Permafrost Characteristics of Alaska

Torre Jorgenson, Kenji Yoshikawa, Mikhail Kanevskiy, Yuri Shur
University of Alaska Fairbanks, Institute of Northern Engineering, Fairbanks, Alaska, USA
Vladimir Romanovsky, Sergei Marchenko, Guido Grosse
University of Alaska Fairbanks, Geophysical Institute, Fairbanks, Alaska, USA
Jerry Brown
International Permafrost Association, Woods Hole, Massachusetts, USA
Ben Jones
U.S. Geological Survey, Anchorage, Alaska, USA

A new permafrost map of Alaska (see inside of front cover), using a terrain-unit approach for mapping permafrost distribution based on climate and surficial geology, is presented. This map represents the third iteration of a permafrost map for Alaska, following the circum-Arctic permafrost map (Brown et al. 1997), which made minor modifications to the initial map by Ferrians (1965). To map permafrost, we developed a rule-based model that incorporated mean annual air temperatures (MAAT) from the PRISM climate map and the surficial geology map of Karlstrom et al. (1964) modified with some new information on geology. We used terrain-permafrost relationships developed by Kreig and Reger (1982) and our knowledge of permafrost distribution to assign permafrost characteristics to each surficial deposit under varying temperatures.

We coded the map with surficial geology, MAAT, primary soil texture, permafrost extent, ground ice volume, and primary thermokarst landforms. The map focuses on the top 10 m of permafrost, where permafrost can be more readily mapped from surface features, determined by simple field measurements, and where ground ice usually is most abundant. Although we used recent MAAT in our model, we note that permafrost distribution is greatly affected by past climates. We relied on many sources for the effort, but are not able to cite all references in this abstract. The main map shows permafrost thickness values based on Ferrians (1965), Péwé (1975), Osterkamp and Payne (1981), Collett et al. (1989), and others.

The following characteristics are shown on small thematic maps on the inside of back cover:

Ground temperatures (usually measured at depths 20 to 30 m) were obtained from boreholes by V. Romanovsky, G. Clow, K. Yoshikawa, D. Kane, and T. Osterkamp as part of the Thermal State of Permafrost project for the International Polar Year (Brown & Romanovsky 2008). Ground ice volumes were estimated for the upper 5 m of permafrost using terrain relationship from Kreig and Reger (1982) and our field data. Ground ice volume near the surface is higher in colder regions due to active ice wedge formation and ice segregation in fine-grained deposits. Pingo distribution was compiled mostly from the literature and by satellite image interpretation. There are >1500 known pingos in Alaska. In central Alaska and bordering Yukon areas, there are ~760 pingos, mostly open-system. Closed-system pingos predominate in the North Slope, Seward Peninsula, and Noatak regions. The distribution of ice wedges was determined from the literature, from polygonal patterns evident on remote sensing imagery, and from our field experience. Ice wedges actively form in the continuous permafrost zone and are mostly inactive in the discontinuous zone (Péwé 1975). Holocene ice wedges are limited to the top 3 to 5 m of permafrost; large, deep (up to 35 m) syngenetic ice wedges formed during the Late Pleistocene. Thermokarst landforms are abundant in all recent and past permafrost zones (Jorgenson et al. 2008). They are varied, due to differences in temperature, ground ice volume, soil texture, slope, and hydrologic conditions.

The permafrost zones underlie 80% of Alaska, including continuous (29%), discontinuous (35%), sporadic (8%), and isolated (8%) permafrost. Permafrost is absent beneath 15% of the State, with glaciers and ice sheets occupying 4% and large water bodies, 1% of the area.

References

Brown, J.B., Ferrians, O.J., Heginbottom, J.A. & Melnikov, E.S. 1997. *Circum-Arctic Map of Permafrost and Ground-Ice Conditions*. U.S. Geol. Surv. Map CP-45, scale 1:10,000,000.

Brown, J. & Romanovsky, V.E. 2008. Report from the International Permafrost Association: State of permafrost in the first decade of the 21st century. *Permafrost and Periglacial Processes* 19: 255-260.

Collett, T.S., Bird, K.J., Kvenvolden, K.A. & Magoon, L.B. 1989. *Map Showing the Depth to the Base of the Deepest Ice-Bearing Permafrost as Determined from Well Logs, North Slope, Alaska.* U.S. Geol. Surv. Oil Gas Inv. Map OM-222, scale 1: 1,000,000.

Ferrians, O.J. 1965. *Permafrost Map of Alaska*. U.S. Geol. Surv. Misc. Geol. Inv. Map I-445, scale 1: 2,500,000.

Jorgenson, M.T., Shur, Y. & Osterkamp, T.E. 2008. Thermokarst in Alaska. *Proceedings of the Ninth International Conference on Permafrost, Fairbanks, Alaska, June 29–July 3, 2008.*.

Karlstrom, T.N.V. et al. 1964. *Surficial Geology of Alaska.* U.S. Geol. Surv. Misc. Geol. Inv. Map I-357, scale 1:1,584,000.

Kreig, R.A. & Reger, R.D. 1982. *Air-Photo Analysis and Summary of Landform Soil Properties Along the Route of the Trans-Alaska Pipeline System.* Alaska Div. Geol. Geophys. Surv., Geologic Rep. 66, 149 pp.

Osterkamp, T.E. & Payne, M.W. 1981. Estimates of permafrost thickness from well logs in northern Alaska. *Cold Reg. Sci. Tech.* 5: 13-27.

Péwé, T.L. 1975. *Quaternary Geology of Alaska*. U.S. Geol. Surv. Prof. Paper 836, 145 pp.

Comparison of Thermal Regimes in Tundra Virgin and Post-Agricultural Soils of the European Northeast

Dmitry Kaverin
Komi Science Center, Russian Academy of Sciences, Syktyvkar, Russia

Introduction

In tundra, agricultural activity transformed the soils and their properties including temperature conditions. Soil thermal regimes are considered to change into ones having no analogues among virgin soils. We studied thermal properties of tundra post-agricultural and virgin soils. Revealing interannual and seasonal temperature dynamics in these soils is important in view of present climate change.

Regional Background

The research was conducted in upland tundra near the town of Vorkuta (67°30′N; 64°02′E) in the east-European Russian Arctic. The terrain is a rolling plain covered generally with silty loams. The area is attributed to the subzone of southern tundra characterized by the distribution of relatively high shrubs: birch and willow. The area under study belongs to the zone of discontinuous permafrost (Oberman & Mazhitova 2003). Massive islands of permafrost occupy slightly dissected hill slopes and hill summits covered with dwarf-shrub/moss vegetation. Permafrost temperatures vary around -1°C.

Mean annual air temperature (MAAT) is -5.8°C, mean annual thawing degree days (DDT) 1005°C-days, and mean annual precipitation 513 mm.

Objects and Methods

Soil temperature regimes were studied in 2 post-agricultural tundra soils. Two undisturbed soils, one permafrost-affected and another one permafrost-free, served as controls. Grassland soils are located in the landscape position similar to that of the control virgin soils.

Soils under study

(1) Abandoned overgrowing sown grassland, soil Epigleyic Gelisol, grass/dwarf-shrub community, willow covers 7–8% of the site area (2005). Permafrost is at 1.35 m depth.

(2) R2 site of the Circumpolar Active Layer Monitoring network, dwarf-shrub/moss tundra, soil Histi-Turbic Cryosol (Reductaquic), permafrost depth is 100 cm;

(3) Abandoned overgrowing arable land, soil Endogleyi-Stagnic Cambisol, grass-moss community, willow covers only 2% of the site area (2005), no permafrost within 2 m depth.

(4) Shrub-moss tundra, soil Dystri-Stagnic Cambisol, no permafrost within 2 m depth.

Post-agricultural sites were abandoned about 10 years ago, and tall shrubs cover up to 10% of the area. Before abandonment, since 1970s the grasslands were annually harvested with periodic rototilling and fertilizing.

The records were conducted with digital Hobo loggers programmed for 8 measurements daily. Loggers were set at depths of 0, 20, 50, and 80 cm and in the upper layer of permafrost in case of its presence. The study was conducted in the period of 2005–2007.

Results and Discussion

By now, there is not much data about the temperature regime of tundra soils in the European Northeast. Kononenko (1986) studied summer temperatures in virgin and agricultural soils but winter thermal regime was quite poorly characterized. Thermal regimes of the soils were not studied at landscape level.

Continuous soil temperature measurements have been conducted in the area since 1996 by Galina Mazhitova. It was revealed that MAST (mean annual air temperature) in all soils of the area is strongly correlated with snow thickness in winter, with permafrost occurring only in the sites with snow thickness less than 50 cm. A progressive increase in shrub coverage is, therefore, the major MAST-controlling factor. Shrubs effectively intensify snow accumulation, catching the snow redistributed by winds (Mazhitova 2001, 2008).

As in previous years during our study, MAST at depth 0–50 cm was commonly above 0°C in all permafrost-free soils. Negative mean annual temperatures in permafrost-affected soils and positive ones in permafrost-free soils are quite typical for discontinuous permafrost zone (Burn 2004).

Studied permafrost-affected soils (No. 1, 2) are located at the southern windward hill slopes. Shallow snow cover (30–40 cm) and quite thick peat layer (10–20 cm) preserve permafrost within the soil profile. Soils of northern slopes located in the same landscape have no permafrost. Such an inversion is resulted from strong winds blowing in winter.

Until 2006, the site with coldest permafrost-affected soil (No. 2) was characterized with negative MAST down all the profile (Mazhitova 2001, 2008). MAST at a depth of 20 cm was -1.9…0.4°C, 50 cm -0.5…-1.9°C. MAST in the upper permafrost layer was -1.2°C with minimum (-4.4°C) in April.

According to MAST and freezing degree days at depths of 0–50 cm the permafrost-affected soil of the abandoned grassland No. 1 was warmer than the virgin soil No. 2. Thus MAST at a depth of 50 cm was -0.35°C versus -0.5°C in the control soil (2006).

The post-agricultural soil (No. 3) was developed in the former shrubby site similar to that of the soil No. 4. It had lower temperatures in comparison with profile No. 4. Despite the absence of thick shrub vegetation, this grassland soil still had no permafrost and was characterized with positive MASTs at depths of 20 cm and 50 cm (+1 +2°C).

The warmest profile was No. 4. Tall shrub vegetation catching thick snow cover causes relatively higher temperatures in winter. It results in higher MASTs.

In 1996–2005, an increasing trend in MAST was observed in the virgin permafrost-affected soil of R2 CALM site (Mazhitova 2008). It was correlated with an increase in both MAAT and active layer depth during the same period (Mazhitova & Kaverin 2007).

In 2006–2007, negative MAST was changed to positive one in the upper soil layer (0–20 cm). This was quite unusual for permafrost-affected soils, but was correlated with extremely hot summer and mild winter that year. MAAT was -2.8°C in 2006–2007. In the soil of arable land, freezing even did not reach a depth of 50 cm during winter 2006–2007.

Zero curtains which are typical for the research area (Mazhitova 2001) observed both in virgin and post-agricultural soils. Zero curtains could be observed from October till January–February. The longest ones are recorded at a depth of 50 cm and more expressed in the permafrost-affected virgin soil.

Conclusions

Removal of virgin vegetation in permafrost-affected sites does not differentiate thermal properties of soils significantly. Post-agricultural permafrost-affected soils were warmer, but permafrost did not disappear just sinking deeper.

In case of removal, tall-shrub vegetation serving as a heat insulation cover in winter soil thermal regime is getting cooler. And still we do not observe permafrost in the post-agricultural soil of the arable land.

Positive mean annual soil temperatures in the permafrost-affected soil were caused by high air temperatures and considered to be an interannual dynamic.

Acknowledgments

The study was supported by NSF (OPP-9732051 and OPP-0225603) and RASHER project of International Polar Year.

References

Archegova, I., Kotelina, N. & Mazhitova, G. Agricultural Use of Tundra Soils in the Vorkuta Area, Northeast European Russia. In: J. Kimble (ed.), *Cryosols (Permafrost-Affected Soils)*. Berlin-Heidelberg-New York: Springer-Verlag, 673-687.

Burn, C.R. 2004. The Thermal Regime of Cryosols. In: J. Kimble (ed.), *Cryosols (Permafrost-Affected Soils)*. Berlin-Heidelberg-New York: Springer-Verlag, 391-414.

Kononenko, A.V. 1986. *Hydrothermal Regime in Taiga and Tundra Soils in the European North-East*. L: Nauka.

Mazhitova, G.G. 2008. Soil Temperature Regimes in the Discontinuous Permafrost Zone in the East European Russian Arctic. *Eurasian Soil Science* 1: 48-62.

Mazhitova, G.G. & Kaverin, D.A. 2007. Dynamics of seasonal thaw depth and surface subsidence at a Circumpolar Active Layer Monitoring (CALM) site in the European Russia. *Earth Cryosphere* 9(4): 20-30 (in Russian).

Mazhitova, G.G. 2001. Structure-functional organization of soils and soil cover in the European North-East. In: F.R. Zaidelman & I.V. Zaboeva (eds.), *Monitoring of Hydrothermal Regime in Tundra Soils*. S-Petersburg: Nauka, 153-162.

Oberman, N.G. & Mazhitova, G.G. 2003. Permafrost mapping of Northeast European Russia based on period of the climatic warming of 1970–1995. *Norsk Geografisk Tidskrift–Norwegian Journal of Geography* 57(2): 111-120.

Massive Ground Ice in the Norilsk Basin: Evidence of Segregation Origin

O.A. Kazansky
Igarka Geocryological Laboratory, Melnikov Permafrost Institute SB RAS, Igarka, Russia
M.Y. Kushchev
Polar Division, MMC Norilsk Nickel, Norilsk, Russia

The Norilsk Basin is situated in the northwestern part of the Putoran Plateau, between Mt. Lontokoisky Kamen and Mt. Kharaelakh. Surficial deposits which consist of glaciolacustrine clays contain massive beds of ground ice up to 15 m in thickness. As is the case with massive ice bodies elsewhere, the origin of the ice in the Norilsk Basin is controversial. The uncertainty regarding this problem impedes understanding of the spatial distribution patterns of massive ground ice and reduces the accuracy of geocryological predictions.

The results of our research suggest that the ice is of segregation origin. This conclusion is based on the field study of sections, as well as on the experimental and theoretical investigations that have demonstrated the possibility of massive ground ice formation by ice segregation during the development of epigenetic permafrost.

The well-known thermal condition for continued ice lens growth is:

$$q_f = q_w + q_i,$$

where q_f is the heat flow from the base of the growing lens to the permafrost table, q_w is the heat flow to the base of the lens from the underlying ground, and q_i is the heat flow required for removal of latent heat of migratory water.

The physico-mechanical requirement for continued lens growth is that no subhorizontal (normal to the heat flow) low-density zones develop in the frozen fringe where new ice lenses that capture the water flow could initiate.

The hydro-physical condition is that the overburden pressure (σ) must not exceed the maximum crystallization pressure (σ_n). Otherwise, migration of water, through the unfrozen water films, from the unfrozen soil connected with an aquifer will cease.

Physically, the process of continued lens growth can be described as follows. During the period when T_s decreases due to a decrease in the permafrost surface temperature T_o (Fig. 1), the thermodynamic equilibrium in the adsorbed water film between the ice lens and the soil particles is disturbed, and part of the water is changed to the ice phase.

As the unfrozen water film becomes thinner, the crystallization pressure increases, pushing the frozen soil upward (Khaimov-Malkov 1959). At the same time, the chemical potential of the adsorbed water decreases in the soil underlying the ice lens with a definite gradient. In order to balance the chemical potential of the adsorbed water and because of the continuity of the films, water flows from the films of the lower-lying particles to the phase change interface.

When the supply of water is matched by the latent heat removal rate according to the thermal boundary condition, the ice lens will continue to grow. If the heat removal is reduced, the thermodynamic balance will be disturbed due to increased T_s and the ice lens will start to melt, while the water will be forced out to the unfrozen zone. If the heat removal increases and a water deficit develops near the bottom of the lens, the freezing zone will be cooled and new crystallization centres will develop below the lowest lens on which migratory water will subsequently settle, resulting in a new ice lens. In this way, a mineral layer forms between the ice lenses.

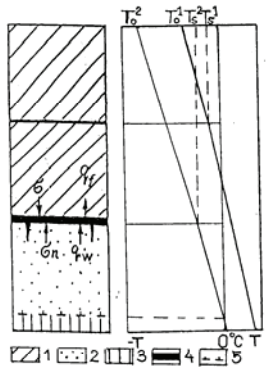

Figure 1. Schematic of the freezing fine-grained soil (Konrad & Morgenstern 1982): 1 – frozen zone; 2 – frozen fringe; 3 – unfrozen soil; 4 – lens of segregated ice; 5 – freezing front.

Any cold wave will be damped at the base of a growing ice lens if it is provided with an adequate supply of water. The wave will not cool the underlying soil until work is done with phase changes. Therefore, in the presence of confined groundwater, continued growth of an ice lens can occur over a long period of time sufficient for the lens to develop into a bed of segregated ice several meters in thickness.

To verify the theoretical concepts considered above, laboratory experiment #15 was conducted in the Igarka permafrost tunnel. Its results corroborate the possibility of continuous growth of a segregated ice lens under the thermal and stress conditions close to those in the field. In the test, a 5.5 cm thick lens was grown in 55 days at a final overburden pressure of 0.25 MPa. Ice lens growth was completely controlled by changing the temperature at the cold side of the sample, simulating the past and present climatic variations. Lowering of the temperature at the base of the ice lens to 0.2°C relative the phase equilibrium temperature corresponding to the applied pressure was allowed. With greater lowering of this temperature, the growing ice lens incorporated soil fragments, resulting in ataxitic (irregular) cryostructure or a

mineral interlayer. Soil and gas inclusions appeared this way in the laboratory-grown ice lenses, which were similar to those observed in natural exposures. The lower the freezing rate is and the larger the soil water pressure is, the better the chance is of continued growth of a segregated ice bed. In the Norilsk Basin, the confined groundwater occurs widely, which easily moves through sandy soils and fissured rocks, providing favourable conditions for the growth of segregated ice.

The transitions between massive ice and ataxitic cryostructure were studied in natural exposures along the Kupets and Norilskaya Rivers, as well as in drill hole cores. In the authors' opinion, such transition between pure ice and ataxitic cryostructure is the only unambiguous evidence so far for the segregated origin of the massive ice beds.

References

Khaimov-Malkov, V.Y. 1959. Thermodynamics of Crystallization Pressure. *Crystal Growth.* Part 2. Moscow: Izd-vo An SSSR, 5-16.

Konrad, J.-M. & Morgenstern, N.R. 1982. Effects of applied pressure on freezing soils. *Can. Geotech. J.* 19(4): 494-495.

Vegetation of Northern West Siberia and its Response to Human-Induced Disturbances

Ludmila Kazantseva
Earth Cryosphere Institute SB RAS, Tyumen, Russia

The significant influence of climate change on ecosystem dynamics was noted long ago (Koloskov 1925, Bocher 1949, Timin et al. 1973, and others) However, long-term ecosystem monitoring in cold regions has been carried out by few researchers (Bliss 1975, Walker 1985, Rannie 1986, Broll et al. 2003). In this connection, the results of long-term ecosystem monitoring at the Nadym site, on which is carried out the conditions of varying climatic and human-induced impact, can be of interest to researchers of arctic and subarctic regions.

The objective of this research is to study vegetation changes under impact of human-induced disturbances. Annual and spatial variability in the structure, species composition, coverage, and frequency of plant species were studied related to changes in seasonal thaw depth and soil temperature.

At the Nadym site located 30 km to the south of the town of Nadym (Moskalenko 2006), detailed descriptions of vegetation on permanent plots are annually carried out, and measurements of seasonal thaw depth and soil temperatures in different landscape conditions are performed.

The zonal vegetation of the Nadym area is birch-larch and birch-pine shrub-moss-lichen light forests. The significant areas are occupied by cloudberry-Labrador tea-peat moss-lichen peatlands and low shrub-sedge-moss bogs. On frost mounds meet cedar Labrador tea-lichen and Labrador tea—peat moss open woodland.

Supervisions were carried out on the 10 x 10 m plots divided grid on meter squares. The plots are situated in natural conditions and in a route of the Nadym-Punga gas pipeline. On each such plot are 100 squares on which the vegetation was described, the soil temperature on a surface and on depth 20 cm was measured, and measurements of seasonal thaw depth were carried out. In a microrelief of plots were described hummocks and space between hummocks and pools; their surfaces were determined with the help of repeated leveling. Microphytocoenoses were registered on dominant species.

The analysis of the received data allowed the compilation of a complete natural and disturbed plots map: spatial structure of microphytocoenoses, microrelief, temperature of soil surface, soil temperature on depth 20 cm, seasonal thaw depth, peat thickness, shrub height.

In Figure 1, two maps of spatial structure show undisturbed and disturbed peat-mineral frost mound results. The microrelief and dominants of microphytocoenoses are shown on these maps.

The vegetation of an undisturbed frost mound is more varied and complicated. There are 3 layers here: (1) shrub layer, height up to 40 cm (*Ledum palustre*); (2) sedge and low

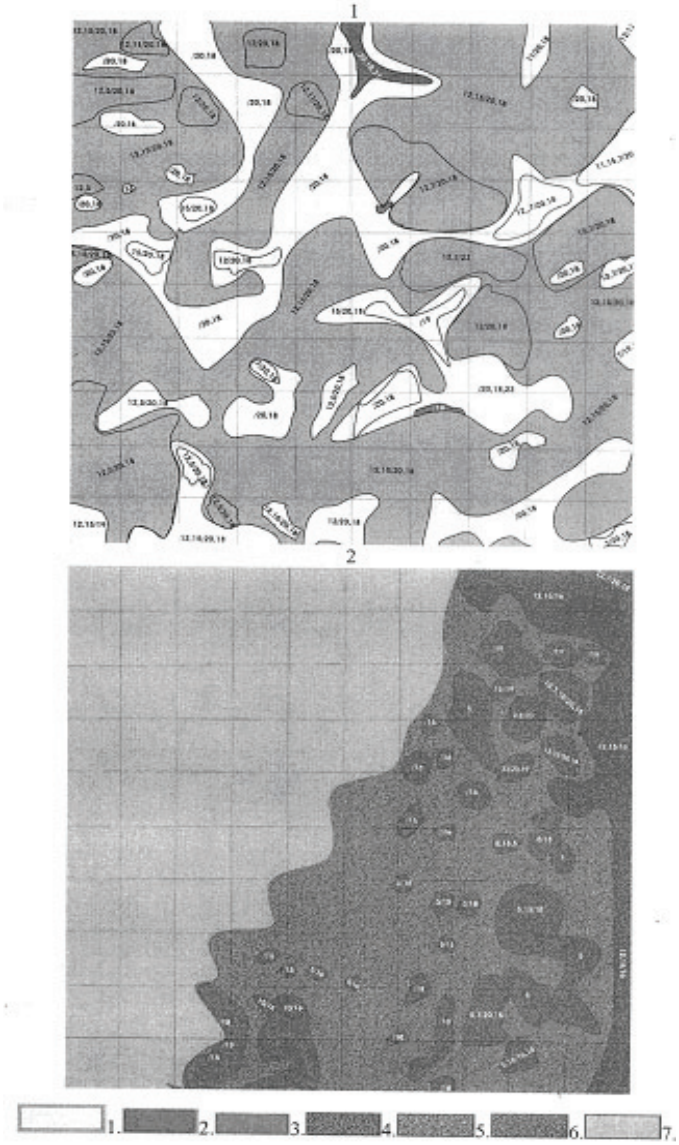

Figure 1. Spatial structure of undisturbed (1) and disturbed (2) frost mound.
Microrelief: 1 – flat surface, 2 – crack, 3 – hummocks, 4 – peaty hummocks, 5 - sandy hummocks, 6 - tussocks, 7 – water
Dominants of microphytocoenoses.
Vascular plants (on the left from line in the index): 4 – Festuca ovina, 5 – Carex globularis, 6 – Juncus filiformis, 7 – Vaccinium vitis-idaea, 8 – Empetrum nigrum, 9 – Dicranum congestum, 10 – Vaccinium uliginosum, 11 – Rubus chamaemorus, 12 – Ledum palustre, 13 – Eriophorum vaginatum, 14 – Andromeda polifolia, 15 – Betula nana, 16 – Pinus sibirica, 17 – Chamaedaphne calyculata.
Mosses and lichen (on the right from line in the index): 18 – Cladina stellaris, 19 – Sphagnum fuscum, 20 – Cetraria islandica, – Cetraria nigricans, 22 – Polytrichum strictum, 23 – Plerozium schreberi.

shrub layer, height up to 10 cm (*Carex globularis, Vaccinium uliginosum)*; and (3) moss and lichen layer (*Cladina stellaris*, *Polytrichum strictum*, *Sphagnum fuscum*).

On a frost mound repeatedly disturbed in 2004 as a result of reconstruction of the gas pipeline, vegetation cover is rare; also it is composed of a small number of species. Vegetation recovery here begins in places where surface peat was kept. More than half of the disturbed plot is flooded with water as a result of infringement of superficial drain by the gas pipeline embankment.

On the natural plot, relative elevations reach 160 cm, and on the disturbed plot, they reach 280 cm due to settlement and flooding of the large part of the plot.

On plot measurements of soil temperature, surface and depth of 20 cm have been carried out. The maps are compiled on the basis of the given temperatures. On the undisturbed frost mound, the maximal temperature of a surface was 14.5°C, on depth 20 cm, -9.7°C; the minimal temperature on a surface was 6.3°C, on the depth 20 cm, -2.7°C. On the disturbed plot, the maximal soil temperature at the depth of 20 cm has increased up to 16°C on peat sites, before covered with lichen, and minimal temperature was 9.5°C. Rise in the soil temperature has made 7°C on the average. Change of temperature influences formation of vegetative cover, the above soil temperature, the more variously specific structure of vegetation on the given site.

Analysis of the given measurements of thaw depth on sites has shown the following: Thaw depth on the undisturbed frost mound was more on the raised sites, occupied with dense Labrador tea; in the space between hummocks occupied with moss-lichen vegetation, thaw depth was less.

The maximal thaw depth was 180 cm; the minimal thaw depth (50 cm) is marked in the frozen crack with lichen cover. According to supervised data, the map of active layer thickness on the undisturbed site is compiled (Fig. 2).

On the disturbed plot, the permafrost table has gone down to a depth of 10 and more meters, according to geophysical works (Ponomareva & Skvortsov 2006).

Measurements of peat thickness have shown that the thickness of peat on a plot changes considerably; it varies in limits from 5 up to 65 cm, depending on the microrelief and vegetation cover. The least thickness of peat is observed on equal sites on which the sedge grows. The greatest thickness of peat is characteristic for peat moss hummocks with cloudberries.

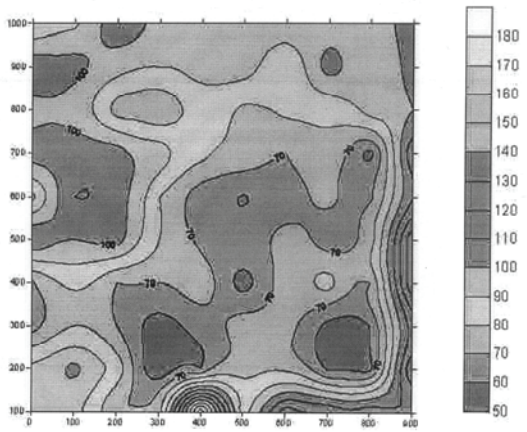

Figure 2. Seasonal thaw depth on undisturbed frost mound (cm).

Human-induced disturbances at construction and operation of the gas pipeline Nadym-Punga in West Siberia rendered significant influence on the vegetation cover and other ecosystem components, which changes are reflected in the complete compiled maps.

These maps can be used for compiling prognostic and ecological maps and also for planning actions related to environment conservation.

Acknowledgments

I thank my colleagues from Earth Cryosphere Institute O.E. Ponomareva, O.L. Opokina, and E.V. Elantsev for help with the fieldwork.

This study was made possible through financial support from the grant of Tyumen governor and the U.S. National Science Foundation (Grants OPP-9732051 and OPP-0225603).

References

Bliss, L.C. 1975. Devon Island, Canada. *Ecolog. Bull*. 20: 17-60.

Bocher, T.W. 1949. Climate, soil and lakes in continental West Greenland in relation to plant life. *Medd. om Gronland*, Bd. 147 (N2,1949): 4.

Broll, G., Tarnocai, C. & Gould, J. 2003. Long-term high Arctic ecosystem monitoring in Quttnir paag National Park, Ellesmere island, Canada. *Proceedings of the Eighth International Conference on Permafrost*, *Zurich, Switzerland, July 21–25 2003*, 1: 85-94.

Koloskov, P.I. 1925. *Climatic Foundations of Agriculture in the Amur Area.* Blagoveshensk: Soviet for Eastern Meteorological Service, 152 pp.

Moskalenko N.G. (ed.) 2006. Anthropogenic changes of ecosystems in West Siberian gas province. *M., RASHN*, 358.

Ponomareva, O.E. & Skvotsov, A.G. 2006. Methods and results of exogenous geological process study in Nadym region of West Siberia. *Proceedings of the International Conference. Tyumen, TGNGU*. 1: 272-274.

Rannie, W.F. 1986. Summer air temperature and number of vascular species in arctic Canada. *Arctic* 39: 133-137.

Timin, M.E., Coller, B.D., Zich, J. & Walker, D.A. 1973. A computer simulation of the arctic tundra ecosystem near Borrow, Alaska. In: *US Tundra Biome Rep*. San Diego State Univ. (73-1): 1-82.

Walker, D.A. 1985. *Vegetation and Environmental Gradients of the Prudhoe Bay Region, Alaska*. Hanover, 239 pp.

Surface Ice and Snow Disappearance in Alpine Cirques and Its Possible Significance for Rock Glacier Formation: Some Observations from Central Austria

Andreas Kellerer-Pirklbauer
Institute of Geography and Regional Science, University of Graz, Austria

Introduction

Active rock glaciers consist of two components: ice (congelation and/or sedimentary ice including "glacier" ice) and lithological material (periglacially and/or glacially-derived rock fragments of different grain size). Considering their long formation period (centuries to millennia) and common climate variability (e.g., temperature, precipitation) in such long time scales, rock glaciers experience strong variations in the rate of nourishment as well as the ratio between ice and debris input to the rock glacier system.

Studies on the climate of rock glaciers reveal that the mean annual air temperature at the rooting zone of active rock glaciers is usually only slightly higher (if at all) than at nearby equilibrium line altitudes (ELA) of normal glaciers and/or the annual precipitation is only slightly lower than at nearby ELA (e.g., Haeberli 1983). This indicates the high sensitivity of rock glacier development to cooler and/or more humid conditions and their close relationship to normal glaciers. However, knowledge regarding incipient formation, entire development period, variations in nourishment rate, and the ratio between ice and rock input seen over a long time span is still far from being complete.

This paper presents data on surface ice and snow disappearance since the Little Ice Age (LIA) at two neighboring cirques in the Central Alps of Austria. Today, one houses a rock glacier and one, a debris-covered glacier remnant. Observations and measurements on thickness variations and thermal conditions of the supraglacial debris cover, on landforms formed from this supraglacial material, and on buried sedimentary ice add to the understanding of rock glacier formation and development.

Study Area and Applied Methods

Kögele Cirque and Hinteres Langtal Cirque

The study area consists of the two neighboring cirques Kögele Cirque (KC) and Hinteres Langtal Cirque (HLC) located in the central part of the Schober Mountains (46°59′N, 12°47′E), Central Alps (Fig. 1). The study area is characterized by crystalline rocks and a continental climate (1500mm at 2000m asl, 0°C mean annual air temperature at 2300 m a.s.l.) causing minor glaciation but a high abundance of rock glaciers. Both cirques are oriented towards the west-northwest, each with comparable high crests and mountain summits (>3000 m a.s.l.) to the south and east (Fig. 1). The HLC is dominated by the Hinteres Langtalkar Rock Glacier (HLRG) which at its front indicates the local lower limit of discontinuous permafrost at 2450 m a.s.l. In contrast, the KC is located some 50 m higher, lacks a rock glacier, but houses a glacier remnant (for details see Kellerer-Pirklbauer & Kaufmann 2007).

Methods

The spatial extent of surface areas covered by glaciers and perennial snow at both cirques was reconstructed for the four stages—c. 1850 (LIA-maximum), 1969, 1997, and 2006—by using morphological evidences (LIA-moraine ridges), air photographs (1969, 1997), and field mapping (Sept. 2006).

Massive sedimentary ice outcrops in the HLC were mapped between summer 2003 and 2007 during fieldwork. In 2006, the thickness of the supraglacial debris mantle in the KC was quantified by digging through and measuring the debris layer to solid ice at 34 sites. These data were used to interpolate the debris cover thickness in the KC, applying the Inverse Distance Weighted interpolator in ArcGIS.

To monitor near-surface temperatures in the supraglacial debris cover, two 3-channel miniature temperature dataloggers (MTLs) (GeoPrecision) were installed in 2006 at 2690 m a.s.l. (KC1) and 2710 m a.s.l. (KC2) in the KC (Fig. 2). Three temperature sensors (PT1000; accuracy +/-0.05°C) were connected to each MTL. The two MTLs operated correctly during the entire period 12.09.2006–25.07.2007, logging values every 0.5 h at depths 0–50 cm (KC1: 0, 10, and 50 cm; KC2: 0, 10, and 20 cm). The lowest sensor at site KC2 was placed at the debris/ice boundary.

Results and Some Related Comments

Surface ice disappearance since 1850

In 1850 A.D., both cirques were covered by glaciers and perennial snow fields covering 0.21 km² of the KC and 0.18 km² of the HLC. In 1969, ice/snow still covered 0.12 km² of the KC and 0.06 km² of the HLC, but by 1997 these values were reduced to 0.06 km² (KC) and 0.01 km² (HLC). In 2006, the extent of surface ice/snow was reduced to a few small patches in the HLC and covered less than 0.01 km² of the KC (Fig. 1).

Supraglacial debris cover and buried sedimentary ice

The supraglacial debris cover in the KC was formed during the last decades by periglacially- and paraglacially-derived sediments from the steadily enlarging supraglacial slopes above the shrinking ice mass. The debris cover is currently relatively thin and increases in thickness down valley, exceeding 70 cm at the lower part of the mapped area (Fig. 2). In contrast to the KC, surface and near-surface (<20 cm), findings of massive ground ice (sedimentary ice judged from the ice appearance) in the HLC are rare and were only noticed at three locations between 2003 and 2007 (Fig. 1). A small lake was observed in the spoon-shaped southern rooting zone of the HLRG in summer 2003 (*2 in Fig. 2), but was absent in the subsequent years. At the upper part of this depression, a narrow massive ice outcrop was seen for the first time in 2006, probably indicating a glacier remnant.

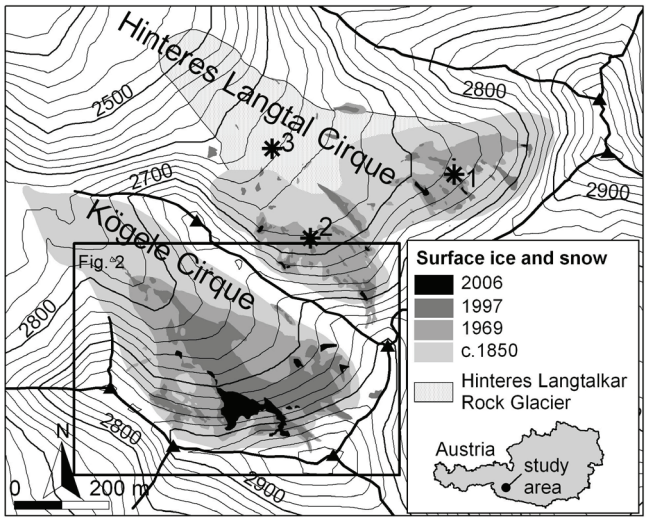

Figure 1. The two cirques Kögele Cirque (KC) and Hinteres Langtal Cirque (HLC) and their extent of surface ice and snow in c. 1850, 1969, 1997, and 2006. The location of the Hinteres Langtalkar Rock Glacier/HLRG (in 2002) is indicated. Findings of sedimentary ice since 2003 in the HLC are asterisked: *1 = in 2006 – below 30 cm of debris; *2 = in 2006 and 2007 – a c. 20 m long and <2 m high massive ice outcrop at the southern rooting zone of HLRG; *3 = in 2007 – below 20–30 cm of debris at the upper edge of a transversal furrow (Viktor Kaufmann, pers. com. 2007).

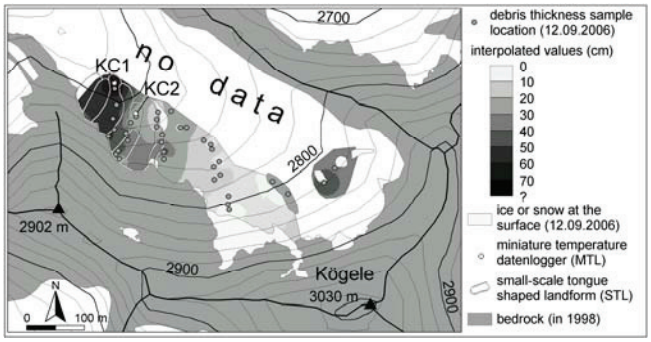

Figure 2. Estimation of the debris cover thickness in the KC, based on 34 sample locations. Locations of the small-scale tongue-shaped landforms (STL) and the two MTLs (KC1 and KC2) are indicated.

Formation of small-scale tongue-shaped landforms

The supraglacial debris cover in the KC does not form a uniform surface. At the southwest margin of the cirque, 9 small-scale tongue-shaped landforms (STL) formed during the last decades are seen on air photographs. Morphometric studies of the STL show heights of the riser of 1–3 m, lengths of 66–125 m, and spatial extents of 859–3276 m². Most of the STL have a down-valley bended appearance in plane view, indicating ongoing movement of the buried glacier remnant. Similar STL features have been observed in the rooting zone of HLRG, hinting a significance of STL for rock glacier nourishment and incipient formation.

Thermal conditions of the supraglacial debris mantle at KC

Data from the MTLs reveal that the mean surface temperature for the period 12.09.2006–25.07.2007 is -1.6°C to -2.4°C at c. 2700 m a.s.l., decreasing with depth (Table 1). The lower temperature at site KC2 seems to be related to longer duration (and thickness?) of winter snow cover. Maximum diurnal temperature fluctuations are >10 K at the surface, 4–5 K at 10 cm depth, 2.2 K at 20 cm depth (at K2 at the ice/debris boundary), and less than 1 K at 50 cm at K1, indicating a substantial damping effect of the debris layer. The lowest sensors at both sites reveal low thawing degree day/TDD values which can be explained by the proximity to the underlying buried ice mass and by a thin active layer at these sheltered locations at such high altitudes.

Table 1. Summarized temperature conditions at different depths at the two sites in the KC for the period 13.09.2006–25.07.2007 (10.5 months) based on MTLs. MPT = mean period temperature in °C; DTF-Max = maximum daily temperature fluctuation during this period in Kelvin; FDD = freezing degree days; TDD = thawing degree days. The snow cover duration was estimated based on low temperature fluctuations (for locations of the MTLs see Fig. 2).

KC1 (snow cover 1.5 months)					KC2 (snow cover 4 months)				
Depth	MPT	DTF-Max	FDD	TDD	Depth	MPT	DTF-Max	FDD	TDD
0	-1.6	11.5	-1010	500	0	-2.4	10.2	-1068	320
10	-1.7	5.3	-924	384	10	-2.8	4.1	-1017	128
50	-2.2	0.8	-742	44	20*	-3.1	2.2	-980	16

*sensor measured at the boundary between debris and glacier ice.

Long-term landscape dynamics: KC versus HLC

The data presented here confirm the fact that, already, slightly different topoclimatic conditions are sufficient to generate over a long time span a rock glacier in one cirque and a normal glacier in the neighbouring cirque. The rate of ice and debris input to the cirque during the past was dominated by the former in the KC, whereas probably by the latter in the HLC. A thin active layer helps to preserve a degrading debris-covered glacier remnant. Subsequent incorporation of such a debris-covered ice mass into a rock glacier body might be regarded as an important nourishment factor; at least this could have been the case at the HLRG.

Acknowledgments

This study was carried out within the framework of the project ALPCHANGE (www.alpchange.at) financed by the Austrian Science Fund (FWF). The air photographs (1969, 1997, and 1998) were kindly provided by Viktor Kaufmann.

References

Haeberli, W. 1983. Permafrost-glacier relationships in the Swiss Alps: Today and in the past. *Proceedings, 4th Intl. Conf. on Permafrost, Fairbanks, AK, July 17–22*: 415-420.

Kellerer-Pirklbauer, A. & Kaufmann, V. 2007. Paraglacial talus instability in recently deglaciated cirques (Schober Group, Austria). *Proceedings, 9th Intl. Symposium High Mountain Remote Sensing Cartography (HMRSC-IX), Graz, Austria, Sept. 14–22, 2006*: 121-130.

Temperatures in Alpine Rock Walls During the Warm Winter 2006–2007 in Austria and Its Significance for Mountain Permafrost: Preliminary Results

Andreas Kellerer-Pirklbauer
Institute of Geography and Regional Science, University of Graz, Austria
Michael Avian
Institute of Remote Sensing and Photogrammetry, Graz University of Technology, Austria
Gerhard Karl Lieb, Matthias Rieckh
Institute of Geography and Regional Science, University of Graz, Austria

Introduction

In a large part of Europe temperatures during autumn and winter 2006–2007 reached a record high. The autumn of 2006 (Sept., Oct., and Nov.) was more than 3°C warmer from the northern side of the Alps to southern Norway if compared to the 1971–2000 average (WMO 2007). The extreme temperature anomaly also affected the high mountains of Austria and caused record temperature values at the Sonnblick Observatory located in the high mountains of central Austria (3106 m a.s.l., 47°03′N, 12°57′E; cf. Fig. 1). At this observatory, the period September 2006 to June 2007 was substantially warmer than the average. Deviations from the mean monthly values of the normal period 1961–1990 are in the range of +2.6°C (Nov. 2006) and +4.9°C (April 2007) with a mean value of +3.2°C for this 10-month period (ZAMG 2007). Comparable extreme atmospheric temperature anomalies are reported to affect near-surface permafrost conditions to depths exceeding 10 m (Isaksen et al. 2007). In particular, monitoring temperature changes in bedrock gives a good indication for the effects of air temperature anomalies on ground thermal conditions (Smith & Riseborough 1996). For this reason, continuous temperature measurements in alpine rock walls for monitoring the effects of climate change on bedrock temperatures (including permafrost) in central and eastern Austria were initiated in summer 2006 within the project ALPCHANGE. Measurements at 9 rock wall sites (RWS) distributed over 5 study areas (SAs) recorded the exceptionally warm 9-month period from 01.10.2006 to 30.06.2007. Preliminary results are presented here.

Study Areas and Instrumentation

Four of the 5 SAs are located in the Hohe Tauern Range, where the highest mountains of Austria reach almost 3800 m a.s.l. At each of the 4 SAs (Dösen Valley, Hintereggen Valley, Hinteres Langtal Cirque, and Pasterze Glacier; Fig. 1, Table 1), 2 RWS with opposed aspects were instrumented with 3 temperature sensors for each rock wall. The fifth SA is located in the eastern part of the Niedere Tauern Range (Hochreichart Cirque), where only one north-facing rock wall at an elevation of 1960 m a.s.l. was instrumented. The 9 RWS are located at elevations between 2220 and 2775 m a.s.l. (3 of them are probably affected by permafrost). All 9 RWS were drilled in different metamorphic bedrock types (Table 1).

To measure bedrock temperatures, 16 mm wide boreholes were drilled at each site 40 cm horizontally into the bedrock by using HILTI drilling equipment connected to an external power set. Due to technical problems, the boreholes at the sites DOV-A, HEV-A, and HEV-B (Table 1) did not reach the intended 40 cm depth. To measure near rock surface temperature, a sensor was installed at 3 cm. The other sensors were installed at depths of 10 and 40 cm (slightly less at the 3 RWS mentioned above) as suggested by Matsuoka (1994). At all RWS, the measurements were recorded every 30 minutes on three-channel miniature temperature dataloggers/MTLs (M-Log6, GeoPrecision). All datasets cover at least the period 01.10.2006 to 30.06.2007. The three sensors are

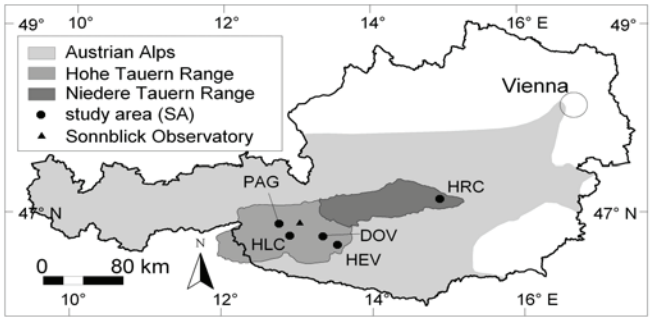

Figure 1. Locations of the 5 study areas in Austria and the Sonnblick Observatory. For abbreviations refer to Table 1.

Table 1. Characteristics of the 9 alpine rock wall sites, where temperature is monitored since summer/early autumn 2006. SA=study area (DOV=Dösen Valley, HEV=Hintereggen Valley, HLC=Hinteres Langtal Cirque, HRC=Hochreichart Cirque, PAG=supraglacial slopes flanking the tongue of Pasterze Glacier); RWS=rock wall site; Bedrock types: GGN=granitic gneiss, AGN=augengneiss, MS=mica schist, GN=Gneiss, CMS=calcareous mica schist; Depths=depths of sensors in borehole.

SA	RWS	Lat.	Long.	Alt. (m asl)	Aspect	Bed-rock.	Depths (cm)
DOV	DOV-A	46°59′N	13°17′E	2630	S	GGN	3,10,32
	DOV-B[1]	46°59′N	13°17′E	2640	N	GGN	3,10,40
HEV	HEV-A	46°55′N	13°23′E	2505	W	AGN	3,10,30
	HEV-B[1]	46°55′N	13°23′E	2530	E	AGN	3,10,30
HLC	HLC-A	46°59′N	12°47′E	2725	SW	MS	3,10,40
	HLC-B[1]	46°59′N	12°47′E	2700	NE	MS	3,10,40
HRC	HRC-A	47°22′N	14°41′E	1960	N	GN	3,10[2],40[2]
PAG	PAG-A	47°05′N	12°44′E	2220	SW	CMS	3,10,40
	PAG-B	47°05′N	12°44′E	2250	NE	CMS	3,10,40

[1] probably with permafrost occurrence (Lieb 1998)
[2] sensor that partly malfunctioned (no data presented in Table 2)

of the PT1000 type with—according to GeoPrecision—an accuracy of +/- 0.05°C, a measurement range between -40 and +100°C and a very high long-term stability (calibration drift <0.01°C/year). Each sensor was connected to the MTL by a teflon cable. After sensors installation, the borehole was refilled with fine quartzite sand and sealed with silica gel to avoid, for example, air circulation in the borehole.

Results and Discussion

Mean temperature values for the 9-month period (MPT), the accumulated freezing degree days (FDD), and the accumulated thawing degree days (TDD) were computed at all 9 RWS for each sensor (Table 2). FDD and TDD equal the number of degree days below and above 0°C, respectively. The results for MPT, FDD, and TDD at the 3 different depths at each RWS are relatively equal, indicating rapid conductive heat transfer in the metamorphic rocks. Maximum value ranges are 0.22°C for MPT (HEV-A), 259 for FDD (DOV-B), and 118 for TDD (HLC-A).

Focusing on the 3 cm values, one might infer that MPT, FDD, and TDD are not correlated with elevation, which can be attributed to differences in the duration of the winter snow cover, aspect, and the small sample size (cf. insert graph in Table 2). The highest location of RWS where positive MPT for the period 01.10.2006 to 30.06.2007 were recorded is located at 2725 m a.s.l., is facing southwest, and was covered by snow for some 3.5 months (HLC-A: 1.55°C). An exceptionally high MPT value of 5.25°C at an elevation of 2220 m a.s.l. with no substantial snow cover was recorded at a southwest-facing RWS (PAG-A). More generally, RWS with absent or short snow cover (1 month or less), located in high as well as lower elevations, reveal positive MPT and relatively low FDD and high TDD values (HEV-A, HEV-B, and PAG-A). In contrary, the lowest MPT (-1.89°C) as well as highest FDD (-679) were recorded at RWS with long snow cover (6 months or more), in north to northeast aspects and in high-elevated permafrost environments (>2640 m a.s.l.). Such conditions have been recorded at HLC-B and DOV-B, where the long-lying snow cover (established around end of November/beginning of December) protected the frozen rock wall from the warm atmospheric conditions during winter and spring.

One might conclude that, based on our data, only rather extreme RWS revealed temperatures during the studied 9-month period 01.10.2006 to 30.06.2007 favorable for permafrost conditions and preservation. Thus, it can be assumed that permafrost regions in central and eastern Austria, with a minor winter and spring snow cover in 2006–2007, experienced very unfavorable conditions. The continuation of our measurements will reveal more details on the significance of this winter over a longer time span.

Table 2. Summarized results of the temperature measurements at all 9 RWS for the period 01.10.2006–30.06.2007: Snow=period with supposed thick snow cover indicated in months; Depth in cm; MPT=mean period temperature in °C; FDD=freezing degree days; TDD=thawing degree days. Insert graph shows relationship between MPT (3 cm) and elevation with respect to snow cover.

DOV-A (Asp. S; Snow 1)			
Depth	MPT	FDD	TDD
3	1.87	-328	839
10	1.93	-312	839
32	1.87	-249	760
DOV-B (Asp. N; Snow 6)			
Depth	MPT	FDD	TDD
3	-1.69	-679	65
10	-1.71	-688	63
40	-1.71	-420	45
HEV-A (Asp. W; Snow 0)			
Depth	MPT	FDD	TDD
3	0.92	-393	646
10	0.91	-384	632
30	0.70	-369	559
HEV-B (Asp. E; Snow 0.5)			
Depth	MPT	FDD	TDD
3	2.11	-249	824
10	2.20	-231	830
30	2.16	-202	791
HLC-A (Asp. SW; Snow 3.5)			
Depth	MPT	FDD	TDD
3	1.55	-302	727
10	1.61	-286	727
40	1.41	-225	609

HLC-B (Asp. NE; Snow 6.5)			
Depth	MPT	FDD	TDD
3	-1.89	-666	149
10	-1.88	-662	148
40	-1.86	-626	118
HRC-A (Asp. N; Snow 0)			
Depth	MPT	FDD	TDD
3	1.99	-303	847
PAG-A (Asp. SW; Snow 0)			
Depth	MPT	FDD	TDD
3	5.25	-101	1535
10	5.42	-81	1560
40	5.10	-37	1429
PAG-B (Asp. NW; Snow 6)			
Depth	MPT	FDD	TDD
3	1.95	-11	544
10	1.77	-28	511
40	1.77	-14	497

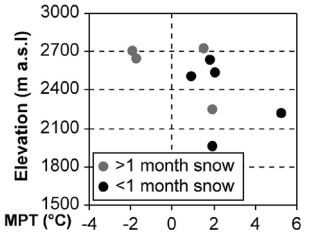

Acknowledgments

This study was carried out within the framework of the project ALPCHANGE (www.alpchange.at) financed by the Austrian Science Fund (FWF).

References

Isaksen, K., Benestad, R.E., Harris, C. & Sollid, J.L. 2007. Recent extreme near-surface permafrost temperatures on Svalbard in relation to future climate scenarios. *Geophysical Research Letters* 34: L17502.

Lieb, G.K. 1998. High-mountain permafrost in the Austrian Alps (Europe). *Proceedings of the Seventh International Permafrost Conference, Yellowknife, Canada, June 23–27, 1998:* 663-668.

Matsuoka, N. 1994. Diurnal freeze-thaw depth in rock walls: field measurements and theoretical considerations. *Earth Surface Processes and Landforms* 19: 423-435.

Smith, M.W. & Riseborough, D.W. 1996. Permafrost monitoring and detection of climate change. *Permafrost and Periglacial Processes* 7: 301-309.

WMO 2007. A warm autumn and winter in Europe. *Newsletter of the World Meteorological Organization* 2007/No. 1: 3.

ZAMG 2007. Present climate data from stations in Austria. http://www.zamg.ac.at (accessed 01.11.2007).

Content and Composition of Organic Matter in Quaternary Deposits on the Laptev Sea Coast

A.L. Kholodov
Geophysical Institute, University of Alaska Fairbanks, USA
Institute of Physical, Chemical, and Biological Problems of Soil Science, RAS, Russia
L. Schirrmeister
Alfred Wegener Institute for Polar and Marine Research, Potsdam, Germany
H. Meyer
Alfred Wegener Institute for Polar and Marine Research, Potsdam, Germany
Ch. Knoblauch
Soil Science Institute of Hamburg University, Germany
K. Fahl
Alfred Wegener Institute for Polar and Marine Research, Bremerhaven, Germany

Introduction

Because of freezing and subsequent preservation of biomass after sedimentation, permafrost areas are considered to be important carbon sinks. Mean TOC contents of frozen Quaternary deposits exposed at the Laptev Sea coast are high and vary between 3.2 to 11.9 wt% (Grigoriev et al. 2004). The organic matter (OM) is preserved in permafrost in the early diagenetic stage of OM maturation. This stage is characterized by a decreasing N content, depletion of products, which have a biological value (carbohydrates, proteins, etc.) and preservation of biopolymers (Bordenave 1993). Deeper thawing caused by climate warming can result in increased decomposition of organic matter and a release of greenhouse gases. This study aims a characterization of the organic matter in different types of Quaternary deposits at the Laptev Sea coast.

The Study Area and Investigated Deposits

Permafrost drilling was carried out on the Bykovsky Peninsula (SW of Lena River Delta) and Cape Svyatoy Nos (NE of Yana River mouth) in 2001 and 2003 (Kholodov et al. 2006). Various types of Quaternary deposits were analyzed from both sampling sites:

1. Middle Pleistocene deposits of the *Kuchchuguy Suite* composed of well-sorted silty loam with numerous thin grass roots. The ice content is in the range from 30 to 50%. The cryostructure is massive. The genesis of these loess-like deposits is still under debate.

2. Late Pleistocene syncryogenic *Ice Complex deposits* of silt or silty loam with sand and peat layers, fragments of twigs and other plant remains, and peat inclusions are characterized by volumetric ice content of up to 80–90% and large wedges (up to 30 m high). The Ice Complex deposits of the Bykovsky Peninsula can be divided into 2 groups: those accumulated due to intensive sedimentation rate and formed under the condition of stable ground surface position. The first group was formed during the MIS-4 and MIS-2 periods. The second group was accumulated during MIS-3 Interstadial. According to previous investigation (Schirrmeister et al. 2002), several periods existed during the MIS-3 time, when rates of sedimentation and freezing decreased and palaeosol horizons were formed over long periods during several thousands of years. The Ice Complex sequences are in places covered by Late Holocene deposits.

3. Late Pleistocene to Holocene *deposits in thermokarst depressions* (alases). The formation of these deposits was a result of thermokarst processes that took place during the Late Pleistocene to Holocene transition period (13–10 kyr BP). This layer can be subdivided into 2 horizons:

a. Taberal deposits, that is, former Ice Complex deposits which were thawed under thermokarst lakes and refrozen after lake drainage. Taberal deposits are silty loams with a volumetric ice content of up to 50%.

b. Lacustrine to boggy (alas) deposits were formed in shallow lakes or in bogs. These deposits are characterized by a high peat and ice (up to 60%) content.

Materials and Methods

The described deposits were cored using a rotary drilling device. The samples were air dried immediately after drilling. Subsequently the material was milled. For determination of TOC and isotopic composition, carbonates were removed from samples by a 1n solution of HCl at 90°C for 3 hours and washed with distilled water.

The following analyses were done:

Water (ice) content and density of soil were determined using a weight method. *Elemental composition* of OM: Total carbon (TC), total organic carbon (TOC), and nitrogen (N) were determined using the VARIO II Element analyzer. *Isotopic composition ($\delta^{13}C$)* was determined with a Finnigan MAT Delta-S mass spectrometer using a FLASH elemental analyzer and a CONFLO III gas mixing system for online determination of the carbon isotopic composition. *Dissolved Organic Carbon (DOC)* was extracted from samples with a $CaCl_2$ solution (4 mM). Subsequently the samples were centrifuged and filtered (0.45 μm) (Zsolnay 2003). *Biomarkers*, to gain better insights into the geochemical composition of the particulate organic carbon n-alkanes (C15 to C37), sterols (sum of 24-Methylcholest-5-en-3ß-ol and

Table 1. Main parameters of organic matter in the investigated deposits.

Type of deposits	n	TC,% *	TOC, % *	TOC/N *	CPI	$\delta^{13}C$, ‰ *;**	DOC (mg gTG) *
Kuchchuguy Suite	14	0.66–1.82 / **1.14**	0.34–1.24 / **0.75**	3.25–9.34/ **6.96**	5–6	-27.28 to -25.70 / **-26.18**	0.13–0.26 / **0.20 (*n*=4)**
Ice Complex	28	0.35–4.53 / **1.91**	0.26–3.89 / **1.48**	1.67–11.38 / **8.75**	–	-27.48 to -23.78 / **-25.34**	0.00–0.95 / **0.36 (*n*=25)**
Taberal deposits	14	0.59–3.28 / **1.64**	0.57–2.65 / **1.08**	0.84–14.63 / **8.44**	4–6	-27.15 to -24.32 / **-25.59**	0.11–0.43./ **0.27 (*n*=9)**
Lacustrine / boggy alas deposits	11	1.01–6.92 / **2.38**	0.93–6.13/ **1.99**	8.20–11.90 / **9.14**	3–5	-26.90 to -23.74 / **-25.33**	0.06–0.61 / **0.27 (*n*=9)**

*Min–max range/average value, ** vs. PDB standard

24-Ethylcholest-5-en-3ß-ol), and fatty acids (carbon length 14 to 30), were analyzed by means of gas chromatography according to Fahl & Stein (1999). The carbon-preference-index (CPI) was calculated after Bray & Evans (1961).

Results and Discussion

The main characteristics of organic matter (TC, TOC, C/N ratio, $\delta^{13}C$, CPI and DOC) in Laptev Sea Quaternary deposits are summarized in Table 1 for the four types of deposits. The mean TC contents are between 1 and 2.5%, most of which (about 60%) is composed of organic carbon. Main differences concerning carbon characteristics between the studied deposit types are lowest TC, TOC, DOC content, C/N ratios and $\delta^{13}C$ values for the Kuchchuguy, whereas Ice Complex, Alas and taberal deposits are similar with regard to their organic composition. The mean $\delta^{13}C$ is about -25.3 to -25.5‰ for these deposits, and very similar ranges let us believe that the ratio between lacustrine/boggy and terrestrial C3 plant remained the same and the degree of reworking is low. The Kuchchuguy deposits, however, are with -26.1‰ slightly lower in $\delta^{13}C$ with similar minimum values, but isotopically lighter (more negative) maximum values. This most likely accounts for the drier conditions and/or higher sedimentation rates during Kuchchuguy deposition, with a lower relative amount of aquatic biomass in the spectrum.

Isotopic composition and C/N ratio indicate a low level of OM decomposition in all investigated deposits. Only buried soils and deposits of the alas complex (both alas and taberal) have C/N values close to the upper (organic) horizons of modern tundra soils. The biomarker data implicate no significant differences between the investigated deposits.

Supply of OM and the grade of its maturity depend on the condition of accumulation. Deposits formed by intensive sedimentation have less OM supply and lowest level of its transformation due to fast burial and subsequent freezing. On the contrary, formed in condition of a stable ground surface, alas deposits and buried soils are characterized by the higher OM supply and level of its maturity.

Conclusion

Frozen Quaternary deposits of the Laptev Sea region are significant reservoirs of low transformed organic matter. The TC content is up to 7 wt%. Most (up to 6 wt%) of this carbon has organic origin and insoluble in water compounds.

Sediments of the highest accumulation rate (Kuchchuguy deposits) have the lowest carbon content and less time to form aquatic organic matter. Decreasing sedimentation rates lead to the accumulation of higher amounts of organic matter from one side and its deeper transformation from another.

Acknowledgments

Current research was supported by RFBR (grant #05-05-64062) and INTAS (YS #04-83-2950).

References

Bordenave, M.L. 1993. *Applied Petroleum Geochemistry*. Enfield, NH: Editions Technip, 524 pp.

Ershov, E.D. 1989. *Geocryology of USSR Eastern Siberia and Far East*. Moscow: Nedra, 515 pp (in Russian).

Fahl, K. & Stein, R. 1999. Biomarkers as organic-carbon-source and environmental indicators in the Late Quaternary Arctic Ocean: problems and perspectives. *Marine Chemistry* 63: 293-309.

Grigoriev, M.N., Rachold, V.R., Hubberten, H.-W. & Schirrmeister, L. 2004. Organic Carbon input to the Arctic Seas through coastal erosion. In: R. Stein & R.W. Macdonald (eds.), *The Organic Carbon Cycle in the Arctic Ocean*. Berlin, Heidelberg, & New York: Springer, 363 pp.

Schirrmeister, L., Siegert, Ch., Kuznetsova, T., Kuzmina S., Andreev, A., Kienast, F., Meyer, H. & Bobrov, A. 2002. Paleoenvironmental and paleoclimatic records from permafrost deposits in the Arctic region of Northern Siberia. *Quaternary International* 89: 97-118.

Zsolnay, A. 2003. Dissolved organic matter: Artefacts, definitions, and functions. *Geoderma* 113: 187-209.

Environmental Controls for the Coastal Processes on Yugorsky Peninsula, Kara Sea, Russia

Artem Khomutov
Earth Cryosphere Institute SB RAS, Tyumen, Russia

Introduction

The study area on Yugorsky Peninsula, coast of the Kara Sea, is noted for active coastal processes (Kizyakov et al. 2006). Dynamics of bluff and thermocirque edges was monitored in 2001–2007, and landscape units were subdivided using satellite image and field data. The paper presents joint analysis of field and remote-sensing data from two key sites: Pervaya Peschanaya and Shpindler. Some aspects of environmental controls for the coastal processes are discussed.

Detailed knowledge of landscape components for remote arctic areas is relatively scarce (Virtanen et al. 2004). Therefore, a combination of remote sensing and field methods was applied to determine response of specific landscape units to coastal processes.

Both key sites were used to work through methods of estimating coastal retreat rate/landscape unit correlation. To understand landscape-coastal process links, a satellite image was classified, and retreat rates at the same plot were measured.

Prior to the field study, main classes were subdivided on a satellite image Landsat 7 ETM+ with 15 m resolution in one panchromatic band. The most suitable combination of multispectral bands was used for accurate identification of classes as specific landscape units subdivided according to the landscape classification of Melnikov (1983). Characteristics of landscape units related to 25 identified classes were based on field studies during the last 3 years (2005–2007). They included descriptions of landforms, vegetation, and active layer depths within each landscape unit. At the coastal bluff and thermocirque edges, retreat was measured in 2001, 2005, 2006, and 2007. Maximum retreat of each of landscape unit was calculated for 2001–2005, 2005–2006, 2006–2007, and for the entire observation period (2001–2007). Then the average annual was calculated by summarizing a maximum retreat for a given landscape during the entire period of measurement divided by 6 years.

Methods

Superposition of the classified satellite image and tacheometric map of the coastal thermocirques at Pervaya Peschanaya and Shpindler key sites shows the following. Landscape resistibility to the coastal processes depends on several environmental factors: slope inclination, moisture/drainage conditions, active layer depth, vegetation complex, and its coverage.

Statistical analysis of the bluff-edge position against landscape units for both key sites provides some indirect retreat rate dependence on environmental controls.

Landscape units subject to coastal processes are subdivided into three groups according to their resistibility to coastal retreat: Irresistible, Medium irresistible, and Resistible. The group of Medium irresistible landscape units is subdivided as a landscape complex, changing its resistibility due to climate change.

Maps for each key site are compiled, showing landscape units, combined into groups marked with different colors depending on their resistibility to coastal processes.

Results and Discussion

Average maximum retreat rates calculated according to the described methodology vary between 1.7– 4.6 m/yr for 6 years. Landscape units are subdivided into 3 groups according to the rate of measured coastal retreat. Irresistible landscapes are those with a maximum annual retreat rate exceeding 7 m/yr. Resistible landscapes are those with a retreat rate less than 3 m/yr. In between are Medium irresistible landscape units. The average maximum retreat rate for a group of Irresistible landscape units is 9.2 m/yr, while the Resistible landscape group shows only 2.4 m/yr average retreat rate. The Medium resistible group is characterized by an average retreat rate of 5.5 m/yr (Table 1).

Landscape components considered as retreat controls are shown in Table 1. They include drainage, slope inclination, surface microrelief, vegetation coverage, and dominating vegetation. Analysis of Table 1 shows that Irresistible landscape units are characterized mainly by slightly poorer drainage conditions compared to Resistible landscapes. As a rule, they are located on steeper slopes, with notable forms of microrelief, such as spot-medallions and hummocks, with rather well-developed vegetation cover and dominating shrubby and mossy complexes. At the same time, landscape units belonging to a Resistant category are generally better drained, level to gently sloping flat surfaces, often bare or poorly vegetated, with graminoid vegetation dominating. Medium irresistible landscape units are characterized by variable landscape features, some of which are closer to the Irresistible type, such as slope inclination and coverage, and some in the middle position between Irresistible and Resistible types.

It should be noted that Medium irresistible are worse drained compared with both extreme types, which means that the combination of even extreme landscape components may cause partial compensation of their effect.

To analyze the role of each retreat rate control, we assigned a numerical score to each of the subdivided environmental factors enumerated in Table 1, based on our experience.

The higher role of the control in retreat rate is presumed, the higher score is assigned. For example, poor drainage (wet surface) is assigned score 3, well drained (dry surface) has score 1. Intermediate drainage is scored as 2.

Table 1. Landscape resistibility to coastal retreat.

Group (average retreat rate, m/yr)	Landscape unit	Average retreat rate, m/yr	Active layer depth range, m	Degree of drainage[1]	Degree of slope inclination[2]	Surface microrelief[3]	Vegetation coverage[4]	Dominating vegetation[5]
Irresistible (9.2)	1	14.6	>1.0	DW	S	H	V	M, Sh, He
	2	8.9	>1.0	D	S	H	BV	Sh, He
	3	8.8	>1.0	D	S	H, SM	V	He, M
	4	8.3	<0.6	DW	G	F	V	M, Se
	5	8.1	0.6–1.0	DW	G	F	V	M, Se
	6	8.0	0.6–1.0	D	L	F	BV	Sh, He
	7	7.6	0.6–1.0	W	G	H, T	V	M, Se
Medium irresistible (5.5)	8	6.6	0.6–1.0	W	G	T	V	Se, M, He
	9	6.3	0.6–1.0	DW	G	F	V	M, Gr
	10	5.95	>1.0	D	S	F	B	
	11	5.9	0.6–1.0	DW	S	H	BV	M
	12	4.95	0.6–1.0	DW	G	F	V	M, Se
	13	4.8	0.6–1.0	D	G	SM	V	M, Sh, Gr
	14	4.1	<0.6	W	L	T	V	M
Resistible (2.4)	15	2.9	>1.0	D	G	H, SM	V	Se, Sh, M
	16	2.7	>1.0	D	L	F	BV	Gr
	17	2.6	>1.0	D	S	F	V	Gr, He
	18	2.4	>1.0	D	L	F	B	
	19	2.3	<0.6	W	L	P	V	Se, M
	20	1.7	>1.0	D	G	F	BV	Gr

[1]D – well drained, DW – poorly drained, W – wet. [2]S – steep, G – gentle, L – level. [3]F – flat, H – hummocky, T – tussocky, SM – with spot-medallions, P – polygonal. [4]B – bare surface, BV – semi-vegetated, V – fully vegetated. [5]Sh – shrubs, He – herbs, Gr – graminoids, M – moss, Se – sedge.

Table 2. Average numerical score analysis of environmental controls.

Groups of landscapes	Environmental controls of maximum retreat rate				
	Dominating vegetation	Vegetation coverage	Degree of slope inclination	Degree of drainage	Surface microrelief
Irresistible	2.4	2.4	2.3	1.7	1.9
Medium irresistible	1.9	2.3	2.1	2.0	1.7
Resistible	1.2	1.8	1.7	1.3	1.5

Scores were summarized and averaged for a group of landscapes as shown in Table 2. Though the table is based on expert judgment, the result expresses an expected pattern: landscape units with a higher retreat rate (Irresistible) according to field measurements show the highest numerical score in all the cases excluding drainage factor, so we consider this approach to give a good qualitative estimate. Analyzing the range of average score for various environmental controls between Irresistible and Resistible landscape groups, we note that the maximum difference (2.4-1.2=1.2, Table 2) belongs to the "dominating vegetation" control, which makes this factor most valuable in determining the degree of resistibility to coastal retreat. Gentle, well-drained slope, though, with moss-shrub vegetation (landscape unit 15) belongs to the category of Resistible landscapes.

Conclusion

Dominating shrubby-mossy vegetation is an indicator of irresistibility of landscapes to maximum coastal retreat, while graminoids indicate the lowest maximum retreat rate. Geomorphological controls are less significant. Most valuable of the geomorphic factors is slope inclination due to gravimetric effect. Microrelief features, such as hummocks and spot-medallions, increase irresistibility of landscape units, especially in combination with steep slopes, because they result from flaws in the active layer.

A combination of environmental controls, even those having a medium numerical score assigned by an expert judgment each, results in a high maximum coastal retreat rate and is a reason for adding this landscape unit in the category of Irresistible.

References

Kizyakov, A.I., Leibman, M.O. & Perednya, D.D. 2006. Destructive relief-forming processes at the coasts of the Arctic plains with tabular ground ice. *Kriosfera Zemli* X(2): 79-89 (in Russian).

Melnikov, E.S. (ed.). 1983. *Landscapes of Cryolithozone of Western-Siberian Gas Province*. Novosibirsk: Nauka Publisher, 166 pp. (in Russian).

Virtanen, T., Mikkola, K. & Nikula, A. 2004. Satellite image based vegetation classification of a large area using limited ground reference data: case study in the Usa Basin, NE European Russia. *Polar Research* 23(1): 51-66.

Carbon Dynamics of the Permafrost Regime, North Slope of Alaska

Yongwon Kim
International Arctic Research Center, University of Alaska Fairbanks, USA
Keiji Kushida
Institute of Low Temperature Science, Hokkaido University, Japan
Masato Shibuya
Graduate School of Agriculture, Hokkaido University, Japan
Hiroshi Enomoto
Department of Civil Engineering, Kitami Institute of Technology, Japan

Introduction

The terrestrial ecosystems, including tundra and boreal forest regions of the Arctic, cover a little less than 18% of Earth's land surface, but they contain more than 40% of all carbon present in the terrestrial biomes (Kasischke 2000), demonstrating about one-third of the carbon sequestered in Pan-Arctic tundra and boreal forests. High-latitude ecosystems are particularly vulnerable to climate change due to the large carbon pools in northern latitude soils. The soil carbon pool estimated for the combined tundra-boreal forest ranges from 21% (Raich & Schlesinger 1992) to 30% (Post et al. 1982) of the global carbon pool.

Recently, Zimov et al. (2006) addressed carbon sequestration from thawing permafrost in the Arctic. The soils of the permafrost region of North America contain 213 Gt of organic carbon—approximately 61% of the carbon in all soils of North America. The soils of the permafrost region of North America are currently a net sink of approximately 11 MtC/yr. The soils of the permafrost region of North America have been slowly accumulating carbon for the last 5–8 thousand years. More recently, increased human activity in the region has resulted in permafrost degradation and at least localized loss of soil carbon.

Considering the wide distribution of permafrost in Alaska's North Slope, the observations of the fluxes of soil CO_2 (e.g., soil respiration) and CH_4, and of the soil carbon/nitrogen contents are extremely significant for a better understanding of soil organic carbon turnover time with the remarkable Arctic climate change (ACIA 2004) on the permafrost regime of Alaska's tundra ecosystem.

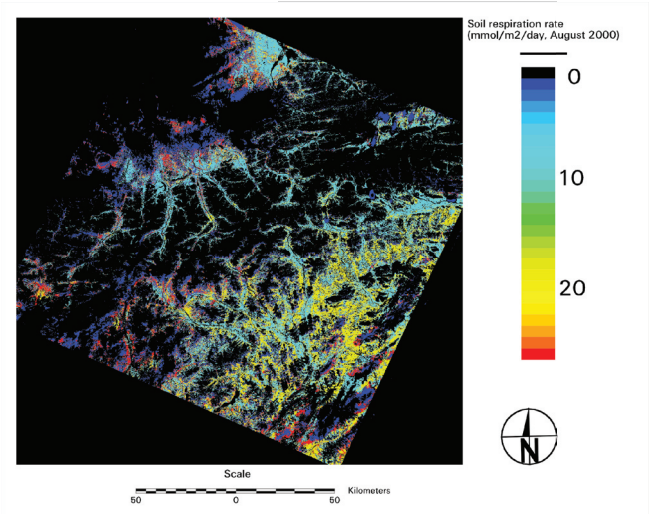

Figure 1. Microbial respiration in subalpine tundra.

Material and Method

Description of study area

The observation sites are shown in Kim & Tanaka (2001), which are coastal tundra (CT) near Deadhorse, upland tundra (UT) north of Toolik Lake station, and subalpine tundra (SaT) north of the Brooks Range along the Trans-Alaska Pipeline during the growing season of 2000/2001. Flux measurements of CO_2 and CH_4 using chambers, soil density, soil water content, and dominant vegetation type and content of soil organic carbon/nitrogen in each site were examined. The chambers used were of two types: one made of transparent material and the other, of nontransparent material. The former is called *light* and the latter is *dark chamber* in this study.

Results and Discussion

Soil respiration and CH_4 flux

Soil respiration consists of heterotrophic (microbial) and root respiration. The average fluxes of CO_2 and CH_4 ranged from -0.058±0.012 (±SE; standard error) in coastal tundra to 0.41±0.08 gCO_2-C/m²/d in upland tundra, and from -1.50±0.33 in subalpine tundra to 1.42±0.23 mg/CH_4-C/m²/d in coastal tundra, respectively. The negative values of CO_2 and CH_4 fluxes indicate photosynthesis and atmospheric CH_4 oxidation. In terms of soil carbon during the growing season, accumulated soil respiration was equivalent to 16±12 and 35±24 gC/m² for light and dark chambers, respectively. It is difficult to estimate seasonal carbon emission for CH_4 flux due to CH_4 oxidation. Gilblin et al. (1991) reported that the soil respiration ranged from 6 to 20 gC/m² in arctic tundra soils during the growing season, and Oechel et al. (1997) measured soil respiration of 4.4 to 44 gC/m² in arctic tussock and wet sedge tundra of Alaska, which is similar to our data during 2000/2001. Figure 1 shows a snapshot of the heterotrophic respiration by soil microbe of soil respiration in alpine tundra using Landsat ETM+ image analysis as well as in situ soil respiration data.

Biomass, soil carbon, and nitrogen

The average content of biomass, carbon and nitrogen,

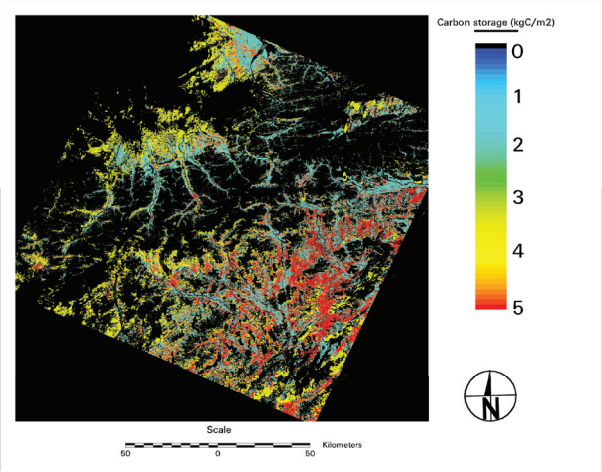

Figure 2. Soil carbon content in subalpine tundra.

and C/N ratio in the upper A0 layer of arctic tundra was 0.13±0.07 kg/m^2, 0.06±0.04 kgC/m^2, 0.001±0.001 kgN/m^2, and 60±18 (n=30), and was 4.31±1.07 kg/m^2, 1.33±1.12 kgC/m^2, 0.053±0.025 kgN/m^2, and 25±3 (*n*=32) in the A0 layer, respectively. The upper A0 layer denotes the layers of shrubs, herbaceous plants, lichen, and moss in surface soils of tundra and boreal forests. Figure 2 shows the soil carbon content in the tundra of Alaska's North Slope during the growing season of 2000/2001.

Turnover time of soil organic carbon

By using soil carbon content and soil respiration from the ground truth data, the turnover time of soil organic carbon on the permafrost regime of Alaska's North Slope varied from 240 years in upland tundra to 570 years in coastal tundra during the growing season of 2000/2001. The coastal tundra is located 32 km south of Deadhorse, which is always saturated by thawed uppermost permafrost water and near-to-peat soil. Thus, it is difficult to decompose the soil organic carbon. Raich & Schlesinger (1992) reported the turnover time was 490 years in the overall tundra of the Arctic. This suggests that the soil organic carbon in tundra is highly vulnerable to intra-tundra regime Arctic warming.

Implication for regional carbon budget

The regional carbon budget in the permafrost regime of Alaska tundra was 0.034±0.025 GtC/season for the light chamber, and 0.074±0.050 GtC/season for the dark chamber during the growing season, respectively, based on 207,000 km^2 of the Alaska tundra area including 73,600 km^2 in subalpine, 62,400 km^2 in the Arctic Foothills, and 71,000 km^2 in the Arctic Coastal Plain. Those are comparable with 0.004 GtC/season in wet sedge and 0.040 GtC/season in the tussock of Alaska's tundra (Oechel et al. 1997).

Acknowledgments

This work was funded by the INIS (IARC-NASDA Information System) and IJIS (IARC-JAXA Information System) projects and in part by the JAMSTEC (Japan Marine Science Technology). We thank Noriyuki Tanaka, Masami Fukuda, Hitoshi Kojima, and Satoshi Tsuda for assisting with the data compilation.

References

ACIA (Arctic Climate Impact Assessment). 2004. *Impacts of a Warming Arctic*. Cambridge: Cambridge University Press, 139 pp.

Gilblin, A.E., Nadelhoffer, K.J. Shaver, G.R. Laundre, J.A. & MaKerrow, A.J. 1991. Biogeochemical diversity along a riverside toposequence in arctic Alaska. *Ecological Monographs* 61: 415-435.

Kasishcke, E.S. 2000. Boreal Ecosystems in the global carbon cycle. In: E.S. Kasishcke & B.J. Stocks (eds.), *Fire, Climate Change, and Carbon Cycling in the Boreal Forest.* New York, NY: Springer, 19-30.

Kim, Y.W. & Tanaka, N. 2001. Temporal and spatial variation of carbon dioxide flux along a latitudinal Alaskan transect. In: T. Nakazawa (ed.), *Proceedings of the 6th International Carbon Dioxide Conference Sendai, Japan:* 465-468.

Oechel, W.C., Vourlitis, G.L. & Hastings, S.J. 1997. Cold season CO_2 emission from arctic soils. *Global Biogeochemical Cycles* 11: 163-172.

Post, W.M., Emanuel, W.R. Zinke, P.J. & Stangenberger, A.G. 1982. Soil carbon pools and world life zone. *Nature* 298: 156-159.

Raich, J.W. & Schlesinger, W.H. 1992. The global carbon dioxide flux in soil respiration and its relationship to vegetation and climate. *Tellus* 44: 81-99.

Zimov, S.A., Schuur, E.A.G. & Chapin, F.S III. 2006. Permafrost and the global carbon budget. *Science* 312: 1612-1613.

Impacts of Climate Warming and Facilities on Rock Temperatures at a Tunnel in High Alpine Continuous Permafrost: Results of Long-Term Monitoring at Kleinmatterhorn, Swiss Alps

Lorenz King
Justus-Liebig-University Giessen, Germany
Clemens Constantin Maag
Justus-Liebig-University Giessen, Germany
Christen Baumann
CEO Zermatt Bergbahnen AG, Switzerland

Introduction

Zermatt is a most popular tourist center in the Swiss Alps, located at approximately 1620 m a.s.l. As the surrounding high mountain ranges often reach above 4000 m a.s.l., the dry and sunny climate generates a high glacier equilibrium line and thus vast unglaciated permafrost areas. Occurrences of sporadic permafrost appear above 2600 m; continuous permafrost exists above 3400 m.

The facilities built on permafrost include hotels, restaurants, mountain huts, railways, funiculars, elevators, or culverts for artificial snow production. In view of climate warming, the subsurface thermal regime requires particular observations, as degradation of permafrost may endanger the proper functioning of these constructions. An appropriate design is crucial and depends on the characteristics of the permafrost occurrences. At present, new constructions and recordings in the continuous permafrost region at Kleinmatterhorn (3820 m) and the previous long-term monitoring at this location enable the study of human influence on this permafrost environment.

Kleinmatterhorn

The mountain peak of Kleinmatterhorn with an altitude of 3883 m a.s.l. is the highest place in the Alps that can conveniently be reached by a cable car and an elevator. The mountain top is located within the continuous permafrost zone. A 176 m long tunnel through the mountain at an altitude of 3820 m and an elevator shaft leading to 3860 m a.s.l. (Fig. 1) present an exceptionally interesting object for permafrost research. Long-term temperature monitoring started in 1998 due to problems caused by refreezing of meltwater in the elevator shaft during a very warm summer. In order to record the bedrock temperatures of the mountain top and the effects of tourist installations, temperature loggers were installed at selected sites of the tunnel.

The permafrost distribution in the Zermatt Valley is quite well known through several studies (cf. references in Philippi et al. 2003). Numerous rock glaciers were the focus of other research projects (Hof et al. 2003, King & Kalisch 1998). Drilling 100 m in depth was carried out on nearby Stockhorn during the EU-project PACE (Harris et al. 2003), indicating a permafrost thickness of 170 m.

At the research site Kleinmatterhorn, air and rock temperatures are monitored at 10 different sites, the

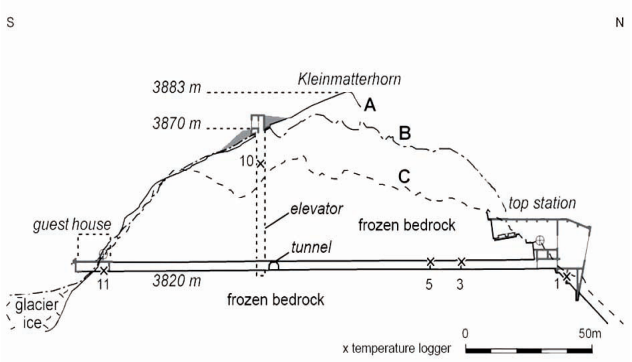

Figure 1. Location of UTL-Loggers (1, 3, 5, 10) at the tunnel system of Kleinmatterhorn mountain peak.

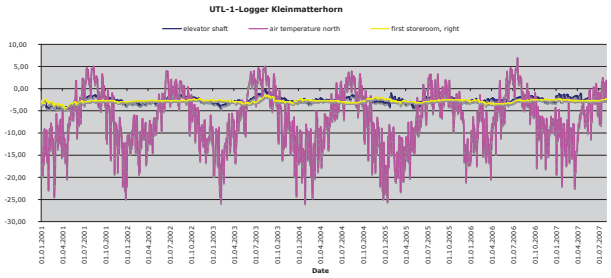

Figure 2. Air, bedrock, and elevator shaft temperatures at Kleinmatterhorn (3820 m) from Jan. 2001 to Aug. 2007.

location of significant loggers are shown in Figure 1. The air temperature (#1) is taken at an undisturbed site near the cable car entrance. Mean annual air temperatures (MAAT) were -8.0°C in 1998 and 1999, attaining -5.7°C in 2006. The mean air temperature in the summer months of July and August 2002 was -0.58°C; it reached +1.98°C in 2003. However, the mean winter temperatures (Dec., Jan., Feb.) also vary considerably with -12.6°C in 2001/02 compared to -15.2°C in 2004/05 and -10.3°C in 2006/07.

Loggers #3 and #5 (located in storerooms that are separated from the passenger tunnel) show small seasonal differences of -2°C and -3°C, with a slightly increasing temperature trend. The elevator shaft temperatures (#10) vary seasonally between -4° and -2°C, however, reaching near zero temperatures in the extremely warm summer of 2003, where also the accumulated positive degree-days are considerably higher than in any other year. Natural ventilation with cold air is a necessary countermeasure to prevent negative effects of heat created by the installations.

Bedrock temperatures around -12°C were reported by Keusen & Haeberli (1983) during the construction phase. The results of the monitoring with 10 loggers since 1998 have proven to be an essential aid for supervising sensitive permafrost areas, thus allowing for preventive measures against the consequences of climate warming and the effects of human activities (heating, inhibited ventilation of cold air etc.) at an early stage.

Actual Construction Activities

One consequence of climate warming in the Alps is that skiing activities tend to concentrate and increase in higher and safer regions. In addition, exceptional attractions help guarantee the success of a tourist resort. The Kleinmatterhorn cable car, constructed from 1976 to 1979, reaches up to 3820 m a.s.l. and arrives at a tunnel cut in the northern wall of the mountain peak. At its southern exit, the ski run starts down to Zermatt.

Currently, three major infrastructure projects are being carried out at the mountain top in order to increase its attractiveness. A new guest house with a larger restaurant will be built at the southern exit of the existing tunnel. The supporting structure will be anchored in the frozen bedrock. From there, two elevators and an ice gallery (cf. Fig. 3) will form a subsurface access to a new "glacier palace" about 15 m below the glacier surface.

The current constructions visualize many engineering and environmental aspects in a sensitive permafrost setting. Future research projects will study the effects on such an intense use of construction and installation for tourism on frozen bedrock and glacier ice, respectively. The mountain guest house accommodating 60 beds will open in late summer of 2008.

At the northern entrance of the tunnel, the construction of a spectacular tower reaching 117 m above the natural mountain top and a viewing platform at an altitude of 4000 m a.s.l. is planned, but has to be approved, consequently providing to the Zermatt resort a sovereign viewpoint.

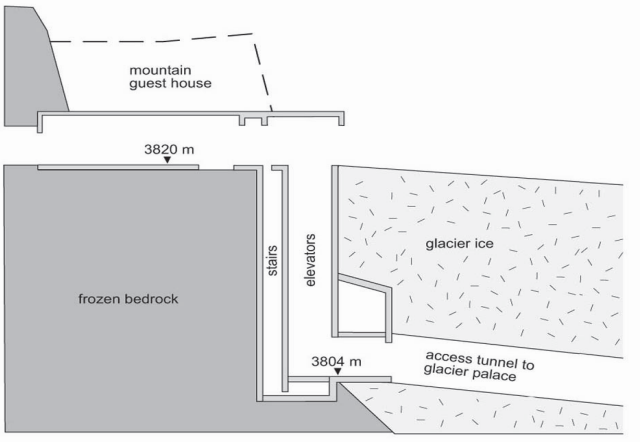

Figure 3. Cross section through guest house, old tunnel (3820 m) and elevator shafts with access to the glacier palace.

Current Research and Future Projects

In February 2008, additional scientific drilling will be carried out in the glacier ice close to the new constructions and at the glacier palace. The mean annual ice temperature will be measured at about 15 m depth. Undisturbed bedrock temperatures near the new construction sites will enable us to establish a good scientific base for new long-term temperature monitoring and 3D modeling of this exceptional mountain peak.

Degradation of permafrost due to both climatic change and an increase in human activity creates a serious challenge for tourist installations, as safety has to be prioritized and ensured in the concerned area. Continuous monitoring will guarantee the required safety.

Acknowledgments

We would like to express our gratitude to Stephan Gruber and Thomas Herz who gave valuable suggestions for fieldwork. The studies were financially supported by the project KI 261/14-1 of the Deutsche Forschungsgemeinschaft.

References

Harris, C., Vonder Mühll, D., Isaksen, K., Haeberli, W., Sollid, J.-L., King, L., Holmlund, P., Dramis, F., Guglielmin, M. & Palacios, D. 2003. Warming permafrost in European mountains. *Global and Planetary Change* 39: 215-225.

Hof, R., King, L. & Gruber, S. 2003. Influence of human activities and climatic change on permafrost at construction sites in Zermatt, Swiss Alps. *Proceeding of the Eighth International Conference on Permafrost, Zurich, Switzerland, July 20–25, 2003*: 65-66.

Keusen, H.R. & Haeberli, W. 1983. Site investigation and foundation design aspects of cable car construction in alpine permafrost at the 'Chli Matterhorn', Wallis, Swiss Alps. *Proceedings of the Fourth International Conference on Permafrost, Fairbanks, Alaska, July 17–22, 1983*: 601-605.

King, L. & Kalisch, A. 1998. Permafrost distribution and implications for construction in the Zermatt area, Swiss Alps. *Proceedings of the Seventh International Conference on Permafrost, Yellowknife, Canada, June 23–27, 1998*: 569-574.

King, L. 1996. Dauerfrostboden im Gebiet Zermatt-Gornergrat-Stockhorn Verbreitung und permafrostbezogene Erschließungsarbeiten. *Zeitschrift für Geomorphologie N.F., Suppl.-Band* 104: 73-93.

Philippi, S., Herz. T. & King, L. 2003. Near-surface ground temperature measurements and permafrost distribution at Gornergrat, Matter valley, Swiss Alps. *Proceedings of the Eighth International Conference on Permafrost, Zürich, Switzerland, July 19–25, 2003*: 129-130.

Differential Estimates of Organic Carbon Pools in Permafrost-Affected Soils of Russia

D.E. Konyushkov, D.I. Rukhovich, N.V. Kalinina, E.A. Dolinina
V.V. Dokuchaev Soil Science Institute, Russian Academy of Agricultural Sciences, Moscow, Russia

At present, a challenge for Russian cryopedologists is to perform differential estimates of organic carbon pools in permafrost-affected soils of Russia on the basis of digitized versions of the 1:2.5 M and 1:1 M scale soil maps. This work is hampered by the absence of adequate databases. For permafrost regions, along with data on the thickness and bulk density of soil horizons and the organic carbon content in them, the databases should include information on the real soil cover complexity, differentiation of thawing depths, the ice content in the soil and the presence of massive ice bodies; the content of gravel and coarser fragments (particularly, for Central and East Siberia); and the depth to the lithic contact. It is important to distinguish between the organic carbon in mineral horizons, the organic carbon in peat layers, and the organic carbon in litter horizons. The organic carbon pool in the transient permafrost layer is a separate problem, as there are little data on the carbon content in it.

Permafrost regions occupy nearly two-thirds of Russia and encompass a wide range of ecosystems with different types of carbon turnover and soil organic carbon (C_{org}) pools: (a) surface accumulation of organic matter in litter, peat, and raw-humus horizons; (b) soil humus accumulation in situ due to the decomposition of root residues; and (c) illuviation of mobile humic substances into humus-illuvial horizons.

The real distribution of C_{org} is a result of various combinations of these processes. A specific feature of permafrost-affected soils is the *cryosequestration of* C_{org} due to (a) cryoturbation and (b) the rise of permafrost table upon the surface accumulation of organic matter, so that the lower part of organic horizons becomes frozen. Another specific feature is the high spatial variability of soil horizons and their intermittent character. In Siberia, these soils are often developed from the residuum of hard bedrock and have high pebble content. The high ice content and the presence of ice wedges are typical of heavy-textured and peat soils. These features should be taken into account in calculations of C_{org} reserves in permafrost regions.

Three major works on carbon reserves in Russian soils are based on different cartographic sources. Orlov et al. (1996) used the *Soil Map of the USSR* (1984, 1:16 M); only major zonal soils were considered. Rozhkov et al. (1996) used a more detailed *Soil Map of Russia and Contiguous Countries* (Gerasimova et al. 1995; 1:4 M); the carbon stored in surface organic horizons and the carbon of soil carbonates were separately calculated. Nilsson et al. (2000) and Stolbovoi (2002) used a generalized version of the *Soil Map of the Russian Federation* (Fridland et al. 1989; 1:2.5 M). The generalized version (1:5 M) contains 168 mapping units and 1300 soil polygons.

In fact, the original map contains 35,000 soil polygons; its legend includes 205 names of individual soils and nearly 100 names of unique soil combinations (soil complexes). The latter are especially typical of the permafrost regions of Russia. The soil cover complexity in the permafrost zone is considerable. Thus, within the permafrost zone of European Russia, 1055 soil polygons encompassing 55 different soils can be found on the 1:2.5 M scale map (Fig. 1). To calculate the reserves of C_{org} on the basis of this map, the attribute database to the digitized version of the map has to be developed.

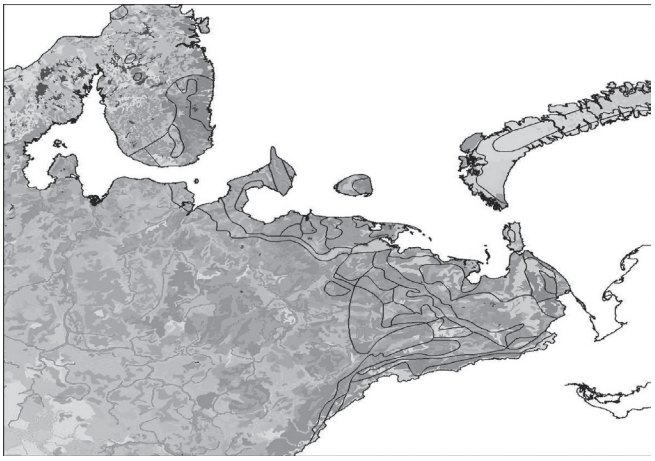

Figure 1. Soil polygons on the 1:2.5 M scale map over the *Circum-Arctic Map of Permafrost and Ground-Ice Conditions* (fragment).

At present, such a database exists for the upper (20 cm thick) soil horizons and, separately, for litters. On this basis, the organic carbon density values used for modeling purposes have been calculated for the European part of Russia (Rukhovich et al. 2007). Figures 2 and 3 illustrate the distribution of C_{org} reserves in the 20 cm thick soil horizons (both mineral and peat soils have been taken into account) and in mineral horizons + litters, respectively. It is seen that the reserves of C_{org} stored in litter horizons play a significant role in the total organic carbon pool within the permafrost zone of European Russia.

However, the database is still incomplete; information on the organic carbon contents and bulk density of the deeper soil horizons is insufficient for final calculations. Information on the content of gravel and coarser fragments is also to be completed for the particular polygons. Finally, in order to calculate C_{org} reserves in the active layer, information on thawing depths is essential.

These problems become more complicated in the case of calculations for the entire permafrost zone of Russia. The database for the map is being developed. The great variability in the soil properties within this vast territory has to be taken into account. A given genetic soil unit may be developed

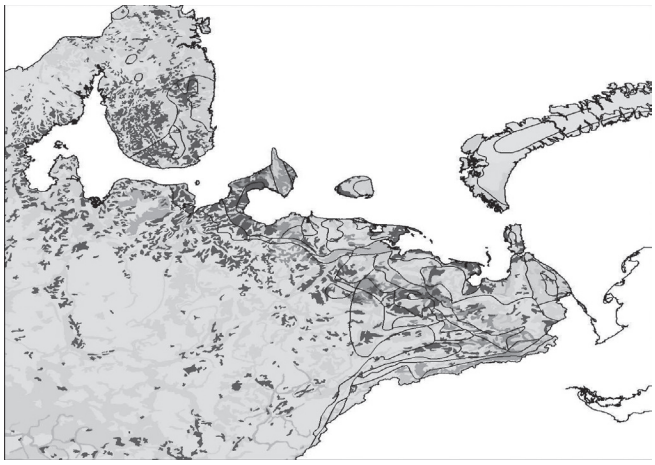

Figure 2. Organic carbon densities in the upper 20 cm thick mineral soil horizons.

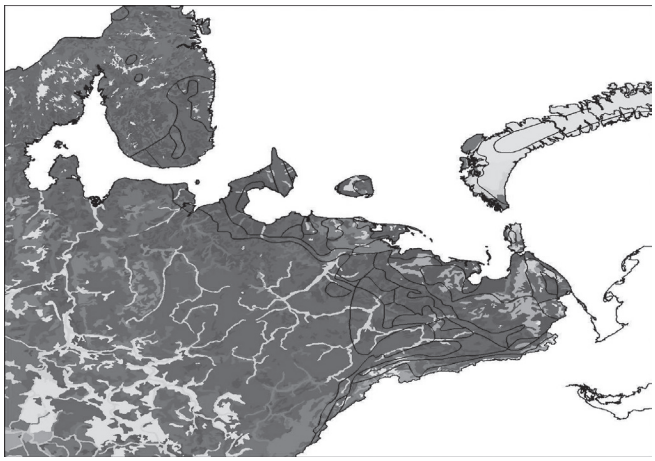

Figure 3. Organic carbon densities in the litters and upper 20 cm thick mineral horizons.

from different parent materials and under somewhat different bioclimatic conditions. As a first approximation, the database is developed for combinations "genetic soil unit + parent material + bioclimatic conditions." In some cases, this information is insufficient. In particular, for mountainous territories and vast plateaus of Siberia, information on the contents of gravel and coarser rock fragments is essential. In calculations of carbon pools for standard depths (50 cm, 1 m), it is also important to take into account the ice content in the soils with a relatively shallow thawing depth and the presence of massive ice bodies and ice wedges in some areas.

Another solid cartographic base for the estimates of organic carbon pools in permafrost-affected soils of Russia is the digitized version of the *State Soil Map* on the 1:1 M scale. This is a much more detailed map. For example, within the European part of the permafrost zone of Russia, 3,427 soil polygons encompassing 155 different soils are shown on this map. In other words, the degree of detail of the 1:1 M soil map is approximately three times higher than that of the 1:2.5 M soil map. It is important that soil polygons distinguished on the 1:1 M soil map display a better correlation with the

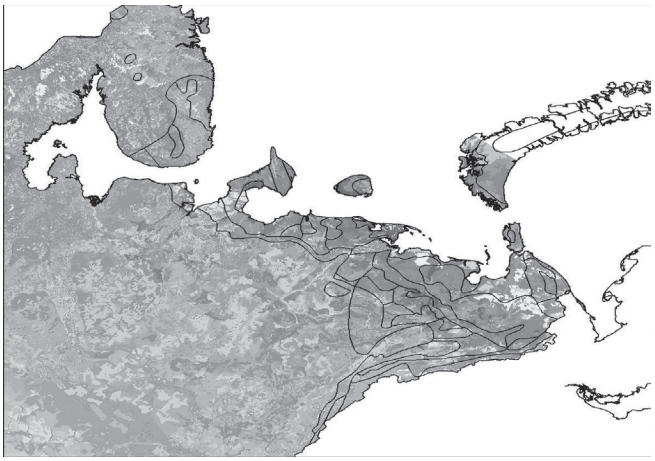

Figure 4. Soil polygons on the 1:1 M map over the *Circum-Arctic Map of Permafrost*.

Circum-Arctic Map of Permafrost, so the use of this map seems to be more promising in the future (Fig. 4).

It is expected that the first results of differential organic carbon estimates for the permafrost zone of Russia on the basis of the digitized version of the 1:2.5 M soil map will be obtained by the end of 2008.

References

Brown, J., Ferrians, O.J. Jr., Heginbottom, J.A. & Melnikov, E.S. 1997. *Circum-Arctic Map of Permafrost and Ground-Ice Conditions.* U.S. Geol. Survey, CP-45. Reston, VA, USA.

Fridland, V.M. (ed.). 1988. *Soil Map of the Russian Soviet Federative Socialistic Republic.* 1:2.5 M scale. Central Administration for Geodesy and Cartography (GUGK), Moscow, Russia, 16 sheets. [In Russian].

Gerasimova, M.I., Gavrilova, I.P., Bogdanova, M.P. et al. 1995. *Soil Map of Newly Independent States.* 1:4 M scale. Central Administration for Geodesy and Cartography (GUGK), Moscow, Russia (in Russian).

Nilsson, S., Shvidenko, A., Stolbovoi, V. et.al. 2000. *Full Carbon Account for Russia.* Interim Report IR-00-021, International Institute for Applied Systems Analysis, Laxenburg, Austria, 180 pp.

Orlov, D.S., Biryukova, O.S. & Sukhanova N.I. 1996. *Organic Matter in Soils of the Russian Federation*. Moscow: Nauka. 256 pp. [in Russian].

Rozhkov, V.A., Wagner, V.B., Kogut, B.M. et al. 1996. *Soil Carbon Estimates and Soil Carbon Map for Russia*. IIASA WP-96-60. Laxenburg, Austria, 44 pp.

Rukhovich, D.I. et al. 2007. Constructing a spatially-resolved database for modelling soil organic carbon stocks of croplands in European Russia. *Regional Environmental Change* 7(2): 51-61.

Stolbovoi, V. 2002. Carbon in Russian soils. *Climatic Change* 55(1-2). The Netherlands: Kluver Academic Publishers, 131-156.

Satellite Observations of Frozen Ground, Snowmelt (1989–2007), and Hydrological Responses at a Discontinuous Permafrost Aquifer (Fort Wainwright, Alaska)

Sarah E. Kopczynski
Cold Regions Research and Engineering Laboratory, Hanover, NH 03755
Joan M. Ramage
Lehigh University, Earth and Environmental Sciences, Bethlehem, PA 18015

Introduction

Snow cover influences permafrost thermal regimes and seasonally frozen ground, and thus impacts groundwater flow, surface runoff, and soil moisture (Ling & Zhang 2003). Within permafrost aquifers, climatic warming will likely increase active layer depth, warm the soil profile, increase soil moisture storage, increase evaporation, cause variable runoff responses, and increase groundwater flux to streamflow (Hinzman & Kane 1992). The aim of this research is to report climate warming impacts at Fort Wainwright and resulting groundwater response over 19 years. Specifically, we investigate timing of spring snowmelt, drawing attention to impacts on permafrost groundwater hydrologic patterns.

Fort Wainwright is located in Interior Alaska east of Fairbanks within the Chena watershed (Fig. 1). Discontinuous permafrost is distributed throughout unconsolidated alluvial sediments and fractured schist bedrock. Groundwater is influenced by the local Chena and regional Tanana Rivers.

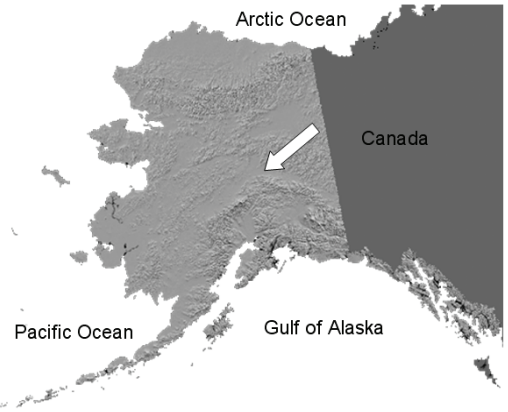

Figure 1. Location of Fort Wainwright, Alaska.

Methodology

Passive microwave remote sensing

This research applies 19 years of multiple daily satellite brightness temperature (Tb) observations of the polar orbiting Special Sensor Microwave Imager (SSM/I) downloaded by online archive. Microwave data measure through darkness, clouds, and precipitation. SSM/I data are used to monitor snowmelt onset and duration (Ramage & Isacks 2002). Snow melts and refreezes when Tb(37V)≥246K and abs(DAV)≥10K. The DAV is the daily amplitude variation of ascending and descending Tb overpasses. Large DAV (>10) indicates melt-refreeze cycles, followed by ripe snow conditions when DAV transitions from abs(DAV)≥10K to abs(DAV)<10.

SSM/I data are used to detect near-surface soil freeze-thaw conditions (Zhang & Armstrong 2001) during 1999. Vertically polarized Tb discriminate frozen from unfrozen ground using a negative spectral gradient (Tb(37V)-Tb(19V))/18<0 together with a cutoff threshold of Tb(37V)<258.2K. Penetration depth is limited to a few centimeters of soil, and observations are only valid when snow cover is absent. Satellite data results are consistent with local thermistor data demarking onset of frozen ground.

Permafrost hydrological responses

Groundwater flow velocities are monitored in situ using high-resolution heat pulse flow sensors throughout the aquifer, which work well in low flow rate higher permeability conditions. Chena and Tanana streamflow are monitored at USGS gauging stations. Soil moisture sensors maintained by UAF provide continuous soil condition records (Hinzman & Lilly 1999).

Results

Between 1989 and 2007, snowmelt onset has occurred 0.86 d/yr earlier (Fig. 2b) with spring snowmelt persisting about 0.7 d/yr longer (Fig. 2c). An example of hydraulic responses to snowmelt (Fig. 3a) in a permafrost-free area and a through-talik in the Fort Wainwright aquifer is shown for 1999–2000. At both sites, rapid snowmelt infiltration causes a soil moisture spike ~8 d before snow is ripe, followed ~10 d later by the local freshet. Soil moisture spikes again during the larger regional freshet. Snowmelt at the permafrost-free site increases flow rates from 2 to 4 ft/d and shifts flow direction 40°. Subpermafrost flow rates respond only to larger basin-wide freshet (1.5 to 4 ft/d), while flow rates at a through-talik respond to both local and regional freshets with peak rates of 1 ft/d and 1.5 ft/d, respectively. Flow directions in the through-talik shift 80° and 100° with each respective freshet. Closed taliks show no statistically significant responses.

Conclusion

This research reports on climate warming impacts at the Fort Wainwright, Alaska, discontinuous permafrost aquifer since 1989. Satellite observations over 19 years show earlier snowmelt (0.86 d/yr) with increasing spring-melt duration (0.7 d/yr). Soil moisture spikes ~8 d before snow is ripe and ~10–20 d before the fluvial freshet. Groundwater velocity increases due to snowmelt infiltration with peak rates of 4 ft/d (permafrost-free site), 4 ft/d (subpermafrost), and ~2 ft/d

in a through-talik. Groundwater velocities in the permafrost aquifer increase during annual active layer freezing when local water levels drop each fall, while there are no comparable responses in permafrost-free areas.

Groundwater velocity measurements are strongly influenced by the timing, magnitude, and duration of snowmelt and ground freezing. These groundwater responses will continue to change as permafrost continues to degrade.

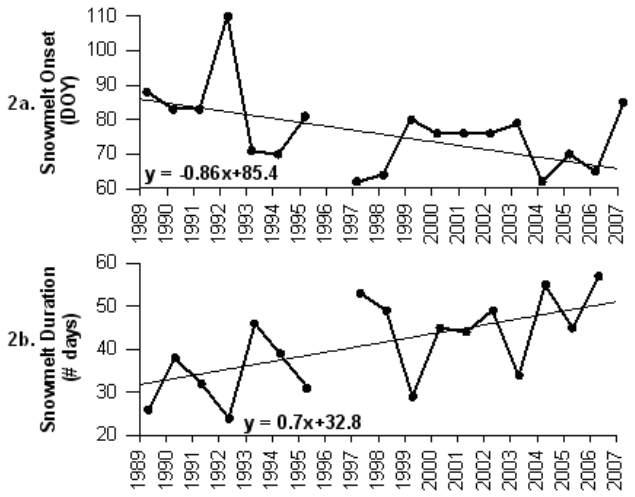

Figure 2. Historical trends in snowmelt onset (a) and duration (b) determined using satellite passive microwave algorithms.

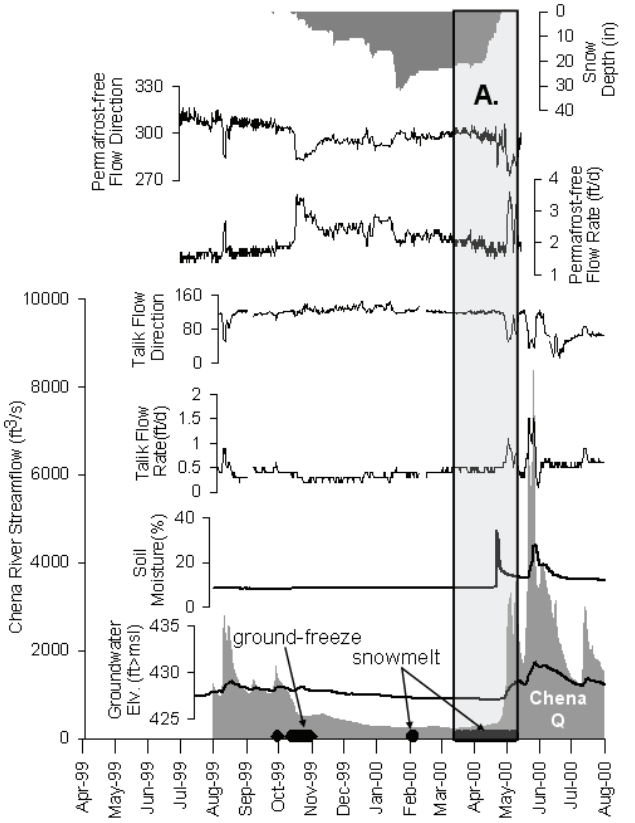

Figure 3. Permafrost-free and through-talik hydrologic responses to ground-freeze and snow melt-refreeze (a) at Fort Wainwright (1999–2000). Snow is ripe after the melt-refreeze interval.

This research establishes long-term baseline observations to underpin investigations of climate warming impacts on permafrost hydrology, and sets the stage for future work to quantitatively model these interactions.

Acknowledgments

This research was funded by NASA Graduate Fellowship NNX06AG08H, U.S. Army Fellowship, NASA Terrestrial Hydrology Grant NNG04GR31G, Lehigh University, U.S. Army Alaska. SSM/I data was provided by the National Snow and Ice Data Center

References

Hinzman, L.D. & Kane, D.L. 1992. Potential response of an arctic watershed during a period of global warming. *Journal of Geoph. Res.–Atmospheres* 97(D3): 2811-2820

Hinzman, L.D. & Lilly, M.R. 1999–2000. Climate data from the Fort Wainwright Hydrology Research. UAF WERC: www.uaf.edu/water/projects/ftww/ftww.html Fairbanks, Alaska. (Ap6009; May99–May00).

Ling, F. & Zhang, T. 2003. Impact of the timing and duration of seasonal snow cover on the active layer and permafrost in the Alaskan Arctic. *Permafrost and Periglacial Processes* 14: 141-150

Ramage, J.M. & Isacks, B.L. 2002. Determination of melt onset and refreeze timing on southeast Alaskan icefields using SSM/I diurnal amplitude variations. *Annals of Glaciology* 34: 391-398.

Zhang, T. & Armstrong, R.L. 2001. Soil freeze/thaw cycles over snow-free land detected by passive microwave remote sensing. *Geoph. Res. Letters* 28(5): 763-766

Low-Frequency Sounding During the Gas Line Engineering Investigations in the Area of the Transition Through Baidaratskaya Bay

A.V. Koshurnikov
MSU-Geophysics, Ltd.
Yu.D. Zykov
The Moscow State University
Yu.V. Kulehsov
Peter Gaz, Ltd.

The main task of this geophysical research was the lateral exploration of frozen and thawed soils in the pipe-laying zone. In that regard, special attention was given to intrasoil ice, thawed soils, and cryopeg detection. Vertical electric explorations were used in the chosen gas pipeline. Vertical electric sounding by a direct current (VES) (Fig. 1), frequency electromagnetic sounding (FS) (Fig. 2), and time domain sounding (TEM) (Fig. 3) were carried out.

To perform the FS, a recently-made hardware system, namely HF-EM, was used. The system includes the generation of square signals with a combination of a discreet set of frequencies from 4 up to 512 kHz. The measuring device and the multiloop frame antenna work simultaneously with the generator. While sounding with VES, a bilateral three-electrode system was used.

Figure.1. VES. Ural, 2006.

Figure 2. FS. Jamal, 2007.

The maximum open pit was 100 m, while the FS sounding distance between the generator and measuring device was 40 m. It takes about 1 minute to measure the signature with the help of FS sounding. Each of these signatures, as *E*

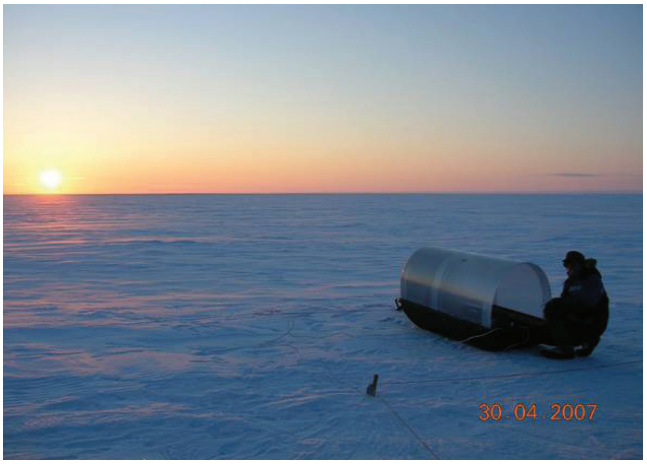

Figure 3. TEM. Jamal, 2007.

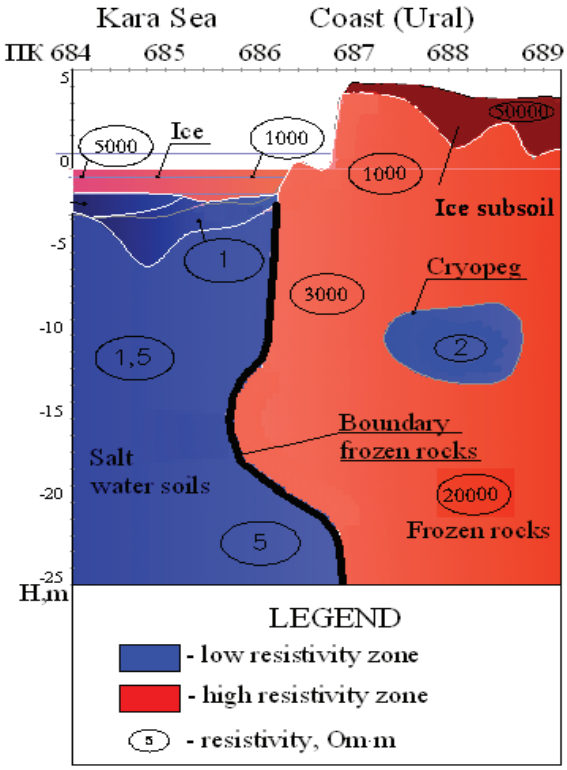

Figure 4. Geoelectric cross section (Ural).

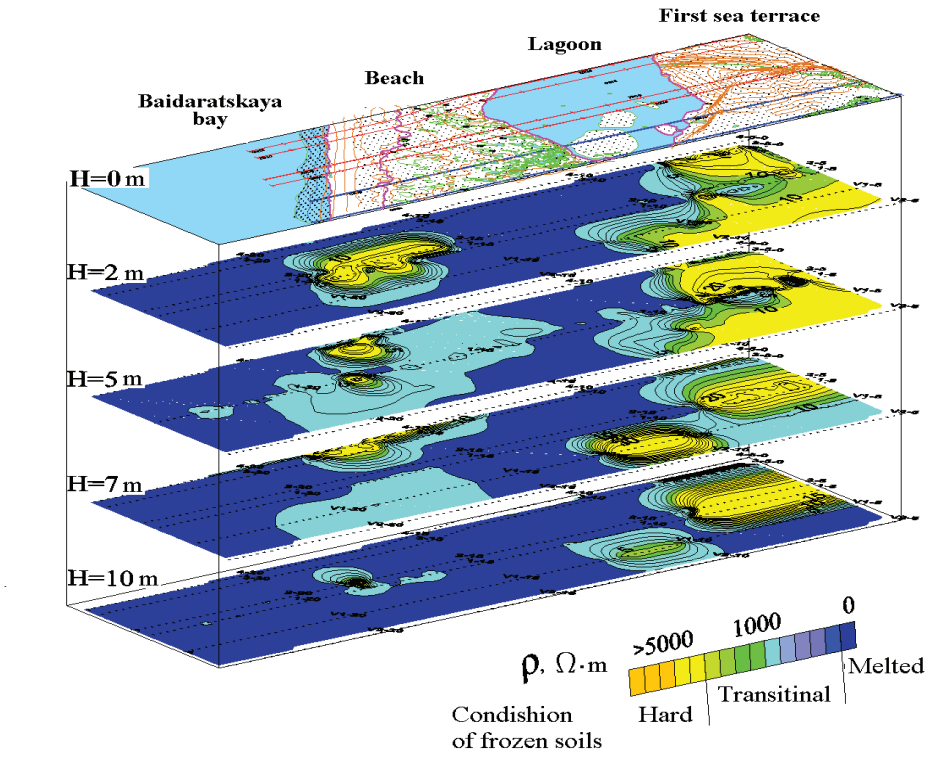

Figure 5. Model of frozen soils condition (Yamal).

against ω, or ρ_ω against ω, can be displayed at the receiver tool screen. For an interpretive translation of the FS data, the EM – 1D programme carrying out 1D inverting ρ_k against ω into simulated resistivity (developed by P. Pushkaryov) was used. The TEM sounding the combine device with square loops sized 20 x 20 (a generator antenna) and 10 x 10 (a receiving antenna) was applied. As a result, it was possible to explore the cut in details to the bottom of 30 m and to solve set tasks.

According to VES data about lithology structure, the maintenance of ice, temperature, and salinity have been obtained (Fig. 4).

According to FS data about position, frozen soil under a beach, a lagoon, and the first sea terrace have been obtained (Fig. 5).

According to TEM, data about deeper borders of thawed and frozen rocks have been obtained (Fig. 4).

The main features of the described methods are as follows:

VES – ability to split the upper part of the cut upon its resistance. But some difficulties are caused due to the presence of a high-resistivity screen (icy subsoil).

FS – ability to map conducting zones (cryopegs); demonstrates the high production, but it is insensitive to the high meanings of resistance.

TEM – ability of depth research.

References

Zykov, Ju.–M. 2007. *Geophysical Methods of Permafrost Studies*. Moscow: Publishing house of the Moscow State University, 272 pp. (in Russian).

Zykov, Ju.D., Buldovich, S., Koshurnikov, A.V. et al. 2007. Opportunity of electromagnetic sounding at geocryology mapping. In: Materials of the international conference "*Cryogenic Resources of Polar Regions" II, Salekhard, 2007*: 149 pp.

Thixotropic Wedges or Frost Cracks: A Review from the Pannonian Basin (Hungary, Europe)

János Kovács
Department of Geology, University of Pécs, Pécs, Hungary
Szabolcs Ákos Fábián
Department of Physical Geography, University of Pécs, Pécs, Hungary
Gábor Varga
Department of Physical Geography, University of Pécs, Pécs, Hungary
István Péter Kovács
Doctoral School of Earth Sciences, University of Pécs, Pécs, Hungary
György Varga
Doctoral School of Earth Sciences, University of Pécs, Pécs, Hungary

Introduction

There is a general consensus about the study and interpretation of soft-sediment deformation structures being helpful in paleoenvironmental reconstructions. During the glacial periods of the Pleistocene, Hungary was subject to a cryogenic environment that produced various relict periglacial features (Dylik 1963, Pécsi 1964, Tarnocai & Schweitzer 1998, Fábián et al. 2000, Kovács et al. 2007). The reason for the cold climate during these glacial periods is Hungary's unique geomorphological setting in the Pannonian Basin. The Carpathians, which surround this large basin, create an almost closed climatic situation, producing climatic conditions not found elsewhere in Europe. In effect, Dylik seems to imply that the climate in Hungary during the glacial periods of the Pleistocene was somewhat similar to the recent climate of the dry tundra regions of North Siberia. According to Maarleveld (1976) and Van Vliet-Lanoë et al. (2004), however, the Pannonian Basin was mostly devoid of continuous permafrost during the Quaternary.

General Setting

In the Pannonian Basin (Fig. 1), the continental crust is thinner and the stress field more complex, owing to a lateral shift to the east of the basin, which is squeezed between the rigid northeast European basement and the Alpine orogene, with transpressional and transtensional phases alternating from the upper Cenozoic to today (Csontos et al. 2002). The present-day seismicity is higher than in northwest Europe, but is still of low magnitude.

As a result of the cold climatic conditions (mentioned above) in the Pleistocene epoch, various types of periglacial features developed and are found in well-preserved relict forms in various deposits. Dylik (1963) summarizes the relict periglacial features of Hungary and discusses their original development, while Pécsi (1964) provides detailed descriptions, including diagrams and photographs, of these features with the locations in which they occur. In the last decade, researchers investigated these cryogenic features for their implication for past climate (Tarnocai & Schweitzer 1998, Fábián et al. 2000, Kovács et al. 2007) and for their distinction between tectonic and periglacial deformation (Van Vliet-Lanoë et al. 2004, Horváth et al. 2005, Magyari et al. 2005).

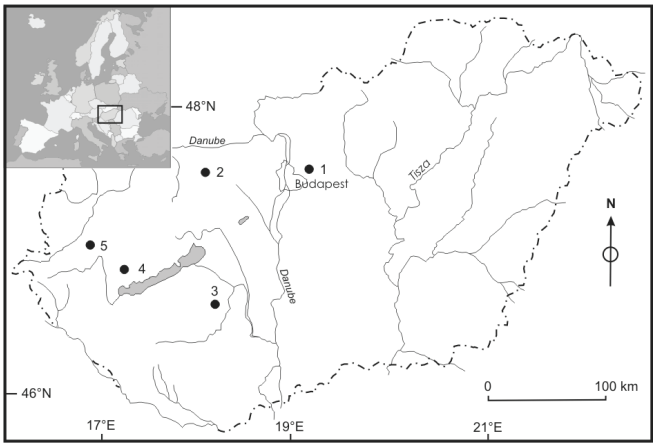

Figure 1. Location of the study sites in Hungary.

Methods

Our interpretation of the periglacial deformations investigated is based on (a) detailed field observations and (b) a synthesis of published data. Polygenetic forms were analysed using criteria defined for the periglacial and seismogenic structures. Sections were cleaned and described using sedimentological and pedological criteria, with respect to the topographical location and available moisture. Samples for grain size analyses and OSL dating were collected from individual fill units, and additional samples were collected for moisture content and background radiation measurement. The samples were dated at the Geological Institute of Hungary.

Results

Thixotropic wedges

Thixotropic wedges, developed in fine sandy-to-pebbly deposits, are formed within the sediment but relatively close to the surface (Montenat et al. 2007). The wedges may be

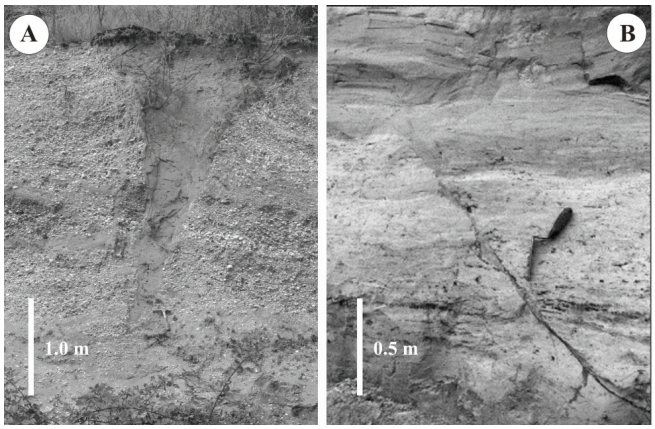

Figure 2. (A) periglacial frost wedge (sand wedge); (B) nonperiglacial synsedimentary transtensive fault (thixotropic wedge).

very narrow and are recurrent (dm to several dm depth); the wedge pattern may be vertically arranged (Montenat et al. 2007). Tension faults (Fig. 2B) are often mistaken for frost (cryodesiccation) fissures, evidence of former ice veins, or even ice-wedge casts, but occur rarely in polygonal networks and extend deeper in depth (Van Vliet-Lanoë et al. 2004). These forms are much narrower than those developed by periglacial thermokarst. Their orientation is parallel or conjugate with tectonic direction (Van Vliet-Lanoë et al. 2004).

Frost wedges

The sand wedges found in the Quaternary sediments have a polygonal system; consequently they are considered sand-wedge polygons. The wedges have an average vertical dimension of 1.5–2.0 m, but some are as much as 3 m (Fig. 2A). The wedge width was measured at right angle of the axial plane of the wedge. Additionally these wedges are 25–30 cm and 50–60 cm or slightly more in width. The sand-filled wedge structures have simple V-shapes with rectilinear or slightly curved sides (convex outward) and pointed toes. The fill of the wedges is subvertically laminated, the sand itself is fine- to medium-grained (1–3 φ) and moderately well sorted. Some wedges near or at the top contain pebbles. The host strata adjacent to a sand wedge is upturned. In plan view, it forms a polygonal network with cracks spaced 2–5 m apart. The cracks are irregular and several meters long.

Conclusions

Several hypotheses for the formation and infill of the wedges were evaluated using detailed physical, stratigraphic, and sedimentological information. The most likely explanation for most of the features is that they are relict cryogenic structures formed by thermal-contraction cracking in permafrost, and filled with wind-blown sediments. The wedges are believed to have formed in the tundra environment that existed in the Pannonian Basin during the coldest parts of the Würm glaciation. Our observations of relict sand wedges support previous inferences for the occurrence of continuous permafrost (which were based on the occurrence of ice-wedge casts and cryoturbations) in Hungary during the Pleistocene. Based on previously reported periglacial features, the local glacial history and OSL dates, these features suggest that the Pannonian Basin was underlain by permafrost during the Late Pleniglacial (22,000–18,000 years ago). We accept that some of the wedge-shaped sedimentary structures may be causally related to paleoearthquakes, but the obvious complexity of the phenomenon requires caution.

Acknowledgments

The authors are grateful to C. Tarnocai and F. Schweitzer for field assistance and useful communications, and to E. Thamó-Bozsó for supervising the OSL measurements.

References

Csontos, L., Benkovics, L., Bergerat, F., Mansy, J.L. & Wórum, G. 2002. Tertiary deformation history from seismic section study and fault analysis in a former European Tethyan margin (the Mecsek-Villány area SW Hungary). *Tectonophysics* 357: 81-102.

Dylik, J. 1963. Magyarország periglaciális problémái. *Földrajzi Értesítő* 12: 453-464.

Fábián, S.Á., Kovács, J. & Varga, G. 2000. Újabb szempontok hazánk periglaciális klímájához. *Földrajzi Értesítő* 49: 189-204.

Horváth, Z., Michéli, E., Mindszenty, A. & Berényi-Üveges, J. 2005. Soft-sediment deformation structures in Late Miocene–Pleistocene sediments on the pediment of the Mátra Hills (Visonta, Atkár, Verseg): Cryoturbation, load structures or seismites? *Tectonophysics* 410: 81-95.

Kovács, J., Fábián, S.Á., Schweitzer, F. & Varga, G. 2007. A relict sand-wedge polygon site in north-central Hungary. *Permafrost and Periglacial Processes* 18: 379-384.

Maarleveld, G. 1976. Periglacial phenomena and the mean annual temperature during the Last Glacial time in the Netherlands. *Biuletyn Peryglacjalny* 26: 57-78.

Magyari, Á., Musitz, B., Csontos, L. & Van Vliet-Lanoë, B. 2005. Quaternary neotectonics of the Somogy Hills, Hungary (part I): Evidence from field observations. *Tectonophysics* 410: 43-62.

Montenat, C., Barrier, P., Ott d′Estevou, P. & Hibsch, C. 2007. Seismites: An attempt at critical analysis and classification. *Sedimentary Geology* 196: 5-30.

Pécsi, M. 1964. Chronological problem of the patterned soils of Hungary. *Biuletyn Peryglacjalny* 14: 279-293.

Tarnocai, C. & Schweitzer, F. 1998. Cryogenic features in Canada and Hungary and their significance for past climate. *Geografia Fisica e Dinamica Quaternaria* 21: 84-92.

Van Vliet-Lanoë, B., Magyari, A. & Meilliez, F. 2004. Distinguishing between tectonic and periglacial deformations of quaternary continental deposits in Europe. *Global and Planetary Change* 43: 103-127.

Potential Inclusion of Vegetation Indices in Mountain Permafrost Modeling

Marian Kremer, Antoni G. Lewkowicz, Michael Sawada, Philip P. Bonnaventure
Department of Geography, University of Ottawa, Ottawa, Canada
Mark Ednie
Geological Survey of Canada, Ottawa, Canada

Introduction

A widely-used method to model the distribution of mountain permafrost employs basal temperature of snow (BTS) measurements as an indicator of the probability of permafrost presence. Multiple regression is used to develop a spatial field of BTS values, and these values are used to predict the distribution of permafrost either through the BTS "rules-of-thumb" or through ground-truthing relationships (e.g., Lewkowicz & Ednie 2004). The best independent variables for modeling BTS values are generally elevation and potential incoming solar radiation (PISR) (e.g., Gruber & Hoelzle 2001, Lewkowicz & Ednie 2004, Ødegård et al. 1999). Multiple regression of BTS against these variables generally results in r^2 values of 0.3–0.4, indicating that there are other important factors affecting BTS values and hence permafrost (Gruber & Hoelzle 2001, Lewkowicz & Ednie 2004), one of which is vegetation.

Vegetation affects the surface offset (Smith & Riseborough 2002) by influencing turbulent energy fluxes, by shading the ground surface in summer and by altering snow distribution in winter, especially in mountain catchments where significant redistribution of snow may occur (e.g., Pomeroy et al. 2006). A small number of attempts have been made to include vegetation in permafrost spatial models using vegetation indices and land cover classifications created from remotely sensed satellite images. However, there is no generally accepted method to represent vegetation for this purpose.

Despite its known theoretical significance, vegetation has proven to be of little importance in the few European mountain permafrost studies that have included it. For example, the Normalized Difference Vegetation Index (NDVI) which was used by Ødegård et al. (1999) in southern Norway did not substantially improve statistical explanation because it was highly correlated with elevation, one of the other independent variables. In Switzerland, Gruber and Hoelzle (2001) used the Soil Adjusted Vegetation Index (SAVI) to correct for the high reflectance of soil in the imagery, but obtained similar results. Without it the r^2 value was 0.386, and with SAVI the r^2 increased by only 0.012 (Gruber & Hoelzle 2001).

Attempts to incorporate vegetation into permafrost modeling using land cover classifications have been more successful. In the Yukon-Tanana Uplands of Alaska, Landsat Thematic Mapper (TM) imagery was used to generate land cover classifications that included types of canopy cover (closed or open) and types of vegetation (coniferous forest, deciduous forest, mixed forest, shrub) (Morrissey & Strong 1986). Using logistic discriminant functions with this classification and data from the thermal band of Landsat TM imagery, which provides similar information to PISR, three classes of permafrost distribution (frozen, discontinuously frozen, and unfrozen) were predicted with reasonable success. In the Mayo region, Yukon, Leverington, and Duguay (1996) also developed a vegetation classification from Landsat TM imagery and used it to test models for predicting active layer depths and the presence or absence of permafrost. The land cover classification was found to be one of the most useful factors for predicting the presence of permafrost. Etzelmüller et al. (2006) combined both land cover classification and NDVI in their multicriteria analysis of mountain permafrost distribution in Mongolia. They found that NDVI was useful only after an initial land cover division into forested and nonforested areas.

Objectives

The goal of this project is to examine which, if any, of the ways discussed above to incorporate vegetation may be suitable for permafrost modeling in the mountains of northwest Canada. Despite their lack of effectiveness in Europe, it is possible that vegetation indices may yet prove useful, given differing patterns of permafrost distribution in relation to vegetation zones. Alternatively, land cover classification or a hybrid approach may be the most effective. By testing models at sites in several climatological zones, we hope to determine if there is a single method that is effective or if adjustments to the methodology must be made to take local vegetation-climate relations into account.

Study Areas

The eight field areas that are being examined for this study represent all the major climatological regions of the southern Yukon and include Wolf Creek near Whitehorse, Johnson's Crossing, Sa Dena Hes mine north of Watson Lake, Faro, Keno, the Top-of-the-World Highway near Dawson, the Ruby Range, and Haines Summit in extreme NW British Columbia. These sites span almost 5° of latitude (59°36′ to 64°05′N), and all fall into zones of discontinuous permafrost (Heginbottom et al. 1995). Elevations in the areas generally vary from about 700 m to 2000 m a.s.l., with the Dawson area extending down to about 320 m. Permafrost is present at higher elevations in all of the areas as well as below tree line in most of them as a result of cold air drainage and hydrological variability.

Results

A preliminary investigation of the relationships between vegetation and the presence or absence of permafrost was undertaken using a dataset collected since 2002 of vegetation descriptions and late-summer probing or temperature profiles in pits at more than 500 mountain sites. Observations were grouped into three vegetation classes that exist in the study areas: northern boreal forest, a shrub tundra zone of willow and birch above treeline, and alpine tundra or bare areas (combined) at the highest elevations.

The percentage of pits exhibiting permafrost for each vegetation type in each study area (organized by increasing precipitation) is shown in Figure 1. The results suggest that precipitation totals may have an impact at the regional scale, but this apparent trend must be interpreted cautiously, as the precipitation values come from low-elevation climatological stations located up to 80 km from the study areas. Organizing the results by latitude (not shown) did not reveal any obvious trends: three sites at virtually the same latitude (Wolf Creek, Johnson's Crossing and Sa Dena Hes) exhibit significant variation in the percentage of permafrost.

Given the link between elevation and vegetation, it is not surprising that the percentage of permafrost is generally higher for alpine tundra sites than for the other two classes. Reasons for the two exceptions (Faro for shrubs and Johnson's Crossing for forest) require further investigation and more field sampling.

The impact of vegetation in affecting the surface offset and, hence, permafrost is best illustrated by the three study areas where shrub sites have the smallest percentage of permafrost (lower than forested sites). This may indicate the importance of trapping snow blown from the tundra above (e.g., Pomeroy et al. 2006) within the shrub zone and the snow's influence on reducing ground heat loss in winter.

These field observations show that vegetation type is highly correlated with elevation, but this brief analysis indicates that it may still affect mountain permafrost distribution independently. It also suggests that these impacts may be site-specific, possibly linked to regional climate. Further investigations of these relationships are planned in order to meet the objectives described above.

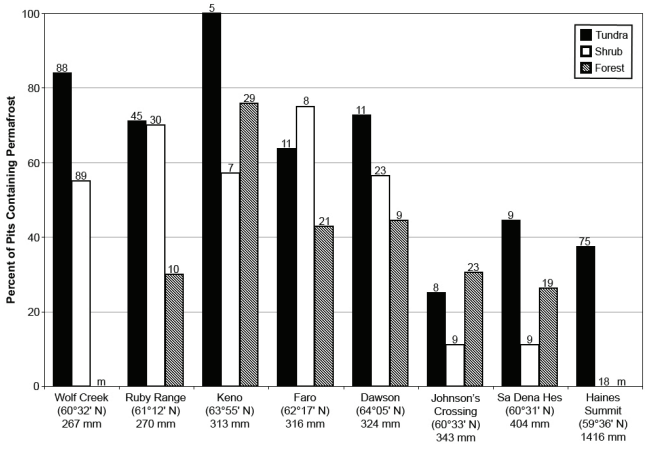

Figure 1. Percent of ground truthing pits that contained permafrost for each vegetation type in each study area. Numbers above the bars indicate the number of pits examined (groups with <5 sites shown as m). Sites organized according to precipitation normals (1971–2000) from the closest climatological station (data source, Environment Canada 2008).

Acknowledgments

Financial support was provided by the Canadian Foundation for Climate and Atmospheric Sciences, NSERC, Geological Survey of Canada, Yukon Geological Survey and the University of Ottawa. Field assistance was provided by Emily Schultz, Dan Odell, and Reid Van Brabant.

References

Environment Canada. 2008. http://www.climate.weatheroffice.ec.gc.ca (accessed February 9, 2008).

Etzelmüller, B., Heggem, E.S.F., Sharkhuu, N., Frauenfelder, R., Kääb, A. & Goulden, C. 2006. Mountain permafrost distribution modeling using a mutli-criteria approach in the Hövsgöl area, northern Mongolia. *Permafrost and Periglacial Processes* 17: 91-104.

Gruber, S. & Hoelzle, M. 2001. Statistical modelling of mountain permafrost distribution: Local calibration and incorporation of remotely sensed data. *Permafrost and Periglacial Processes* 12: 69-77.

Heginbottom, J.A., Dubreuil, M.A. & Harker, P.T. 1995. Canada Permafrost. 1:7,500,000 scale. In: *The National Atlas of Canada*, 5th ed., sheet MCR 4177. Ottawa: National Resources Canada.

Leverington, D.W. & Duguay, C.R. 1996. Evaluation of three supervised classifiers in mapping "depth to late-summer frozen ground", central Yukon Territory. *Canadian Journal of Remote Sensing* 22: 163-174.

Lewkowicz, A. & Ednie, M. 2004. Probability mapping of mountain permfrost using the BTS method, Wolf Creek, Yukon Territory, Canada. *Permafrost and Periglacial Processes* 15: 67-80.

Morrissey, L.A., Strong, L.L. & Card, D.H. 1986. Mapping permafrost in the boreal forest with thematic mapper satellite data. *Photogrammetric Engineering and Remote Sensing* 52: 1513-1520.

Ødegård, R.S., Isaksen, K., Mastervik, M., Billdal, L., Engler, M. & Sollid, J.L. 1999. Comparison of BTS and Landsat TM data from Jotunheimen, southern Norway. *Norsk Geografisk Tidsskrift* 53: 226-233.

Pomeroy, J.W., Bewley, D.S., Essery, R.L.H., Hedstrom, N.R., Link, T., Granger, R.J., Sicart, J.E., Ellis, C.R. & Janowicz, J.R. 2006. Shrub tundra snowmelt. *Hydrological Processes* 20: 923-941.

Smith, M.W. & Riseborough, D.W. 2002. Climate and the limits of permafrost: A zonal analysis. *Permafrost and Periglacial Processes* 13: 1-15.

Thermal Conditions in Martian Permafrost: Past and Present

Mikhail A. Kreslavsky
University of California – Santa Cruz

Present Conditions

Global cryosphere

The temperature of the Martian surface has been monitored by several orbital thermal infrared sensors. These measurements, accompanied by careful and cautious modeling, give rather accurate knowledge of the thermal regime of the uppermost meters of the surface in the present epoch.

The year-average surface temperature on Mars is well below 0°C everywhere on the planet, meaning a thick global cryosphere. The day-average temperature also never exceeds the ice melting point, meaning the absence of the active layer of Martian permafrost in the present epoch.

Observations with orbital gamma-ray and neutron sensors sensitive to the presence of hydrogen in the uppermost meter of the surface have indicated that high latitudes (above ~ 60° in both hemispheres) contain much hydrogen, which obviously means the presence of water ice. This ice is abundant, and its amount in the soil noticeably exceeds 50% by volume. At mid and low latitudes, ice in the upper meter is less abundant or absent. The hydrogen content in equatorial regions is spatially variable and in some regions exceeds 10 wt% water-equivalent by weight. Deeper in the ground, ice may be present virtually everywhere.

Calculations of the ground ice stability against diffusion of water vapor to the atmosphere (e.g., Mellon & Jakosky 1995, Schorghofer & Aharonson 2005) show that the ground ice is stable at high latitudes and unstable at low latitudes; in addition to latitude, surface albedo and thermal properties influence stability.

Patterned ground

High-resolution images reveal a great variety of polygonal patterns (e.g., Mangold et al. 2004), totally covering more than one-quarter of the planet (predominantly at high latitudes). The extent of massive polygonal pattern occurrence somewhat exceeds the limits of the observed high hydrogen content. Polygonal patterns are often forming hierarchical systems of different scales (Fig. 1). These patterns were probably initiated by thermal cracking of ice-rich permafrost. On Earth, thermal cracking of permafrost usually leads to formation of ice-wedge polygons due to seasonal thaw of the active layer. On Mars, seasonal thaw does not occur, and the cracks evolve into sand-wedge polygons and/or sublimation polygons, features, observed in extremely cold and dry terrestrial environments (Marchant et al. 2002).

Thermal cracking of ice-rich frozen soils occurs due to an anomalously high bulk thermal expansion coefficient of the ice-soil mixtures. However, the thermal expansion coefficient decreases with the temperature decrease. Very high seasonal temperature amplitude at high latitudes on Mars favors thermal cracking, while generally low temperatures are not favorable.

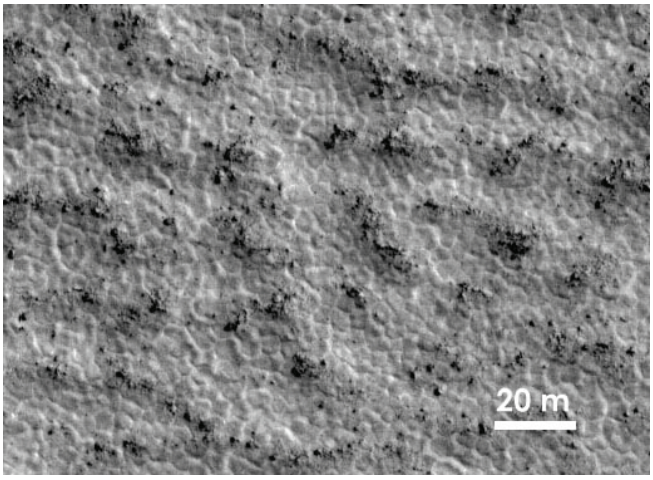

Figure 1. Two scales of polygonal pattern on Mars. HiRISE image PSP_001404_2490, 69°N, 106°W.

The absence of polygons in the *low-latitude* hydrogen-rich regions has been interpreted as evidence for the absence of water ice in the soil (the hydrogen being bound in hydrated minerals). However, in these regions, the seasonal temperature amplitudes are modest (typically, 20–30 K; <50 K in any place) and temperatures (~210 K year average) are very low. The hydrogen-rich regions coincide with the regions of low-thermal-inertia dust cover. This ice-free cover would further reduce the seasonal temperature amplitude at the hypothetical ice table. Formation of the thermal contraction cracks is not probable under such conditions, and their absence cannot be considered as an argument against subsurface ice.

The polygonal patterns at *high latitudes* show remarkable uniformity over large areas, as well as significant regional variability partly correlated with latitude (e.g., Kostama et al. 2006, Levy et al. 2008). The polygon-covered surface at high latitude is almost devoid of small (tens of meters) impact craters, which indicates geologically recent deposition of meters-thick icy material ("mantle") and/or thorough reworking of the surface by cryoturbaton. Thus, patterned ground bears a record of processes related to recent climate change on Mars.

Recent Past

Kostama et al. (2006) found that the crater retention age for tens-of-meters-scale craters in the high northern latitudes is on the order of 100 ka, and is highly variable regionally and latitudinally. Recent measurements of the present-day cratering rate on Mars (Malin et al. 2006, Kreslavsky 2007) make that estimate more certain. Thus the polygonal pattern

records the most recent climate variations and can be used to constrain timing of other recent geological events (e.g., the most recent gully activity).

Stresses causing thermal cracking are proportional to the seasonal amplitude of the surface temperature. At high latitudes on Mars the winter temperature is buffered by condensation of the atmospheric carbon dioxide at ~140 K. Thus, the amplitude of seasonal surface temperature variations is solely defined by the year-maximum day-average temperature. On Mars, weak atmosphere is mostly thermally decoupled from the surface, and the surface temperature is controlled mostly by direct insolation, other contributions being minor. The year-maximum day-average temperature is an increasing function of the year-maximum day-average insolation. Since the winter temperature is the same, the year-average surface temperature is also an increasing function of the year-maximum day-average temperature, and hence, of the insolation. Thus, the year-maximum day-average insolation is a good proxy of the climate signal with regard to cryoturbation and formation of the polygonal patterns.

The insolation regime is controlled by evolution of spin and orbit parameters of Mars. For the recent epoch, these parameters were accurately calculated by Laskar et al. 2004. Figure 2 presents evolution of the year-maximum day-average insolation at high latitudes (70°) in both hemispheres

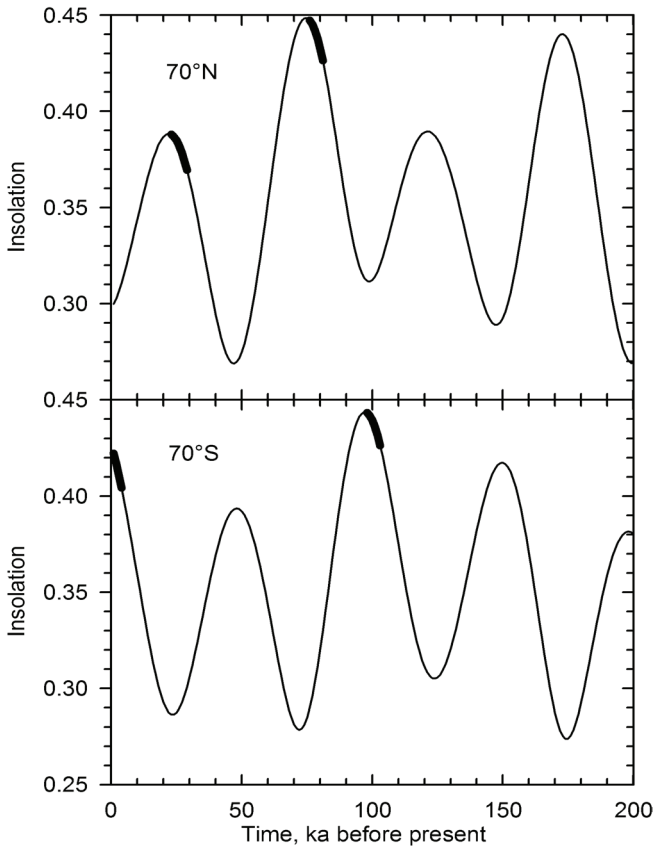

Figure 2. Evolution of the year-maximum day-average insolation (in parts of the martian solar constant) over the last 200 ka for horizontal surfaces at 70° latitude in the Northern (top) and Southern (bottom) Hemispheres. Bold segments show probable most recent periods of intensive polygon formation

over the last 200 ka. Formation of new cracks is expected to be on increasing insolation branches close to the insolation maxima, as marked on the plots (Fig. 2).

In the Southern Hemisphere, the polygon formation can be active at the present time. Older crack systems can have been formed 100 ka ago. If even older polygonal cracks are observed in the southern high latitudes, they may date back to 400 ka ago (not shown in Fig. 2). In the Northern Hemisphere, the most recent insolation peak occurred 20 ka ago, but it was lower than the present-day insolation at the south. The more probable period of activity is 75 ka ago, and it is most close to the age estimates by Kostama et al. 2006. An earlier high insolation peak occurred 275 ka ago.

Applying these results to the geologic studies, we need to keep in mind that the other factors, such as surface albedo (which can change due to painting of the surface with thin layers of fine dust) and thickness of dry layer above the ground ice (which depends on atmospheric water vapor content) can strongly influence the formation of polygonal patterns.

References

Kostama, V.-P., Kreslavsky, M.A. & Head, J.W. 2006. Recent high-latitude icy mantle in the northern plains of Mars: Characteristics and ages of emplacement. *Geophys. Res. Lett.* 33: L11201.

Kreslavsky, M.A. 2007. *Statistical Characterization of Spatial Distribution of Impact Craters: Implications to Present-Day Cratering Rate on Mars*. 7th Conf. on Mars, LPI Contribution No. 1353: 3325.

Laskar, J. et al. 2004. Long term evolution and chaotic diffusion of the insolation quantities of Mars. *Icarus* 170: 343-364.

Levy, J.S., Head, J.W. & Marchant, D.R. 2008. Mars thermal contraction crack polygon classification and distribution: Morphological characterization at HiRISE resolution. *Lunar Planetary Sci. XXXIX*: #1171.

Malin, M.C. et al. 2006. Present-day impact cratering rate and contemporary gully activity on Mars. *Science* 314: 1573-1577.

Mangold, N. et al. 2004. Spatial relationships between patterned ground and ground ice detected by the Neutron Spectrometer on Mars. *J. Geophys. Res.* 109: E08001.

Marchant, D.R. et al. 2002. Formation of patterned-ground and sublimation till over Miocene glacier ice in Beacon Valley, Antarctica. *Geol. Soc. Am. Bull.* 114(6): 718-730.

Mellon, M.T. & Jakosky, B.M. 1995. The distribution and behavior of Martian ground ice during past and present epochs. *J. Geophys. Res.* 100: 11781-11799.

Schorghofer, N. & Aharonson, O. 2005. Stability and exchange of subsurface ice on Mars. *J. Geophys. Res.* 110: E05003.

Collapse of the Bérard Rock Glacier (Southern French Alps)

Jean-Michel Krysiecki
Institute of Alpine Geography, University of Grenoble, France
Xavier Bodin
University Paris-Diderot (Paris 7), Institute of Alpine Geography, University of Grenoble, France
Philippe Schoeneich
Institute of Alpine Geography, University of Grenoble, France

Introduction

In the Mediterranean French Alps, the summer 2006 has been marked by the sudden collapse of the Bérard rock glacier (Parpaillon Range, Alpes de Haute Provence, France), a very rare event and exceptional by the amount of disturbed material estimated to be about 2 millions m^3 (Fig.1).

Located near the southern limits of the European Alpine permafrost, the Bérard rock glacier case is perhaps representative of the potential consequences of mountain permafrost degradation under present global warming, and raises questions about the evolution of ice-debris mixtures on steep slopes; for example, rock glacier under permafrost conditions. An atmospheric warming of 0.5 to 1°C between 1900 and 2000 is indeed currently observed in the Alps (Casty et al. 2005). In the same way, recent observations on thermal evolution of the ground in high mountains (Harris et al. 2003), as well as the occurrence of new and unexpected phenomena, for example, acceleration of rock glacier flow (Ikeda & Matsuoka 2002, Roer et al. 2005, Delaloye et al. 2006, Kääb et al. 2006, Delaloye et al. 2008) or rock glacier collapse (Evin et al. 2007), seem to indicate that mountain permafrost could respond much faster to global warming than expected, and that areas at its lower limits could experience a morphogenetic crisis.

Crucial questions in terms of natural hazards and associated dangers are being raised (Harris et al. 2000): the speed-up of creeping landforms (Kääb et al. 2006), the destabilisation of the frontal part of rock glaciers (Arenson 2002), and an increase of the rockfall activity (Haeberli et al. 1997, Noetzli et al. 2003) and of the frequency of debris flow have already been observed in mountain permafrost areas.

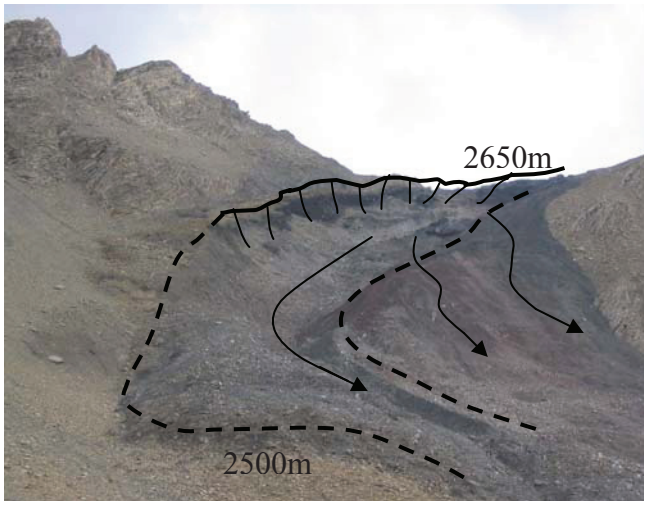

Figure 1. An upward-looking view of the collapsed Bérard rock glacier (July 2007).

In this context, the main objective of our study is to understand the mechanisms that triggered the Bérard rock glacier collapse, which could subsequently gain new insights into the destabilisation of ice-rich deposits on mountain catchments.

The Bérard Rock Glacier Situation

The Bérard rock glacier is located in the Parpaillon Range, one of the southernmost ranges of the European Alps, including the summits of Grand Bérard (3046 m) and La Chalanche (2984 m). Topoclimatic and geomorphological conditions are favorable to permafrost occurrence in this valley.

Methods

Within a larger research project intending to study the consequences of permafrost degradation in the French Alps, a complete monitoring of the site has hence been set up. This includes:

- the geodetic survey (Differential and Permanent GPS) of marked blocks during the summer, in order to quantify the velocity and the characteristics of the movement;
- the use of radar interferometry to reconstruct the history of the event during the previous years and to map the main destabilised areas;
- the interpretation of electrical resistivity and refraction seismic tomographies to assess the physical properties of the internal structure of the rock glacier;
- the analysis of the ice to determine its origin and its main physical properties;
- the survey of the climatic parameters (air temperature, solar radiation, wind speed and direction, snow height) with an automatic weather station; and
- the survey of the thermal state of the ground (with miniature temperature dataloggers) to allow the monitoring of pertinent indicators; for example, mean annual ground surface temperature (MAGST) or mean annual active layer temperature.

First Results

Among the above-mentioned methods, geomorphological study, DGPS results, and ice analyses have given first results.

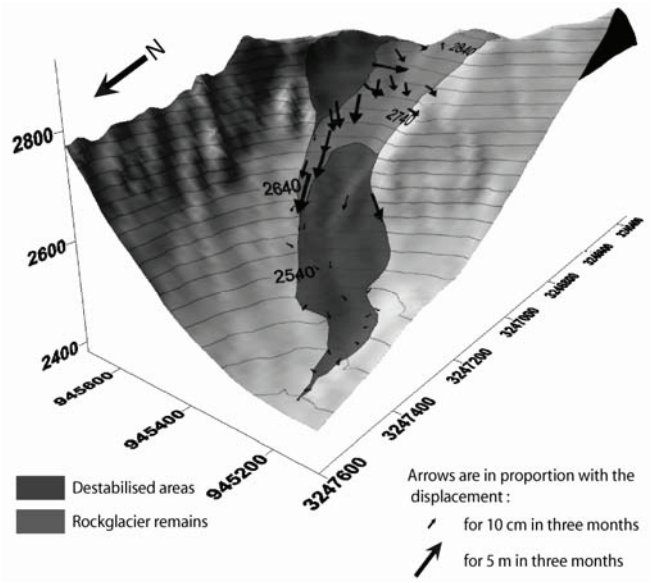

Figure 2. 3-D displacement of marked blocks on the Bérard rock glacier between June and September 2007.

The geomorphological study of the site has already revealed that the breaking of the rock glacier is probably partly related to an underlying rockslide in the schist series, which may have been activated by storms during summer 2006.

First results are DGPS measurements of more than 40 marked blocks on the Bérard rock glacier and the slided mass, in June and September 2007. The 3-D vectors map shows that the slided mass has not experienced important movements during the three surveyed months. *Z* values suggest a general settling (about 5–15 cm), certainly due to the ice melt in debris. Remains of the rock glacier, especially near the collapse area, are affected by large movements (more than 5 m in three months) and the destabilisation is effective as far as the saddle point (displacements are around 1 m in three months). Permanent GPS, located above the scar on a flat area, indicates a mean displacement of 6.4 $mm.day^{-1}$ in the north direction, corresponding to an annual displacement of more than 2 m, which fits with the surrounding DGPS measurements.

Stratigraphic observations on near-surface ice outcrops reveal that Bérard rock glacier has been affected by periglacial and glacial mechanisms. Preliminary analyses of ice structure have revealed the sample to be similar to glacier ice (Vallon, pers. com.). Little Ice Age period is suspected in this mechanism change, but other analyses have to confirm that.

Our study, thanks to the various monitoring devices, has already clarified the respective roles of the meteorological conditions, the recent climatic warming, and the geological settings in the collapse of the Bérard rock glacier. Most of the results are coming during the summer 2008 and will bring new precision on the Bérard rock glacier event.

References

Arenson, L.U. 2002. *Unstable Alpine permafrost: A potential important natural hazard – Variations of geotechnical behaviour with time and temperature.* PhD Thesis, ETH Zurich.

Casty, C. et al. 2005. Temperature and precipitation variability in the European Alps since 1500. *International Journal of Climatology* 25: 1855-1880.

Delaloye, R. et al. 2006. ERS InSAR for detecting slope movement in a periglacial mountain environment (western Valais Alps, Switzerland). *Ninth International Symposium on High Mountain Remote Sensing Cartography* (HMRSC-IX), Graz, Austria.

Delaloye, R. et al. 2008. Recent interannual variations of rock glacier creep in the European Alps. *Proceedings of the Ninth International Conference on Permafrost, Fairbanks, Alaska, 29 June–3 July 2008*.

Evin, M. et al. 2007. Rupture et glissement en masse d'un glacier rocheux dans le vallon du Bérard (Massif du Parpaillon, Alpes du Sud, France) au cours de l'été 2006, Grenoble, *SHF - Section Glaciologie/ Nivologie*.

Gruber, S. et al. 2004. Interpretation of geothermal profiles perturbed by topography: the Alpine permafrost boreholes at Stockhorn Plateau, Switzerland. *Permafrost and Periglacial Processes* 15(4).

Haeberli, W. et al. 1997. Slope stability problems related to glacier shrinkage and permafrost degradation in the Alps. *Eclogae Geol. Helv*. 90: 407-414.

Ikeda, A. & Matsuoka, N. 2002. Degradation of talus-derived rock glacier in the Upper Engadin, Swiss Alps. *Permafrost and Periglacial Processes* 13: 145-161.

Kääb A. et al. 2006. On the response of rockglacier creep to surface temperature increase. *Global and Planetary Change* 56(1–2): 172-187, doi:10.1016/j.gloplacha.2006.07.005.

Noetzli, J. et al. 2003. Mountain permafrost and recent Alpine rock-fall events: A GIS-based approach to determine critical factors. *Proceedings of the Eighth International Conference on Permafrost, Zürich. Swets & Zeitlinger, Lisse.*

Roer, I. et al. 2005. Rockglacier "speed-up" throughout European Alps: A climatic signal? *Second European Conference on Permafrost*, Potsdam, Alfred-Wegener-Stiftung.

Studies of the Freezing Soil Process at the Railway Contact System Supports to Provide Safe Transportation and Operation of Facilities

S.A. Kudryavtsev, D.G.Tsvigunov
Far Eastern State Transport University (FESTU), Khabarovsk, Russia

Introduction

Maintenance and efficient operation of railway power engineering facilities in regions with seasonal freezing and permafrost soils are faced with serious difficulties connected with the bulging of contact system supports. Seasonal soil freezing is one of the major factors taken into consideration for contact system support foundations.

The problem of frost heaving is characterized not only by the number of repaired contact system supports, but also by safe transportation, too. On sections of the Far Eastern railway, which pass through a permafrost area, a large number of contact system supports has to be restored annually. To develop a reliable and stable foundation structure, an exact estimation of thermophysical and stress-deformed conditions of heave-probable soils both at freezing and thawing is required.

Studies of freezing, frost heaving, and thawing of soils and their effect on contact system supports are complicated processes and require further development. Their complexity is first of all explained by a great number of interactive factors, changing in time and space. Studying these processes in natural conditions requires observations for a long period of time, because the data of short-term observations may be accidental.

Thermometric Observations

To check correctness of foundation designs used and search for new decisions in the field of construction, calculations, the utilization of structures, as well as establishing the character of their interaction must be considered. With seasonal freezing soils, monthly thermometric observations have been organized on the Khabarovsk Section of the Far Eastern Railway (8540 km.).

They are:

1. Thermal regime of the soil at the contact system support.
2. Geodesic control of the contact system support position.

To watch the thermal regime, a temperature monitoring system, Thermoscan, had been used. It is designed to do work for measuring temperature in continuous and single regimes.

The Thermoscan set includes a measuring block with a controller, a measuring bus duct with temperature "sensors," a pocket PC, a storage battery, and Thermoscan software.

Numerical Modeling of the Freezing Process

Measurements of the thermo-moisture regime were made with the help of numerical modeling. By analyzing

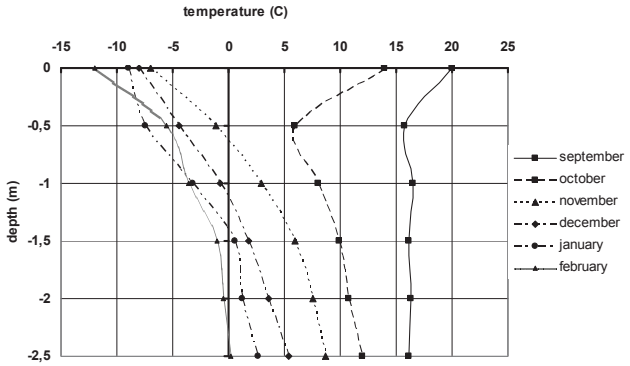

Figure 1. Thermometric observation data.

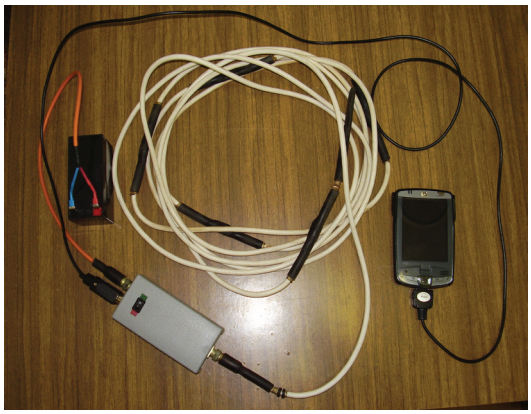

Figure 2. The Thermoscan temperature monitoring system.

the existent models of freezing and thawing of soils, a mathematical model of numerical modeling of freezing, frost heaving, and thawing in an annual cycle has been developed by the method of finite elements in the space set, being a component of the programmed complex "FEM-models."

This complicated geotechnical task is done in two stages: The first stage solves the thermo technical task of defining temperature and moisture fields for each period of time. The second stage solves the task of defining stress-deformed conditions of fundamental soils in the process of freezing and thawing.

We have simulated the process of freezing and heaving of the railway trial sector. Monthly calculations were made for yearly changes of the monthly average temperature in the region. The maximum depth of soil freezing in the contact system support, without principally the thermal insulation layer, was 2.0 m in March.

Deformation of the principal area of the railway bed caused by frost penetration is equal to 6 cm, and horizontal deformation of the contact system support, about 3.5 cm. Use of expanded polystyrene thermal insulation materials lowers the freezing front (zero isotherm) to 1.4 m under the

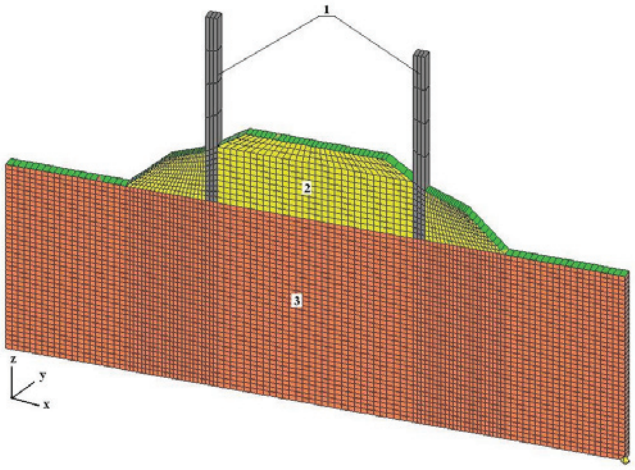

Figure 3. Calculations simulation scheme. 1 – contact system support; 2 – dusty loan embankment; 3 – basement.

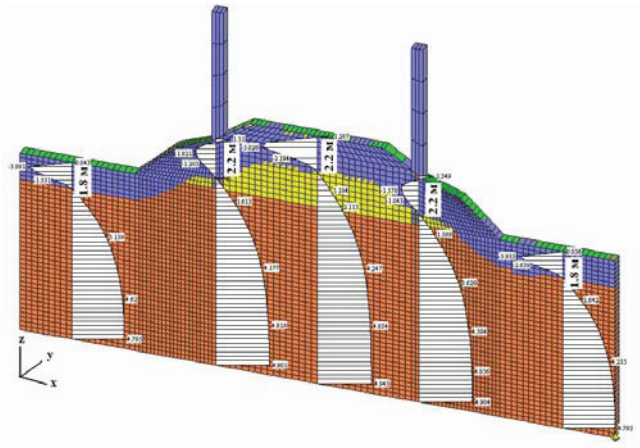

Figure 4. Temperature epures of the embankment body and basement.

center line of the track, and, accordingly, with deformation decrease down to 1.5 cm, frost heaving forces become lower. In the embankment slope, frost heaving forces have a serious effect on the stability of the contact system support, exerting normal and horizontal action, as the zero isotherm catches the foundations. This causes horizontal deformation of the supports, worsening their operational qualities.

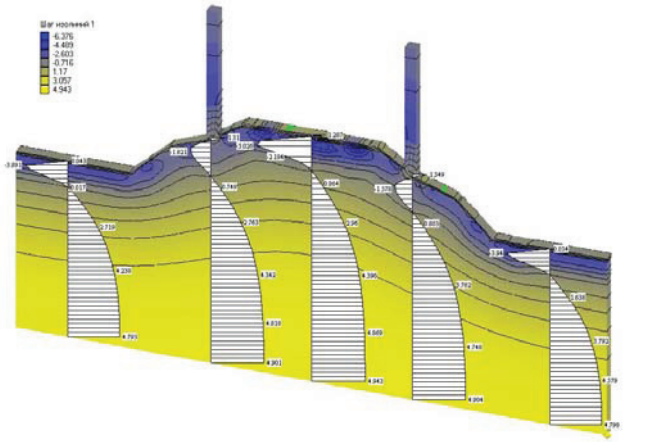

Figure 5. Temperature isolines and epures of the embankment body and basement.

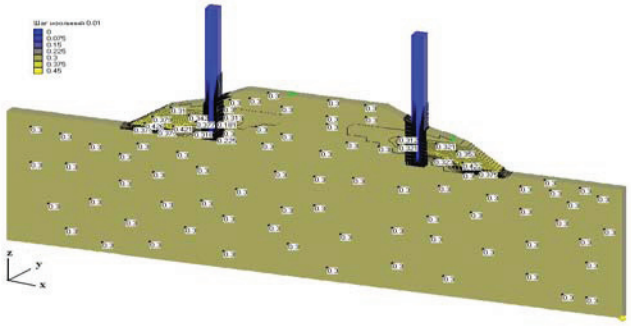

Figure 6. Isolines of moisture distribution in the body of embankment and basement in winter.

References

Kudryavtsev, S.A., Ulitsky, V.M., Paramonov, V.N., Shashkin, K.G. & Lisyuk, M.B. 2003. Contemporary geotechnologies providing safe operation of railway embankments in permafrost conditions. *Proceedings of the Eighth International Conference on Permafrost. Extended Abstracts, Reporting Current Research and New Informational Zurich, Switzerland, 20–25 July 2003:* 167-168.

Temporal Variability in Plant Cover and Carbon Balance of Permafrost-Affected Tundra Ecosystems

Peter Kuhry
Department of Physical Geography and Quaternary Geology, Stockholm University, Sweden

Introduction

The extant tundra in Northeast European Russia is characterized by high spatial variability. Previous studies highlight the fine mosaic of microsites with different vegetation, soil, permafrost, carbon storage, and methane emission characteristics (e.g., Kuhry et al. 2002, Heikkinen et al. 2004). This investigation points in addition to high temporal landscape dynamics in relation to recent climate and/or permafrost changes, which represents a further challenge for the past reconstruction and future prediction of the tundra carbon balance.

Methods

The temporal ecosystem dynamics in a tundra site at Lek-Vorkuta (Northeast European Russia) is traced using high resolution (1–2 cm depth intervals), absolute dating, geochemical, and plant macrofossil analyses of a 22 cm thick top organic sequence in permafrost-affected peaty soil. The LVPS3 profile was excavated from a small hummock in wet tundra (67°40′N, 63°35′E). The upper permafrost table at the time of collection (August 3, 1999) was located at 25 cm. This implies that the entire top organic horizon is located within the active layer. Although the profile at the site showed considerable deformation of the original layers, no evidence was found for complete stratigraphic inversions (Fig 1).

The LVPS3 sequence was dated through a combination of ^{210}Pb dating of the upper 16 cm and ^{14}C AMS wiggle-matching of the lower 7 cm of the top organic deposit. The geochemical analyses of the sequence included bulk density, loss-on ignition (550°C) and carbon/nitrogen ratio measurements. Figure 2 presents the gross stratigraphy of the profile and the samples (intervals and materials) utilized for the different types of analyses performed.

Figure 1. Collection site and material of the LVPS3 profile.

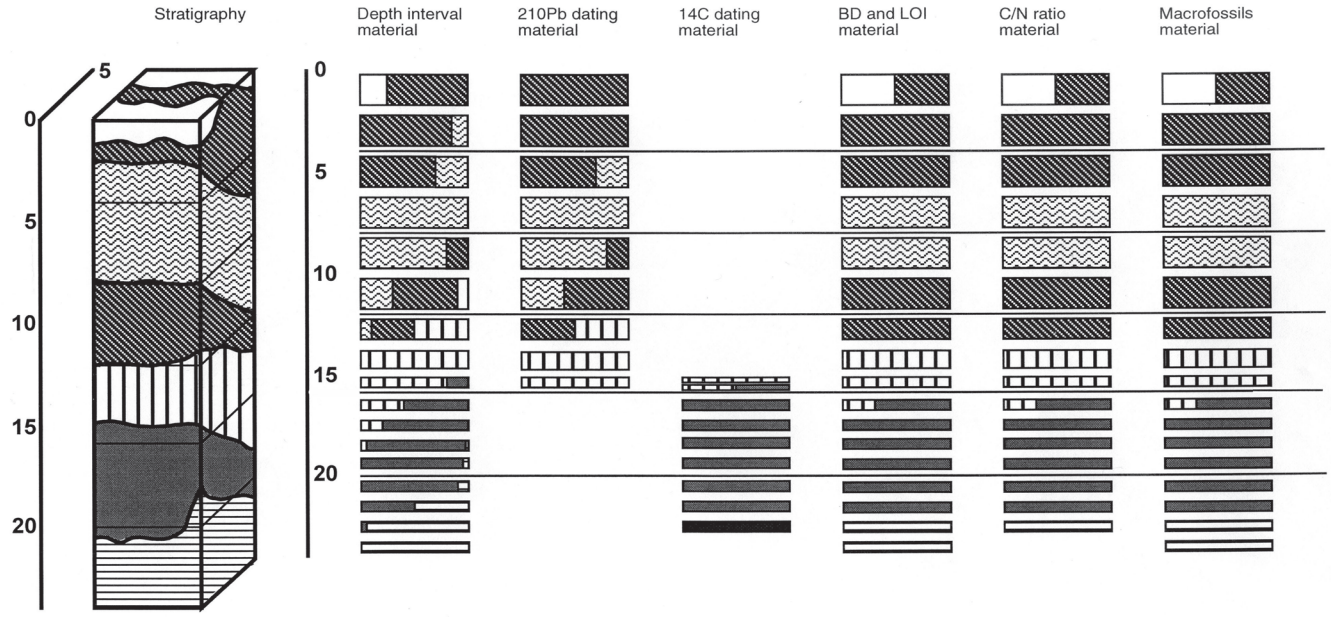

Figure 2. LVPS3 gross stratigraphy and samples analyzed for different analytical procedures. Stratigraphy from base to top: horizontal dash (mineral subsoil); uniform grey (organic soil); vertical dash (monocot peat); diagonal dash, two layers (*Polytrichum/Dicranum* peat); horizontal wave (*Sphagnum* peat); white (present lichen cover).

Results

The most plausible age-depth model suggests that the deposit represents ca. 650 calendar years with a rapidly declining net carbon accumulation rate due to cumulative decay of the organic matter with age. There has been a (near) complete turnover of organic material deposited prior to this time, leaving no evidence of the older history at the site.

Chronological control becomes increasingly more accurate towards the present, allowing a more detailed reconstruction of the timing and duration of successive vegetation phases.

Macrobotanical remains reveal significant changes in surface conditions at the site over time. The first recorded phase, characterized as dwarf-birch tundra, lasted until ca. 1860 AD. At this time the site paludified, resulting in the formation of an *Eriophorum*-dominated wetland. After about 40 years, drier surface conditions developed starting with *Sphagnum fuscum* and culminating in a *Polytrichum/ Dicranum* phase. Wetter conditions reappeared in the 1930s as indicated by *Sphagnum* Sect. Cuspidata. In recent decades the surface became drier again with a *Sphagnum fuscum* phase, followed by the present *Polytrichum/Dicranum*/ lichen phase.

An assessment will be made whether these recent changes in surface conditions can be linked to monitored long-term climate variability in the region. Alternatively, the observed temporal dynamics can be associated with permafrost aggradation following the development of a thick organic layer in the dwarf-birch phase and subsequent differential frost heave/ground subsidence at and in the immediate vicinity of the investigated site.

The final objective is to assess net carbon storage and methane emission characteristics throughout the recent history of the site with the aim to reconstruct the variable net radiative climate forcing originating from this type of dynamical tundra ecosystems.

Acknowledgments

The collection of the material was funded through the EU 4th Framework Environment and Climate Programme (TUNDRA project) and the EU INTAS Programme (PERUSA project). Current analyses of the material are supported by a grant from the Swedish Research Council.

References

Heikkinen, J.E.P., Virtanen, T., Huttunen, J.T., Elsakov, V. & Martikainen, P.J. 2004. Carbon balance of East European tundra. *Global Biogeochemical Cycles* 18, doi:10.1029/2003GB002054.

Kuhry, P., Mazhitova, G., Forest, P.A., Deneva, S., Virtanen, T. & Kultti, S. 2002. Upscaling soil carbon estimates for the Usa Basin (Northeast European Russia) using GIS-based landcover and soil classification schemes. *Danish Journal of Geography* 102: 11-25.

Temperatures of Upper Permafrost in Northern West Siberia

Anna N. Kurchatova, Alexander V. Boytsov
Tymen State Oil and Gas University, Russia
Alexei B. Osokin, Gregory K. Smolov
Gas Company "Nadymgasprom," Russia

Introduction

A monitoring net of permafrost observatories was established in 2004 by the Subarctic Centre (Tyumen State Oil and Gas University) and "Nadymgasprom" Company in Northern West Siberia. The southern part of the submeridian transect is located in continental territory between Nadym and Pur Rivers (Medvezhye and Yubileinoe gas fields); the northern end is situated on Yamal Peninsula (Kharasavay and Bovanenkovo gas-condensate fields). The observational sites are located on the main geomorphological levels of the territory and are presented by different landscapes. Boreholes (from 1 to 3 at observatory, up to 30 m depth) are equipped by automatic systems for temperature measurements made by "GEOTECHCENTRE," Russia. Measurements are taken every 6 hours at the 15s levels. At Bovanenkovo gas-condensate field (Yamal), a soil-climate station (by Campbell Scientific Ltd.) was established in 2006 for registration of standard meteorological parameters and the temperature-moisture regime of the active layer. On the territory of Yubileynoe gas field, 4 CALM sites were created for long-term dynamics of the active layer. The first results of these measurements are presented in this report.

Permafrost Temperatures

Analyses of meteorological data in West Siberia show a general increase in mean annual air temperature for about 30 years mainly due to decreasing of the temperature sum of the winter period. The first publications about the tendency of permafrost warming within the layer of the annual amplitudes appeared in the early 1990s. Long-term research at the geocryological stations in West Siberia (Marre-Sale – Pavlov 1994, and Nadym – Pavlov & Moskalenko 2002) shows the warming tendency of the frozen ground temperature during the last decades. For the last years, relative stability of the annual air temperature is accompanied by an increase in the positive temperature sum that can lead to melting of the ice-bearing permafrost table. And as a result, activity of cryogenic processes or local degradation of frozen ground from the top down at the drained sites in the southern cryolithozone can occur.

Observatories located at weakly drained watersheds of high geomorphological levels composed of mineral soils are the most representative for understanding permafrost's reaction to climate change. Zonal landscapes along the submeridian transect are changed from northern forest to tundra. Local factors can play a main role in the ground temperature regime: In depressions, a formation of snow cover occurs mainly due to the strong wind influence; the high ice content and moss cover provide thermal stability for the frozen peatlands in summer.

The temperature ground regime of the boreholes shows relative stability in different zonal landscapes (Fig. 1A). In the southern cryolithozone, taliks with deep permafrost table are widespread even within watersheds. The first results show that the depth of zero annual amplitude at these sites is about 15 m despite water-saturated sands in the upper part of the soil section. On Yamal Peninsula at the sites composed by clayish sediments, the annual thermal turnover reaches ≈10 m depth, explained by low temperature of freezing and low thermal conductivity of saline marine sediments and widespread cryopegs there. However, at the sandy denuded areas at the high marine terraces, the depth of zero annual amplitude can reach 20 m.

The mosaic landscape structure of forest-tundra has resulted in the high dynamics of the thermal ground state (Fig. 1B, C, D). Sparse growth of larches with dense shrubs is a clear indicator of taliks because of higher snow accumulation (1 m depth and more, I-1; 0.3–0.4 m at the peat bogs, I-2). The zero-temperature regime of the high river terraces has been kept by the warm input of melting snow water and the first liquid precipitation down into the dry frozen sands up to 3–5 m depth despite deep freezing during winter (I-3).

Disturbances of the soil surface (fires and construction) are a more common cause of ground temperature change, and especially of an increase in active layer depth. The substantial increase in the mean annual soil temperature at the base of the active layer within polygonal peatland was caused by a fire and destruction of the moss-lichen cover after the anomalous high air temperature in July 2007 (Fig. 1B, I-2). However, the disappearance of insulating moss cover can also result in fast freezing of the active layer in the beginning of winter, and then to the substantial decrease in soil temperature. We observed the formation of a new frost-cracking system at the other site after a similar fire in 2005.

Acknowledgments

Funding for the research was provided by the INTAS Infrastructure Action (Ref. Nr. 04-87-689) and Tyumen regional grants. We are grateful to the leaders of "Nadymgasprom" Company for the support of drilling and fieldwork, and to Drs. V. Romanovsky and N. Shiklomanov for equipment and assistance in the creation of CALM sites.

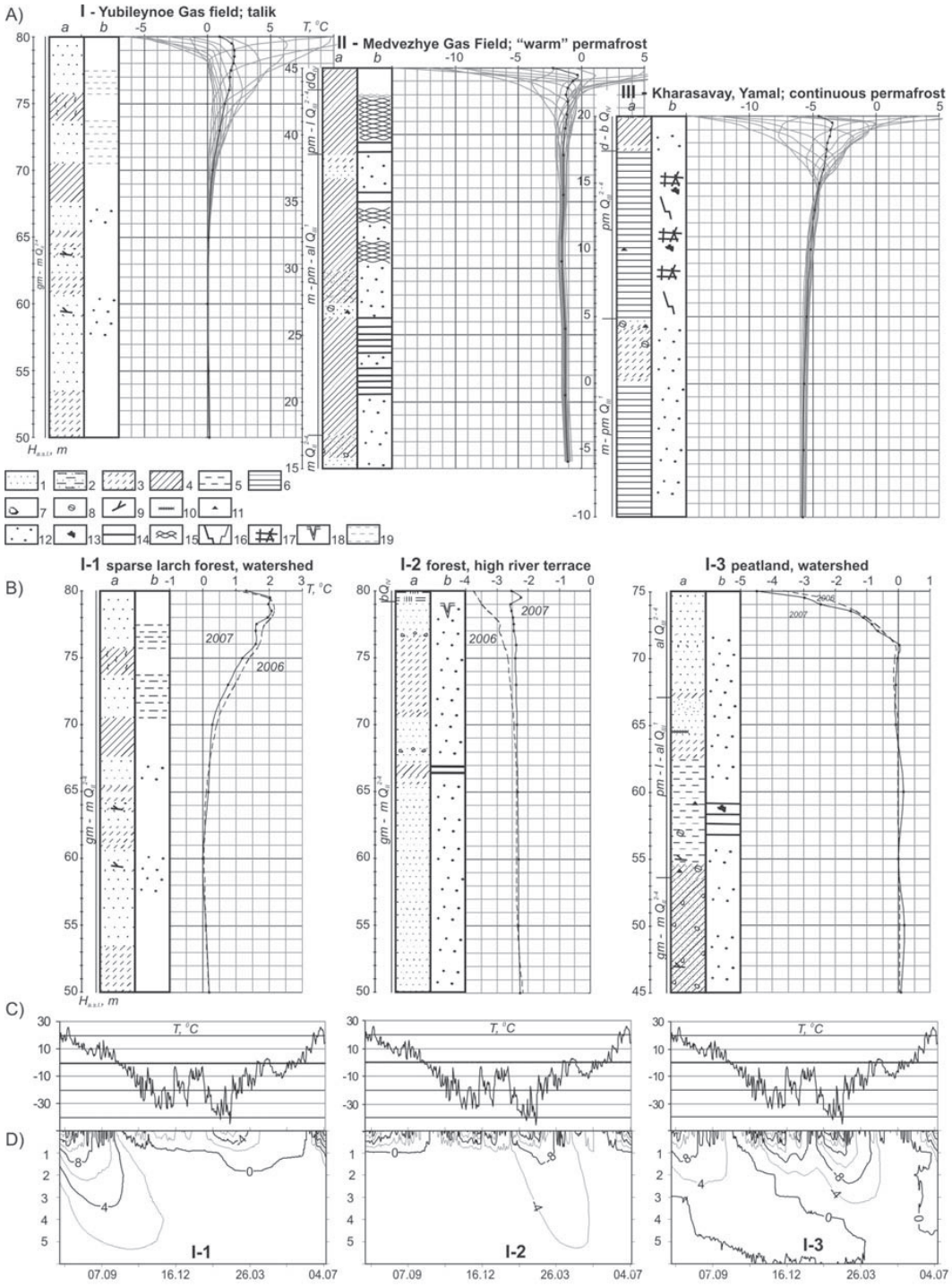

Figure 1. A: Mean annual (black line) and month (gray line) ground temperatures in Northern West Siberia; B: Changes in the mean annual ground temperatures at observatory I (Yubileynoe gas field) in 2006–2007; C: Mean daily air temperature at Novy Urengoy for 07.2006–07.2007; D: Active layer dynamics at observatory I in the different landscapes.
Lithology: 1-sand; 2-silty sand; 3-sandy-loam; 4-loam; 5-silt; 6-clay; 7-pebbles; 8-clayish fragments; 9-wooden remnants; 10-allochtonous peat; 11-carbonized organic debris. Cryostructure: 12-massive; 13-ice agglomerate; 14-layered; 15-reticulate; 16-vertical veins; 17-reticulate-blocky; 18-ice wedge; 19-water saturated soils.

References

Pavlov, A.V. 1994. Current changes of climate and permafrost in the Arctic and Sub-Arctic of Russia. *Permafrost and Periglacial Processes* 5: 101-110.

Pavlov, A.V. & Moskalenko, N.G. 2002. The thermal regime of soils in the north of Western Siberia. *Permafrost and Periglacial Processes* 13: 43-51.

Two-Dimensional Geoelectrical Monitoring in an Alpine Frozen Moraine

Christophe Lambiel
Institute of Geography, University of Lausanne, Switzerland
Ludovic Baron
Institute of Geophysics, University of Lausanne, Switzerland

Introduction

As defined by Haeberli (1979), push moraines are frozen sediments deformed by a glacier advance. In the Alps, push moraines are typically encountered in the margin of small glaciers, at altitudes comprised between 2500 and 3000 m a.s.l., in the belt of discontinuous permafrost (see e.g., Reynard et al. 2003, Delaloye 2004). In order to better know the internal structure and the ice content and repartition of this type of landform, a monitoring of the resistivity variation has been initiated on the Col des Gentianes push moraine (Swiss Alps).

Site Description and Methods

The Col des Gentianes moraine is located at 2900 m a.s.l., on the orographic left side of the Tortin glacier (Fig. 1). A cable car station for ski activity was built on the northern part of the moraine at the end of the 1970s. In October 2006, the road located between the building and the glacier was excavated for ski-run landscaping purposes. Massive ice layers were encountered at depths of 50 cm to 2 m. Congelation and sedimentary ice were present. Ground temperatures have been recorded in a 20 m deep borehole since November 2002 (Lambiel 2006). They attest the presence of permafrost conditions in the moraine, with temperatures of -0.5°C to -1°C between 5 and 20 m depth (Fig. 2).

Two-dimensional (2-D) resistivity imaging is an efficient tool to characterize permafrost extension in recently deglaciated glacier forefields (e.g., Marescot et al. 2003, Kneisel 2004). To provide information on both lateral and vertical variations of the resistivity and to monitor the temporal evolution of the resistivities in the Col des Gentianes moraine, a permanent 2-D electrical profile was installed on the upslope part of the road (Fig. 1). Two acquisitions were carried out on 13 August and on 23 October 2007 with the Wenner-Schlumberger configuration. Data were inversed with the software RES2DINV.

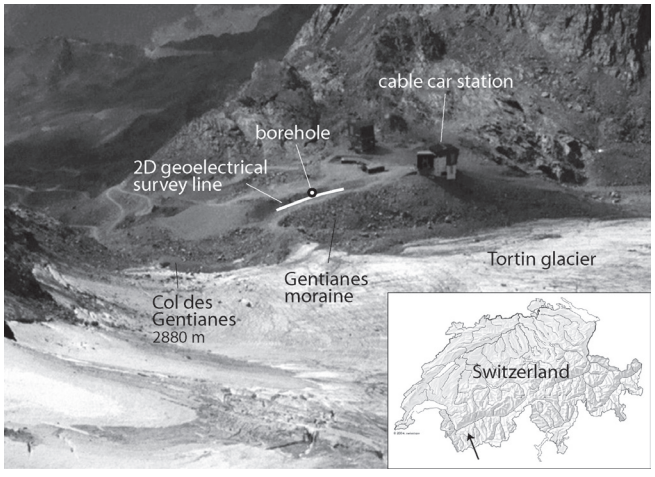

Figure 1. View of the Gentianes moraine with location of the borehole and of the 2-D geoelectrical survey line.

Results and Discussion

The first acquisition (13 Aug. 2007) reveals resistivities overall higher than 5 kΩm, with a clear increase towards the south (Fig. 3). Two lenses of higher resistivities (max. 150 kΩm) are clearly visible near the middle and in the south side of the profile. They probably correspond to massive ice lenses, like those which were observed in the excavation in October 2006. In the centre, resistivities are relatively low (<6 kΩm) below 10 m depth. However, the borehole, which is located near the center of the survey line, indicates negative temperatures throughout the first 20 m of the moraine. Thus, we can conclude that the frozen material is very little resistant in places. Such low resistivities may be explained by an increase of the specific surface. This implies that the deep layers would contain a high proportion of fine-grained sediments.

The second acquisition (23 Oct. 2007) shows a strong increase of the resistivities in the upper layers. The two resistant lenses are still visible, but the resistivities have been multiplied by 2 for the south lens and by 5 for the central one. In the northern half of the profile, at about 6 to 10 m depth, we can observe, on the contrary, a slight decrease of the resistivities.

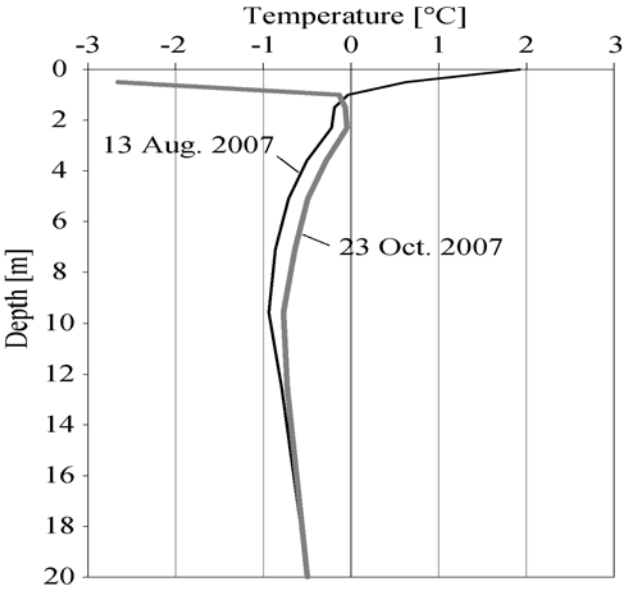

Figure 2. Thermal profiles of the moraine at the time of the two geoelectrical acquisitions.

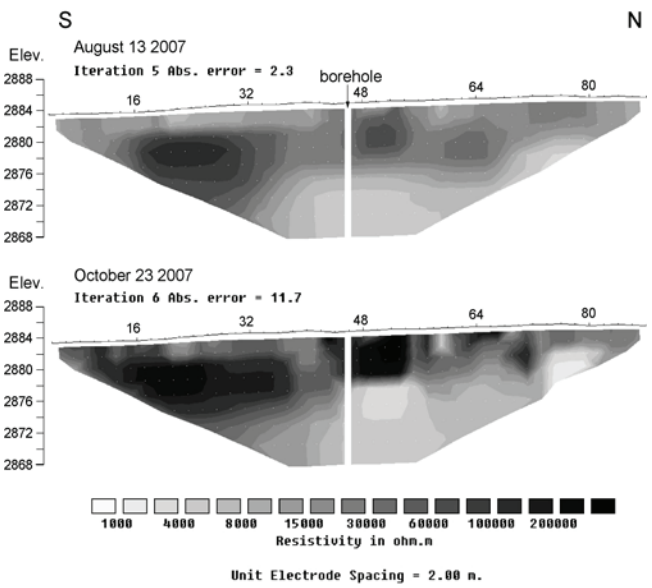

Figure 3. Two-dimensional resistivity profiles on 13 August and 23 October 2007 on the Col des Gentianes moraine.

Borehole data indicate warmer temperatures between 1 and 13 m depth in October than in August (Fig. 2). At the same time, we observe a strong increase in resistivities between the 2 acquisitions up to 6–10 m deep. Now, below 0°C, many studies reported that decreasing temperatures provoke increasing resistivities (e.g., Hauck 2001). Thus, the change in resistivities that we observe cannot be explained by a change in ground temperatures.

A hypothesis which could explain these different resistivities is the existence of 2 completely different climatic conditions during the 2 weeks preceding the 2 acquisitions. In August, the weather was very rainy, whereas October was dry and very cold at the acquisition time. As a consequence, the active layer was probably saturated with unfrozen water in August, whereas it was dry and frozen in October (Fig. 2). This led to higher resistivities at the subsurface. The strong increase in resistivities below the active layer is more difficult to understand, but we can assess that the difference in resistivity contact due to difference in surface humidity played an important role in the inversion process at greater depth.

According to the 2-D resistivity imaging, the ground stratigraphy is very heterogeneous. This is not surprising, insofar as a push moraine is often a complex landform incorporating, for instance, frozen sediments and sedimentary ice from the glacier. The presence of unfrozen lenses cannot then be excluded. Thus, it is possible that water could penetrate the deep layers during the rainy episode of August, which could have provoked lower resistivities.

Finally, the slight resistivity decrease at 6–10 m deep in the center of the profile may be explained by slight warming of the ground between the two acquisitions (Fig. 2).

Conclusion

The measurements show that the internal structure of the moraine is very heterogeneous. Massive ice lenses are probably present above 10 m depth. This assumption is supported by the observation of different ice types (sedimentary, congelation) in an excavation. An unexpected and strong increase in resistivities occurred in relatively deep layers between August and October. Totally different climatic conditions before the acquisitions and the influence of the first layer on the inversion process are probably the only way to explain such differences. However, further acquisitions and modeling of the first layer influence are necessary to validate this hypothesis.

References

Delaloye, R. 2004. *Contribution à l'étude du pergélisol de montagne en zone marginale*. Thèse. Fac. Sciences, Univ. Fribourg, Geofocus 10: 240 pp.

Haeberli, W. 1979. Holocene push-moraines in alpine permafrost. *Geografiska Annaler* 61A(1–2): 43-48.

Hauck, C. 2001. Geophysical methods for detecting permafrost in high mountains. *Mitteilungen der VAW, ETH Zürich,* 171.

Kneisel, C. 2004. New insights into mountain permafrost occurrence and characteristics in glacier forefields at high altitude through the application of 2-D resistivity imaging. *Permafrost and Periglacial Processes* 15: 221-227.

Lambiel, C. 2006. *Le pergélisol dans les terrains sédimentaires à forte déclivité: distribution, régime thermique et instabilités*. Thèse, Université de Lausanne, Institut de Géographie, coll. "Travaux et Recherches," n° 33: 260 pp.

Marescot, L., Loke, M.H., Chapellier, D., Delaloye, R., Lambiel, C. & Reynard, E. 2003. Assessing reliability of 2D resistivity imaging in mountain permafrost studies using the depth of investigation index method. *Near Surface Geophysics* 1: 57-67.

Reynard, E., Lambiel, C., Delaloye, R., Devaud, G., Baron, L., Chapellier, D., Marescot, L. & Monnet, R. 2003. Glacier/permafrost relationships in forefields of small glaciers (Swiss Alps). *Proceedings of the Eighth International Conference on Permafrost, Zürich, Switzerland, July 21–25, 2003*: 947-952.

Impacts of Small-Scale Surface Variations on the Energy Balance of Polygonal Tundra on Samoylov Island, Lena River Delta, Siberia

M. Langer
Alfred Wegener Institute for Polar and Marine Research, Potsdam, Germany
J. Boike
Alfred Wegener Institute for Polar and Marine Research, Potsdam, Germany
K. Piel
Alfred Wegener Institute for Polar and Marine Research, Potsdam, Germany
G. Stoof
Alfred Wegener Institute for Polar and Marine Research, Potsdam, Germany

Introduction

To quantify the magnitude of energy balance variations of a typical polygonal tundra system, two typical polygons at different succession stages were chosen for study. At each polygon site, surface characteristics were analyzed under the aspect of energy exchange processes. The focus rests upon the energy transfer processes due to the emission and absorption of radiation. The study is complemented through the analysis of soil heat fluxes and the corresponding thermal ground characteristics, such as soil heat capacity and conductivity.

Site Description

The investigated polygons have the following characteristics: The center of the first polygon consists of water-supersaturated peat. The groundwater level is at or just above the soil surface. The first polygon rim is elevated 10 cm above the water table. The uppermost soil layers consist of peat with high air content. The soil surface is covered by different moss types associated with dry conditions.

The polygonal crack is 10 cm wide and extends down to the ice wedge. The crack is filled with a combination of water and organic material of hydrophilic mosses.

The second polygonal rim consists of an elevated region and a lower transition zone towards the second polygon center. The soil in this elevated region still holds a considerable air fraction, but has an increased mineral fraction compared to the first polygonal rim. The transition zone shows increasing soil moisture toward the second polygon center. The second polygon center consists of water-saturated peat with the water table just underneath the ground surface. The second polygonal center is dominated by different hydrophilic mosses.

Methods

For detecting variations of the radiation balance, the investigated polygons were instrumented with a radiation scanner system bridging a 10 m transect. The scanner is capable of measuring reflected and emitted shortwave and longwave radiation at high spatial and temporal resolutions of 20 cm and 30 min, respectively.

The system consists of a photo pyranometer and an infrared sensor that were fixed on the scanner wagon 70 cm above the ground surface. An air temperature and relative humidity probe, as well as a photosynthetic active radiation sensor, were attached adjacent to the main sensors. Meteorological variables, such as incoming radiation, were measured at a climate tower located 5 m from the scanner system.

Soil heat fluxes were calculated based on temperature and moisture measurements directly beneath the soil surface at eight different locations along the scanner transect. Two-point temperature measurements were used for thermal diffusivity calculations based on a one-dimensional numerical solution of the heat transfer equation. Soil heat capacities were approximated based upon literature values of different soil types and soil moisture measurements.

Results

The scanner system directly provides surface temperatures and reflected solar radiation fluxes. By estimating surface emissivities, the surface temperatures can be transformed into emitted longwave radiation fluxes. The consistency of the data was controlled by comparing the spatial mean of the emitted and reflected radiation to the radiation measurements at the climate tower.

The scanner system was operated during periods of different weather conditions. The surface temperatures always varied significantly along the profile. At periods of high solar angles the surface temperatures of the dry rims are generally increased compared to the wet locations. During these time spans the polygonal rimes are about 5°C warmer than the wet polygonal centers. Less evident is the reverse situation that occurs during low sun positions, when the wet locations are slightly warmer than the dry polygonal rims. Observed temperature differences are about 3°C. The highest spatial temperature differences were observed during periods of clear sky conditions when radiative transfer is at a maximum.

The observed albedo values also display spatial variations corresponding to the different surface structures. The reflectivity at the rims is about 20% and about 15% at the polygonal centers. These observations are verified through spectrometer data. Instrumentation failures such as sensor

orientation may have strong effects on the measurements. These errors are magnified as measurements decrease in value. Therefore, reflectivity data at periods of low sun angles must be considered with caution. The approximated albedo values are based on midday observations, occurring around 12:00 (local time).

Soil heat flux measurements along the transect display marginal differences within the daily average. More significant are the differences in the diurnal heat flux amplitude, which varies about 10–20 W/m² among the particular locations. The polygonal centers and the crack display more pronounced heat flux amplitudes compared to the polygonal rims. This can be explained by differences in thermal diffusivity due to unlike soil moisture conditions. The varying heat capacities and conductivities lead to higher absorption and re-release of energy at the wet locations.

Discussion

The different surface temperatures indicate variations in the partition of the energy balance at the ground surface. This implies different contributions of sensible, latent, or ground heat fluxes. The results display only slight variations in ground heat fluxes among the different surface structures. Moreover, the comparatively small ground heat fluxes are of secondary importance within the complete energy balance. Thus, the energy partition at the ground surface primarily affects sensible and latent heat processes. Most likely at the dry polygon rims, more energy is available for sensible heat processes, while at the wet polygonal centers, the majority of radiation is consumed through the evapotranspiration process.

Non-Summer CO_2 Measurements Indicate Tundra Ecosystem Annual Net Source of Carbon Double Net Summer Sink

Cheryl Laskowski
San Diego State University, San Diego, CA, USA
George Burba
LiCor, Inc., Lincoln, NE, USA
Walter Oechel
San Diego State University, San Diego, CA, USA

Introduction

The Arctic tundra ecosystems are dominated by winter conditions, but data during the non-summer months is often lacking in Arctic annual carbon exchange estimates. The extreme conditions (temperatures regularly below freezing, low light levels, and snow-covered frozen ground) are often less than ideal for biological processes, and it has been largely assumed that little activity occurs under these conditions (McKane et al. 1997). While winter arctic conditions may not be ideal for high levels of photosynthesis and respiration, biological activity still occurs under snow and in subzero temperatures (Romanovsky & Osterkamp 2000, Sturm et al. 2005). Although there is substantial evidence showing the importance of non-summer periods to Arctic carbon metabolism, the difficulty of making ecosystem measurements under Arctic winter conditions means that estimates of carbon flux rates across the tundra are typically made based solely on summer (June–August) carbon flux data (Kwon et al. 2006, Vourlitis & Oechel 1999).

Annual estimates that ignore the non-summer period are likely to be largely in error with respect to the annual carbon balance (Oechel et al. 1997). Given that snowmelt is occurring earlier (Stone et al. 2002) and the growing season has lengthened (Chapman & Walsh 1993, Keyser et al. 2000), the traditional 10- to 12-week field campaign no longer encompasses even the full snow-free period. Prior attempts to predict annual carbon budgets based on winter field measurements have often lacked continuous monitoring throughout the year, relying on a few data points to model seasonal carbon estimates (Zimov et al. 1996, Oechel et al. 1997). Attempts at continuous monitoring (i.e., through the eddy covariance method) have had limited success while highlighting some of the major limitations. The limitations that have posed the greatest hindrance to continuous monitoring in the past are now diminishing, and include instrument icing (minimized by heaters), instrument operating limits (that have been recently modified to operate at very low temperatures), and mismatch between CO_2 flux estimates and ecological/biological theory (for which there is a new correction provided by Burba et al. 2006).

Methods

Direct and continuous measures of mass (water vapor and CO_2), momentum, and energy exchange were measured near the village of Atqasuk, Alaska, located 100 km south of Barrow, Alaska, during 2006. Net ecosystem exchange was measured using the open-path eddy covariance method and included an open-path infrared gas analyzer (IRGA, Li-7500, LiCor, Inc., Nebraska, USA) and ultrasonic anemometer (R3, Gill Instruments, Lymington, England).

Eddy covariance data were calculated in half-hour data series using the EdiRe program (University of Edinburgh, Edinburgh, England), and applying standard corrections for simultaneous latent and sensible heat measurements (Webb et al. 1980) and quality control techniques (AmeriFlux 2006). Data gaps were filled using techniques outlined in Falge et al. (2001) to represent seasonal/annual carbon exchange estimates. In addition, the data are corrected for an apparent-uptake signal due to heating of the air mass in the absorption path of the IRGA. The correction is modified from Burba et al. 2006, to account for non-vertical sensor mounting angle.

Results

Weather conditions during 2006 were typical of historic climate averages for Atqasuk, Alaska, with July as the warmest month of the year and March, the coldest month (air temperatures of 8.2°C and -29.8°C, respectively). Eddy covariance data availability varied greatly, from a low of 14% in February to a high of 80% in June. Average summer (June–August) data recovery was 71%, and data were primarily rejected due to precipitation events. Average non-summer (September–May) data recovery was 36%, and data loss was mainly due to icing events and conditions outside of the instruments' operating specifications.

Summer carbon flux data showed a distinct diurnal pattern characterized by a midday CO_2 drawdown and slight mid-night release, with the pattern being strongly temperature- and light-dependent. Non-summer diurnal patterns were not evident, due to the lack of intense solar radiation during much of the season.

Cumulative carbon exchange during the summer months resulted in a net uptake of 21.5 g C m^{-2}, whereas the cumulative non-summer carbon exchange showed a net loss of 53.5 g C m^{-2}. This resulted in an annual carbon release of 31.8 g C m^{-2} to the atmosphere (Fig. 1).

Discussion

The results show that non-summer season carbon exchange is not only significant, it can be of greater cumulative magnitude than summer carbon exchange—in this case,

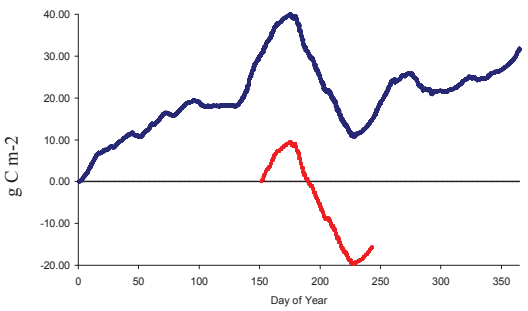

Figure 1. Cumulative carbon exchange for Atqasuk, Alaska, 2006, in g C m^{-2}. Line from day of year 0–365 represents the cumulative annual carbon exchange, while the line from day of year 152–243 (June–August) represents the summer-only cumulatie carbon exchange.

nearly 2.5 times the summer estimate. This also emphasizes the importance of year-round estimates in determining source versus sink activity. Capturing only summer-season carbon exchange would result in a net uptake of carbon rather than a net release. These results indicate that not only is winter carbon emission for tundra ecosystems important in annual carbon estimates, it dominates the annual signal, shifting the net carbon exchange from a sink to a source.

Disproportionately more data were rejected or lost in non-summer months, primarily due to instrument icing. This results in higher uncertainty of non-summer data compared to summer data. Reducing data loss by using heaters or increased site visits may lessen data loss. In addition, the correction factor (Burba et al. 2006) used in this study must be further tested to verify the accuracy of the correction parameters. These features are currently being implemented at this and other sites. However, these data are, to our knowledge, the first near-continuous carbon exchange data for Alaskan Arctic tundra, and provide evidence that not only is the non-summer season important, it may in fact be dominant over summer season net carbon exchange.

Acknowledgments

We would like thank D. Whiteman, R. Bryan, S. Delapena, N. Panzarini, A. Sharma, BASC, VPR, NSB, and NSF's Study of the Northern Alaskan Coastal System's research grant number 046177.

References

Burba, G.G., Anderson, D.J., Xu, L. & McDermitt, D.K. 2006. Additional term in the Webb-Pearman-Leuning correction due to surface heating from an open-path gas analyzer. *Eos Trans. AGU* 87(52), Fall Meet. Suppl., C12A-03.

Chapman, W.L. & Walsh, J.E. 1993. Recent variations of sea ice and air-temperature in high-latitudes. *Bulletin of the American Meteorological Society* 74(1): 33-47.

Falge, E. et al. 2001. Gap filling strategies for long term energy flux data sets. *Agricultural and Forest Meteorology* 107(1): 71-77.

Kappen, L. 1993. Plant activity under snow and ice, with particular reference to lichens. *Arctic* 46(4): 297-302.

Kwon, H.J. et al. 2006. Effects of climate variability on carbon sequestration among adjacent wet sedge tundra and moist tussock tundra ecosystems. *Journal of Geophysical Research-Biogeosciences* 111(G3).

McKane, R.B. et al. 1997. Climatic effects on tundra carbon storage inferred from experimental data and a model. *Ecology* 78(4): 1170-1187.

Oechel, W.C. et al. 1997. Cold season CO_2 emission from arctic soils. *Global Biogeochemical Cycles* 11(2): 163-172.

Romanovsky, V.E. & Osterkamp, T.E. 2000. Effects of unfrozen water on heat and mass transport processes in the active layer and permafrost. *Permafrost and Periglacial Processes* 11(3): 219-239.

Stone, R.S. et al. 2002. Earlier spring snowmelt in northern Alaska as an indicator of climate change. *Journal of Geophysical Research-Atmospheres* 107(D10).

Sturm, M. et al. 2005. Winter biological processes could help convert arctic tundra to shrubland. *Bioscience* 55(1): 17-26.

Vourlitis, G.L. & Oechel, W.C. 1999. Eddy covariance measurements of CO_2 and energy fluxes of an Alaskan tussock tundra ecosystem. *Ecology* 80(2): 686-701.

Webb, E.K. et al. 1980. Correction of flux measurements for density effects due to heat and water-vapor transfer. *Quarterly Journal of the Royal Meteorological Society* 106(447): 85-100.

Zimov, S.A. et al. 1996. Siberian CO_2 efflux in winter as a CO_2 source and cause of seasonality in atmospheric CO_2. *Climatic Change* 33(1): 111-120.

Accelerated Arctic Land Warming and Permafrost Degradation During Rapid Sea Ice Loss

David M. Lawrence
National Center for Atmospheric Research, Boulder, CO, USA
Andrew G. Slater
Cooperative Institute for Research in the Environmental Sciences, Boulder, CO, USA
Robert A. Tomas, Marika M. Holland, Clara Deser
National Center for Atmospheric Research, Boulder, CO, USA

Introduction

In September 2007, the annual minimum sea ice extent shattered the previous observational-record low. CRUTEM3 data indicate that 2007 August to October western Arctic land temperatures were the warmest of the last 30 years (+2.3°C warmer than the 1978 to 2006 average). The striking sea ice decline in 2007 raises the specter that a period of abrupt sea ice loss, such as those simulated in Community Climate System Model (CCSM3) 21st century A1B simulations (Holland et al. 2006), is a distinct possibility. Rapid sea ice loss events (RILEs) in CCSM3 typically last between 5 and 10 years and exhibit negative sea ice extent trends that are roughly 4 times larger than average simulated (or recently observed) trends.

Whether or not the 2007 sea ice record minimum is a precursor of a sustained period of rapid loss remains to be seen, but it provides motivation to assess the potential consequence for adjacent land climate. Here, we evaluate Arctic land temperature response to RILEs in CCSM3. We find that the secular 21st century land-warming trend is augmented by a factor of 3.5 during RILEs, which is likely to have adverse impacts on permafrost. Through idealized experiments with the Community Land Model (CLM), we assess the impact of a RILE and its timing on permafrost. The results presented here are excerpted from Lawrence et al. (2008).

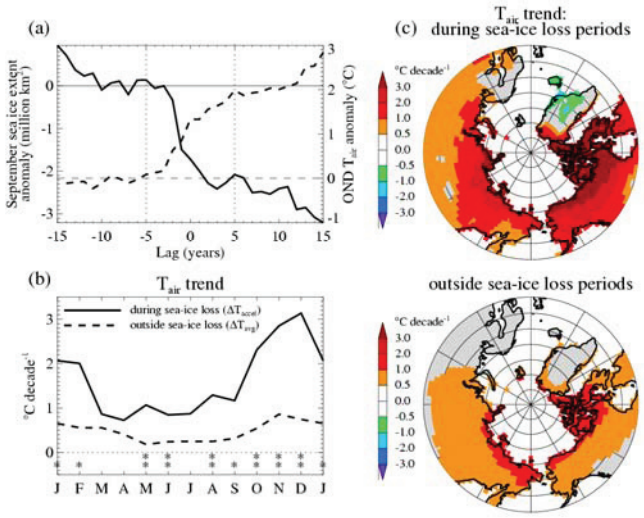

Figure 1. (a) Composite lagged time series of September sea ice extent (solid line) and OND T_{air} (dashed line) over Arctic land area (65°–80°N, 60°–300°E). Composites are centered around the mid-points of the nine rapid sea ice loss events seen in the CCSM3 A1B simulations. Results shown as anomalies from the average of years -10 to -5. (b) Average monthly Arctic land air temperature trends during rapid sea ice loss periods and outside sea ice loss periods. Trend is statistically significant at the 90% (*) and 95% (**) levels. (c) Maps of air temperature trends for OND during and outside abrupt sea ice loss periods.

Arctic Land Temperature Trends During Rapid Sea Ice Loss

Nine RILEs are identified across the eight-member CCSM3 A1B 21st century ensemble (Holland et al. 2006b). By computing a lagged composite of sea ice extent anomalies across the nine events, we form a picture of the typical sea ice extent trajectory during abrupt loss periods (Fig. 1a). A corresponding composite for western Arctic October to December (OND) land T_{air} shows an increase in warming during RILEs (Fig. 1a). Figure 1b shows the western Arctic linear T_{air} trend during and outside RILEs. Warming is accelerated during RILEs throughout most of the year with statistically significant increases in warming rates apparent in the summer and early autumn, likely due to increased open water area, as well as in late autumn and winter, when the thinner ice pack less efficiently insulates the atmosphere from the comparatively warm ocean water below. Accelerated warming spans most of the terrestrial western Arctic juxtaposed to the area of sea ice contraction in CCSM3. It is strongest along the Arctic coast where it is as high as 5°C decade^{-1} in the autumn, but a signal of enhanced warming can extend 1500 km inland (Fig. 1c). Annually averaged, the warming trend during RILEs is 3.5 times greater than outside these periods (1.60°C decade^{-1} versus 0.46°C decade^{-1}).

Impact of Accelerated Warming on Permafrost

To evaluate the impact of abrupt warming and its timing on permafrost, we construct four synthetic trend scenarios based on the results shown in Figure 1. We then use these scenarios to force a version of CLM (Oleson et al. 2004) that includes some improvements in permafrost dynamics, namely explicit representation of the thermal and hydrologic properties of organic soil (Lawrence & Slater 2007) and a 50 m soil column that represents thermal inertia provided by deep ground (Lawrence et al. 2008).

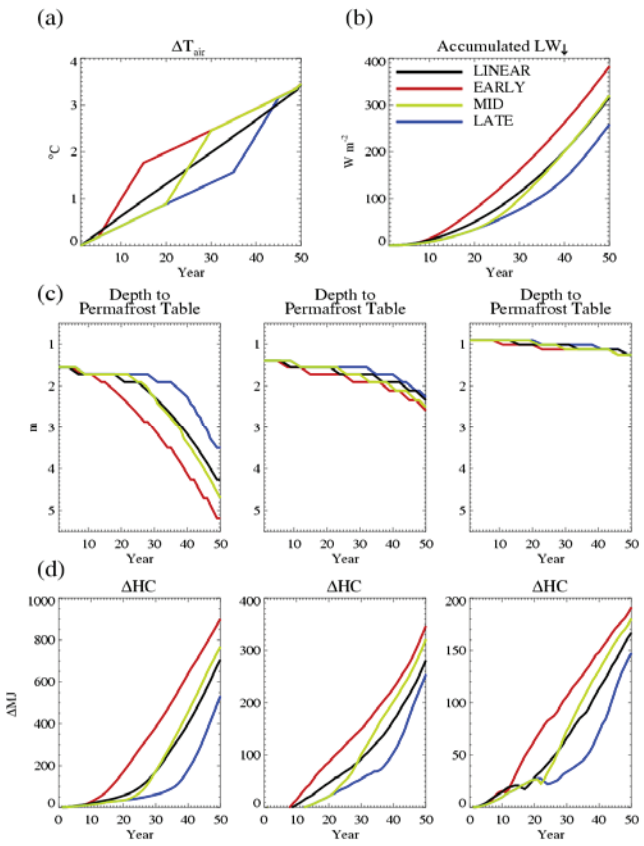

Figure 2. (a) Annual mean T_{air} anomaly time series for the four experiments. Note that monthly air temperature anomalies used in the forced experiments contain the annual cycle structure shown in Fig. 1c. (b) Accumulated LW↓ anomaly time series. (c) Depth to permafrost table (DPT). (d) Change in soil heat content (ΔSHC) for three different initial permafrost states; $\overline{T_{soil}(PT, y=1)}$ = -0.3°C, -1.5°C, and -5.8°C from left to right.

The impact of accelerated warming is shown for three illustrative ground conditions representing differing initial permafrost states (warm to cold) (Figs. 2c and 3d). These cases all exhibit minimal snow depth change (< 10%) over the 50-yr simulation. For initially cold permafrost, the timing of accelerated warming has little influence on the rate of active layer deepening. All four scenarios simulate an ~0.35m deepening of the active layer (Table 1). However, the soil heat content (SHC) gained in EARLY (191 MJ m^{-2}) is 30% larger than in LATE (147 MJ m^{-2}). The additional heat gained in EARLY corresponds to +0.41°C more warming over the 50 m column. The increase in heat accumulation preconditions permafrost for earlier and/or more rapid degradation under continued warming.

For warm permafrost, the timing of accelerated warming has a more dramatic influence. In all four scenarios, DPT increases slowly at first, but accelerates rapidly once a layer of perpetually unfrozen ground forms above the permafrost table (talik) at ~2 m depth. This occurs much sooner in EARLY with accelerated warming instigating talik formation by year 12. By year 50, the warm permafrost soil column in EARLY has absorbed 900 MJ m^{-2}, 68% more than LATE,

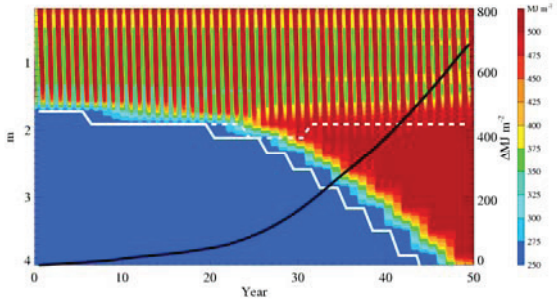

Figure 3. Time series of depth of warming (white solid line) and cooling (white dashed line) fronts from LINEAR experiment for warm permafrost case. Contours indicate SHC. Change in SHC is shown as black line.

and the DPT is 3.6 m deeper compared to only 1.9 m deeper in LATE. Why does talik formation coincide with a strong increase in SHC accumulation rates? Taliks form when the downwelling summer heating wave extends deeper than the corresponding winter cooling wave, thereby preventing the talik from refreezing in winter. Near isothermal soil layers at 0°C beneath the talik also limit cooling from below. At this point, with continued warming, heat accumulates at the maximum depth of the heating wave and permafrost degrades rapidly (Fig. 3).

References

Holland, M.M., Bitz, C.M. & Tremblay, B. 2006. Future abrupt reductions in the summer Arctic sea ice, *Geophys. Res. Lett*. 33: L23503, doi:10.1029/2006GL028024.

Lawrence, D.M., & Slater, A.G. 2007. Incorporating organic soil into a global climate model. *Clim. Dyn.*: doi:10.1007/s00382-007-0278-1.

Lawrence, D.M., Slater, A.G., Romanovsky, V.E. & Nicolsky, D.J. 2008. The sensitivity of a model projection of near-surface permafrost degradation to soil column depth and representation of soil organic matter. *JGR-Earth Surface* (in press).

Lawrence, D.M., Slater, A.G., Tomas, R.A., Holland, M.M. & Deser, C. 2008. Accelerated Arctic land warming and permafrost degradation during rapid sea ice loss. *Geophys. Res. Lett*. (submitted).

Oleson, K.W. et al. 2004. *Technical description of the Community Land Model (CLM)*. NCAR Tech. Note TN-461+STR, 174 pp.

The Sensitivity of a Model Projection of Near-Surface Permafrost Degradation to Soil Column Depth and Representation of Soil Organic Matter

David M. Lawrence
National Center for Atmospheric Research, Boulder, CO, USA
Andrew G. Slater
Cooperative Institute for Research in the Environmental Sciences, Boulder, CO, USA
Vladimir Romanovsky
University of Alaska Fairbanks, AK, USA
Dmitry Nicolsky
University of Alaska Fairbanks, AK, USA

Introduction

Coupled global climate models (GCMs) are advancing to the point that many of the biogeophysical, biogeochemical, and hydrological interactions and feedbacks that are directly or indirectly related to permafrost degradation are or will soon be captured. Here, we describe and analyze improvements in the depiction of permafrost in the Community Land Model (CLM), CLM is the global land-surface scheme that is included in the Community Climate System Model (CCSM). These improvements to CLM represent another step towards a more complete depiction of the integrated Arctic processes in a global modeling system.

In Lawrence and Slater (2005), we presented data from CCSM3 simulations indicating that the extent of near-surface permafrost may contract substantially during the 21st century as arctic temperatures soar. Here, we examine the sensitivity of these near-surface permafrost degradation projections to the incorporation of a deeper soil column and the explicit treatment of the thermal and hydrologic properties of soil organic matter. The results presented here are excerpted from our recently published study (Lawrence et al. 2008).

Model

CLM (for a detailed technical description see Oleson et al. 2004) can be run in both offline mode or as a component of CCSM. The land surface is represented by fractional coverage of lakes, wetland, bare soil, glacier, and up to four plant functional types (PFT) for each grid box. Processes simulated by CLM include heat transfer in soil and snow, hydrology of canopy, soil, and snow, and stomatal physiology and photosynthesis. Fluxes of energy and moisture are modeled independently for each surface type and aggregated before being passed to the atmosphere model. CLM3 includes a five-layer snow model which simulates processes such as accumulation, melt, compaction, snow aging, and water transfer across layers. Simulations with the standard version of CLM are referred to as CONTROL.

Organic soil

Nicolsky et al. (2007) show that accounting for the physical properties of soil organic matter significantly improves soil temperature simulations. In Lawrence and Slater (2007), we describe how organic soil and its impact on soil thermal and hydraulic properties can be implemented into CLM. Briefly, a geographically distributed and profiled soil carbon density dataset for CLM is derived by taking the gridded Global Soil Data Task soil carbon content dataset and distributing the carbon content for each grid box vertically through the CLM This dataset is then used to calculate the organic soil or mixed organic and mineral soil thermal and hydrologic properties for each soil layer. Simulations using this organic matter dataset along with the revised parameterizations are referred to as SOILCARB.

Deep soil

Alexeev et al. (2007) demonstrate that the depth of the bottom boundary condition strongly influences seasonal and longer time-scale soil temperature dynamics. Soil depths of greater than 30 m are preferred to reasonably simulate the annual cycle and decadal trends of subsurface temperatures. We test CLM with soil depths ranging from 25 m to 125 m by adding from 4 to 7 exponentially thicker layers to the original 10 level soil model. Experiments with a deep soil configuration (and organic matter) are referred to as SOILCARB_DS50 and SOILCARB_DS125.

Results

Figure 1 shows annual cycle-depth temperature plots for CONTROL, SOILCARB, and SOILCARB_DS50 compared to observed annual cycle-depth temperatures. The broad qualitative improvements in the simulation are immediately apparent. The active layer thickness (ALT), defined as the depth to which the soil thaws each summer, is much shallower in SOILCARB and SOILCARB_DS50, and its level is in much closer agreement with observations. Soil temperatures below the active layer are also improved, especially in SOILCARB_DS50, where the removal of the zero flux boundary at 3.5 m results in smaller and more realistic seasonal temperature variations at depths below 2 m.

We then force the improved CLM with 6-hourly data from a fully coupled CCSM3 20th and 21st century simulation. The resulting time series of near-surface permafrost extent are shown in Figure 2 for the CONTROL, SOILCARB, SOILCARB_DS50, and SOILCARB_DS125 experiments.

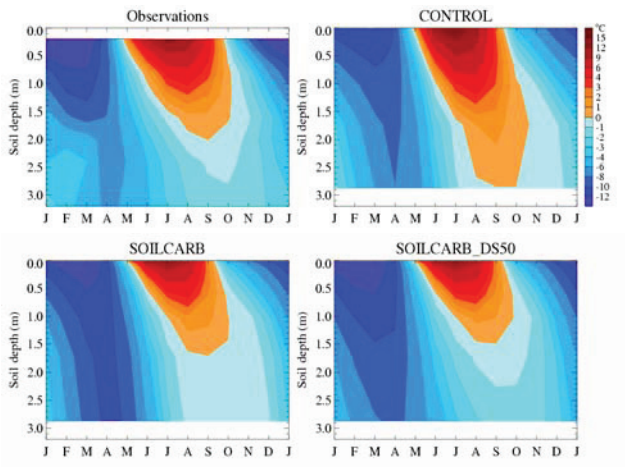

Figure 1. Annual cycle-depth plots of soil temperature averaged for selected stations in Russian soil temperature dataset (Zhang et al. 2001). Stations include those that exhibit perpetually frozen soil in top 3 m. Equivalent locations extracted and averaged over the same time period from offline CLM simulations forced with observed data.

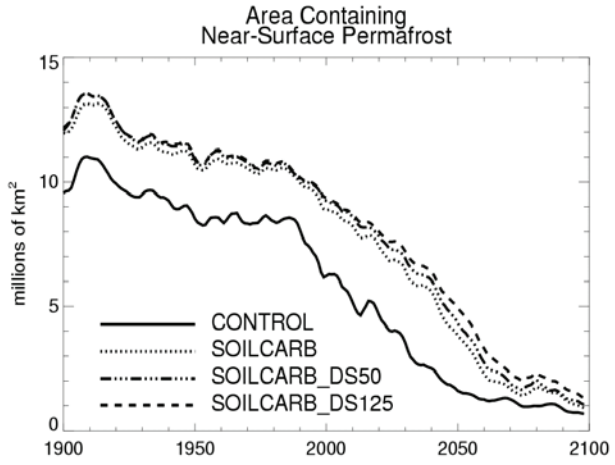

Figure 2. Time series of total area containing near-surface permafrost (north of 45°N and excluding ground underneath glaciers) for selected experiments.

$CONTROL_{CCSM3}$ and $CONTROL_{CLM3}$ are not shown for the sake of clarity, but lie roughly in between the curves for CONTROL and SOILCARB. As noted above, experiments that include soil organic matter are substantially cooler, and near-surface permafrost extent is correspondingly broader. The observed estimates for the area of continuous permafrost (90–100% coverage) and discontinuous permafrost (50–90% coverage) combined are 11.2–13.5 million km^2 (for the region poleward of 45°N (Zhang et al. 2000). The total area simulated in CONTROL is clearly biased low at 8.5 million km^2. In the organic soil and deeper soil column experiments, the area with near-surface permafrost increases to 10.5 and 10.7 million km^2, respectively, which compares reasonably with the observed permafrost extent although still biased a little low.

The rate of near-surface permafrost extent contraction is slower between 1990 and 2040 in SOILCARB (87,000 km^2 yr^{-1} versus 111,000 km^2 yr^{-1} in SOILCARB and CONTROL, respectively). In simulations with a deeper soil column, the average rate of loss decreases further to 81,000 km^2 yr^{-1} and 76,000 km^2 yr^{-1} (1990–2040) in SOILCARB_DS50 and SOILCARB_DS125. However, even though near-surface permafrost degrades at a slower rate in the latter three experiments, the total degradation by 2100 is almost as extensive as that seen in CONTROL.

Although much of the simulated near-surface permafrost degrades in all experiments, it should be stressed that this does not mean that all permafrost disappears. As noted above, each grid box is represented by a single soil column which means that sporadic and isolated permafrost cannot be explicitly detected in the model. For regions where the maximum soil temperature rises above 0°C, but only marginally, it can be assumed that sporadic or isolated patches of permafrost would still be present in the warmer climate. Additionally, for the deep soil experiments, we find that most of the deep permafrost remains at the end of the 21st century.

References

Alexeev, V.A., Nicolsky, D.J., Romanovsky, V.E. & Lawrence, D.M. 2007. An evaluation of deep soil configurations in the CLM3 for improved representation of permafrost. *Geophys. Res. Lett.* 34: L09502, doi:10.1029/2007GL029536.

Lawrence, D.M. & Slater, A.G. 2005. A projection of severe near-surface permafrost degradation during the 21st century. *Geophys. Res. Lett.* 24: L24401, doi:10.1029/2005GL025080.

Lawrence, D.M. & Slater A.G. 2007. Incorporating organic soil into a global climate model, *Clim. Dyn.* doi:10.1007/s00382-007-0278-1.

Lawrence, D.M., Slater, A.G., Romanovsky, V.E. & Nicolsky, D.J. 2008. The sensitivity of a model projection of near-surface permafrost degradation to soil column depth and representation of soil organic matter. *JGR-Earth Surface* (in press).

Nicolsky, D.J., Romanovsky, V.E., Alexeev, V.A. & Lawrence, D.M. 2007. Improved modeling of permafrost dynamics in a GCM land-surface scheme, *Geophys. Res. Lett*. 34: L08501, doi:10.1029/2007GL029525.

Oleson, K.W. et al. 2004. *Technical description of the Community Land Model (CLM)*. NCAR Tech. Note TN-461+STR, 174 pp.

The Influence of Snowdrift on the Geothermal Field of Permafrost: Results from Three-Dimensional Numerical Simulations at a Local Scale

Anne-Marie LeBlanc
Centre d'études nordiques, Université Laval, Québec (QC), Canada
Richard Fortier
Centre d'études nordiques, Université Laval, Québec (QC), Canada
Michel Allard
Centre d'études nordiques, Université Laval, Québec (QC), Canada
René Therrien
Département de géologie et de génie géologique, Université Laval, Québec (QC), Canada

Introduction

Three-dimensional (3-D) numerical simulations of the thermal regime of permafrost were carried out to study the effect of thermal insulation of snow and the impacts of climate warming on the permafrost evolution. The thermal regime of permafrost is closely related to not only the climate variability but also the surface conditions controlling the heat exchange between the ground and the air. Among the parameters affecting the surface conditions, the snow cover is probably the most important because it is recognized as a good thermal insulator preventing the ground cooling in winter (Goodrich 1982). The spatial distribution of snow at a local scale depends on the snow falls, prevailing winds, vegetation, changes in topography, obstacles, and snow removal. While open areas prone to strong winds are characterized by thin snow cover, snowdrifts form in the areas protected from the wind transport and erosion such as depressions, thick embankments, and tall infrastructures. Since the spatial distribution of snowdrifts is highly variable at a local scale, the influence of snowdrifts on the geothermal field of permafrost only can be modeled using 3-D numerical simulation.

Study Site

The Inuit community of Salluit (62°12′N, 75°40′W) is located in the continuous permafrost zone along the southern shore of Hudson Strait, in Nunavik, Canada. The village lies in a valley, and most infrastructures are built on ice-rich marine sediments.

3-D Numerical Simulation

A 3-D finite-element heat conduction model taking into account the phase change was developed to predict the geothermal field of permafrost in the valley of Salluit. The Quaternary deposits and permafrost conditions in the valley were mapped at a scale of 1:2000. These deposits were then divided into 52 vertical layers, with layer thickness increasing from 0.2 m near the surface up to 5 m at a depth of 100 m. The element side varied from 2 to 50 m according to the dimensions of the surface conditions to be simulated. Thermal properties were then given at each voxel of the 3-D model according to the previous mapping. The lower boundary condition at a depth of 100 m corresponded to the geothermal heat flux of 0.03 W/m^2 measured in a deep borehole in the Katinniq plateau, 150 km southeast of Salluit. The complex heat transfer function between the air and the ground was simulated using simultaneous recordings of air and ground surface temperatures at various locations in the valley during two consecutive years. Mean monthly air temperatures from the Canadian Regional Climate Model (Music & Caya 2007) were used to drive the simulations from 1961 to 2100 according to the SRES A2 scenario (IPCC 2000).

Results

Figure 1 shows the predicted mean monthly ground surface temperatures (MMGST) beneath a snowdrift from October 2002 to September 2003 in close match with the observed MMGST at the same location over the same period. The predicted MMGST at this location for the year 2099–2100 is also given in Figure 1. According to SRES A2 scenario, the increase in air temperature of 6ºC over one century, from 2002–2003 to 2099–2100, will shorten the winter period of at least two months. The ground surface will be still snow free in October 2099, and the snowmelt will take place in May 2100; one month earlier than in 2003. The method for predicting the MMGST was based on the assumption that there is no interannual variability in snow thickness and spatial distribution of snow. In the case of a windy environment such as Salluit, this assumption is valid. Even if the variation in snow height was not simulated, the long-term modification in MMGST is similar to the results of the SNOWPACK model presented in Luetschg et al. (2003).

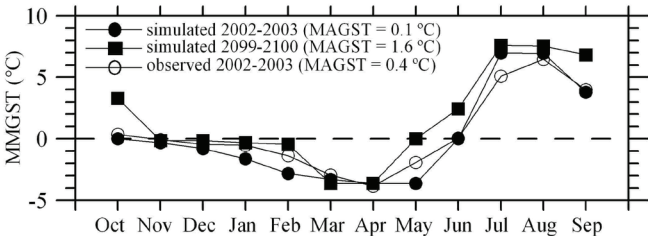

Figure 1. Observed and simulated mean monthly ground surface temperatures (MMGST) beneath a snowdrift.

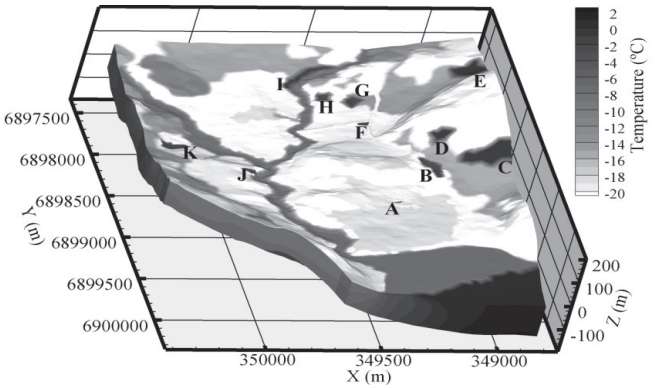

Figure 2. 3-D geothermal model. Snowdrifts *A* to *K*.

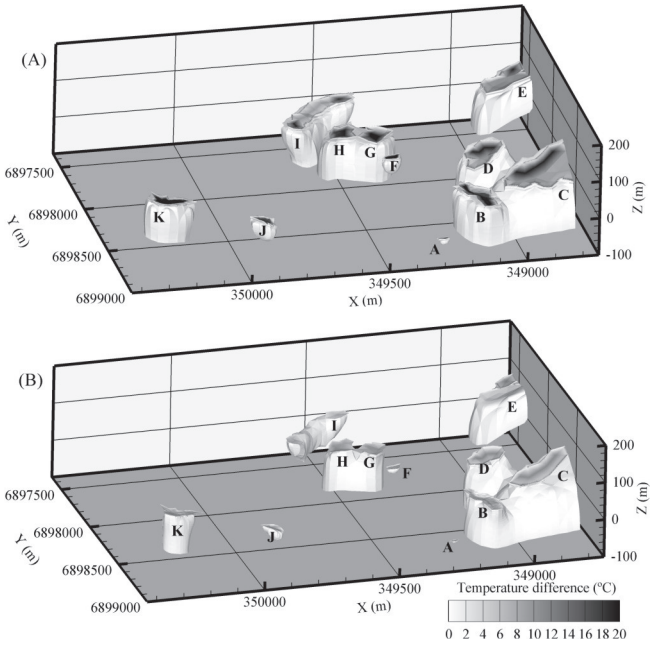

Figure 3. Ground temperature difference between the simulations with snowdrift surface conditions and the bare surface: (A) In January 2005; (B) In January 2100.

The 3-D geothermal model for the month of January 2005 in the valley of Salluit is shown in Figure 2. Among the snowdrifts mapped in the valley, 11 were integrated in the model. They are identified with letters from A to K in Figure 2.

Several numerical simulations were performed for assessing the thermal effect of snowdrifts. The ground temperature difference between the simulations integrating the snowdrift surface conditions and without integrating these conditions is shown in Figures 3a and 3b in January 2005 and 2100, respectively. Ground temperature differences below the cutoff value of 0.5 C are not shown. In 2005, the thermal effect of snow insulation on ground temperatures can reach depths as high as 100 m except for the snowdrifts *A* (16 m), *F* (42 m) and *J* (56 m). The surface area of snowdrift *A* is small, restricting the depth of snow influence on ground temperatures. For similar snowdrift surface area, till and sand transmit the heat more efficiently than clay due to their higher thermal conductivity and their lower water content. The thermal effect of snow on ground temperatures

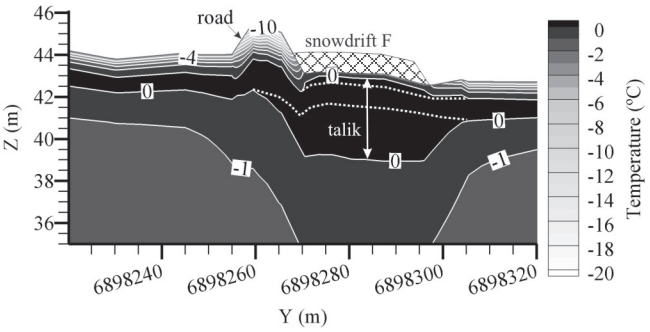

Figure 4. 2-D section of predicted ground temperatures underneath a road embankment and a thick snowdrift in January 2100. The dotted lines are the ground temperatures for a thin snow cover.

is limited, therefore, under the snowdrifts *F* and *J* compared to snowdrift *H* (Fig. 3a) due to the difference in soil types. In 2100, the climate warming will lead to a reduction in temperature difference at the surface: 10°C (Fig. 3b) instead of 20°C (Fig. 3a). The ground volume affected by the snowdrifts will also decrease. In a context of climate warming, the ground temperatures affected by a thin snow cover or under bare surface conditions will increase faster than the ground temperatures beneath snowdrifts.

A 2-D section of predicted ground temperatures underneath a road embankment and a thick snowdrift lying on the right embankment shoulder is shown in Figure 4 to illustrate the major thermal effect of snowdrift. A 4 m thick talik is present beneath the snowdrift, while the talik is only 1 m when considering a thin snow cover (dotted lines). The thermal effect of the snowdrift propagates also underneath the road embankment, inducing a ground warming. However, no attempt was made to take into account the water migration at shallow depths and to accommodate thaw settlement. These two factors can influence the geothermal field of permafrost.

References

Goodrich, L.E. 1982. The influence of snow cover on the ground thermal regime. *Canadian Geotechnical Journal* 19: 421-432.

IPCC 2000. *Special Report on Emission Scenarios*. N. Nakicenovic & R. Swart (eds.). UK: Cambridge University Press, 570 pp.

Luetschg, M., Bartelt, P., Lehning, M. & Toeckli, V. 2003. Numerical simulation of the interaction processes between snow cover and alpine permafrost. *Proceedings of the Eighth International Conference on Permafrost*, *Zurich, Switzerland*: 697-702.

Music, B. & Caya, D. 2007. Evaluation of the hydrological cycle over the Mississippi river basin as simulated by the Canadian Regional Climate Model. *Journal of Hydrometeorology* 8(5): 969-988.

Spatial Variation in CO_2 Release from Arctic Tundra as a Result of Permafrost Thawing and Thermokarst Development

Hanna Lee
Department of Botany, University of Florida, Gainesville, FL 32601-8526, USA
Edward A.G. Schuur
Department of Botany, University of Florida, Gainesville, FL 32601-8526, USA
Jason G. Vogel
Department of Botany, University of Florida, Gainesville, FL 32601-8526, USA

Introduction

One of the biggest potential feedbacks to global climate change from high latitude ecosystems may come from thawing of permafrost, which stores 30% of the total global terrestrial soil organic carbon (SOC) (Gorham 1991). Permafrost thawing may accelerate decomposition of soil organic matter (SOM) and increase carbon dioxide (CO_2) emissions, which could lead to further climatic warming (Oechel et al. 2000). In particular, thermokarst formation in response to permafrost thawing could change C cycling in high latitude ecosystems beyond simple increases in temperature because it has unique effects on soil conditions.

When permafrost thaws and drains in ice-rich areas, it creates localized surface subsidence called thermokarst (Jorgenson et al. 2001). The changes in the ground surface topography can induce variations in soil properties such as soil temperature, moisture content, and nutrient availability (Chapin et al. 2000). Our objective was to determine how permafrost thawing and thermokarst development affect SOM decomposition and ecosystem C exchange. We hypothesized that there will be a positive relationship between the degree of ground subsidence and CO_2 emissions from SOM.

Materials and Methods

Field site

This study was established at the Eight Mile Lake (EML) tundra site located 5 miles outside of Denali National Park. Previous work by Osterkamp and Romanovsky (1999) monitored deep soil temperatures at this site to 27 m belowground for the previous two decades and observed increased permafrost temperatures and thermokarst development (Osterkamp 2007).

Three sites were established at EML as an observational natural gradient study based on the degree of thermokarst development. The observed gradient was divided into three categories: Minimal Thaw, where typical tussock tundra appears least disturbed; Moderate Thaw, where thermokarst development started about 20 years ago; and Severe Thaw, where there were significant surface depressions. Based on 1951 aerial photographs, thermokarst development at Severe Thaw was estimated to be present for at least 50 years (Schuur et al. 2007).

Defining microtopography

We defined the degrees and patterns of depression created by thermokarst using a topographic survey. Twelve transects were established within a 50 m × 50 m plot at each of the three sites, and 600 (±50) points were surveyed. The major independent variable was elevation representing variation in microtopography created by thermokarst; lower surfaces represent subsidence by thermokarst development.

Establishing the plots

A 50 × 25 m subplot was established within the surveyed area at each site. In each plot, 50 equally spaced points were selected and surveyed again with a fine-scale GPS (Trimble 5700) unit within the plot to relate microtopography to soil temperature, moisture, active layer thickness, ecosystem respiration, and photosynthesis.

Soil properties

Soil temperature, volumetric water content (VWC), and active layer thickness were measured across the sites. A handheld soil temperature probe was used to measure soil temperature at 10, 20, and 30 cm during the growing season. VWC was measured at 10 and 20 cm belowground using a soil moisture reflectometer (Campbell Scientific CS616), and a 1/8 inch rod was used as a depth probe to measure active layer thickness.

Carbon emissions

CO_2 flux was quantified 4 times during the summer of 2006 and 2007 at the peak of the growing season to measure net ecosystem exchange of carbon using an IRGA (infrared gas analyzer, LiCOR820) attached to a 40 × 40 × 40 cm plastic chamber. Both dark CO_2 chamber measurement and light measurement were taken covered with a reflecting cloth, completely intercepting light and uncovering the chamber. Dark measurements estimate the rate of carbon emissions from ecosystem respiration, whereas light measurements estimate carbon emissions from ecosystem respiration as well as carbon uptake by photosynthesis. Differences between light and dark measurement served as an estimate of photosynthesis.

Analyses

To compare the effects of microtopography among sites, the plot level elevations were normalized to relative values within each site and semivariograms and correlograms were calculated to mathematically define the surface structure. A multiple regression with stepwise selection was used to obtain the best relationship between microtopography and measured soil and ecosystem properties.

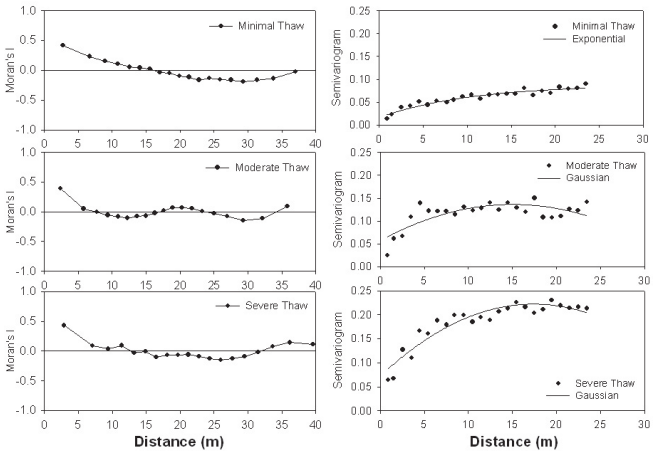

Figure 1. Semivariogram and correlogram of microtopography of the three sites in EML. Semivariograms show autocorrelation of microtopography as a function of distance. Minimal Thaw site has homogeneous surface; Moderate Thaw site has patchy depression within the thermokarst; and Severe Thaw site has large scale depression and is heterogeneous.

Results

Microtopographic patterns

Our semivariogram and correlogram results show that Minimal Thaw site has the most uniform surface pattern of all 3 sites. There are patchy depressions within Moderate Thaw site, while Severe Thaw site shows large-scale heterogeneous depressions that are not autocorrelated over 15 m (Fig. 1).

Soil properties

All of the measured soil properties were significantly correlated to topographic patterns, except for soil temperature due to a measurement error. Among the soil property measurements, VWC showed the strongest relationship with topographic patterns ($p < 0.008$) for all three sites, implying that soil moisture conditions changed the most due to thermokarst development (Table 1).

Carbon emissions

Multiple regression analyses (Fig. 2) showed a negative correlation between ecosystem respiration and micro-topography at Severe and Minimal Thaw sites. Among the environmental variables, the best predictor variable for ecosystem C exchange was VWC from changes in soil properties.

Conclusions

Changes in microtopography created by thermokarst development alter soil properties, especially soil moisture content by redistributing water when the ground surface subsides. Subsided areas showed higher CO_2 emissions; therefore, we suggest thermokarst development may stimulate CO_2 emissions in high latitude ecosystems.

Table 1. Probability of each significant variable in a stepwise regression at each site.

Site	Variables	Step	Sig. Prob.
Minimal Thaw	VWC20cm	1	0.0000
	VWC10cm	2	0.0683
Moderate Thaw	Active Layer	1	0.0000
	VWC20cm	2	0.0000
Severe Thaw	Active Layer	1	0.0000
	VWC10cm	2	0.0008

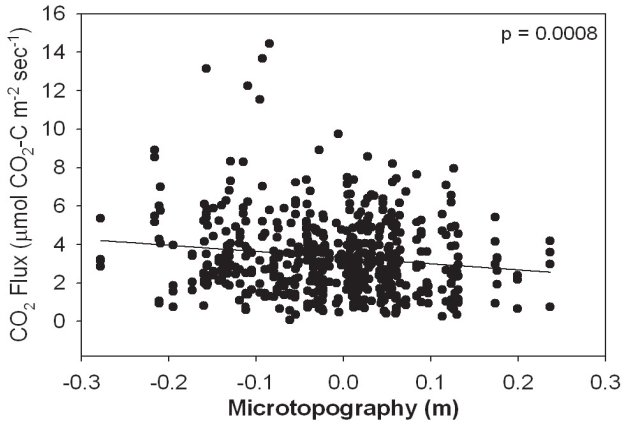

Figure 2. Relationship between microtopography and ecosystem respiration measured using dark CO_2 chamber.

Acknowledgments

We thank C. Staudhammer and M. Lavoie for advice on spatial analysis; UNAVCO for Trimble rental and training. This research was funded by NSF grant DEB-0516326 awarded to EAGS.

References

Chapin III, F.S. et al. 2000. Arctic and boreal ecosystems of western North America as components of the climate system. *Global Change Biology* 6: 211-223.

Gorham, E. 1991. Northern peatlands: Role in the carbon cycle and probable responses to climatic warming. *Ecological Applications* 1: 182-195.

Jorgenson, M.T., Racine, C.H., Walters, J.C. & Osterkamp, T.E. 2001. Permafrost degradation and ecological changes associated with a warming climate in central Alaska. *Climate Change* 48: 551-579.

Oechel, W.C. et al. 2000. Acclimation of ecosystem CO_2 exchange in the Alaskan Arctic in response to decadal climate warming. *Nature* 406: 978-981.

Osterkamp, T.E. & Romanovsky, V.E. 1999. Evidence for warming and thawing of discontinuous permafrost in Alaska. *Permafrost and Periglac. Process* 10: 17-37.

Osterkamp, T.E. 2007. Characteristics of the recent warming of permafrost in Alaska. *Journal of Geophysical Research* 112: F02S02, DOI: 10.1029.

Schuur, E.A.G., Crummer, K.G., Vogel, J.G. & Mack, M.C. 2007. Plant species composition and productivity following permafrost thaw and thermokarst in Alaskan tundra. *Ecosystems* 10: 280-292.

Soil Structural Change Effects on Greenhouse Gas Production and Carbon Loss in Thawing Soils

G.A. Lehrsch
USDA-ARS Northwest Irrigation & Soils Research Laboratory, Kimberly, ID, USA
R.S. Dungan
USDA-ARS Northwest Irrigation & Soils Research Laboratory, Kimberly, ID, USA

Introduction

Freezing alters soil structure, affects microbial populations and activities, increases the emission of greenhouse gases (GHG) such as CO_2 and N_2O, and redistributes the soil solution and its constituents within soil profiles. None of these processes are well characterized, being affected in various ways by the interacting effects of numerous factors, including initial soil water content, freezing rate, and number of freeze-thaw cycles (FTC) experienced (Lehrsch 1998, Lehrsch et al. 1991). As a soil freezes, its soil water is redistributed, at times and in places strengthening aggregates and elsewhere fracturing them. Increases in aggregate stability are thought to be due to clay accumulation or to the precipitation, at particle contact points within aggregates, of soil solution constituents, such as Ca^{2+} or soluble silica (Lehrsch et al. 1991). Experimental evidence for such processes, however, is lacking. Moreover, aggregate breakdown could release soluble organic C (SOC). Increased SOC concentrations in the soil solution, upon thawing, may spur localized microbial activity, increasing GHG emissions. The extent and speed with which soil water is redistributed determines whether these processes will occur and, if so, their extent and significance. The exposing of new fracture surfaces from broken aggregates may increase N_2O flux, since there may then be more nitrogen in the soil solution and more substrate available to support microbial denitrification (Sehy et al. 2004). Since wintertime losses of N_2O from agricultural soils can be 2 to 4 times as great as summertime losses, the study of physicochemical and microbial processes affecting wintertime N_2O flux are critically needed to assess global N_2O budgets (van Bochove et al. 2000). As active layer or seasonally frozen soils thaw, greenhouse gases are emitted but little is known about the effects of freezing-induced soil structural changes upon in situ microbial production of CO_2 and N_2O. Thus, in the laboratory, we characterized the effects of organic carbon, soil water content, and FTC on aggregate stability and the emissions of CO_2 and N_2O from thawing soils.

Methods and Materials

We studied three lots of Portneuf silt loam (Durinodic Xeric Haplocalcid) collected from the 0 to 0.15 m depth of a field site (42°31′N, 114°22′W) located about 2.1 km southwest of Kimberly, Idaho, USA, on 3 October 2007. One lot (hereafter referred to as soil with aged manure) had received about 35 Mg ha^{-1} (dry weight) of dairy manure each spring for 2 y prior to sampling, one lot 35 Mg ha^{-1} of fresh manure at study initiation, and one lot no manure. The Portneuf's Ap horizon contained about 560 g silt kg^{-1}, 220 g clay kg^{-1}, and where no manure had been added, about 9.3 g kg^{-1} of organic carbon (C). When collected, the Portneuf's aggregate stability was about 88%. Field-moist soil (water content of 0.07 kg kg^{-1}) passing an 8 mm sieve was packed to a dry bulk density of 1.15 Mg m^{-3} into 97 mm diameter, 0.13 m long plastic cylinders then, at a temperature of +2° C, slowly wetted to saturation and thereafter drained by tension to a matric potential of -5 or -10 kPa (approximate water contents of 0.48 and 0.37 m^3 m^{-3}, respectively). The packed cylinders, insulated using extruded foam to ensure freezing downward from the surface, in an environmental chamber were then subjected to 0, 1, 2, or 4 FTC, each of which consisted of slow freezing at -7°C for 72 h, then thawing at +2°C for 72 h. The 0, 1, 2, and 4 FTC were chosen for study because (1) the greatest microbial effects occur with the first few cycles, and (2) important structural changes occur with the first few cycles (Lehrsch 1998). The unfrozen controls (0 FTC) were held at +2° C for the entire period of all FTC. A calibrated, infrared photoacoustic detector (Field Gas-Monitor Model 1412, Innova™ AirTech Instruments, Ballerup, Denmark) was used to simultaneously measure CO_2 and N_2O concentrations, after correction for water vapor, in gas samples collected every 8 to 12 h from the 560 ml headspace of intact but thawing cores in sealed containers held at 2, 10, 20, or 30°C for 72 h in an environmental chamber. After each sample had been frozen for the last time but not yet thawed, it was removed from the cylinder and sectioned into 20 to 25 mm thick layers. After each layer was split longitudinally, water content and aggregate stability were measured on one half, and CO_2 and N_2O emitted from the other half using the photoacoustic detector as the soil thawed in a sealed container at 2, 10, 20, or 30°C for 72 h. Before measuring aggregate stability, the frozen soil was thawed at +2°C for 72 h. Thereafter, aggregate stability was measured by wet sieving 1 to 4 mm aggregates in deionized water for 180 s.

Results and Discussion

Soil water and soil structure

Preliminary data revealed that relatively slow freezing at -7°C redistributed the water in the relatively wet soil core (Fig. 1A). Due primarily to thermal potential gradients, water flowed from the 33 mm depth to the 10 mm depth. Compared to the water content at 33 mm, the water content at 10 mm increased about 19%, to a water content of about 0.44 m^3 m^{-3}

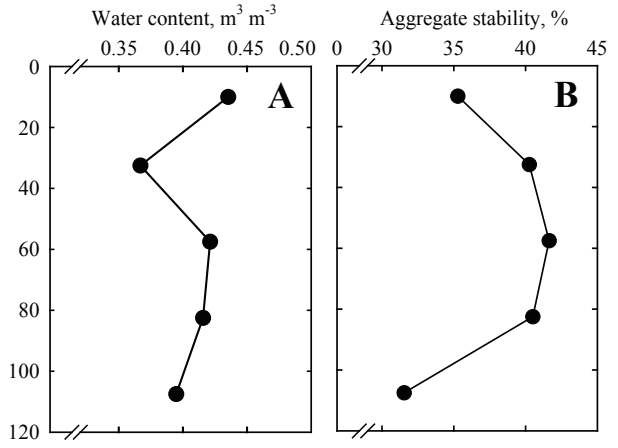

Figure 1. Soil water contents and aggregate stability in a relatively wet core of Portneuf silt loam after freezing at -7°C.

(Fig. 1A). There was little change in water content below 58 mm. Lehrsch et al. (1991) found that water content of 0.34 m^3 m^{-3} in Portneuf silt loam was sufficient to decrease its aggregate stability when it was frozen, then thawed. In this study, at water content nearly one-third greater, structural changes will occur.

Indeed, soil structure near the surface reflected the oft-observed inverse relationship between water content and aggregate stability after freezing (Fig. 1B) (Lehrsch et al. 1991). As water content decreased with depth, aggregate stability increased from 35% at the 10 mm depth to 40% at the 33 mm depth, a 1.14-fold increase. In the middle of the core, however, aggregate stability changed little. The relatively low aggregate stability near the bottom of the core may have been a consequence of difficulty experienced when dissecting the core prior to analysis.

CO_2 and N_2O emissions

Preliminary data revealed that both CO_2 and N_2O concentrations measured in the headspace above intact soil cores increased with time as once-frozen soil containing aged manure thawed at +2°C (Fig. 2). CO_2 concentrations increased by about 200 ppmv (37% greater than ambient) in the first 30 h after air temperatures in the environmental chamber were increased from -7 to +2°C. For subsequent FTC and thawing temperatures of +2°C, CO_2 emissions from intact cores may not be as great. The C pool that provides the substrate for microbial production of CO_2 as repeatedly frozen soils thaw is apparently limited in size, since Herrmann and Witter (2002) found that most CO_2 was produced in the first 4 FTC. Data in Figure 2 also reveal that N_2O concentrations after one incidence of freezing increased by about 5.7 ppmv (more than eight times greater than ambient) in the first 30 h after thawing began. The concentration of CO_2 peaked about 24 h, and N_2O peaked about 26 h after the temperature was increased (Fig. 2). Lysed microbial cells may have provided substrate for microbial denitrification (Sehy et al. 2004).

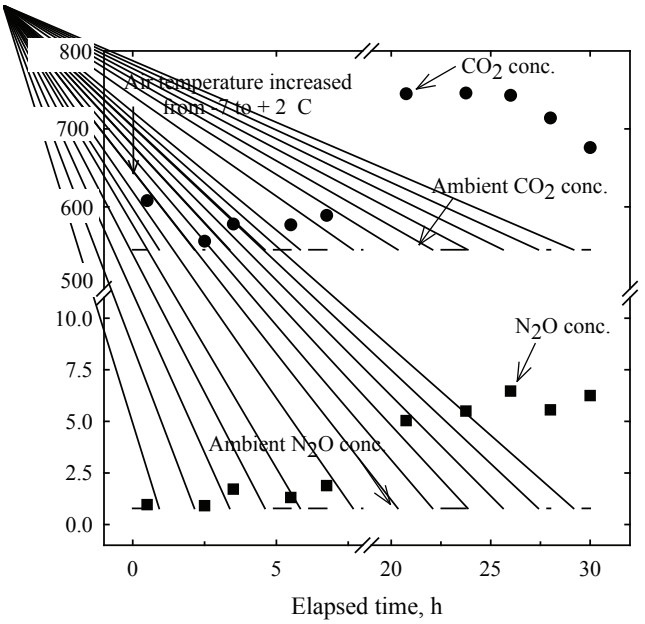

Figure 2. CO_2 and N_2O emissions as a function of thawing time from intact cores frozen once.

Summary

Available data indicate that FTC (1) caused soil water to redistribute and (2) interacted with water content to alter the near-surface aggregate stability of wet soil. Moreover, compared to ambient conditions, emissions of CO_2 increased by a third, and N_2O increased by a factor of eight, each peaking 24 to 26 h after thawing began, from intact cores of soil frozen only once and thawed at only +2°C.

References

Herrmann, A. & Witter, E. 2002. Sources of C and N contributing to the flush in mineralization upon freeze-thaw cycles in soils. *Soil Biology & Biochemistry* 34: 1495-1505.

Lehrsch, G.A. 1998. Freeze-thaw cycles increase near-surface aggregate stability. *Soil Science* 163: 63-70.

Lehrsch, G.A., Sojka, R.E., Carter, D.L. & Jolley, P.M. 1991. Freezing effects on aggregate stability affected by texture, mineralogy, and organic matter. *Soil Science Society of America Journal* 55: 1401-1406.

Sehy, U., Dyckmans, J., Ruser, R. & Munch, J.C. 2004. Adding dissolved organic carbon to simulate freeze-thaw related N_2O emissions from soil. *Journal of Plant Nutrition and Soil Science* 167: 471-478.

van Bochove, E., Jones, H.G., Bertrand, N. & Prevost, D. 2000. Winter fluxes of greenhouse gases from snow-covered agricultural soil: Intra-annual and inter-annual variations. *Global Biogeochemical Cycles* 14: 113-125.

Relation of Active Layer Depth to Vegetation on the Central Yamal Peninsula, Russia

M.O. Leibman
Earth Cryosphere Institute SB RAS, Tyumen, Russia
H.E. Epstein
Department of Environmental Science, University of Virginia, USA
A.V. Khomutov
Earth Cryosphere Institute SB RAS, Tyumen, Russia
N.G. Moskalenko
Earth Cryosphere Institute SB RAS, Tyumen, Russia
D.A. Walker
Institute of Arctic Biology, University of Alaska Fairbanks, USA

Introduction

The purpose of this study was to obtain ground observations in support of remote sensing data. The normalized difference vegetation index (NDVI) and leaf area index (LAI) were measured within a Circumarctic Active Layer Monitoring (CALM) program grid and compared to active layer depth (ALD) measurements. Additional data on active layer properties (soil texture and moisture content), surface features (spot-medallions, hummocks, polygonal pattern and windblown hollows), vegetation complexes, organic mat thickness, and shrub height were analyzed.

The study area is located on the central Yamal Peninsula in the watershed of the Se-Yakha and Mordy-Ykha Rivers. A CALM grid was placed on the top and slope of a highly dissected alluvial-lacustrine-marine plain, affected by landslides with sandy to clayey soils.

Active surface aeolian and landslide processes common in the study area produce vast areas of bare ground. The rate of revegetation and plant succession at such sites related to climate fluctuations was examined through repeated descriptions of vegetation coverage and species in 1993 and 2007.

Previous studies have shown that the main controls of the active layer dynamics are the types of surficial deposits, moisture content in the fall, thickness of organic cover, and air temperature in summer. In general, maximum ALD (1–1.2 m) is found in sands on bare surfaces or with sparse vegetation and low moisture content (up to 20%). Minimum ALD (50–60 cm) is found in peat or clay deposits covered by thick moss and with moisture contents more than 40%.

Methods

The active layer was monitored using a metal probe according to the procedure accepted by the CALM program (Brown et al. 2001) within a grid 100 x 100 m in 10 m increments. Ground and vegetation characteristics were recorded at each grid node. NDVI was measured using a portable ASD PSII spectroradiometer, and LAI was estimated using a LICOR-2000 plant canopy analyzer. NDVI is essentially an index of green, photosynthesizing vegetation, as it strongly depends on the absorption of red light. LAI (as estimated by the LICOR-2000) is the total area of aboveground plant tissue divided by the ground area that is covered by the extent of the plant canopy. Both NDVI and LAI are highly, positively correlated with the mass of aboveground vegetation, and this is true for Low Arctic tundra vegetation (Riedel et al. 2005).

A database was compiled that included ALD, NDVI, LAI, organic mat thickness, shrub height, dominant plant species, and cover of each plant community. The spatial distribution of various parameters was analyzed on a map compiled by interpolation of numerical data between grid-nodes using Surfer software, and field mapping of descriptive data (map not shown).

Active layer measurements in 2007 were accompanied by vegetation descriptions and measurements at each grid-node (121 points and their vicinities were characterized in the database). The data were sorted into three categories of ALD, the averages of all the parameters were calculated, and relations between these averages were analyzed within each category.

Results and Discussion

In general, for the entire CALM grid, the higher the vegetation indices and parameters the lower the ALD (Fig. 1). This result is within the generally accepted effect of vegetation insulation on ground temperatures and ALD (Melnikov et al. 2004).

Analysis of dominant plant species supports the idea that vegetation acts as an insulating mat. Of all the plant groups, moss showed the highest negative correlation with ALD, while lichens and shrubs were more favorable for thawing (or deep thaw was favorable for lichen and shrub growth) (Fig. 2).

Eight vegetation units (Table 1) were recognized within the grid. "Moist grass-sedge-dwarf shrub lichen-moss and green moss hummocky tundra" (#5, Table 1) is most widespread. Partly bare surfaces (#1, 2, 3, and 8, Table 1) are also common, though no bare nodes occurred on the windblown sands, due to recent vegetation recovery.

When the CALM grid was established in 1993, five bare surface grid-nodes occurred in windblown hollows (Leibman 1998). Revegetation of windblown sands started after

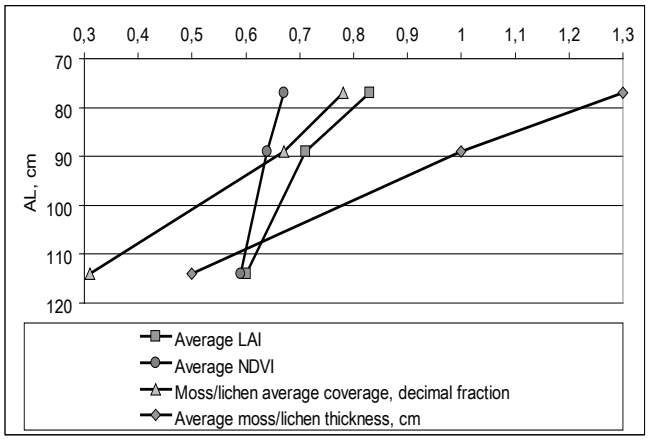

Figure 1. Relation between the active layer depth and average vegetation indices at a CALM grid, research polygon Vaskiny Dachi.

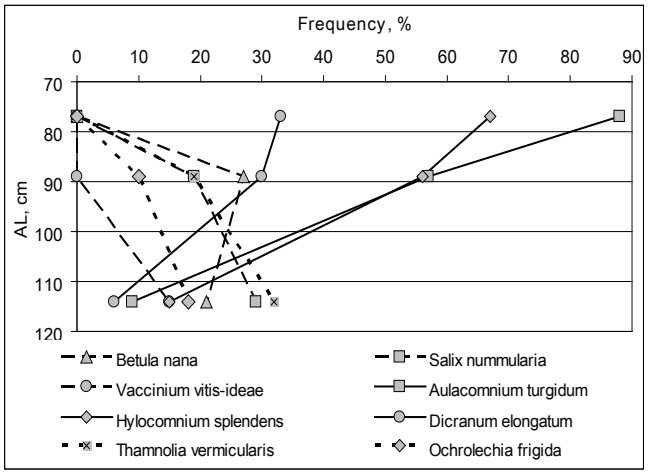

Figure 2. Relation between the active layer depth and frequency of dominant plant species at a CALM grid, research polygon Vaskiny Dachi.

Table 1. Legend for vegetation map of the CALM grid Vaskiny Dachi.

##	Vegetation complex (% bare surface)	Number of grid-nodes
1	Dry blowout sands	0
2	Dry grass-prostrate dwarf shrub-green moss-lichen tundra with spot-medallions (40–60%)	24
3	Dry grass-prostrate dwarf shrub-green moss and green moss-lichen tundra with spot-medallions (10–30%)	12
4	Moist grass-dwarf shrub lichen-moss and green moss tundra	4
5	Moist grass-sedge-dwarf shrub lichen-moss and green moss hummocky tundra	61
6	Moist grass-sedge-low shrub moss tundra	6
7	Wet willow-cotton grass cover	9
8	Moist willow-sedge-grass cover (30–50%)	5

considerable warming in 2000, so the observed revegetation resulted from eight years of change. Shear surfaces of two landslides within the CALM grid were exposed during the landslide event in 1989. Twelve grid nodes became bare surfaces following these events. A survey in 2007 showed that seven grid nodes were entirely revegetated (100% coverage by willow-cotton grass complex, #7, Table 1), and five grid-nodes were partly revegetated (up to 50% coverage by willow-sedge-grass complex, (#8, Table 1) in 18 years.

Conclusion

The active layer depth is negatively related to both LAI and NDVI. This is potentially helpful for mapping active layer depths, using remotely sensed vegetation indices and products. Organic matter coverage and thickness are also negatively related to active layer depth; this is especially true for moss cover. Contrary to the moss species, there is an ordinal relation between ALD and lichen/shrub species.

Temporal patterns of vegetation dynamics on bare surfaces after 10–18 years of revegetation result in the formation of dwarf shrub-lichen cover on dry sandy tops and gentle slopes, willow-cotton grass cover on wet landslide shear surface sites, and willow-sedge-grass cover on moist sites.

Acknowledgments

This research is part of the CALM project funded by the U.S. National Science Foundation (Grant No. OPP-9732051), and the Yamal Land Cover Land Use Change project of the International Polar Year (IPY) funded by NASA Grant No. NNG6GE00A.

References

Brown, J., Hinkel, K.M. & Nelson, F.E. 2001. The Circumpolar Active Layer Monitoring (CALM) program: Research designs and initial results. *Polar Geography* 24: 165-258.

Melnikov, E.S., Leibman, M.O., Moskalenko, N.G. & Vasiliev, A.A. 2004. Active layer monitoring in West Siberia. *Polar Geography* 28(4): 267-285.

Leibman, M.O. 1998. Active layer depth measurements in marine saline clayey deposits of Yamal Peninsula, Russia: procedure and interpretation of results. *Proceedings of the 7th Intl. Conference on Permafrost, Yellowknife, Canada, June 23–27, 1998*: 635-639.

Riedel, S.M., Epstein, H.E & Walker, D.A. 2005. Biotic controls over spectral indices of arctic tundra vegetation. *Intl. Journal of Remote Sensing* 26: 2391-2405.

Rock Glacier Response to Post-Little Ice Age Warming: Spruce Creek Rock Glacier, Ten Mile Range, Colorado, USA

Eric M. Leonard
Department of Geology, Colorado College, Colorado Springs, CO, USA
Stephen G. Weaver
Department of Geology, Colorado College, Colorado Springs, CO, USA
James A. Bradbury
Department of Geosciences, University of Massachusetts, Amherst, MA, USA
Erica E. Langbecker
Department of Geology, Colorado College, Colorado Springs, USA
Jeffrey A. Wollenberg
Department of Geology, Colorado College, Colorado Springs, USA

Introduction

In this study, we use multiple methods to document changes in flow velocity, internal deformation, and surface geometry of the Spruce Creek rock glacier in the Ten Mile Range of central Colorado. Our methods include lichenometry, photogrammetry, and detailed ground surveying. The data provide evidence of strong rock glacier response to both Little Ice Age cooling and post-Little Ice Age warming. Response to warming over the last century appears to have occurred with little lag time.

Methods

Long-term flow variations are evaluated through measurement of lichens (*Rhizocarpon s.l.*) on the rock glacier surface, which provide a record of surface ages, and thus flow rates, spanning the last 2500–3000 years. Lichen measurements are calibrated using a modified version of Benedict's (1993) *Rhizocarpon* growth curve for the Colorado Front Range. Aerial photographs taken at several intervals since 1938 provide a more detailed record of changing flow rates over the last seven decades. Repeated ground surveys begun in the 1985 provide information on changing velocities, strain rates, and strain patterns, and thinning of the rock glacier over the last two decades.

Results

Lichenometry provides only approximate surface ages and thus only approximate flow rates. During the 2000-year interval before about 1600 A.D., mean centerline flow rate at Spruce Creek was approximately 6 cm/yr. The flow rate increased dramatically after about 1600 A.D. For the following three centuries, until the late 19th century, a time interval corresponding to the global peak of the Little Ice Age, mean flow rates were on the order of 40–55 cm /yr. By the mid 20th century, flow rate had declined again to about half of this peak rate, and from the mid 1980s through 2000 A.D., centerline flow rates had declined further to 5.9–10.2 cm/yr on three surveyed transects. Mean flow rates along the three transects over this interval ranged from 4.5 to 6.7 cm/yr. The relatively fast-moving upper portion of the rock glacier, which formed initially during the Little Ice Age, slowed down by 25% between the late 1980s and the late 1990s, and strain rates measured at 12 strain diamonds distributed across the rock glacier declined by an average of 19% over the same interval. Lowering of the rock glacier surface was general, but spatially highly variable, over the period from 1985 to 2000 A.D. Mean surface lowering exceeded 1 m during this period.

Records from the nearest continuously operating meteorological station, at Climax, Colorado, 8–9 km southwest of the Spruce Creek rock glacier, and the more comprehensive records from Niwot Ridge in the Colorado Front Range about 75 km to the northeast, both indicate strong summer warming after the mid 1970s. The velocity and strain rate decreases and surface lowering measured at the rock glacier since the mid 1980s appear to be a response to that warming.

Ongoing Research

During summer 2008, we will resurvey the rock glacier to examine its response to continued warming. Since 2000, summer (June through August) temperatures at Climax have averaged 0.96°C higher than during the initial 15 years of our survey.

Reference

Benedict, J.B. 1993. A 2000-year lichen-snowkill chronology for the Colorado Front Range, USA. *The Holocene* 3: 27-33.

Mapping the Permafrost in China Using Remotely Sensed Land Surface Temperature Data

Xin Li, Shuguo Wang, Rui Jin, Youhua Ran
Cold and Arid Regions Environmental and Engineering Research Institute, Chinese Academy of Sciences Lanzhou 730000, China
World Data Center for Glaciology and Geocryology in Lanzhou, Lanzhou 730000, China

The permafrost area in China is about 1.72×10^6 km^2. The area of altitudinal/mountain permafrost is approximately 1.36×10^6 km^2 (Li et al. 2008), which ranks first in the world in terms of middle- and high-altitude permafrost area. The permafrost in China is very sensitive to climatic warming. Significant permafrost degradation has occurred and is occurring in most permafrost regions in China, and has resulted in an increase of environment fragility and related hazards (Li et al. 2008, Jin et al. 2000, Jin et al. 2006).

Mapping the permafrost is of critical importance therefore. The existing small-scale permafrost/frozen soil maps in China include the map of snow, ice, and frozen ground in China (1:4,000,000) (Shi et al. 1988), permafrost map of the Qinghai-Tibet Plateau (1:3,000,000) (Li & Cheng 1996), the map of geocryological regionalization and classification in China (1:10,000,000) (Qiu et al. 2000), and the map of glaciers, frozen ground, and deserts in China (1:4,000,000) (Wang et al. 2006). In additional, the circum-Arctic map of permafrost and ground-ice conditions (1:10,000,000) (Brown 1998) can be subset to be used as a regional map.

These maps provide a good summary of geocryological research in China; however, there are two weaknesses of these existing small-scale permafrost maps. The first is that the classification systems of these existing maps are inconsistent. All of the legends are continuity-based, but each map uses a different and incomparable map legend itself. The inconsistence is caused, partially, by the ambiguity of the definition of continuity, which is based on the surrounding region it is lying in and, therefore, is scale-dependent (Nelson & Outcalt 1987). Obviously, a consistent and unified legend system is needed for both altitudinal and latitudinal permafrost mapping in China. The lack of it hinders the monitoring and modeling of permafrost.

Another weakness of traditional permafrost mapping is the data unavailability. Global and regional permafrost mapping usually relies on meteorological data. That most commonly used is air temperature, but it is sparse in many permafrost areas, e.g., the Qinghai-Tibetan Plateau. The scarcity of data is an obstacle of high-resolution permafrost mapping.

To address the first weakness, we propose using a stability-based classification system proposed by Cheng (Cheng 1984) to unify the legends of altitudinal and latitudinal permafrost maps. This classification uses temperature criteria, which is more objective than the continuity criteria. It is also more applicable when using GIS mapping technology, because GIS mapping is usually grid-based, which is easy for presenting the existence of permafrost in a grid cell, but not the percentage of permafrost distribution.

To address the second weakness, we propose to use remote sensing data. As stated above, air temperature isotherm is usually used to delineate permafrost zonation. However, many investigators suggested that the air temperature is not an optimal predictor of permafrost distribution, because the very large effects of snow cover and other variables influencing permafrost occurrence are ignored. Instead, land surface skin temperature (LST) should be used (Nelson & Outcalt 1987, Cheng, pers. com.). The LST, though a more ideal criterion, is traditionally more unavailable than air temperature and its heterogeneity is very strong so that extracting LST to data-void regions is more difficult. The remote sensing era has changed this situation. Thermal infrared remote sensing is providing direct observations of LST in high spatial and temporal resolutions, being capable of bridging the gap between permafrost mapping and data unavailability.

The paper aims to develop a new, general, and high-resolution permafrost map of China by applying the thermal stability-based classification system (Cheng 1984) and using remotely sensed LST and snow depth data.

References

Cheng, G.-D. 1984. Problems of zonation of high-altitude permafrost. *ACTA Geographica Sinica* 39(2): 185-193.

Jin, H.J., Li, S.X., Cheng, G.D., Wang, S.L. & Li, X. 2000. Permafrost and climatic change in China. *Global and Planetary Change* 26(4): 387-404.

Jin, H.J., Zhao, L., Wang, S.L. & Jin, R. 2006. Thermal regimes and degradation modes of permafrost along the Qinghai-Tibet Highway. *Science in China D: Earth Sciences* 49(11): 1170-1183.

Li, S.D. & Cheng, G.D. 1996. *Permafrost Distribution Map on the Qinghai-Tibet Plateau*. Lanzhou: Gansu Culture Press.

Li, X., Cheng, G.D., Jin, H.J., Kang, E.S., Che, T., Jin, R., Wu, L.Z., Nan, Z.T., Wang, J. & Shen, Y.P. 2008. Cryospheric change in China. *Global and Planetary Change,* doi:10.1016/j.gloplacha.2008.02.001.

Nelson, F.E. & Outcalt, S.I. 1987. A computational method for prediction and regionalization of permafrost. *Arctic and Alpine Research* 19(3): 279-288.

Qiu, G.-Q., Zhou, Y.-W., Guo, D.-X. & Wang, Y.-X. 2000. *The Map of Geocryological Regionalization and Classification in China*. Beijing: Science Press.

Shi, Y.F. & Mi, D.S. 1988. *Map of Snow, Ice, and Frozen Ground in China, 1:4,000,000*. Beijing: SinoMaps Press.

Wang, T., Wang, N.L. & Li, S.X. 2006. *Map of the Glaciers, Frozen Ground and Desert in China.* 1:4,000,000. Beijing: Chinese Map Press.

The Effect of Spatially Distributed Snow Cover on Soil Temperatures: A Field and Modeling Study

Anna Liljedahl
University of Alaska Fairbanks, USA
Larry Hinzman
University of Alaska Fairbanks, USA
Sergei Marchenko
University of Alaska Fairbanks, USA
Svetlana Berezovskaya
University of Alaska Fairbanks, USA

Introduction

Due to its insulative properties, snow cover has been shown to play a significant role in the 20th century warming of permafrost (Osterkamp 2007, Stieglitz et al. 2003) and thermokarst formation (Osterkamp 2007). Although the effects of snow cover characteristics on soil temperatures have been studied by others (Ling & Zhang 2003, Osterkamp 2007, Overduin et al. 2007, Stieglitz et al. 2003), small-scale geographical variations have been given limited attention. The combination of snow redistribution, hydraulic gradients induced by polygonal features, nutrient limited vegetation, soil mineralization, and respiration impaired by the cold soils calls for a fine-scale analysis to understand the interactions among the Arctic systems and how they would respond to any changes in air temperature and precipitation.

We examine the effects of snow depth and soil thermal properties on micro-scale (>0.6 m horizontal, >0.01 m vertical) soil temperature distribution through field measurements and computer modeling across a single polygon.

Study site

The study site is located inside the boundaries of the Barrow Environmental Observatory (BEO) close to Barrow on the North Slope of Alaska (Fig. 1). The BEO hosts an intensively monitored area called the Biocomplexity site (71°16′47″N, 156°36′2″W), which is a 1 km^2 watershed containing a drained lake basin and low- and high-centered polygons. Sedges and sphagnum moss represent the major vegetation at the Biocomplexity site.

The mean annual air temperature in Barrow during the years 1973–2006 was -12°C with 32% of mean daily air temperatures colder than -20°C. The latter ranged from -45°C to 16°C yr 1973–2006. Adjusted precipitation (Yang et al. 1998) averaged 168 mm/yr with 72 mm falling June–August (1973–2006). Summer 2007 was a warm summer (5.4°C compared to 3.3°C yr 1973–2007) with a low amount of precipitation (24 mm), resulting in unusually dry soils prior to freezing. The Circumpolar Active Layer Monitoring site (Brown et al. 2000), located at the northern end of the BEO, experienced a mean active layer depth of 35 cm yr 1995–2007. The area of focus for this study is a low-centered polygon represented by relatively high (0.5 m) and wide (5 m) rims.

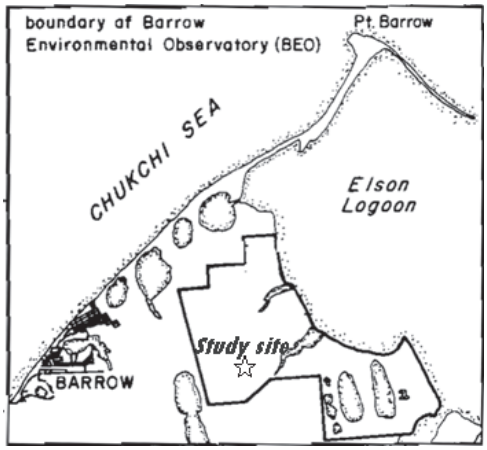

Figure 1. The location of the Biocomplexity site inside the boundaries of the Barrow Environmental Observatory. Original image courtesy of K.M. Hinkel.

Methods

We combined distributed modeling and field observations of snow depth and soil temperatures, focusing on the active layer thermal regime. Output from a snow distribution model was used as input to a soil thermal regime model in both daily and hourly time steps. SnowTran-3D (Liston et al. 2007) provided wind-driven snow depth evolution over topographically variable terrain. Required model inputs include topography, vegetation, and weather data (precipitation, air temperature, humidity, wind speed and direction). In order to simulate the spatially distributed temperatures of permafrost and active layer thickness for the investigated area, both equilibrium and transient models have been applied. The equilibrium model is a spatially distributed permafrost model based on an approximate analytical solution of soil freezing and thawing, which includes an estimation of thermal offset due to the difference of frozen and thawed soil thermal properties (Romanovsky & Osterkamp 1995). The numerical (transient) model simulates soil temperature dynamics and depth of seasonal freezing and thawing by solving nonlinear heat equation with a phase change. In this model, the process of soil freezing/thawing occurs in accordance with the unfrozen water content curve and soil thermal properties, which are specific for each soil layer (Marchenko et al. 2008). The model requires input of

upper (air temperature, snow, and vegetation) and lower (geothermal heat flux) boundary conditions, initial conditions (temperature distribution with depth), soil water content, and soil thermal properties. Topography was resolved in 1 m and 0.04 m horizontal and vertical scale, respectively, with finer pixels available in the near future. Vegetation was mapped into 2.8 m horizontal resolution.

The simulations were validated with field measurements of soil temperature and snow depth. An installation of 116 thermistors (YSI model 44033 and Hobo U23-004) and 29 water content reflectometers (CS616, Campbell Scientific) was made in late September 2007 across the polygon. The thermistors were placed 0.6–20 m apart at three depths per site (1) at the interface of living and dead organic, (2) 7–10 cm below the interface, and (3) at the bottom of the active layer. One soil moisture sensor was placed in the organic layer 7–10 cm below the living and dead organic interface. Thermal conductivity, volumetric specific heat, diffusivity, and temperature were measured with a Kd2Pro sensor (Decagon) throughout the different soil layers in fall 2007.

Results and Discussion

Active layer depths ranged from 18 (troughs) to 46 cm (rims) in 2007 with a mean of 31 cm across the studied polygon. In the thawed polygon soil profile a 2–10 cm thick live moss layer (mean 4 cm) overlaid a 5–25 cm organic layer (mean 10 cm). The thicker moss layers were found in troughs, while the thickest thawed organic layers were found at the inner edge of the rim. Organic layer thermal conductivity in fall 2007 varied between 0.16–0.60 W m^{-1} K^{-1} (n = 68) with moss thermal conductivity from 0.11 to 0.91 W m^{-1} K^{-1} (n = 6). Measurements of moss thermal conductivity could only be obtained at a limited number of sites where ice formation had not occurred. However, five of the six measurements were obtained at the same day, where four sites showed higher thermal conductivities in the moss layer than in the organic layer below (ratio 2.3 to 5.6).

Field measurements showed large variation in near-surface soil thermal properties on short horizontal and vertical scales. Despite relatively small differences in vegetation and topography, a heterogeneous snow accumulation is to be expected due to redistribution by wind. The distribution of winter soil temperatures across the polygon are likely to vary significantly due to the combined effects of snow depth and soil thermal characteristics.

Acknowledgments

The authors are grateful to Matthew Sturm, Robert Busey, Steve Hastings, and B.A.S.C. for field assistance. Financial support was provided by Gålö Foundation, Center for Global Change and Arctic System Research, and the National Science Foundation through the International Arctic Research Center (Grant number 0327664).

References

Brown, J., Hinkel, K.M. & Nelson, F.E. 2000. The circumpolar active layer monitoring (CALM) program: Research designs and initial results. *Polar Geogr.* 24(3): 165-258.

Ling, F. & Zhang, T. 2003. Impact of the timing and duration of seasonal snow cover on the active layer and permafrost in the Alaskan arctic. *Permafrost and Periglac. Process.* 14: 141-150.

Liston, G.E., Haehnel, R.B., Sturm, M., Hiemstra, C.A., Berezovskaya, S. & Tabler, R.D. 2007. Simulating complex snow distribution in windy environments using SnowTran-3D. *J. of Glaciol.* 53(181): 241-256.

Marchenko, S.S., Romanovsky, V.E. & Tipenko, G.S. 2008. Numerical modeling of spatial permafrost dynamics in Alaska. *Proceedings of the Ninth International Conference on Permafrost*, *Fairbanks, Alaska, June 29–July 3, 2008.*

Osterkamp, T.E. 2007. Causes of warming and thawing permafrost in Alaska. *Eos Trans.* 88(48): 522-523.

Overduin, P.P., Boike, J., Kane, D.L. & Westermann, S. 2007. Soil temperatures under a rage of organic and snow covers. *Eos Trans.* 88(52), Fall Meet. Suppl., Abstract C12A-0061, 31:737-747.

Romanovsky, V.E. & Osterkamp, T.E. 1995. Interannual variations of the thermal regime of the active layer and near surface permafrost in Northern Alaska. *Permafrost and Periglac. Process*. 6(3): 313-335.

Stieglitz, M., Déry, S.J., Romanovsky, V.E. & Osterkamp, T.E. 2003. The role of snow cover in the warming of arctic permafrost. *Geophys. Res. Lett.,* 30(13): 1721, doi:10.1029/2003GL017337.

Yang, D., Goodison, B.E. & Ishida, S. 1998. Adjustment of daily precipitation data at 10 climate stations in Alaska: Application of WMO intercomparison results. *Water Resours. Res.* 34(2): 241-256.

The Omnsbreen Glacier: Possible Aggrading Permafrost, Southern Central Norway

Karianne Staalesen Lilleøren
Department of Geosciences, University of Oslo, Norway
Ole Humlum
Department of Geosciences, University of Oslo, Norway

Introduction

The Omnsbreen Glacier is a small (< 0.5 km^2) mountain glacier situated in southern central Norway about 1500 m a.s.l. Presently, the glacier exists approximately 100 m below the regional equilibrium line altitude (ELA), due to local accumulation of wind-redistributed snow.

During the "Little Ice Age" (LIA), the glacier was of a considerable size and extent (approximately 6 km^2) and occupied the whole valley, where today it occupies only parts of the western slope. The maximum size was reached around 1750, as for most of the glaciers in southern Norway (Andreassen et al. 2005). At that time, the effect of snow accumulating by wind on the glacier was significantly reduced because of the glacier's different geometry, filling up the valley.

From the LIA maximum and until around 1930, the glacier remained relatively stable in shape and size. Between 1930 and 1985, however, the bulk of the glacier disappeared. Since then, the glacier has lost mass at a much lower rate compared to the years before, until recent years when the glacier apparently has stagnated with a fairly constant size.

An ongoing study aims at explaining the rapid disappearance of Omnsbreen since 1930 by using local and regional climate data (temperature, precipitation, and wind) and also tries to explain the apparent recent stagnation of the glacier. Couplings between the glacier, the climate, and mountain permafrost is investigated (Lilleøren 2007).

Climatology and Area Description

Location

The Omnsbreen Glacier is located close to Finse (1220 m a.s.l.) at the northwestern margin of the flat Hardangervidda area (Fig. 1). Finse is situated in a transition zone between the marine western coast and the more continental eastern parts of Norway, and has a high mountain climate. The mean annual air temperature (MAAT) was -2.1°C (1970–2000), and the mean annual precipitation in the same period was 1030 mm, according to measurements by the Norwegian Institute of Meteorology at Finse (DNMI 2007).

Temperature

In the before-mentioned ongoing study of the Omnsbreen area, Tinytag-Loggers measuring air temperature, bottom temperature of winter snow cover (BTS), and ground temperature were placed in the area close to the glacier, and the mean difference in air temperature measured between Finse and Omnsbreen was found to be 2.1°C, with the lowest

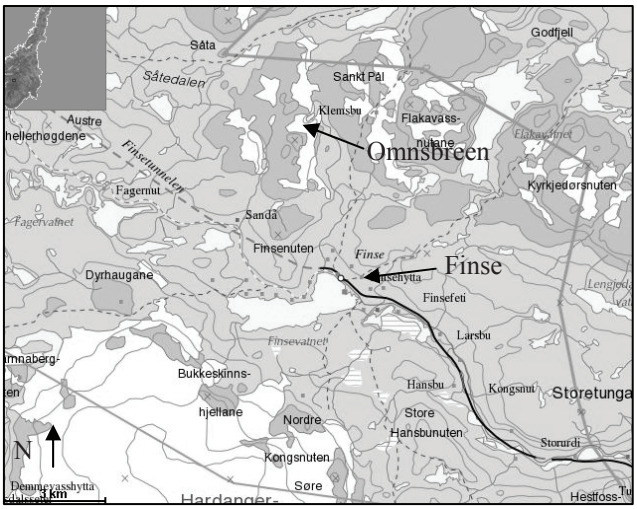

Figure 1. Location of Finse and Omnsbreen, southern central Norway.

temperatures at Omnsbreen for the period 06/08/22 through 07/08/19. The picture is complicated by large temperature inversions in the area, especially during the winter. Finse is situated in a valley bottom that efficiently traps heavy cold air cooled in higher elevations.

Wind

Mapping of snow cover surface forms demonstrated that the mean winter wind direction is from the west or slightly southwest. Omnsbreen's valley has a north–south extension, and snow transported by westerly winds can efficiently accumulate in the valley's east-facing slopes. When studying the wind directions measured by the meteorological station at Finse, it seems like there has been a shift in the wind directions since the 1970s, from a wide directional spread during the winter to a more consistent wind direction from west in the 1980s. This shift also coincides with the reduction in the mass loss from the Omnsbreen glacier.

Permafrost?

Of the loggers measuring the BTS today (four places) in the area earlier covered by ice, one had a stable temperature close to -4°C, which can be interpreted as an indication of permafrost in the area (Fig. 2). The MAAT in the area presumably is too high to allow widespread permafrost, but some sporadic permafrost may exist at this altitude at wind-exposed sites. Situated in a transition area between maritime and continental climate types, the area experiences large differences in snow cover from one year to the next,

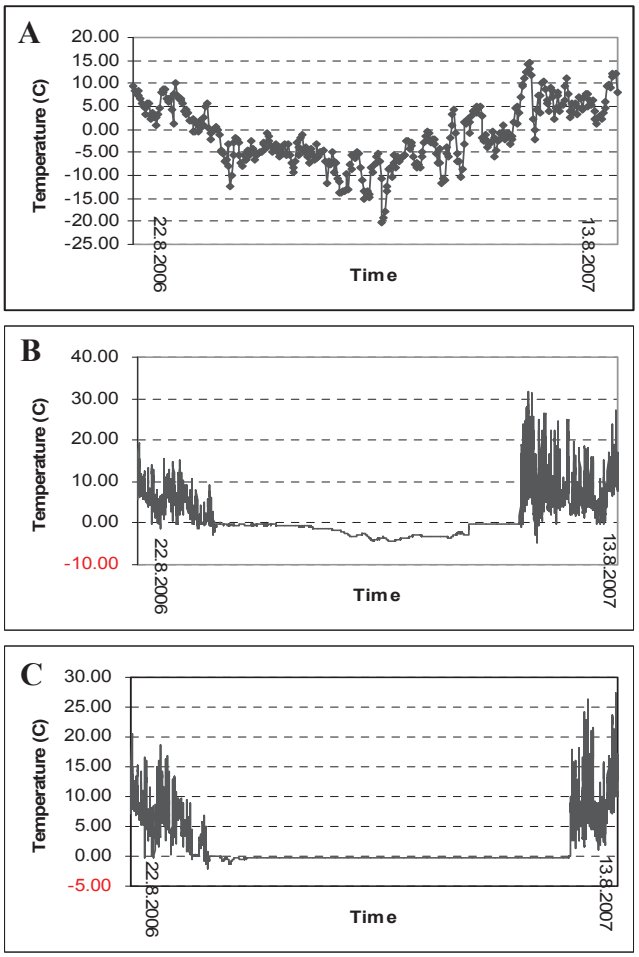

Figure 2. A: Air temperature at Omnsbreen for the period 06/08/22–07/08/13. B: Ground surface temperature (GST) in the Omnsbreen area (1559 m a.s.l.). Snow from mid-October, temperature at ca. -4°C from mid-February to May. C: GST in the Omnsbreen area (1431 m a.s.l.).

including wind-redistributed snow. This situation also changes the permafrost conditions from year to year. In this area, differences in snow cover might be more important for the permafrost distribution than temperature changes, compared to areas further northeast where permafrost is known to exist (Etzelmüller et al. 2003).

The zone covered by ice during the LIA is today characterized by landforms created beneath a warm-based glacier such as flutings, eskers, striae, and crag-and-tails, which indicates non-permafrost conditions at that time. Based on the findings of sporadic permafrost in this area today, the paraglacial zone might be subject to aggrading permafrost (Etzelmüller & Hagen 2005).

Discussion

During the LIA, the Omnsbreen Glacier filled the whole valley. The geometry of the glacier itself probably made accumulation of wind-redistributed snow hard at that time, and it is more likely that the summit areas of the glacier were object to erosion by the wind. As the glacier became smaller, it also became possible for wind-redistributed snow to accumulate in the western parts of the valley. Today's glacier is probably depending on this amount of wind transported snow to exist.

One cannot ignore the possibility that similar wind and topography-induced changes between two stable situations have occurred several times in the history of the Omnsbreen Glacier.

Permafrost

In the following years, time series will be established on BTS, air temperature, and snow cover distribution, considering especially the conditions for permafrost to exist.

References

Andreassen, L.M., Elvehøy, H., Kjøllmoen B., Engeset, R. V. & Haakensen, N. 2005. Glacier mass-balance and length variations in Norway. *Annals of Glaciology* 42: 317-325.

DNMI. 2007. *eKlima*. Oslo: The Norwegian Meteorological Institute.

Etzelmüller, B., Berthling, I. & Sollid, J.L. 2003. Aspects and concepts on the geomorphological significance of Holocene permafrost in southern Norway. *Geomorphology* 52: 87-104.

Etzelmüller, B. & Hagen, J.-O. 2005. Glacier-permafrost interaction in Arctic and alpine mountain environments with examples from southern Norway and Svalbard. In: C. Harris & J.B. Murton (eds.), *Cryospheric Systems: Glaciers and Permafrost.* London: Geological Society, London, Special Publications, 242: 11-27.

Lilleøren, K.S. 2007. *Omnsbreen. Utbredelse og dynamikk under "Den lille istid" og gjennom det 20. århundre.* (English: *The Omnsbreen glacier. Extent and dynamics during the "Little Ice Age" and the 20th century.)*. M.Sc. Thesis. Oslo: Department of Geosciences, University of Oslo.

A Permafrost and Building Foundation Monitoring System to Help Design Adaptable Foundation Structures in a Changing Climate

Michael R. Lilly
GW Scientific, Fairbanks, Alaska, USA
Ron F. Paetzold
GW Scientific, College Station, Texas, USA
Daniel Reichardt
GW Scientific, Anchorage, Alaska, USA

Introduction

Designing foundations for homes and buildings in northern regions will face many challenges in future years as climate changes impact permafrost regions. Permafrost stability may be adversely affected by climate change, and new buildings need to be designed to withstand or adapt for such changing conditions. Past approaches have focused on stabilizing permafrost, making the assumption that the building structure was the primary source for any change in permafrost. As climate changes increase, the potential for associated impacts to foundation systems within the design lifespan of the building will become more common, and the expense and difficulty associated with stabilizing warming permafrost will likely become greater.

The Cold Climate Housing Research Center (CCHRC) was created to promote, develop, and test cold climate building technology. The Center's Research and Testing Facility (RTF) is a 15,000 square foot building designed as a multipurpose structure containing office space, research laboratories, meeting rooms, and a library. The building is located in a setting having shallow permafrost conditions. Additional information about the Center and the RTF may be found on their website: http://www.cchrc.org/.

The RTF was built to adjust to degrading permafrost by having an adjustable foundation system. This is different than past methods, which focus on maintaining frozen conditions. With warming climatic conditions, this places a foundation-stabilization system at odds with the natural state of the environment. The building's foundation is designed with piers that are equipped with 50-ton jacks to keep the building level by compensating for any differential settlement resulting from permafrost degradation.

To help evaluate, respond, and demonstrate this type of foundation system for buildings, a permafrost and active layer monitoring system was installed to help provide data for the life of facility operations. The RTF and the areas beneath and around the building have been thoroughly instrumented to monitor conditions, especially those related to temperature and moisture.

The temperature monitoring network was established to help look at background permafrost conditions, as well as conditions under the building and at various sections of the building foundations that may be impacted by seasonal freezing. The site has a supra-permafrost, unconfined, aquifer in unconsolidated silts. The groundwater flow impacts heat transfer between the building and underlying permafrost. The water-table elevation varies seasonally with snowmelt recharge in the spring. The general groundwater gradient is from west to east.

Additional monitoring includes unfrozen soil-moisture sensors. While the building limits future vertical drainage into the subsurface, annual rising and falling groundwater tables can contribute to the unsaturated moisture levels under the building. Changing permafrost conditions may increase or decrease groundwater fluxes and vertical changes under the building.

A better understanding of the subsurface environment and changing permafrost conditions will be important for future evaluations of the adjustable foundations systems and the transferability to developing cold regions.

Materials and Methods

The depth to permafrost at the building site varies from 3.7 m (12 feet) at the southwest corner to more than 8.5 m (28 feet) on the northeast corner.

Construction began on the RTF in the middle of July 2005. The building was completely enclosed in January 2006 and was completed in September of 2006. Sensors were installed during building construction. Layout of the facility is shown in Figure 1.

Several monitoring wells were drilled into permafrost and allowed to freeze back. The wells can be used for two purposes: measurements of the top of the water-table aquifer and the top of permafrost. A background site was installed away from the facility (weather station site), on the up-gradient side of the building in shallow permafrost, and on the downstream side of the facility, where the maximum impact should come from thermal heat loss from the building. A

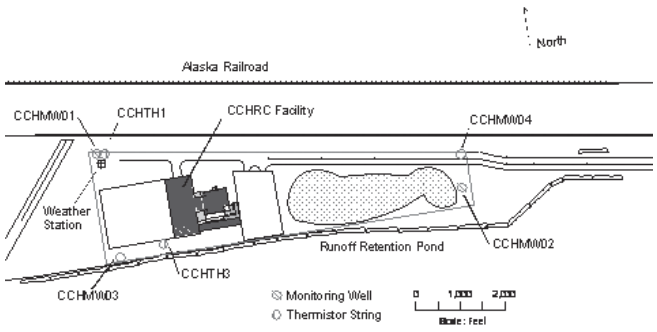

Figure 1. Site location map for CCHRC facility, showing location of observation wells and thermistor borings.

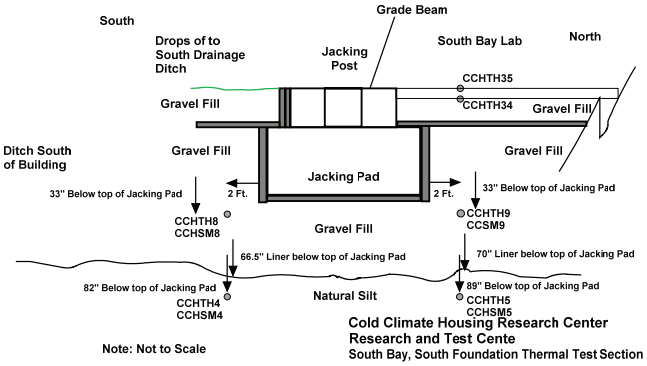

Figure 2. South Bay south foundation thermal test section sensor locations.

number of sensors were also installed under all the building foundation systems to help characterize the heat loss from the building.

Soil temperature is monitored at various points using sensors fabricated with triplicate YSI thermistors or strings of 12 YSI thermistors at a predetermined spacing. The calibration for each sensor was verified. Figure 1 shows the location of two of the thermistor strings: CCHTH1 and CCHTH3.

Soil-water content was monitored with Campbell Scientific, Inc. CS616 TDR-type sensors. These sensors indicate the volumetric amount of unfrozen water content, based on changes in soil bulk dielectric properties.

Water levels in observation wells are manually recorded at selected observation intervals. The groundwater wells are located near the four property corners, as shown on the map in Figure 1.

Sensor readings at each station were controlled and recorded with a Campbell Scientific, Inc. CR1000 datalogger. Data are transmitted hourly to a central processing server though an Internet connection.

Figure 2 shows sensor locations near one of the foundation jacking pad test sections. CCHTH## sensors are temperature sensors consisting of triplicate thermistors. CCHSM## sensors are soil-moisture sensors.

Results and Discussion

The south foundation thermal test section is taken as representative. Figure 3 shows soil temperatures since September 1, 2006, for the sensors in the gravel fill and natural silt to 2.26 m below the top of the jacking pad. The soil temperature did not fall below freezing here.

Figure 4 shows soil-water content since September 1, 2006, for the sensors in the gravel fill and natural silt to 2.26 m below the top of the jacking pad. The sensors in the natural silt, below the gravel fill, show the soil to be very moist, near saturation. The gravel fill is very dry, between about 5 to 7 percent by volume. The graph shows seasonal variability in soil-water content in the silt. The driest time is in the spring. Fall 2007 shows higher soil-water content than the same period in 2006. The monitoring needs to continue in order to ascertain if this is simply seasonal variability, if the soil

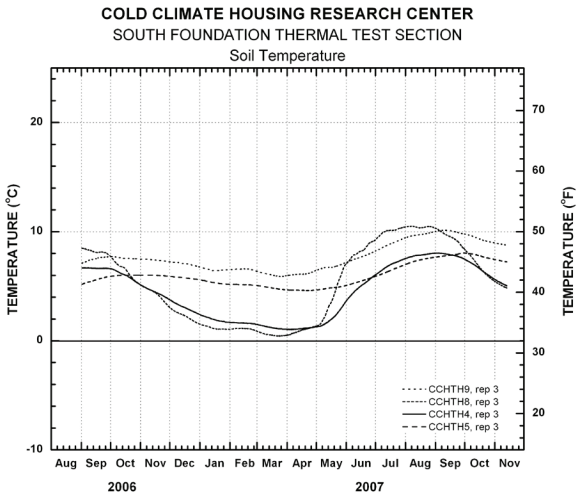

Figure 3. South foundation thermal test section: soil temperature in the gravel fill and in the natural silt.

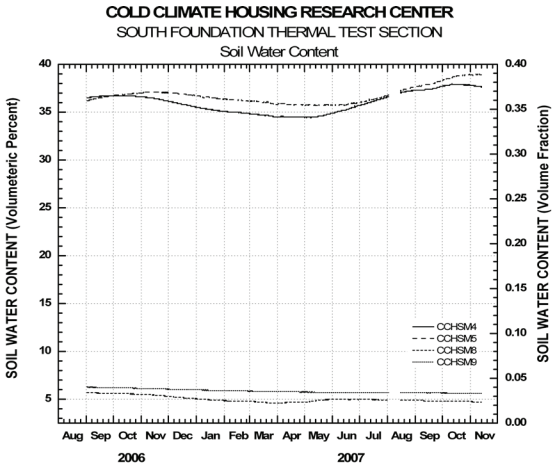

Figure 4. South foundation thermal test section: soil-water content in the gravel fill and in the natural silt.

is getting wetter, or if the soil was dried during construction and is returning to a stable state.

Summary

The CCHRC RTF is a state-of-the-art facility located on shallow permafrost. The building foundation is designed to allow compensation for any differential settlement resulting from permafrost degradation. The building and surrounding area is heavily instrumented to allow soil-temperature and soil-moisture monitoring. The monitoring system is designed for long-term use. Preliminary results are given, but it is too soon to tell if the ground beneath the building has reached equilibrium after the disturbance resulting from the construction.

References

Murton, J.B. & French, H.M. 1994. Cryostructures in permafrost, Tuktoyaktuk coastlands, western Arctic Canada. *Canadian Journal of Earth Sciences* 31: 737-747.

The Role of Permafrost in the 2002 Ten Mile Creek Debris Torrent, Yukon, Canada

Panya Lipovsky
Yukon Geological Survey, Whitehorse, Canada
Crystal Huscroft
Thompson Rivers University, Kamloops, Canada
Antoni Lewkowicz
University of Ottawa, Ottawa, Canada
Bernd Etzelmüller
University of Oslo, Oslo, Norway

Introduction

In June 2002, a catastrophic debris torrent initiated from a moderate north-facing slope in the headwaters of Ten Mile Creek, in central Yukon, Canada. Field evidence indicates that permafrost was a major contributing factor that caused an initial landslide which then triggered the debris torrent. The mechanism of failure in the initial landslide appears to be unique in comparison to other permafrost-related landslides (i.e., retrogressive thaw failures and active layer detachments) documented in the region (Lipovsky et al. 2006, Lipovsky & Huscroft 2007, Lyle 2006).

Setting

The landslide source zone is located at 1084 m elevation, 15 km southeast of the town of Carmacks in central Yukon, Canada (61°58′45.4″N, 136°08′20.7″W). Based on field observations and aerial photograph analysis of the terrain immediately surrounding the source zone, the pre-failure slope is estimated to have been moderately steep (up to 27°) with a typical boreal forest cover consisting of low shrubs, mosses and mature spruce trees.

The landslide left a bowl-shaped scar up to 160 m wide and 100 m long with a steep headwall 12–31 m high (Fig. 1). Springs flow from the base of a secondary slump scar in the floor of this bowl. Following the initial failure, an ensuing debris torrent descended 500 m in elevation and traveled 4.7 km down the narrow *v*-shaped valley of Ten Mile Creek. The main debris lobe came to rest after crossing the South Klondike Highway, clogging its culvert and filling the adjacent ditch with debris. Superelevation measurements taken on a channel bend in the runout zone indicate that the torrent traveled at a maximum velocity of 11 m/s (40 km/hr) with a peak discharge of 1300 m^3/s.

Along much of the debris torrent path, a swath of trees averaging 35 m wide was cleared through mature forest adjacent to the former stream channel. Silty loam diamicton (containing 35–43% coarse fragments) was deposited up to 1.3 m thick along most of the debris torrent path, except within a 600 m long canyon segment confined by steep rock walls. Ongoing remobilization of these deposits by subsequent stream flow has caused sedimentation of local salmon habitat at the mouth of the creek where it flows into Nordenskiold River.

Surficial geological materials exposed in the landslide headwall consist of a stony till blanket up to 12.5 m thick overlying at least 22 m of glaciofluvial sand and gravel exhibiting prominent bedding structures. At numerous locations up to 3.7 km downstream from the source zone, discrete blocks of sandy material deposited by the debris torrent and originating from this lower glaciofluvial unit show intact primary bedding structures. In order to preserve these features over such a long transport distance, the sediment must have been frozen both before and during transport. This implies that in the landslide source zone permafrost must have extended into the glaciofluvial unit found at least 12.5 m below the ground surface.

Local Permafrost Conditions

Ten Mile Creek is located within Yukon's extensive discontinuous permafrost zone. Permafrost is commonly found on north-facing slopes in this region, particularly

Figure 1. Aerial view of landslide source zone showing debris torrent channel exiting at lower left corner. Maximum height of the headwall is 31 m and the bowl is approximately 160 m wide.

beneath thick organic mats associated with boreal forest cover.

Surface probing behind the landslide headwall in late summer 2004 indicated an active layer thickness of 42–86 cm where the organic mat was at least 40 cm thick. Where the organic mat was thinner, the permafrost table was not encountered within 1.05 m of the ground surface, however it was assumed to be present at greater depth. Thermistor measurements and lateral probing into the lower headwall did not detect permafrost in the glaciofluvial unit at this time (ground temperatures 1 m into the face were ~1°C).

DC resistivity surveys conducted in 2006 suggest that permafrost is up to 5 m thick on the gentle north-facing slope behind the landslide headwall, and up to 15 m thick on the steeper north-facing slope adjacent to the landslide source zone (Fig. 1). The resistivity surveys also confirmed the absence of permafrost in the landslide headwall, implying that rapid lateral thaw has occurred since the failure occurred in 2002.

Landslide Failure Mechanism

Unfrozen glaciofluvial sand and gravel exposed in the lower unit of the landslide headwall are highly permeable and porous, with a capacity to store and transmit a large amount of groundwater. This is confirmed by the presence of springs flowing from the floor of the landslide source zone scar. Based on aerial photograph interpretation, these sediments are part of a larger geological unit consisting of bedded glaciofluvial deltaic materials that extend laterally further upslope and capture groundwater from the upper drainage basin. As a result of this geomorphic configuration, the site of the landslide source area represents the location of greatest groundwater convergence within that basin. We hypothesize, therefore, that the base of the impermeable permafrost layer within these sediments confined groundwater flow and allowed high pore pressures to accumulate below the permafrost during the spring snowmelt period in June 2002. During the same time period, no abnormal precipitation was recorded and no earthquakes occurred in the vicinity. We suggest that pore pressures increased until a threshold was reached that allowed rupture or "blow-off" (Cavers 2003) of the unfrozen materials and detachment of the entire permafrost layer above.

We infer that subsequent rapid drainage of stored groundwater supplied a large volume of water which facilitated the catastrophic debris torrent. Similar failure mechanisms are common in non-permafrost areas throughout western Canada where groundwater pressures are instead confined by surficial material stratigraphy rather than by frozen ground (Cavers 2003). Alternatively, the initial movement could have partially blocked a small stream channel to the northeast allowing water to accumulate in a pond. However, we were unable to locate any evidence of such ponding in the field.

Local and regional climatic data show that at least four decades of climate warming have occurred in central Yukon since 1930. Any corresponding permafrost warming and/or thinning may have weakened the permafrost layer and lowered the pore pressure threshold required to initiate a failure and cause detachment. Dataloggers were installed in 2005 to monitor the long-term air and ground surface temperatures above the landslide source zone.

Implications

The results of this study have important implications for future development and land use planning in the area, as the geomorphic setting of the landslide source zone is widespread throughout much of central Yukon. This case study illustrates that significant hazards are associated with this type of landslide. It also highlights the need to perform detailed evaluations of basin characteristics, permafrost conditions, and surficial material stratigraphy several kilometers upslope of any area targeted for human land use. In particular, stream crossing designs and development on fans in permafrost regions should carefully consider the risk of debris torrents triggered by groundwater blow-off failures beneath frozen ground.

Acknowledgments

Funding was provided by NSERC and the University of Ottawa to A. Lewkowicz; by the University of Oslo to B. Etzelmüller; and by the Yukon Geological Survey to P. Lipovsky and C. Huscroft.

References

Cavers, D.S. 2003. Groundwater blow-off and piping debris flow failures. *Proceedings, 3rd Canadian Conference on Geotechnique and Natural Hazards, Edmonton, Alberta, June 9–10, 2003*: 151-158.

Lipovsky, P. & Huscroft, C. 2007. A reconnaissance inventory of permafrost-related landslides in the Pelly River watershed, central Yukon. In: D.S. Emond, L.L. Lewis & L.H. Weston (eds.), *Yukon Exploration and Geology 2006*. Yukon Geological Survey, 181-195.

Lipovsky, P.S., Coates, J., Lewkowicz, A.G. & Trochim, E. 2006. Active-layer detachments following the summer 2004 forest fires near Dawson City, Yukon. In: D.S. Emond, G.D. Bradshaw, L.L. Lewis & L.H. Weston (eds.), *Yukon Exploration and Geology 2005*. Yukon Geological Survey, 175-194.

Lyle, R.R. 2006. *Landslide susceptibility mapping in discontinuous permafrost, Little Salmon Lake, Central Yukon*. M.Sc.E. Thesis. Queen's University, 351 pp.

Carbon Gas Fluxes from Contrasting Boreal Lakes During Intensive Rain Events

Jessica López Bellido
University of Helsinki, Department of Ecological and Environmental Science, Niemenkatu 73, FIN-15140 Lahti, Finland
Anne Ojala
University of Helsinki, Department of Ecological and Environmental Science, Niemenkatu 73, FIN-15140 Lahti, Finland

Introduction

The variability in climate and weather are typical characteristics in the Northern Hemisphere, which by itself already has a strong impact in the hydrology and ecology of freshwater ecosystems. Change in climate variables, such as temperature and precipitation, will definitely impact aquatic species at various trophic levels and alter the physical and chemical processes that act on and within the lake ecosystem. Nevertheless, not only will the extreme seasonality affect the aquatic ecosystems, but also their surrounding areas. For instance, the Nordic region has a vast variety of terrains which contain a significant number and diversity of lakes. This linked pathway makes the lakes vulnerable to changes due to the direct impact from the adjacent terrestrial ecosystem, leading to the reduction or abundance of organic matter which, in turn, significantly impacts aquatic production, that is, agriculture, forestry, and urbanization. Under this process of human disturbance, the flux of gases between land, water, and atmosphere has been radically altered; thus, the increase of greenhouses gases to the atmosphere, mainly of carbon dioxide and methane.

At high latitudes, wetlands (i.e., lakes, ponds, and peatlands) are the key feature of the landscape. Among wetlands, lakes are the most important areas where radical changes in water management or climate can significantly affect the quality of human life. On the other hand, lakes themselves can affect the climate system. Globally, lakes are supersaturated with CO_2 and CH_4 (Cole & Caraco 1998). Lakes in Finland have also been shown to be supersaturated with these greenhouse gases (Kortelainen 2000). They play an important role, therefore, in the exchange of CO_2 and CH_4 at the regional and global scale due to the amount of carbon stored in these ecosystems. This is actually a concern due to the projections in global climate change in Nordic areas, where today's sinks can be turned into sources of carbon dioxide and methane.

In this study, we explored CO_2 and CH_4 fluxes from two lakes with contrasting limnological characteristics in southern Finland: Lake Ormajärvi, a clear-water lake, and Lake Pääjärvi, a humic brown–water system. The main hypothesis was that the two lakes differ in their carbon gas fluxes, where the humic lake, which processes more organic carbon of terrestrial origin, shows larger CO_2 fluxes, whereas CH_4 fluxes were higher from the more eutrophic clear-water lake. Due to the limnological distinctions supposedly resulting in differences in timing and intensity of mixing periods, differences in seasonal flux patterns were examined as well as their relation to biological carbon uptake and carbon mineralization in the epilimnion of the pelagic zone. For instance, it was also hypothesized that fluxes from the clear water Lake Ormajärvi are more closely connected to autochthonous carbon uptake, whereas in the brown-water Lake Pääjärvi, the system is fueled more by allochthonous carbon; thus fluxes and mineralization processes are tied together. Finally, since during the study year 2004 the summertime precipitation in the area doubled from the ordinary 200–220 mm to 413 mm and the extra rain poured down in four events June–July, the opportunity allowed the study of lake response to an extreme weather event.

Methods

Measurements of CO_2 and CH_4 fluxes were based on surface water concentrations as well as gas accumulation in floating closed chambers.

Primary production was measured by the radiocarbon technique, using light/dark bottle incubations (Schindler et al. 1972). Plankton community respiration, that is, biological mineralization of organic carbon, was estimated from the consumption of dissolved oxygen. For final results, the rates of oxygen consumption were converted to rates of CO_2 release using a value of one for the respiratory quotient (RQ) (Wetzel & Likens 2000). To facilitate the comparison between the two different lakes, the data from respiration measurements as well as primary production were areally integrated. Pelagic CO_2 net production due to biological processes was then calculated by subtracting the primary production from the pelagic mineralization.

Results and Discussion

Both lakes presented seasonalities in fluxes, so the gases accumulated under ice and in the hypolimnion were ventilated out in spring and autumn. The annual CO_2 fluxes from Lake Ormajärvi and Lake Pääjärvi were 3.6 mol m^{-2} y^{-1} and 6.1 mol m^{-2} y^{-1}, respectively, and both lakes acted as a source of CO_2. The corresponding values for CH_4 were 24.5 mmol m^{-2} y^{-1} and 18.5 mmol m^{-2} y^{-1}. In terms of global warming potential on annual basis, CH_4 had contributed 7.4% and 19.0% in Lake Pääjärvi and in Lake Ormajärvi, respectively.

The most distinctive results of this study were the overwhelming importance of rain events to gas fluxes. In Lake Pääjärvi, the high precipitation resulted in a large peak in CO_2 and CH_4 fluxes which lasted for a couple of weeks and contributed to 46% in CO_2 and 48% in CH_4 annual fluxes. In Lake Ormajärvi, the contribution of the rainy period to carbon gas fluxes was 39% and 37% for CH_4 and CO_2, respectively. The response of Lake Ormajärvi fluxes to high

precipitation was not as sudden and immediate as in Lake Pääjärvi, but the outcome was more radical, since before the rainy period the lake was autotrophic; that is, photosynthesis exceeded respiration. When the rains started, however, the lake turned to heterotrophy with respiration exceeding photosynthesis. Opposite to Lake Ormajärvi, Lake Pääjärvi appeared net heterotrophic throughout the study period. By thoroughly analyzing the results on biological processes within the lakes, the "extra" CO_2 and CH_4 did not originate from mineralization processes within the lakes, but the gases were flushed into the lakes from the surrounding terrestrial soil and were of allochthonous origin.

Conclusion

This study demonstrated that the link between the catchment and the lake is more immediate than anticipated and is strongly controlled by hydrology. Also, the role of input of CO_2 and CH_4 can be significant even in summertime, when there is an extreme rainfall event. In northern Europe, these kinds of high extremes of precipitation are very likely to increase in magnitude and frequency due to climate change. Thus, for correct estimates of carbon exchange of terrestrial ecosystems, the role of lakes as efflux sites of carbon gases of terrestrial origin should be taken into account.

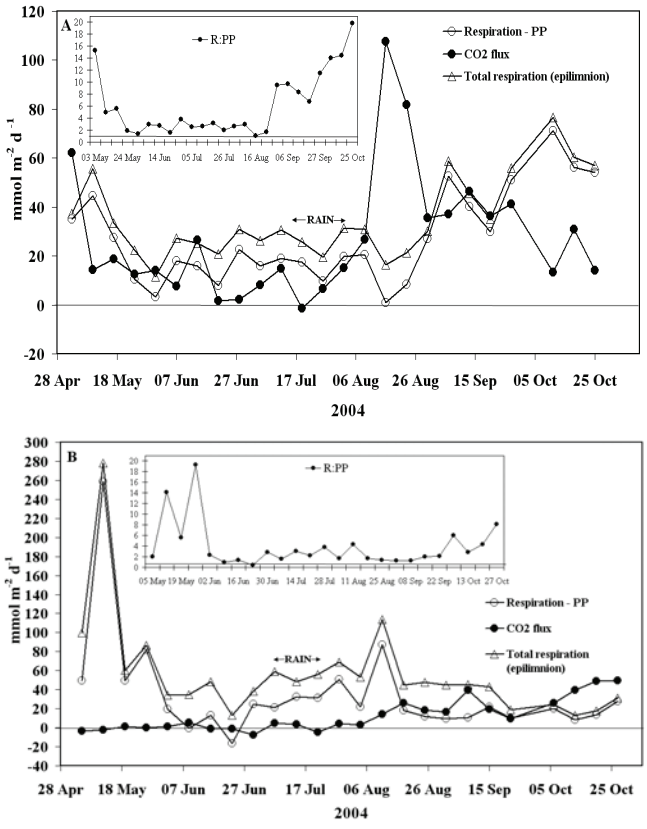

Figure 1. CO_2 net production and community respiration in relation to ΔCO_2 flux in (A) Lake Pääjärvi and (B) Lake Ormajärvi. The period of heaviest rains is shown with arrows. The inserts display R:PP ratios in both lakes.

Acknowledgments

Financial support was provided by NECC (Nordic Center of Excellence for Studies of Ecosystem Carbon Exchange and its Interactions with Climate Ecosystem). Thanks are also to Lammi Biological Station of the University of Helsinki.

References

Cole, J.J. & Caraco, N.F. 1998. Atmospheric exchange of carbon dioxide in low-wind oligotrophic lake measured by the addition of SF_6. *Limnol. Oceanogr*. 43: 647-656.

Kortelainen, P., Huttunen, J., Väisänen, T., Mattsson, T., Karjalainen, P. & Martikainen, P. 2000. CH_4, CO_2 and N_2O supersaturation in 12 Finnish lakes before and after ice melt. *Verh. Int. Ver. Limnol*. 27(3): 1410-1414

Schindler, D.W., Schmidt, R.V. & Reid, R. 1972. Acidification and bubbling as an alternative to filtration in determining phytoplankton production by the ^{14}C method. *J. Fish. Res. Board Can*. 29: 1627-1631.

Wetzel, R.G. & Likens, G. 2000. *Limnological Analyses*, 2nd ed. New York, NY: Springer Verlag.

The Sensitivity of SiBCASA-Simulated Carbon Fluxes and Biomass to North American Interannual Climate Variations

Lixin Lu
Department of Atmospheric Science, Colorado State University, Fort Collins; and CIRES and ATOC, University of Colorado, Boulder, Colorado
Kevin Schaefer, Tingjun Zhang
CIRES and NSIDC, University of Colorado, Boulder, Colorado
Ian Baker
Department of Atmospheric Science, Colorado State University, Fort Collins

Introduction

Simple Biosphere model (SiB2.5) (Sellers et al. 1996a,b) is coupled with Carnegie-Ames-Stanford Approach model (CASA) (Potter et al. 1993, Randerson et al. 1996) to form a new model, SiBCASA, which is capable of simulating diurnal to interannual variations of terrestrial carbon fluxes and biomass at plot to global scales (Shaefer et al. 2008a). While prescribing leaf biomass derived from remotely sensed Normalized Difference Vegetation Index (NDVI), SiBCASA can dynamically allocate carbon to leaf, root, and wood pools, and explicitly calculate autotrophic respiration.

To improve winter-process simulations, Schaefer et al (2008b) improved the snow and soil freeze- and thaw-related algorithms in SiBCASA. These modifications include, incorporating Sturm et al. (1995) snow classification system, adopting the Lawrence and Slater (2005) organic soil model, and extending the soil column depth to 15 m with an increased number of soil layers. These changes greatly improved the SiBCASA-simulated snow density, snow depth, as well as soil temperature, to more realistic ranges with observations.

Study Sites and Experiment Design

Nine eddy covariance flux tower sites (include Barrow, Bondville, Boreas old black spruce, Harvard Forest, Howland Forest, Lethbridge, Niwot Ridge, Park Falls, and Winder River) across a range of the climate-ecosystem zones are selected for initial evaluations of SiBCASA-simulated biophysical and biogeochemical processes (shown in Fig. 1). The meteorological forcings are derived from 32-km grid-spacing North American Regional Reanalysis product spanning 1979 through 2003 at 3-hourly time-step. Modeled carbon fluxes and biomass at these sites are evaluated against tower-observed values. In particular, the parameterizations describing cold-land processes were developed and implemented to better represent the interactions between snow cover, soil thermodynamics, and soil freeze-thaw processes, as well as their influences on carbon cycle over permafrost regions.

A suite of sensitivity experiment is performed by perturbing the atmospheric forcing variables one at a time. Maximum and minimum temperatures are increased and decreased 2°C, while precipitations are increased and decreased 25% of their original values. SiBCASA-simulated carbon fluxes and biomass are also sensitive to the initial conditions

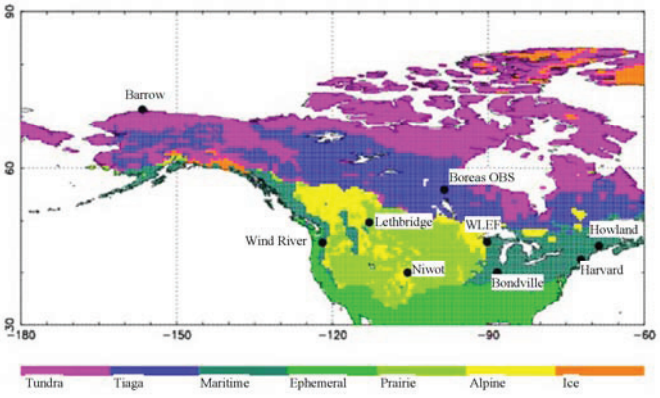

Figure 1. The distribution of nine study sites over the North America domain. These sites are coincident with Ameriflux eddy covariance flux tower sites.

of soil moisture and temperature, snow depth, and initial woody pool size. Statistical analyses are being carried out to understand how these climate perturbations and changes in initial conditions influence the predictions of carbon fluxes and biomass. These experiments, by artificially manipulating the input data to imitate possible future scenarios, will enable us to assess and quantify the sensitivity of North American carbon cycle to large-scale climate change.

Preliminary Results

Heat fluxes

The upper two panels in Figure 2 show SiBCASA-simulated latent and sensible heat fluxes from 1982 through 2004 at the Barrow site. Monthly mean values are plotted to highlight the interannual variations. From year to year, both sensible and latent heat fluxes show changes up to 30% and 40% of their averaged values, respectively. A mid-year latent-heat-flux depression persists throughout the simulation time period, indicating that soil might be drying out due to surface evapotranspiration and soil hydrology before it is replenished by summer rainfalls. The latent heat fluxes share the same sign of temperature changes, up to 30% of their original values when temperature increases or decreases by 2°C. The sensible heat fluxes only vary up to 10% of their original values with the same magnitude of temperature changes as in the latent heat flux experiment, and most importantly, they are in opposite sign of temperature changes. Both heat fluxes respond to precipitation perturbations in much

smaller magnitude and a more non-linear fashion. Most of the time, increased precipitations result in increased latent heat fluxes and reduced sensible heat fluxes, and vice versa. These results imply that the heat fluxes at the Barrow site are more controlled by temperatures than precipitations; it is an energy-limited moist site.

Carbon fluxes and pools

Figure 3 shows clear seasonal cycles and large interannual variability of Net Ecosystem Exchange (NEE) and wood pool modeled by SiBCASA. During summer months, when temperatures increase, the photosynthesis uptake exceeds the respiratory carbon release, resulting in increased net CO_2 uptake. This might be a result of very long daylight hours in Arctic summer. The model shows minimal sensitivity of NEE in winter months, largely because the negligible *R* during very cold winter and the complete shutdown of photosynthetic uptake. In general, increase temperatures and precipitations lead to increased wood pools, and vice versa.

Presently, more detailed statistical analyses are being performed to the results from the SiBCASA sensitivity experiments.

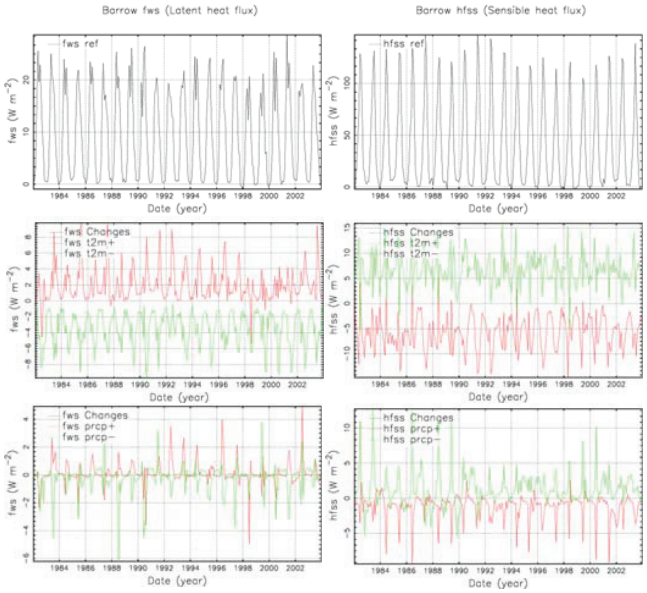

Figure 2. SiBCASA-simulated latent and sensible heat fluxes from 1982 through 2004 at the Barrow site. Also shown are changes in heat fluxes to perturbations of temperatures and precipitations. In these plots, monthly mean values are aggregated from 15-minute time-step model outputs.

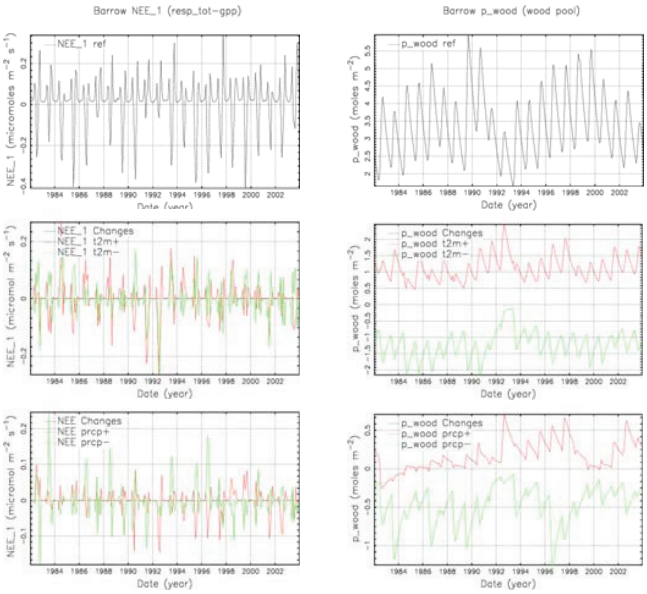

Figure 3. SiBCASA-simulated net ecosystem exchange and wood pools from 1982 through 2004 at Barrow site. Also shown are changes in NEE and wood pool to perturbations of temperatures and precipitations. In these plots, monthly mean values are aggregated from 15-minute time-step model outputs.

Acknowledgments

This study is supported by the U.S. National Aeronautics and Space Administration (NASA) grant NNX06AE65G to the University of Colorado at Boulder.

References

Lawrence, D.M. & Slater, A.G. 2005. A projection of severe near-surface permafrost degradation during the 21st century. *Geophys. Res. Lett*. 32(24): doi:10.1029/2005GL025080.

Potter, C.S., Randerson, J.T., Field, C.B., Matson, P.A., Vitousek, P.M., Mooney, H.A., & Klooster, S.A. 1993. Terrestrial ecosystem production: A process-oriented model based on global satellite and surface data. *Global Biogeochem. Cycles* 7: 811-842.

Randerson, J.T., Thompson, M.V., Conway, T.J., Field, C.B. & Fung, I.Y. 1996. Substrate limitations for heterotrophs: Implications for models that estimate the seasonal cycle of atmospheric CO_2. *Global Biogeochem. Cycles* 10(4): 585-602.

Schaefer, K, Collatz, G.J., Tans, P, Denning, A.S., Baker, I., Berry, J., Prihodko, L., Suits, N. & Philpott, A. 2008a. The combined Simple Biosphere/Carnegie-Ames-Stanford Approach (SiBCASA) terrestrial carbon cycle model. *J. Geophys. Res*. (in press).

Schaefer, K., Zhang, T.J., Lu, L. & Baker, I. 2008b. Applying snow classification system and organic soil properties to the SiBCASA model. *JGR-Atmosphere* (to be submitted).

Seller, P.J., Randall, D.A., Collatz, G.J., Berry, J.A., Field, C.B., Dazlich, D.A., Zhang, C., Collelo, G.D. & Bounoua, L. 1996a. A revised land surface parameterization of GCMs, Part I: Model Formulation. *J. Clim*. 9(4): 676-705.

Sellers, P.J., Los, S.O., Tucker, C.J., Justice, C.O., Dazlich, D.A., Collatz, G.J. & Randall, D.A. 1996b: A revised land surface parameterization of GCMs, Part II: The generation of global fields of terrestrial biosphysical parameters from satellite data. *J. Clim.* 9(4): 706-737.

Sturm, M., Holgren, J. & Liston, G.E. 1995. A seasonal snow cover classification system for local to global applications, *J. Clim*. 8(5): 1261-1283.

Permafrost Characteristics and Climate Change Consequences at Stockhorn and Gornergrat (Swiss Alps)

Clemens Constantin Maag, Oliver Wild, Lorenz King
Justus-Liebig-University Giessen, Germany
Martin Baum, Sebastian Klein, Christin Hilbich
Friedrich-Schiller-University Jena, Germany

Introduction

The Stockhorn-Gornergrat tourist area is of high interest for the study of mountain permafrost and aspects of climate change. Within the EU-project PACE, a 100 m deep drilling located at 3405 m a.s.l. points to a permafrost thickness of about 170 m at the Stockhorn Plateau. Since then, long-term monitoring of the bedrock and permafrost conditions started. A reorganization of the ski region due to changed tourist expectations led to both new ski slopes and cable car connections. The necessary construction work provides the opportunity for new findings of the existing permafrost conditions. Stockhorn qualifies as a salient research area, as it is only marginally affected by the tourist industry yet is within the well-examined Zermatt research area, and only 10 km by airline from Kleinmatterhorn (3883 m a.s.l.) (King et al. 2008). These conditions allow observation of climatic developments due to climate change and construction measures.

Alpine Natural Hazards at Gornergrat

Climate change and accompanying effects like rising temperatures have created new alpine phenomena and dangers. Avalanches, rockfalls and water inclusions may appear more often due to the steady warming of the atmosphere. In 2003, the rise of temperatures resulted in permafrost thaw and exceptional rockfalls (Gruber et al 2004b). As further research projects showed, characteristics of rock walls and their temperature depend not only on the quality of solar radiation and air temperature, but also on their topographic distribution (Gruber et al. 2004).

As the Stockhorn and Gornergrat are highly frequented by large numbers of tourists and skiers, the characteristics of this area must be constantly monitored.

Ground Ice at Kelle

The area Kelle at the northern slopes of the east–west running Gornergrat crest (3135 m) and Hohtälli (3286 m a.s.l.) is well known for its permafrost occurrences. Visible indicators are rock glaciers and perennial snow patches. Scientific studies consisted of measurements of ground temperatures and BTS values (Philippi 2003) and the development of permafrost models (Gruber 2000). In summer 2007, excavation work for a new ski run and a culvert system for artificial snow was carried out, and ground ice was exposed at various sites. The new ski run has a length of 2.5 km and 300 m altitudinal difference, and crosses rock glaciers and rock glacier-like features. Near-surface top layers were removed down to a depth of 8 to 10 m at some places. This offered the rare opportunity to have a look inside these features. The excavation was accompanied throughout 2007 by researchers of different universities. Geophysical measurements were carried out (Hilbich et al. 2007), ice samples taken, and the course of the ski track surveyed (Giessen, Zurich). Melting of the ground ice was already observed during the construction period.

Figure 1. Ground ice of the rock glacier with water conduit for artificial snow production (lower right).

Geophysical Analyses

In order to observe climate-related permafrost degradation, a fix ERT monitoring system was installed at the Stockhorn plateau in summer 2005 (Hilbich et al. 2008) in close co-operation with the PERMOS network (Permafrost Monitoring Switzerland). It enables regular (preferably seasonal) semi-automatic measurements of the apparent electrical resistivity of the ground. The ERT section consists of 55 electrodes with a spacing of 2 m, resulting in a length of 108 m in total. The vertical penetration depth is about 20 m.

Figure 2 shows the computed results of an ERT measurement made in September 2007. The position of the PACE boreholes are marked; however they may have a lateral offset of about 10 m to the ERT line.

In addition, the electrode array was complemented by a coinciding fix transect for refraction seismic monitoring in summer 2007. For the refraction seismic monitoring, one short (2 m spacing) and one long (4 m spacing) section with 24 geophones each were installed to account for both high spatial resolution (at a length of 46 m) and extension across the whole ERT line (96 m).

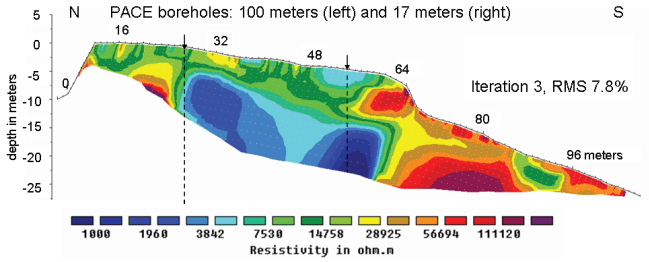

Figure 2. ERT results at Stockhorn Plateau and positions of the PACE boreholes 60/00 (left) and 61/00 (right).

In order to analyze the computed results of the seismic and geo-electric measurements, 4 temperature loggers were installed at a depth of 30 cm, with a lateral offset of about 5 m all along the section.

First results of the geophysical monitoring reveal a pronounced seasonal active layer dynamic up to a depth of about 3 to 5 m. Variations are due to the distinctive topography of the plateau with steeply inclined northern and southern slopes. This characteristic topography also influences the 3D subsurface temperature field, which has to be considered at the interpretation of borehole temperatures.

The combination of both geo-electric and seismic analysis allows the determination of the total content and temporal change of frozen and unfrozen water and air-filled pore space in the subsurface of this plateau (Hauck et al. 2008).

The PACE Monitoring Site Stockhorn

The studies at Stockhorn and Gornergrat directly relate to actual and current aspects of permafrost research under tourist aspects. The various continuous approaches allow a full understanding of the described factors in the high mountain area. Future research will aim at the investigation of the collected PACE data and the embedding into the general research in Valais. The data of both boreholes (100 m and 17 m) will be compared at a depth of 10 m in order to classify the results. Therefore one aspect is to develop a concept for the interpretation of the ongoing measurements under consideration of the natural disturbances and the modeling of corresponding temperature histories. To what extent the overall influence of climate change on both rock and air temperature is intensified by building measures in the alpine regions is of great interest for the tourism industry. A newly structured implementation of this area into the tourist concept generates unique scientific research possibilities due to the rather peripheral location within the Zermatt alpine region.

Acknowledgments

The authors are especially thankful for the support provided by the Zermatt Bergbahnen AG, which made the scientific research possible. Stephan Gruber (Zurich) and Thomas Herz (Giessen) were a crucial help in the data analyses.

References

Gruber, S. 2000. *Slope Instability and Permafrost, a Spatial Analysis in the Matter Valley, Switzerland*. Unpublished master thesis, Germany: Institute of Geography, Justus Liebig University Giessen.

Gruber, S., King, L., Kohl, T., Herz, T., Haeberli, W. & Hoelzle, M. 2004. Interpretation of geothermal profiles perturbed by topography: The alpine permafrost boreholes at Stockhorn Plateau, Switzerland. *Permafrost and Periglacial Processes* 15: 349-357.

Gruber, S., Hoelzle, M. & Haeberli, W. 2004a. Rock-wall temperatures in the Alps: Modelling their topographic distribution and regional differences. *Permafrost and Periglacial Processes* 15: 299-307.

Gruber, S., Hoelzle, M. & Haeberli, W. 2004b. Permafrost thaw and destabilization of alpine rock walls in the hot summer of 2003. *Geophysical Research Letters* 31: doi:10.1029/2004GL020051.

Hauck, C., Bach, M. & Hilbich, C. 2008. A 4-phase model to quantify subsurface ice and water content in permafrost regions based on geophysical datasets. *Proceedings of the Ninth International Conference on Permafrost, Fairbanks, Alaska, June 23–July 3, 2008.*

Hilbich, C. Roer, I & Hauck, C. 2007. Ground truth observations of the interior of a rockglacier as validation for geophysical monitoring data sets. *Eos Trans. AGU* 88(52), Fall Meet. Suppl., Abstracts C21a-0056.

Hilbich, C. et al. 2008. A geo-electric monitoring network and resistivity-temperature relationships of different mountain permafrost sites in the Swiss Alps. *Proceedings of the Ninth International Conference on Permafrost, Fairbanks, Alaska, June 23–July 3, 2008.*

King, L., Hof, R., Herz, T & Gruber, S. 2003. Long-term monitoring of borehole temperatures and permafrost-related data for climate change research and natural hazard management: Examples from the Mattertal, Swiss Alps. *Proceedings of the Eighth International Conference on Permafrost, Zurich, Switzerland, July 20-25, 2003*: 77-78.

King, L. Maag, C.C. & Baumann, C. 2008. Impacts of Climate Warming and Facilities on Rock Temperatures at a Tunnel in High Alpine Continuous Permafrost: Results of Long-Term Monitoring at Kleinmatterhorn, Swiss Alps. *Proceedings of the Ninth International Conference on Permafrost, Fairbanks, Alaska, June 23–July 3, 2008.*

Philippi, S., Herz, T. & King, L. 2003. Near-surface ground temperatures and permafrost distribution at Gornergrat, Matter valley, Swiss Alps. *Proceedings of the Eighth International Conference on Permafrost, Zurich, Switzerland, July 20-25, 2003*: 129-130.

The Microtopography of Periglacial Landforms on Mars

Nicolas Mangold
Laboratoire IDES, CNRS and Université Paris Sud, 91405 Orsay, France

Introduction

The planet Mars is covered by many landforms involving water ice, either at surface or at depth. These landforms are important in studying the geographic distribution of water ice, its temporal variation, and the possibility of freeze-thaw cycles in past epochs. Geologically recent Martian hillside gullies, discovered in Mars Orbiter Camera (MOC) Narrow Angle (NA) images (Malin & Edgett 2000), exhibit characteristic morphologies similar to terrestrial debris flows in mountain or arctic regions, formed by flowing water or water-rich slurries, leading Malin and Edgett (2000) to suggest that they, too, were formed by the action of water. Processes other than water erosion have been proposed to explain the formation of gullies, including the action of CO2-based debris flows (e.g., Musselwhite et al. 2001) and granular avalanches or mass wasting of CO2 frost (e.g., Ishii & Sasaki 2004). The role of liquid water is still debated, especially given the subfreezing mean temperature (-60°C) that might only reach submelting temperatures during high obliquity periods of the past (Costard et al. 2002). The origin of the fluid is also questioned. Various mechanisms for the formation of gullies by water have been proposed, although fundamentally they can be divided into either atmospheric or groundwater processes depending on the source of the water.

Until recently the only available images with sufficient resolution to detect gullies have been MOC NA data, and most previous studies have used this dataset. However, the HiRISE camera of the Mars Reconnaissance Orbiter provides high resolution (<30 cm/pixel) images that allow us a detailed observation of these landforms (Fig. 1). The microtopography can be measured thanks to methods of photoclinometry that use photometric properties of the surface (sun angle, spacecraft position, material property). This enables us to extract topographic profiles at the scale of the image sampling, thus a few tens of centimeters. We apply this method to the recent gullies, and especially to their transverse profile to examine their depth and their levee size. Indeed, the presence of levees and the end of the channel on slopes steeper than 5° are major arguments favoring a plastic or viscous behavior. These parameters help us to estimate the properties of the flowing material (Mangold et al. 2003), such as flow rate and viscosity, showing that a Bingham law might best explain the presence of levees and channels on slopes higher than 10°.

Methods

Photoclinometry can be used to extract topographic data from an image. Photoclinometry is difficult to use in terrains of various albedo like many regions of Mars, but gullies regions are often of regular albedo due to a thin dust mantle which is favorable to this method. Photoclinometric models are developed using the method described by Davis and Soderblom (1984). Models were calibrated using MOLA (Mars Observer Laser Altimeter) profiles as an envelope for the topography, but at the scale of gullies, MOLA data cannot be used directly because MOLA shot data are 300 m spaced. Cross sections for photoclinometry were chosen orthogonal to the flow, enabling us to assume a horizontal profile between both sides of the channel. Indeed, assuming that the flow is in the direction of the main slope, orthogonal profiles should have the same elevation on both sides of the gullies. Sinuous gullies are frequent on this image. Several studies have noted that debris flow levees are commonly higher on outsides of bends than on insides. This characteristic allows us the determination of the velocities of debris flows (Johnson & Rodine 1984). Indeed, the surface of the flow tilts toward the center of curvature of the bend as a result of the radial acceleration of the debris. The consequence of this tilt after the flow is the presence of larger and broader deposits on the outsides of channel bends. The levees are much narrower on the insides of channels bends. According to Johnson and Rodine (1984), the mean angular velocity of the flow inside the bends can be deduced from the radial acceleration a:

$$a = \frac{V^2}{R} \tag{1}$$

with V the velocity, R the radius of curvature. This radial acceleration is also equal to:

$$a = g \cos\alpha \tan\beta \tag{2}$$

with β the tilt estimated from the difference of elevation of levees (g is gravity and α is the slope).

$$V = \sqrt{gR \cos\alpha \tan\beta} \tag{3}$$

This method gives good measurements of velocities on Earth (Johnson & Rodine 1984).

Results

We have measured levees thickness, width, and channel size for different gullies of the selected image (Fig. 1). The method of levees dissymmetry in bends gives us estimates for the flow velocity. The example of Figure 2 shows typical levees size of 1.7 m on one side and 1 m on the other side, implying a tilt of 2.5° of the flow in this bend. The channel thickness is estimated from the average of the levees at 1.2 m. We find flow rates from 1.1 to 2.9 m/s. These values are small especially because of the small radii of curvature of most gullies of only 20 to 40 m. These flow rates also enable us to estimate the viscosity of the flow by using the measured depth, giving values from 200 to 1500 Pa.s. These viscosities

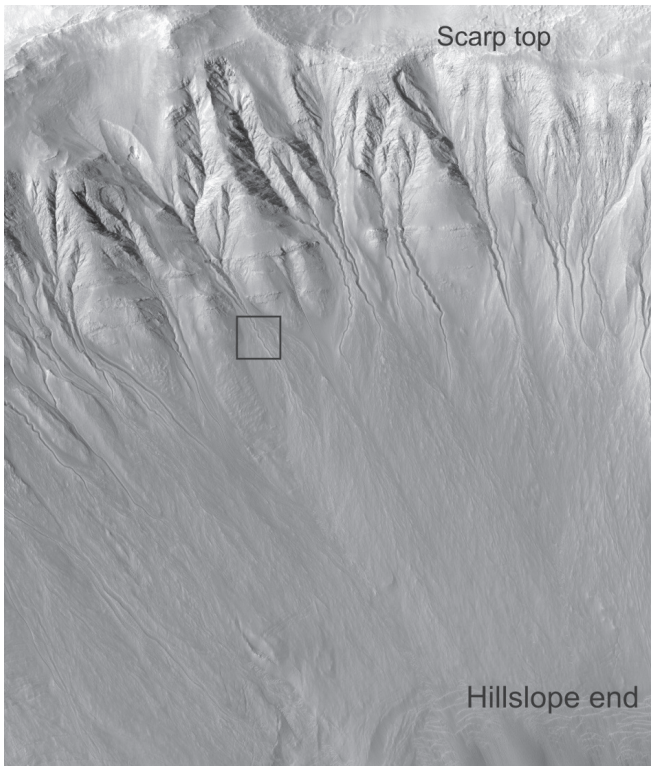

Figure 1. General view of HiRISE image 3464–1380 in Newton Basin. The scarp is about 1 km high. Many gullies are visible showing alcoves in the upward section, channels which typically are found on 10–20° slopes, and large aprons on the downward part. The image is about 2 km large.

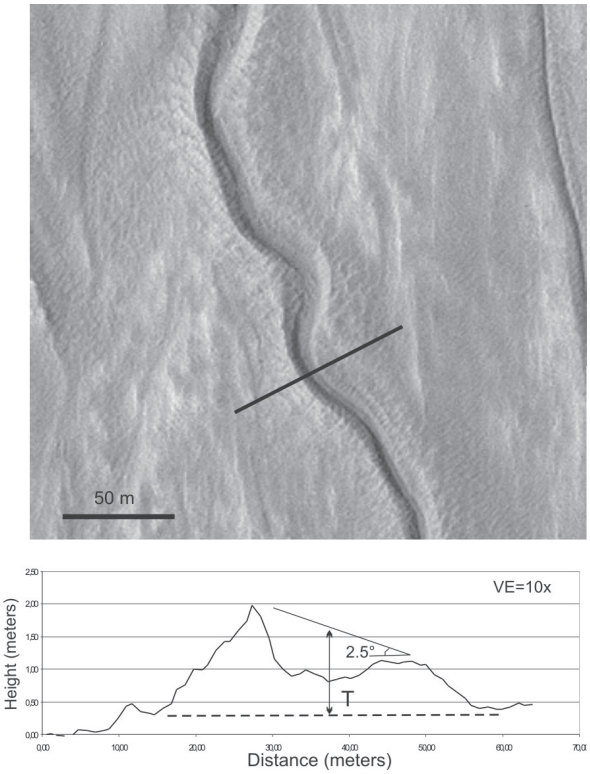

Figure 2. Close-up of Figure 1 on a sinuous channel. The profile shows the topography extracted from photoclinometry. Elevations are exaggerated about 10 times.

and flow rates are typical of viscous debris flows formed by 20 to 40% of liquid water mixed with rocks. This does not exclude other types of material to explain these properties, but excludes granular flows and pure liquid water as a good explanation for the channels observed. More data will be processed as soon as more images become available.

Our study is only preliminary among the large amount of data that are acquired throughout years. We show that the method used is powerful in extraction of material properties from remote sensing data. These results confirm material properties estimates of previous works using MOC images. Given the cold temperatures of Mars, liquid water might form especially from melting of an active layer in summer. Debris flows activity would occur only on the steepest slopes (>20°).

References

Costard, F., Forget, F., Mangold, N. & Peulvast, J.-P. 2002. Formation of recent Martian debris flows by melting of near-surface ground ice at high obliquity. *Science* 295: 110-113.

Davis, P.A. & Soderblom, L.A. 1984. Modeling crater topography and albedo from monoscopic orbiter images 1. Methodology. *J. Geophys. Res.* 89 (B11): 9449-9457.

Ishii, T. & Sasaki, S. 2004. Formation of recent Martian gullies by avalanches of CO_2 frost. *35th Lunar and Planetary Science Conference, 2004,* Abstract 1556.

Johnson, A.M. & Rodine, J.R. 1984. Debris flow. In: D. Brundsen & D.B. Prior (eds.), *Slope Instability*. Wiley and Sons, 257-361.

Malin, M.C. & Edgett, K.S. 2000. Evidence for recent groundwater seepage and surface runoff on Mars, *Science* 288: 2330-2335.

Mangold, N., Costard, F. & Forget, F. 2003. Debris flows over sand dunes on Mars: Evidence for liquid water. *J. Geophys. Res*. 108(E4): 5027.

Musselwhite, D.S., Swindle, T.D. & Lunine, J.I. 2001. Liquid CO2 breakout and the formation of recent small gullies on Mars. *Geophys. Res. Let.* 28(7): 1283-1285.

Coastal Erosion Since 1950 Along the Southeast Chukchi Sea, Alaska, Based on Both GIS and Field Measurements

William F. Manley
INSTAAR, Univ. of Colorado, Boulder, CO 80309-0450
James W. Jordan
Antioch University New England, Dept. of Environmental Studies, Keene, NH 03431
Leanne R. Lestak
INSTAAR, Univ. of Colorado, Boulder, CO 80309-0450
Owen K. Mason
Geoarch Alaska, P.O. Box 91554, Anchorage, AK 99509
Eric G. Parrish
INSTAAR, Univ. of Colorado, Boulder, CO 80309-0450
Diane M. Sanzone
BP Exploration (Alaska) Inc., Anchorage, AK 99519

Coastal environments at high latitudes are experiencing rapid change (e.g., Solomon 2005, Jorgenson & Brown 2005, Mars & Houseknecht 2007). Coastal erosion threatens a variety of nearshore marine, terrestrial, and freshwater habitats, and may be accelerating with Arctic warming. To better understand impacts for national parks in northwestern Alaska, a collaborative study has begun to document coastal change in the southeast Chukchi Sea.

A field-based component includes repeat photography, mapping and description of sediments and landforms, and periodic ground-truth measurements of shoreline change since 1987 at 27 coastal monitoring sites. A geospatial component began with creation of digital orthoimagery over a large area (>6000 km^2) at high resolution (1.0 m or better)

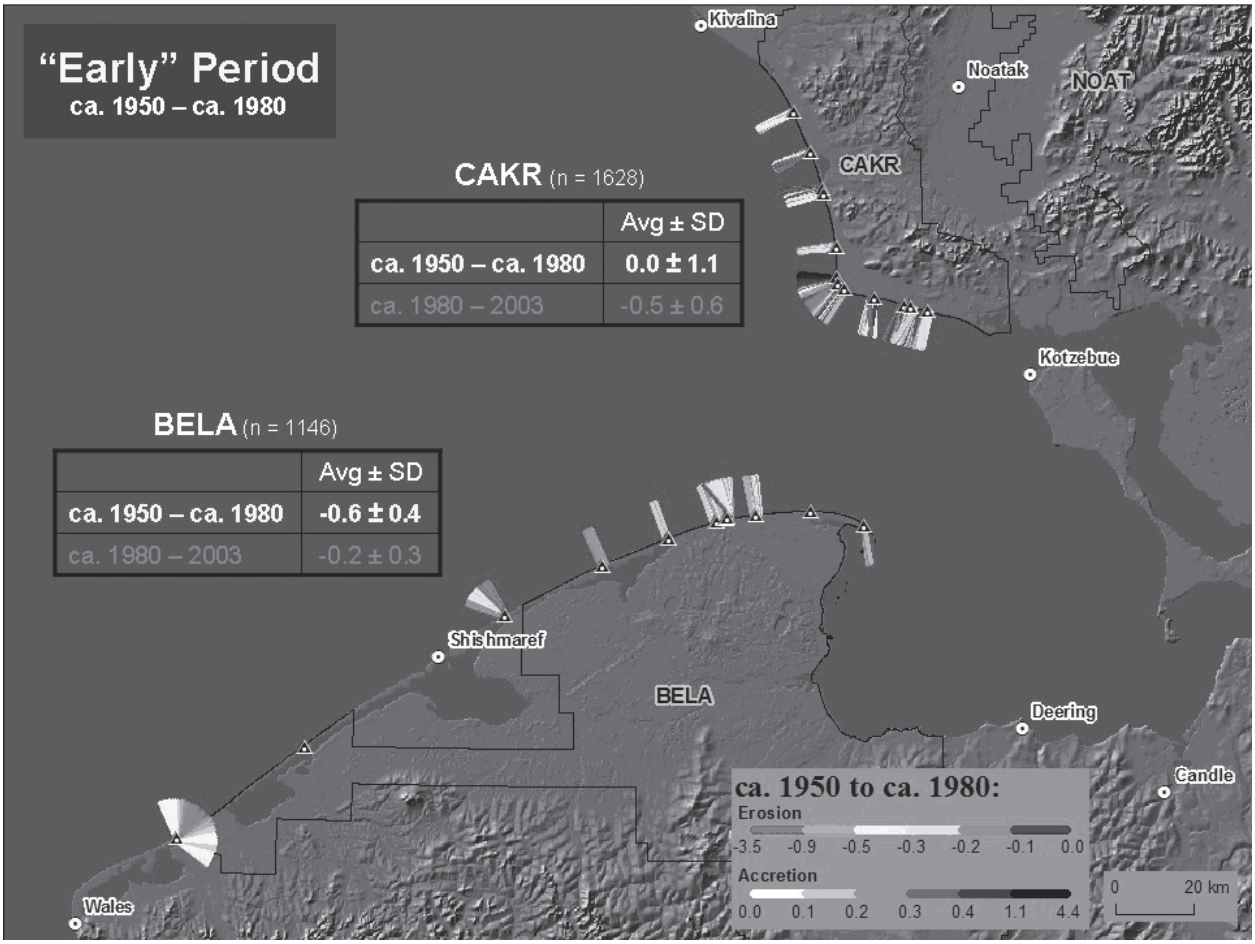

Figure 1. Bluff accretion and erosion near coastal monitoring stations during the "Early" period, from approx. 1950 to approx. 1980 (depending on air photo acquisition dates), in m/yr.

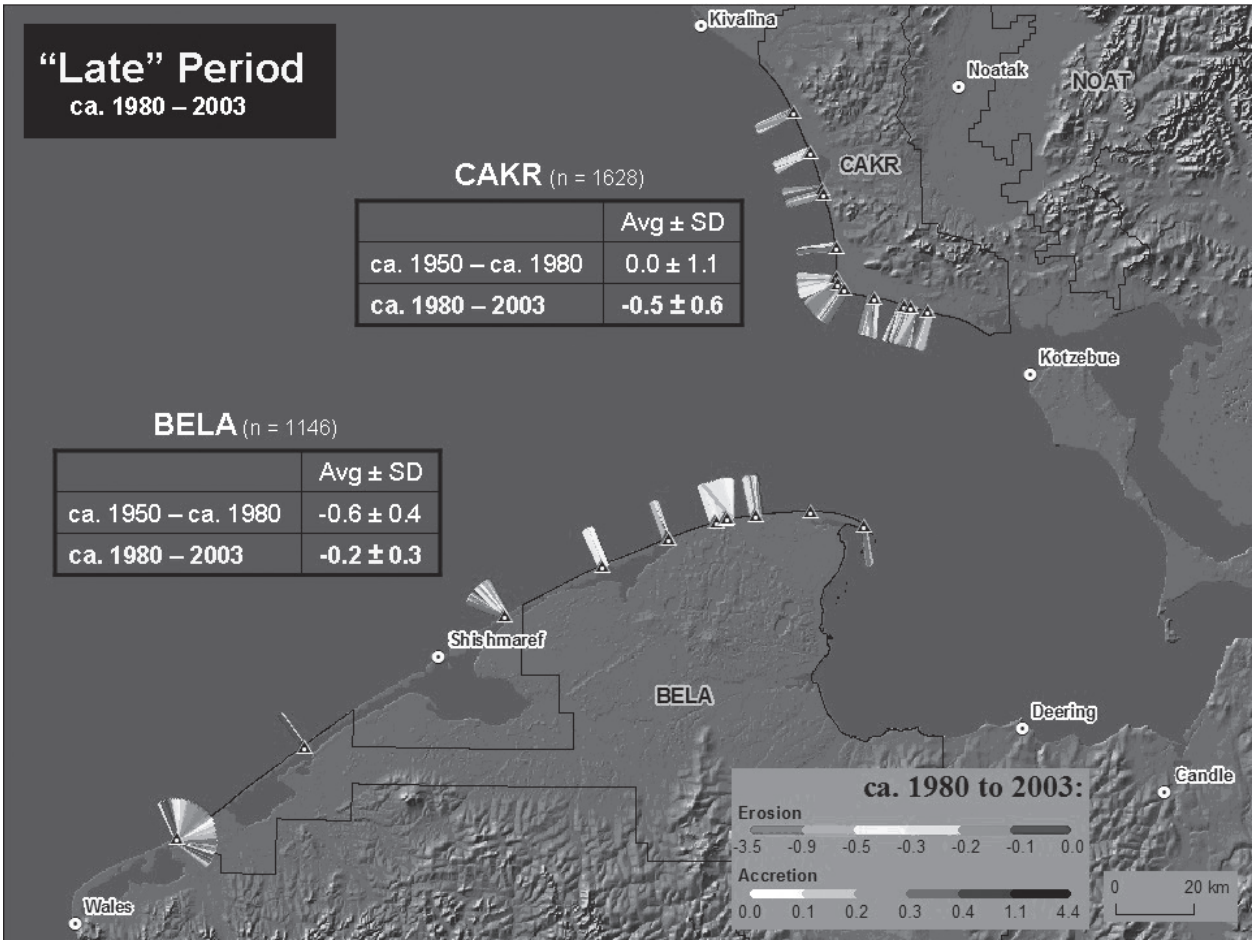

Figure 2. Bluff accretion and erosion during the "Late" period from approx. 1980 to 2003, in m/yr.

for three "timeslices": approx. 1950, approx. 1980, and 2003 (Manley et al. 2007). Spatial analysis of bluff retreat was conducted for selected areas near the monitoring sites using the USGS DSAS extension to ArcGIS (Thieler et al. 2005). Results indicate that the GIS-based measurements have acceptably low errors (+/- 0.1 m/yr or better).

Transects with 20 m spacing reveal high spatial variability related to coastal morphologies and processes (Figs. 1, 2). A comparison of the two time intervals suggests temporal variability also. For example, bluff erosion rates appear to have decreased after 1980 for the north-facing coast of Bering Land Bridge National Park (BELA), while increasing after 1980 for the west-facing coast of Cape Krusenstern National Monument (CAKR). In general, most of the >600 km-long coast from Wales to Kivalina has experienced erosion in the past five decades, with long-term average rates of 0 to -3 m/yr. Direct impacts include beach and bluff retreat, overwash deposition, migration or closure of inlets and lagoons, capture of thaw-lake basins, and release of sediment and organic carbon to nearshore waters. Higher temporal resolution is needed, but the coastal ecosystems in the region appear to be sensitive to the frequency and intensity of storm events, increasing temperatures, permafrost melting, sea-level rise, and the increasing length of the summer ice-free season.

References

Jorgenson, M.T. & Brown, J. 2005. Classification of the Alaskan Beaufort Sea Coast and estimation of carbon and sediment inputs from coastal erosion. *Geomarine Letters* 25: 69-80.

Manley, W.F., Parrish, E.G., Sanzone, D.M. & Lestak, L.R. 2007. *High-Resolution Orthorectified Imagery for the Coastal Areas of Bering Land Bridge NP (BELA) and Cape Krusenstern NM (CAKR)*. Northwest Alaska, Fairbanks, AK: National Park Service, Arctic Network I & M Program. Digital Media.

Mars, J.C. & Houseknecht, D.W. 2007. Quantitative remote sensing study indicates doubling of coastal erosion in past 50 yr along a segment of the Arctic coast of Alaska. *Geology* 35: 583-586.

Solomon, S.M. 2005. Spatial and temporal variability of shoreline change in the Beaufort-Mackenzie region, northwest territories, Canada. *Geomarine Letters* 25: 127-137.

Thieler, E.R., Himmelstoss, E.A., Zichichi, J.L. & Miller, T.L. 2005. Digital Shoreline Analysis System (DSAS) version 3.0: An ArcGIS extension for calculating shoreline change. *U.S. Geological Survey Open-file Report* 2005-1304.

Importance of Changes in Moisture for Geomorphic Responses to Rapid Climatic Warming in the Western Brooks Range and the Arctic Foothills, Northern Alaska: Lessons from the Past

Daniel Mann
Institute of Arctic Biology, University of Alaska, Fairbanks, AK 99775, USA
Pamela Groves
Institute of Arctic Biology, University of Alaska, Fairbanks, AK 99775, USA
Michael Kunz
Arctic Field Office, Bureau of Land Management, Fairbanks, AK 99709, USA

Climate changes between 12,500 and 8,000 ^{14}C yr BP triggered sweeping changes in vegetation cover, slope stability, and floodplain dynamics in the Brooks Range and Arctic Foothills of northern Alaska. Some of these climate changes involved rapid warming, so they provide analogs to the warming predicted for the coming century. Using palynology and radiocarbon-dated basal peats, Mann et al. (2002a) inferred that peat deposition (paludification) began, and shrub vegetation became widespread, ca. 12,500 ^{14}C yr BP, probably in response to a warmer and wetter climate. Stream-bank stratigraphy reveals that increased slope erosion caused rapid alluviation in valleys at the same time that *Populus* trees spread northward along braided floodplains before ca. 11,000 ^{14}C yr BP (Bockheim et al. 2003). During the Younger Dryas (YD) Chronozone (11,000–10,000 ^{14}C yr BP), lake levels fell and streams incised, probably in response to a drier, cooler climate that caused active layers to thin and the erosion of slopes to slow. A hiatus in records of *Populus* suggest that its geographic range contracted during the YD, and pollen records of other species suggest a cooler and drier climate during this interval. Basal peats dating to the YD are rare, suggesting that paludification slowed. Starting ca. 10,000 ^{14}C yr BP, lake levels rose, streams aggraded rapidly again, intense solifluction seems to have occurred, and *Populus* re-invaded the region (Mann et al. 2002a).

Paleoindian people occupied the Arctic Foothills briefly at the close of the YD, though there is increasingly good evidence that they were also present several centuries before the YD began ca. 11,000 ^{14}C yr BP (Kunz & Reanier 1994, Rasic 2000, Kunz, unpubl. data). We speculate that the spread of moist acidic tundra between 10,000 and 8,500 ^{14}C yr BP, along with the wet, organic-rich soils characteristic of the present landscape, caused the Paleoindians and their prey species to disappear from the region.

Floodplain dynamics are of particular interest for understanding the responses of arctic landscapes to climate changes, because they are centers of primary productivity and biodiversity (Walker et al. 2001). Floodplains aggraded at rates of meters/century just prior to 11,000 ^{14}C yr BP and immediately after 10,000 ^{14}C yr BP. Aggradation at such rapid rates must have been accompanied by widespread slope erosion, which suggests intense and widespread thermokarst formations.

Dating of relict alluvial fans in the western Brooks Range suggests several periods of increased deposition from headwater streams over the course of the Holocene. This work is in progress, but currently we have evidence for fan building ca. 4,000 ^{14}C yr BP and ca. 2,000 ^{14}C yr BP. Systematic observations begun in 2005 of floodplains in the western Brooks Range reveal that rapid aggradation is now underway in the headwater reaches of some stream systems. This aggradation is associated with mass movements of several different kinds occurring on hill slopes and in stream channels. Our observations suggest that we are at the cusp of another major ecosystem transition in the Brooks Range.

Most of the landscape-scale changes in the Arctic Foothills during the Pleistocene-Holocene transition involved changes in moisture balance, many imply changes in active-layer thickness, and some occurred very rapidly. The vulnerability of ecosystems in northern Alaska to changes in moisture balance is still evident today in the sensitive threshold existing between sand dunes and the vegetation surrounding them (Galloway & Carter 1993, Mann et al. 2002c). During the Late Pleistocene and early Holocene, the encroachment of marine water caused by rising global sea level was probably a major driver of increasing effective moisture on Alaska's North Slope (Mann et al. 2002b). Today, the moisture balance, which is still poorly constrained by predictive climate models, may be changing under the influences of increased winter snowfalls that accompany warmer winter temperatures, by northward shifts in the summer position of the Polar Front over the western Brooks Range and by net thawing of ice-rich permafrost as the result of warming in both summer and winter. Just as it was during the early Holocene, we suspect that moisture balance will be the key, proximal driver of ecosystem change in northern Alaska and in other arctic regions during the coming century.

References

Bockheim, J.G., O'Brien, J.D., Munroe, J.S. & Hinkel, K.M. 2003. Factors affecting the distribution of *Populus balsamifera* on the North Slope of Alaska, U.S.A. *Arctic, Antarctic, and Alpine Research* 35: 331-340.

Galloway, J.P. & Carter, L. D. 1993. Late holocene longitudinal and parabolic dunes in northern Alaska: Preliminary interpretations of age and paleoclimatic significance. *U.S. Geological Survey Bulletin* 2068: 3-11.

Kunz, M.L. & Reanier, R.E. 1994. Paleoindians in Beringia: evidence from arctic Alaska. *Science* 263: 660-662.

Mann, D.H., Peteet, D.M., Reanier, R.E. & Kunz, M.L. 2002a. Responses of an arctic landscape to late glacial and early Holocene climatic changes: the importance of moisture. *Quaternary Science Reviews* 21: 997-1021.

Mann, D.H., Reanier, R.E., Peteet, D.M. & Kunz, M.L. 2002b. Environmental change and arctic paleoindians. *Arctic Anthropology* 38: 119-138.

Mann, D.H., Heiser, P.A. & Finney, B.P. 2002c. Holocene history of the Great Kobuk Sand Dunes, Northwestern Alaska. *Quaternary Science Reviews* 21: 709-731.

Rasic, J.T. 2000. *Prehistoric lithic technology at the Tuluuk Hill Site, Northwest Alaska*. Master thesis, Department of Anthropology, Washington State University, Pullman, Washington.

Walker, D.A., Bockheim, J.G., Chapin, F.S., Eugster, W., Nelson, F.E. & Ping, C.L. 2001. Calcium-rich tundra, wildlife, and the Mammoth Steppe. *Quaternary Science Reviews* 20: 149-163.

Toward a Permafrost Map of Central Asia

Sergei Marchenko
Geophysical Institute, University of Alaska Fairbanks, USA
N. Sharkhuu
Institute of Geoecology, Mongolian Academy of Sciences, Ulaanbaatar, Mongolia
Xin Li
Cold and Arid Regions Environmental and Engineering Research Institute, Chinese Academy of Sciences, Lanzhou, China
Mamoru Ishikawa
Faculty of Environmental Earth Science, Hokkaido University, Sapporo 060-0810, Japan
Jerry Brown
International Permafrost Association, Woods Hole, MA, USA
Vladimir Romanovsky
Geophysical Institute, University of Alaska Fairbanks, USA
Dmitri Drodzov
Institute of the Earth Cryosphere, Moscow, Russia

Introduction

Although national permafrost maps exist for China, Kazakhstan, Mongolia, and Russia, there is no consistent cartographic or temperature criteria on which to base a unified permafrost map for the more topographically complex regions that prevail in Central Asia. The International Permafrost Association's (IPA) "Circum-Arctic Map of Permafrost and Ground-Ice Conditions" (1:10,000,000) employed an international legend developed primarily for continental (lowland) permafrost regions (Brown et al. 1997). That classification was applied to mountainous and high altitude regions with considerable uncertainties.

The retreat of glaciers and permafrost degradation in Central Asia in recent years is unprecedented as a consequence of warming. Accelerated warming of permafrost in mountainous, highland, and plateau regions of Asia could result in the disequilibria of the water cycle, increased mass wasting processes, and related sediment transport and slope hazards. Without a unified and verified regional permafrost map, these processes cannot be assessed adequately. Mapping, modeling, and monitoring strategies in mountain regions are under development to test and to verify climate-change scenarios and models.

In response to the difficulties involved in classifying and mapping of the region's permafrost, recommendations were approved at the IPA-sponsored International Symposium on Mountain and Arid Land Permafrost, Ulaanbaatar, Mongolia, September 2001 (Brown 2001). These included a request that an international team of experts prepare a unified permafrost map of Central Asia.

The workshop on the distribution and mapping of the permafrost distribution of Central and Eastern Asia was held prior to the Asian Conference on Permafrost, in Lanzhou, China, August 5–6, 2006, and was hosted by the Cold and Arid Regions Environmental and Engineering Research Institute (CAREERI). The workshop participants agreed that conventional mapping and modeling approaches of permafrost in this region recognize both latitudinal and altitudinal permafrost zonation, furthermore, and that the category of mountain permafrost be recognized as a subset of altitudinal zonation or, if appropriate, remain as a separate class. The proposed map should delineate each of these permafrost zones and contain actual and calculated ground temperatures and active layer thickness as point observations. Where available, estimates of ground ice would be included. However, for this next-generation map, classes of ground ice and spatial continuity (percentages) will not be part of the classification.

Mapping of Permafrost in Central Asia

Permafrost classifications

A major difficulty is in reconciling the usage of "continuous permafrost zonation," as it is commonly applied to continental permafrost (greater than 90% of the land surface; see Heginbottom 2002 for a comparison of classification schemes). A comparison of the spatial classifications in use in the four countries is presented in Table 1.

Modeling approach

An alternative approach of altitudinal permafrost mapping is modeling the ground temperature and permafrost distribution using the process-based models. Such an approach allows for spatial and temporal extrapolation of permafrost thermal state and distribution and also is well suited for studies with respect to permafrost response to climate change. But the process-based model requires an extensive set of input data such as meteorological data, surface characteristics (vegetation, snow cover), ground thermal properties, and topography. For the modeling of altitudinal permafrost within the rugged topography of the Altai Mountains, the basic dataset at 100 m resolution for the digital elevation model (DEM) was generated. The spatial permafrost model with a grid box size of 5 km uses gridded fields of monthly air temperature (topographically adjusted

Table 1. Classifications of permafrost continuity for China, Kazakhstan, Mongolia, and Russia.

Country (authors), landform, and region	Principle of permafrost zonation	Terminology for permafrost distribution	Permafrost extent
China			
1.1 Middle height mountain regions in Northeast China (Xu & Guo 1982)	Latitudinal zones	Islands	<30%
		Predominantly continuous	30 – 75%
1.2. Quinghai-Xizang High Plateau (Cheng 1983)	Index or degree of permafrost thermal stability	Lower belt	0°C – -0.5°C
		Middle belt	-0.5°C – -3°C
		Upper belt	< -3°C
1.3. Alpine mountains in West and East China (Zhang et al. 1985)	Altitudinal belts	Islands	
		Predominantly continuous	
Kazakhstan			
High Alpine Tien Shan and Pamirs Mountains (Gorbunov et al. 1996)	Altitudinal subbelts	Sporadic	<30%
		Discontinuous	30 – 90%
		Continuous	> 90%
Mongolia			
Middle height (Altai, Hovsgol, Khangai, & Khentei) mountain and adjacent arid land regions (Gravis et al. 1990, Sharkhuu 2006)	Latitudinal zones	Sporadic	< 1%
		Scattered islands	1 – 5%
		Islands	5 – 40%
		Discontinuous	40 – 80%
		Continuous	> 80%
Southern Russia			
Mountainous regions with depressions and separate plateaus and plains (Ershov 1991)	Latitudinal zones	Southern discontinuous	> -0.5. °C – -2°C
		Northern discontinuous	< -0.5°C – -2°C

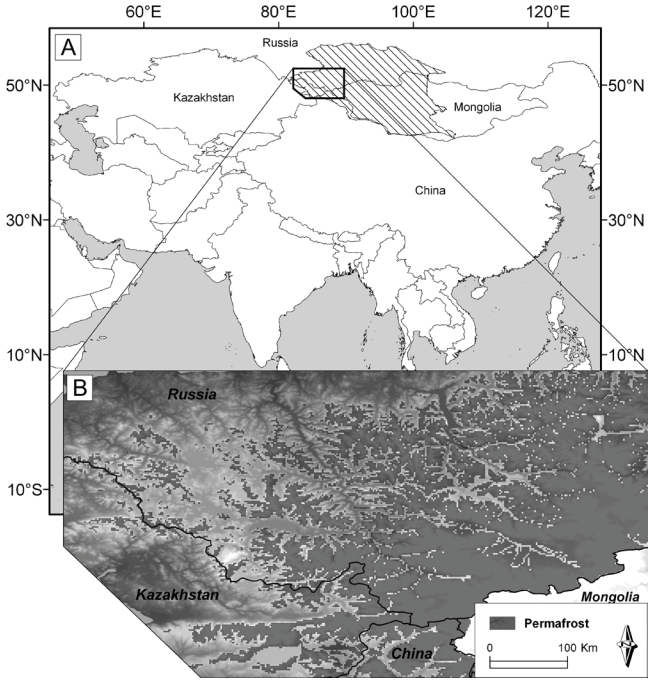

Figure 1. (A) The entire Altai-Sayan region (shaded area) and (B) modeled permafrost distribution within the northwest part of the region.

using the altitudinal air temperature gradients for the various parts of the Altai), incoming amount of solar radiation, vegetation, snow, and soil thermal properties. Figure 1 illustrates the results of the spatially-distributed permafrost model within the northwest part of the Altai Mountains.

Acknowledgments

We thank Alan Heginbottom, Emeritus, Geological Survey of Canada, who provided advice and information on existing classification schemes. We thank all the participants of the two workshops for their interest, discussions, and cooperation.

References

Brown, J. 2001. International Symposium on Mountain and Arid Land Permafrost and Field Excursion in Mongolia. *Frozen Ground News Bulletin* 25: 7-11.

Brown, J., Ferrians, O.J. Jr., Heginbottom, J.A. & Melnikov, E.S. 1997. *Circum-Arctic Map of Permafrost and Ground-Ice Conditions.* U.S. Geological Survey Circum-Pacific Map CP-45, 1:10,000,000, Reston, Virginia.

Cheng, G. 1983. Vertical and horizontal zonation of high-altitude permafrost. *Proceedings of the Fourth International Conference on Permafrost, Fairbanks, Alaska, 1983*: 136-131.

Gravis, G.F., Sharkhuu, N. & Zabolotnik, S.I. 1990. Geocryology and geocryological zonation. *National Atlas of Mongolia. GUGK of Mongolian Republic and* USSR. Ulaanbaatar: Moscow Plates, 40-41, (scale 1:4,500,000).

Heginbottom, J.A. 2002. Permafrost mapping: A review. *Progress Physical Geography* 26: 623-642.

Yershov, E.D. 1991. *Geocryological Map of Russia and Neighbouring Republics.* 16 sheets, 1:2,500,000. Moscow: Moscow State University.

Methane Ebullition During Field-Simulated Lake Expansion and Permafrost Degradation

Olivier Mazéas
University of California, Berkeley, Dept. of Geography 507 McCone Hall #4740, Berkeley, CA 94720-4740, USA
Joseph von Fischer
Colorado State University, Dept. of Biology, Fort Collins, CO 80523, USA
Robert Rhew
University of California, Berkeley, Dept. of Geography 507 McCone Hall #4740, Berkeley, CA 94720-4740, USA

Introduction

The Arctic accounts for 30% of the global emissions of methane (CH_4), a potent greenhouse gas, to the atmosphere (Christensen 1993). Within the Arctic, tundra and lakes are major sources, although they exhibit exceptionally high spatial variability. In arctic lakes, CH_4 ebullition is the major transport mechanism from the sediments to the atmosphere (95%). Ebullition rates are the greatest near the edges of the lakes, where active erosion occurs (Walter et al. 2006). In regions of continuous permafrost, arctic lakes have been expanding in recent decades, owing to permafrost melting and development of thermokarst (Smith et al. 2005). Lake expansion occurs when margins erode into water, supplying large amounts of organic rich material to the sediment-water interface. This allows carbon that was previously stored in the soil (permafrost and active layer) to become bioavailable and subject to decomposition. An increase in arctic CH_4 emissions as a result of permafrost thawing and lake expansion would constitute a positive feedback to arctic warming.

In order to better understand processes associated with lake CH_4 emissions, we conducted an experiment in a thaw lake on the Arctic Coastal Plain during the summer and fall of 2007. Different layers of tundra soil were incubated in chambers at the bottom of the lake, and methane ebullition was monitored.

Material and Methods

Eleven incubations were initiated in mid-July 2007 at a depth of 1 m in Cake Eater Lake, on the Barrow Environmental Observatory (BEO), Alaska. Each experimental chamber consisted of a bucket (yielding an exposed surface area of 0.07 m^2) fixed beneath an inverted funnel equipped with a sampling port to capture and collect the emitted gases.

The nearby tundra soil was vertically stratified in 3 distinct layers, which we extracted separately. First, the unfrozen (upper) section of soil, hereafter called the active layer, was sampled down to the depth of frozen soil, and included live plants and decaying peat material (3 adjacent points, ~20 cm deep and 13 kg each, $n = 3$). Next, the seasonally frozen layer soil (~12 cm thick) was sampled with a mechanical auger, homogenized, and divided into separate buckets (about 8 kg each, $n = 3$). Finally, a layer of permafrost was sampled (~12 cm deep), homogenized, and placed into buckets (about 8 kg each, $n = 3$). Although these soils were initially frozen, the samples thawed before the initiation of the experiment.

In addition to these 9 incubations, 2 others were added for comparative purposes: a control incubation using an empty bucket and another one containing sawdust mixed in with thawed permafrost. This sawdust provided cellulose, which is a major component of plant tissue, and its fermentation was expected to yield substrates for methanogenesis.

Ebullition gas volume determination and sampling were performed at variable time points along an 11-week period, ending on the days of initial lake freeze-up at the beginning of October.

From each gas sample, a 0.5 ml subsample was analyzed using a laser-based analyzer (Los Gatos Research) for methane and carbon dioxide determination. Nitrogen (N_2) was used as the carrier gas, and a calibration curve was run for each sequence (Matheson Tri-Gas grade CH_4).

The initial carbon content was determined using a Carbon-Nitrogen analyzer (NC2100, Carlo Erba). Water and sediment temperatures were recorded using in situ dataloggers, and wind speed and atmospheric pressure were also monitored throughout the experiment.

Results and Discussion

Only the active layer consistently emitted gases via ebullition throughout the experiment, with an average rate of 15 ml day^{-1}. The seasonally frozen and permafrost layers sporadically emitted small volumes of gas (typically 0 to 1 ml per day), with cumulative volumes ~20 times smaller than the active layer. The ebullition frequency was highly variable, and significant ebullition events could not be correlated with any of the environmental parameters monitored.

Daily ebullition events were consistently observed from the active layer incubations from the first day of the experiment, with large ebullition rates (> mean) occurring within 7–15 days and some of the highest rates starting within 3–4 weeks. The replicates show a similar overall trend; however, one replicate could not be monitored after the fifth week of incubation due to technical problems. Ebullition significantly decreased or ceased during the last 7 to 10 days prior to lake freeze-up, a period when the water temperature dropped to between 1 and 0°C. In contrast, no temporal pattern of ebullition rates was observed for the frozen soil layers.

The gas composition of the collected bubbles also differed

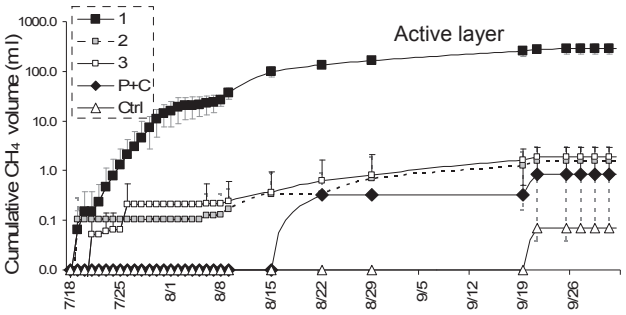

Figure 1. Cumulative CH_4 volume emitted from the beginning of the experiment to the lake freeze-up (logarithmic *Y* axis). Means and error bars are indicated for the replicate incubations. 1: Active layer; 2: Seasonally frozen layer; 3: Permafrost, P+C: Cellulose-enriched permafrost; Ctrl: Control.

between the active layer and frozen layers below. Gas samples from the active layer had CH_4 concentrations that increased gradually during the first two weeks, reaching concentrations in the same range as the ones measured during the following higher gas emission period (~30%). However, when ebullition decreased at the end of the season, slightly higher concentrations (~50% CH_4) were observed. Meanwhile, CO_2 concentrations remained below the detection limit (<0.5%).

The seasonally frozen and permafrost replicates, as well as the cellulose-enriched incubation, were associated with much smaller CH_4 concentrations than the active layer, even when relatively large volumes of gas were emitted. A few samples exhibited high CH_4 concentrations, but were always associated with small ebullition volumes.

Cumulative CH_4 release from the active layer was approximately 160 times higher in the active layer than in the 2 frozen layers (Fig. 1). Meanwhile, cumulative ebullition volumes from the frozen layers were not significantly different from each other. The large variability associated with the seasonally frozen layer was because one of the replicates showed very low emissions, comparable to the control experiment.

Emission rates normalized to carbon content in soil samples were ~50 times higher for the active layer than for the permafrost or the frozen active layer, further demonstrating the unexpected low emissions from the frozen layers (Fig. 2).

Even though there was less carbon in the frozen soil incubations, the particularly low emission from the cellulose-enriched incubation suggests the pattern is not due to carbon limitation, but rather that there are insignificant methanogen or syntrophic organism populations in the formerly frozen soils, even after 11 weeks in the lake, where existing microbes could have colonized the incubated substrates.

We calculated a mean emission rate of 39 mg CH_4 m^{-2} day^{-1} for simulated thermokarst erosion of the active layer. Such a rate is in the range of background ebullition reported by Walter et al. (2006). This corresponds to 0.2 mg CH_4 day^{-1} per kg of active layer.

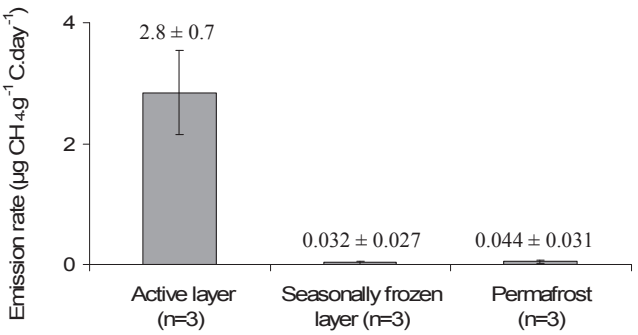

Figure 2. Overall methane ebullition rates in µg CH_4 per day per grams of initial tundra carbon (± standard deviation).

Conclusions

During the first 11 weeks of immersion, the thawed active layer emitted significant amounts of CH_4 while frozen soils only sporadically produced gas bubbles, with CH_4 volumes about 160 times smaller. These low rates could be due to the lack of indigenous methanogen populations in the frozen soils and slow subsequent colonization during the incubation period. The active layer incubations exhibited an average of 39 mg CH_4 m^{-2} day^{-1} during the experiment. This rate is in the range as background ebullition observed by Walter et al. (2006) in Siberian lakes, which is believed to represent 25% of total lake ebullition.

We hope to continue monitoring these incubations over several years and add additional treatments (autoclaved active layer, combined layers, low and high center polygonal tundra) to better define the timing, amplitude, and chemical signatures of methane ebullition as well as its primary physical, chemical, and biological controls. Moreover, we hope to perform additional analyses, such as carbon isotopic determination of CH_4, microbial community characterization, and dissolved oxygen measurements. Similar incubations should also be initiated in larger thermokarst lakes in order to compare ebullition under different chemical and physical parameters.

Acknowledgments

We thank Jerry Brown, the Barrow Arctic Science Consortium, and the Ukpeagvik Iñupiat Corporation for facilitating work at the BEO; A. Kear for gas analyses; and M. Whelan, M. Nguyen, and A. Atwood for field assistance.

References

Christensen, T.R. 1993. Methane emission from Arctic tundra. *Biogeochemistry* 21: 117-139.

Smith, L.C., Sheng, Y., MacDonald, G.M. & Hinzman, L.D. 2005. Disappearing Arctic lakes. *Science* 308: 1429.

Walter, K.M., Zimov, S.A., Chanton, J.P., Verbyla, D. & Chapin III, F.S. 2006. Methane bubbling from Siberian thaw lakes as a positive feedback to climate warming. *Nature* 443: 71–75.

A Provisional 1:50,000 Scale Soil Map of Wright Valley, Antarctica

M. McLeod
Landcare Research, Private Bag 3127, Hamilton, New Zealand
J.G. Bockheim
Department of Soil Science, University of Wisconsin, 1525 Observatory Drive, Madison, WI 53706-1299, USA
M.R. Balks
Department of Earth and Ocean Sciences, University of Waikato, Private Bag 3105, Hamilton, New Zealand

Introduction

During the austral summers of 2005–2007, we mapped soils and permafrost form within Wright Valley, Antarctica, for use at a scale of 1:50,000. Wright Valley, within the McMurdo Dry Valley region of Northern Victoria Land, extends 53 km from the Wright Lower Glacier, a lobe of the Wilson Piedmont Glacier, to the Wright Upper Glacier, an outlet glacier from the East Antarctic ice sheet. The Onyx River flows seasonally from Wright Lower Glacier inland 30 km to Lake Vanda, which is 90 m a.s.l. The study area also includes the Dais, Labyrinth and the North and South Forks. Although many soils have been described in central Wright Valley, they have primarily been used to aid and interpret surficial geologic deposits and assign ages/names to develop a glacial chronology. Renewed interest in environmental classification in a spatial framework (Waterhouse 2001) has led to the demand for soil and permafrost maps of Antarctica. This paper presents preliminary results from those investigations.

Methods

Stereo-pair aerial photographs of Wright Valley were examined with preliminary soil boundaries plotted onto a GIS-based geo-referenced satellite image (http://usarc.usgs.gov/ant-ogc-viewer/declasdownload.htm) and a hill shade image built from a 2 m post-processed resolution LIDAR file (http://usarc.usgs.gov/ant-ogc-viewer/lidardownload.htm) at 1:50,000 scale.

Fieldwork was undertaken to validate the preliminary boundaries and determine the nature of surface geology, soils, and permafrost. About 300 small test pits were excavated, described, and classified following Soil Taxonomy (Soil Survey Staff 2003) and located by GPS. The soil pits were then backfilled. Weathering stage follows Campbell and Claridge (1975), while salt stage follows Bockheim (1990). Soil boundaries were upgraded daily in the field using the GPS and soil pit information. At 118 locations larger pits were dug to at least 70 cm (unless ice-cemented permafrost or boulders were encountered), with the soil being sampled by horizon. Both <2 and >2 mm fractions were weighed, with the <2 mm fraction being retained for analysis.

Analysis for pH, EC, water soluble cations (Ca, Mg, K, Na) anions (Cl, nitrate-N, SO_4) followed methods at http://www.landcareresearch.co.nz/services/laboratories/eclab/eclabtest_list.asp#water. Total soluble salts to 70 cm (TSS_{70}) were calculated following Bockheim (1979).

Results

Broadly, eight groups of soil parent materials have been identified. They are:

- Peleus till, a silty olive-coloured till with few stones and the oldest drift recognized in the valley, was deposited before 3.9 Ma, by a wet-based glacier draining the East Antarctic Ice Sheet.
- Drift from up to 8 westward glacial advances from grounded ice within Ross Sea Embayment.
- Drift from 4 advances (Alpine I–IV) of alpine glaciers along the south valley wall. These drifts are out of phase with the westward flowing glaciers as a result of the snow-gun effect (Prentice 1991), resulting in a complex cross-cutting pattern of surficial geology and in some cases, soil classification.
- Drift from 3 eastward advances of Upper Wright Glacier (which has acted as an alpine glacier) tentatively correlated with Alpine I, IIa and III advances within the lower Wright Valley.
- Rock glaciers in the North and South Forks tentatively correlated with the Alpine IIb advance (Bockheim & McLeod submitted) and two rock glaciers flowing from the south wall of the main valley, immediately to the east of the Dais.
- Alluvium deposited by the Onyx River.
- Colluvium on valley walls and footslopes. Generally, on the north wall, ice-cemented permafrost is not encountered at a soil depth of less than 70 cm (in mid-summer), whereas on the south wall and especially in western reaches, ice-cemented permafrost is commonly encountered at a soil depth of less than 70 cm.
- Bare rock associated with valley walls and valley floor dyke systems. Bedrock consists predominantly of Precambrian to Paleozoic metasediments, granite-gneisses, and lamprophyre and rhyolite porphyry dikes, Devonian-to-Jurassic Beacon Supergroup sandstones intruded by the Jurassic Ferrar Dolerite (McKelvey & Webb 1962).

Soils were classified into the Gelisol order to the family level (Soil Survey Staff 2003); mineral soils with one or more horizons that are cryoturbated are classified as Turbels. Soils without cryoturbation are Orthels. Both suborders are divided into Great Groups on the basis of soil climate and other soil properties. Within Wright Valley soils are both hydrous and anhydrous conditions, as it is soil moisture conditions that are classified rather than atmospheric conditions. Therefore, the soils are classified as Haplorthel/Haploturbels, where ice-cemented permafrost first occurs within 70 cm of the soil

surface or as Anhyorthel/Anhyturbels, where ice-cemented permafrost first occurs below 70 cm. Gelisols were further subdivided into subgroups on the basis of presence or absence of soluble salts (e.g., salic, gypsic, nitric, petrosalic, and petrogypsic).

Discussion

Although 8 broad groups of parent materials have been identified, the soil pattern is also strongly influenced by soil climate. At low elevation (<100 m) from the east along the valley floor to the western end of Lake Vanda, the valley lies within coastal Zone 1 (Marchant & Denton 1996), where the climate is relatively mild, with precipitation at Vanda station approximately 80 mm y^{-1}. Especially near the coast, the precipitation allows recharge of soil water lost to evaporation. Thus ice-cemented permafrost remains close to the soil surface, and soil development is hindered (Bockheim 1979). Similarly, where soil water is recharged from the Onyx River or on foot slopes below a meltwater source, ice-cemented permafrost remains close to the soil surface (McLeod et al. 2008). Generally, in these locations a Typic Haplorthel/Haploturbel association is mapped in recognition of the cryoturbated zones, creating patterned ground around flat-centred polygons.

With increasing age of drift material, and away from the influence of soil moisture recharge, aerosol salts accumulate in the soil, developing firstly increased total salts within the soil until a salic horizon (Soil Survey Staff 2003) develops. When the salic horizon is ultimately cemented, "Petro" subgroups are classified. It follows, therefore, that the combination of a Salic Subgroup under a Haplorthel Great Group is unlikely to occur.

Salt accumulation in the soil profile is relatively low at the coastal eastern end of the valley and highest in the central valley, where we recorded an indurated salic horizon with TSS_{70} of approximately 10 500 mg cm^{-2}. Towards the western end of the valley and in the North and South Forks, salt accumulation does not appear to be so great, possibly because of the low precipitation and the consequent low aerosol deposition of salts.

Soils with a water table were described from two different zones. In the hyporheic zone of the Onyx River, predominantly Typic Haplorthels were mapped, whereas in a bouldery hyporheic zone near the terminus of the Onyx River, a Typic Aquorthel was identified that contained low chroma mottles. In contrast, adjacent to Don Juan Pond in the South Fork, groundwater is sufficiently salty to prevent freezing, and Salic Aquorthels with TSS_{70} of approximately 4000 mg cm^{-2} were described.

Acknowledgments

This work was partially funded by the New Zealand Foundation for Research, Science, and Technology under contract C09X0307. Antarctica New Zealand provided logistical support.

References

Bockheim, J.G. 1979. Ice core and ice cement effects on soil development, eastern Wright Valley, Antarctica. *New Zealand Journal of Geology and Geophysics* 22(4): 487-493.

Bockheim, J.G. 1990. Soil development rates in the Transantarctic Mountains. *Geoderma* 47: 59-77.

Campbell, I.B. & Claridge, G.G.C. 1975. Morphology and age relationships of Antarctic soils. Quaternary Studies. *Royal Society of New Zealand Bulletin* 13: 83-88.

Marchant, D.R. & Denton, G.H. 1996. Miocene and Pliocene Paleoclimate of the Dry Valley region, Southern Victoria Land: A geomorphological approach. *Marine Micropaleontology* 27(1–4): 253-271.

McKelvey, B.C. & Webb, P.N. 1962. Geological investigations in northern Victoria Land, Antarctica –Geology of Wright Valley. *New Zealand Journal of Geology and Geophysics* 5(1): 143–162.

McLeod, M., Bockheim, J.G. & Balks, M.R. 2008. Glacial geomorphology, soil development and permafrost features in central-upper Wright Valley, Antarctica. *Geoderma*. In press.

Prentice, M.L. & Matthews, R.K. 1991. Tertiary ice sheet dynamics: The snow gun hypothesis. *Journal of Geophysical Research* 96(B4): 6811–6827.

Soil Survey Staff 2003. *Keys to Soil Taxonomy*. U.S. Department of Agriculture, Natural Resources Conservation Service. soils.usda.gov/technical/classification/tax_keys/keysweb.pdf

Waterhouse, E.J. 2001. A state of the environment report for the Ross sea region of Antarctica. *Ross Sea Region 2001*. New Zealand Antarctic Institute, Christchurch .

Improving the Parameterization of Snow Processes to Model the Implications of Shrub-Tundra Expansion on Soil Temperatures

Cecile Menard
Centre for Ecology and Hydrology, Wallingford, UK
Richard Essery
School of GeoSciences, University of Edinburgh, UK
Douglas Clark
Centre for Ecology and Hydrology, Wallingford, UK

Introduction

Field observations, satellite remote sensing, and models suggest that the recent warming of the Arctic has caused an increase in shrub cover (Sturm et al. 2005, Jia et al. 2006, Tape et al. 2006). This change in vegetation structure is expected to significantly affect snow distributions and interactions between the land surface and the atmosphere, with consequences for the hydrology, ecology, carbon, and energy balances of the region. Shrubs capture wind-blown snow, increasing snow depths, and decreasing winter water losses through sublimation. The low thermal conductivity of snow insulates the soil, deepening the active layer and affecting the permafrost regime. Thus, snow/permafrost interactions will be at the core of feedback loops leading to further shrub expansion. For example, warmer winter soil temperatures lead to increased microbial activity and hence to greater nutrient availability, which will further stimulate shrub growth (Chapin et al. 2005, Tape et al. 2006). Carbon cycling will also be affected, although the environmental effects of greater shrub abundance are uncertain. Sturm et al. (2005) suggest that the Arctic may become a carbon sink because of increasing production of above-ground shrub biomass. On the other hand, thawing of permafrost is expected to liberate large amounts of carbon currently sequestered in frozen organic soils (Solomon et al. 2007).

Land surface models (LSMs) are required to calculate energy and water fluxes between the land and the atmosphere in global climate models (GCMs), but the representation of cryospheric processes is generally crude in current LSMs. In this paper, two different snow schemes are tested offline to assess the implications for soil processes of the predicted northward expansion of shrub-tundra.

Methods

Field site

Meteorological measurements and soil temperatures were obtained at two sites in the Wolf Creek Research Basin (60°36′N, 134°57′W), Yukon Territory, Canada (Pomeroy et al. 2004):

1. An alpine tundra site (1615 m a.s.l.), characterized by 0.01–0.3 m tall vegetation (willow, dwarf birch, grass, and lichen) and bare rock, within the widespread discontinuous permafrost zone (Lewkowicz & Ednie 2004). Soil temperatures were measured at 3 cm depth.
2. A shrub tundra site (1250 m a.s.l.), with 0.4–3 m tall vegetation (willow, sparse white spruce, dwarf birch and grass), within a sporadic discontinuous permafrost zone. Soil temperatures were measured at 11 cm depth.

Data for the one-year period starting on 1 August 1998 are used here. Air temperatures at both sites were similar from November to February, but the alpine site was generally 2°C colder than the shrub tundra site for the rest of the year. Because the alpine site is more exposed, the annual average wind speed was greater by 2.3 ms^{-1}. Although the snowfall is almost the same at the two sites, increased wind ablation and reduced trapping by shrubs give lower snow depths at the alpine site. The importance of snow insulation is reflected in differences in soil temperatures; the greatest differences occurred in March, for which average soil temperatures were -9°C at the alpine site but -4°C at the shrub tundra site. Summer differences were smaller, and down to 0.4°C in June and August (7°C at the alpine site and 6.6°C at the shrub tundra site).

Model parameterization

Snow depths and soil temperatures at the two sites have been simulated with the JULES (Joint UK Land Environment Simulator; Blyth et al. 2006) LSM using two different snow schemes. Simulations were first performed with the present version of JULES, which represents snow as a composite with the top soil layer. The insulating properties of snow are incorporated by adjusting the thermal conductivity and thickness of the layer (Cox et al. 1999). The temperature of this top layer is taken to be at the layer midpoint, whether snow is present or not, hence it may reflect the soil or the snow temperature depending on snow depth. A new snow model using a multilayer representation of snow has now been developed for JULES. Simple representations of snow compaction, and retention and refreezing of liquid water, all of which were neglected in the original model, have been included.

Model results

Figures 1 and 2 compare simulated snow depths and soil temperatures with measurements. Simulations with the original snow model underestimate winter soil temperatures, particularly for the alpine site where the measurement depth lies within the model's composite snow-soil layer, but also for the shrub tundra site where the measurements are below this layer. The greater snow insulation simulated by the new model greatly improves the soil temperature simulations,

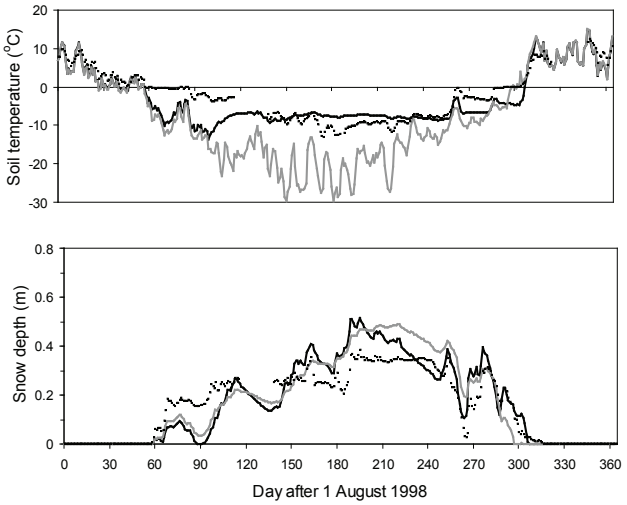

Figure 1. Daily average soil temperatures and snow depths from observations (dotted lines), the composite snow model (grey lines), and the multilayer snow model (black lines) for the alpine site.

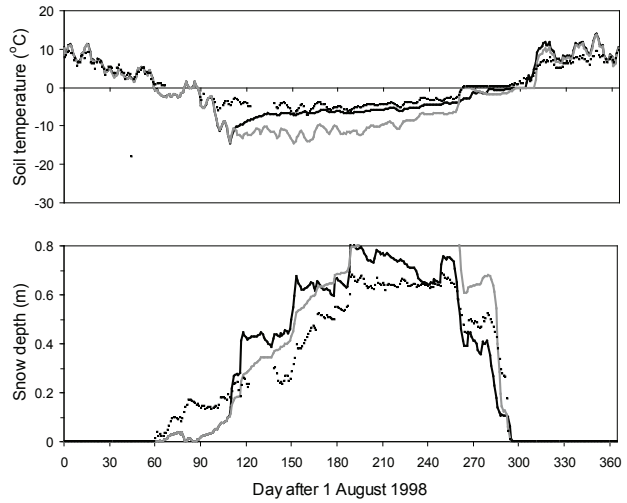

Figure 2. As Figure 1, but for the shrub tundra site.

except for periods such as November when the simulated snow depth is underestimated at both sites.

Additional runs will be made to assess how much of the soil temperature variation between sites can be explained by meteorology and how much by vegetation cover. One way to address this will be to perform simulations with vegetation characteristics at one site used as model input at the other.

Acknowledgments

Field data were supplied by John Pomeroy, University of Saskatchewan. Cecile Menard is supported by a NERC studentship.

References

Blyth, E.M. et al. 2006. JULES: a new community land surface model. *IGBP Newsletter* 66: 9-11.

Cox, P.M. et al. 1999. The impact of new land surface physics on the GCM simulation of climate and climate sensitivity. *Climate Dynamics* 15: 183-203.

Chapin, F.S. et al. 2005. Role of land-surface changes in Arctic summer warming, *Science* 310: 657-660.

Jia, G.J., Epstein, H.E. & Walker, D.A. 2006. Spatial heterogeneity of tundra vegetation response to recent temperature changes. *Global Change Biology* 12: 42-55.

Lewkowicz, A.G. & Ednie, M. 2004. Probability mapping of mountain permafrost using the BTS method, Wolf Creek, Yukon Territory, Canada. *Permafrost and Periglacial Processes* 15: 67-80.

Pomeroy, J., Essery, R. & Toth, B. 2003. Implications of spatial distributions of snow mass and melt rate on snowcover depletion: observations in a sub-arctic mountain catchment. *Annals of Glaciology* 38(1): 195-201.

Solomon, S. et al. (eds.). 2007. *IPCC 2007, Climate Change 2007: The Physical Science Basis. Contribution of Working Group I to the Fourth Assessment Report of the Intergovernmental Panel on Climate Change*. Cambridge: Cambridge University Press.

Sturm, M. et al. 2005. Winter biological processes could help convert arctic tundra to shrubland. *Bioscience* 55: 17-26.

Tape, K., Strum, M. & Racine, C. 2006. The evidence for shrub expansion in Northern Alaska and the Pan-Arctic. *Global Change Biology* 12: 686-702.

Pyrogenic Dynamics of Cryosols and Carbon Pools in Open Forests of Northeast Eurasia

N.S. Mergelov
Institute of Geography RAS, Moscow, Russia

There is no sufficient data on fires and postpyrogenic functioning of ecosystems at the north tree boundary at the Kolyma River Lowland (Russia). Our studies carried out in larch open forests of the northeast part of this region (69°N, 161°E) showed that fires are among the major factors influencing vegetation and soil successions. All loamy cryohydromorphic soils (Turbic, Turbi-Saprihistic, Gleyi-Turbic & Endogleyi-Turbi-Histic Cryosols; Gelic Gleysols) formed at watersheds on loess-icy complex sediments represent various stages of postpyrogenic development.

The most mature ecosystem of the study site is old (quasi-climax) larch open forest (~ 200 years old). Postpyrogenic recovery of vegetation occurs through various nonstable ecosystems: highly productive dense larch forest (30–60 years old), larch open forest (60 years old), treeless areas with grass and low shrubs (15–40 years old), and others (Fig. 1).

The strong fire in combination with absence of seeds for tree reproduction could lead to formation of treeless areas with low shrub-grassy vegetation, stable to larch reproduction during at least 30 years. In later stages, larch appears in such areas forming open woodlands.

The trend of postpyrogenic succession depends primarily on the type (ground or crown fire, ground fires prevail) and intensity of fire. Among others important factors is the availability of the sufficient amount of viable seeds. In the presence of surplus amounts of seed, the plant succession could develop through the stage of highly productive dense larch forest, which subsequently thins out.

The trends in transformation of soil cover generally for initial postpyrogenic stages (increase of the active-layer thickness, increase of soil moisture due to the melting of ice lenses and wedges, intensification of cryoturbations and gleyic processes) differ significantly in the later stages and depend on direction of postpyrogenic plant succession (Fig. 2).

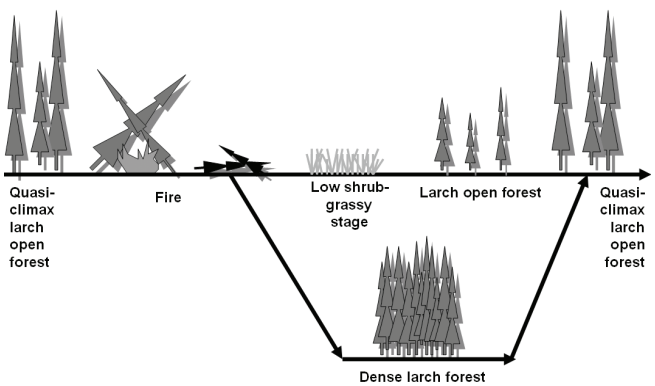

Figure 1. Sequence of postpyrogenic succession change.

Development of dense larch forest with thick lichen-low shrub–moss ground cover leads to a more stable state of the soil cover since thermokarst processes are not so intensive. Active-layer thickness strongly decreases (from 120–140 cm to 30–50 cm). Morphological gleyic and cryoturbation features are not strongly expressed in the soil profile. Due to autoregulation of the ecosystem, dense larch forest thins out. This process is accompanied by raising of diversity of the ground vegetation: the share of mosses decreases while the share of lichens increases. The ground vegetation of mature larch open forest comprises regular low shrub-moss and moss-lichen parcels-polygons. The difference in thermal capacity of mosses and lichens—parcel-forming plants, leads to heterogeneity in thawing depth, which varies also on a regular basis. The average active-layer thickness under low-shrub moss parcel is 25 cm; under moss-lichen parcel is 45 cm.

The treeless areas with low shrub-grassy vegetation even 30–40 years after the fire have high active layer thickness of 90–120 cm, thermokarst processes are still active, and polygonal microtopography is formed. Thermokarst

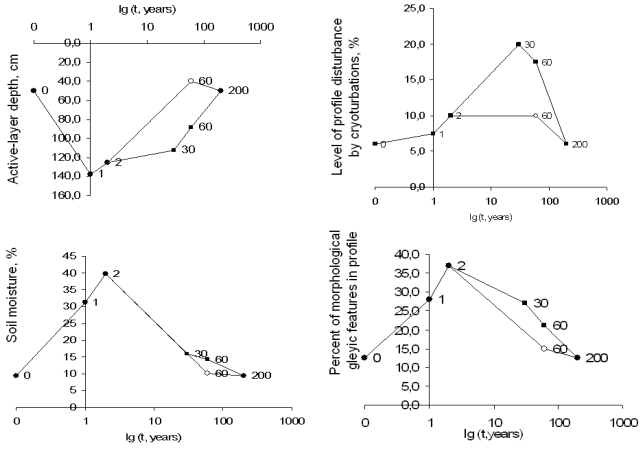

Figure 2. Soil properties alteration in dependence to fire age and/or type of postpyrogenic succession.
● = consecutive postpyrogenic development of larch open forest;
o = development through stage of dense larch forest
Legend:

Time passed after the last fire (years)	Postpyrogenic stages of vegetation recovery
1	Burn without arboreal vegetation
2	Burn without arboreal vegetation
30	Burn without arboreal vegetation (low shrub-grassy stage)
60	Larch open forest
60	Dense larch forest
200	Old (quasi-climax) larch open forest

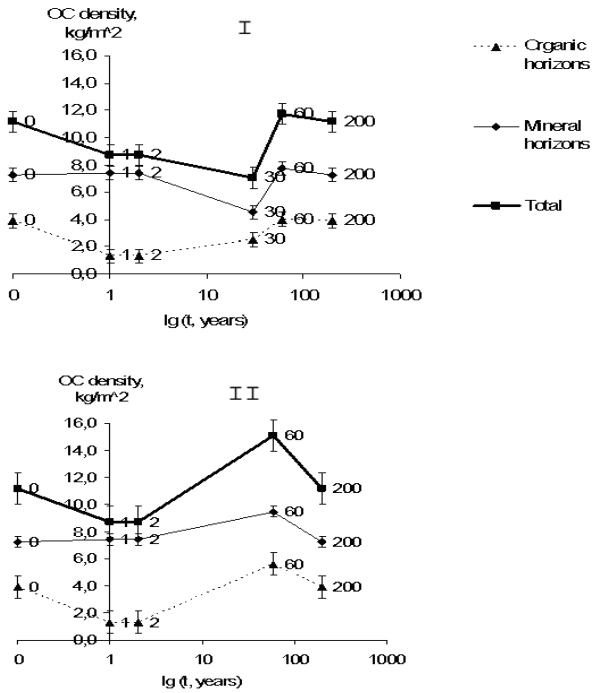

Figure 3. Alteration of OC densities in organic and mineral horizons in dependence to fire age and/or type of postpyrogenic succession (for the legend see Fig. 2).
I – consecutive postpyrogenic development of larch open forest
II – development through stage of dense larch forest

depressions (1–4 m in diameter) indicate an intersection of ice wedges, which partially melt when vegetation is destroyed during the fire. The soil profiles are strongly disturbed by cryoturbations.

Postpyrogenic successions of vegetation and soils are cyclical. This fact provided an opportunity to estimate dynamics of soil features including organic carbon (OC) densities (in similar lithological and geomorphological conditions) (Fig. 3).

OC densities in mineral horizons were calculated for the 50 cm layer. OC storage in organic horizons was estimated for its actual thickness. "Expected" postpyrogenic reduction of OC density is most significant in organic horizons (from 3.9 to 0.5 kg C/m^2). However, 60 years after the fire, OC density reached its initial values in larch open forest and even exceeded initial values in a highly productive ecosystem of dense larch forest (Δ = 1.7 kg C/m^2) with thick moss cover stimulating active peat accumulation. Alteration of OC densities in mineral horizons is less evident. For the larch open forest ecosystem 30 years after the fire, the reduction was fixed (Δ = -1.6 kg C/m^2); however, at the next measuring point (60 years after the fire), an intensive increase has been revealed (Δ = 2.5 kg C/m^2). Such "unobvious" change was primarily induced by two factors: active layer thickness and cryoturbations. According to our data, in a 30- to 60-year period after the fire, active layer thickness decreases, reaching its initial values; at this time cryoturbations reach the highest intensity. Cryoturbations in the presence of two conditions—close permafrost table and already formed thick organic cover—most intensively enrich mineral horizons with organic matter. A similar trend was observed for the succession developing through the stage of dense forest.

Thus, the influence of fires on soil carbon pools has a dual nature: in the first stages, "expected" dramatic reduction of carbon pools in organic horizons and less expressed in mineral horizons; in the later stages, postpyrogenic effect of organic matter accumulation on the mineral surface and OC enrichment of mineral horizons due to intense recovery processes in the ecosystem.

References

Tarabukina, V.G. & Savvinov, D.D. 1990. Influence of fires on cryogenic soils. *Novosibirsk*: 120 pp.

NORPERM: The Norwegian TSP Permafrost Database

Kirsti Midttømme
Geological Survey of Norway, NGU
Geir Strand
Geological Survey of Norway, NGU
Håvard Juliussen
Department of Geology, The University Centre in Svalbard, Norway
Hanne H. Christiansen
Department of Geology, The University Centre in Svalbard, Norway

Introduction

According to the IPY data policy, all data from IPY projects should be stored in international data repositories, ensuring long-term preservation and sustained access. Also, the increasing amount of ground temperature data in Norway and Svalbard collected as part of different projects needs to be managed and stored centrally in a standard format database. The Geological Survey of Norway (NGU) is the managing institution for geological data in Norway, and is thus the obvious institution to host the Norwegian ground temperature database. A Norwegian permafrost database—NORPERM—is thus being developed at NGU as part of the IPY project "Permafrost Observatory Project: A Contribution to the Thermal State of Permafrost in Norway and Svalbard (TSP NORWAY)" (Etzelmüller et al. 2008). This database will include temperature data from about 40 existing boreholes, hundreds of miniloggers measuring shallow ground temperatures, Bottom Temperature of Snow (BTS) campaigns, and from similar research projects such as the CRYOLINK project (Etzelmüller et al. submitted). NORPERM will be the important data legacy from the TSP NORWAY project.

Data Sources – The TSP NORWAY Project

The observatories and data of the TSP NORWAY project are used as templates for NORPERM. There are two main permafrost observatories in TSP NORWAY: Troms in northern Norway and Nordenskiöldland in Svalbard (Fig. 1). Within the observatories, individual measurement sites (boreholes, miniloggers, etc.) are grouped together at specific so-called permafrost locations (e.g., mountains, valleys, etc.). Temperature data to be included in NORPERM are ground temperatures in 10–20 m deep boreholes, shallow ground temperatures using miniloggers, and traditional BTS data. There are 11 TSP boreholes in northern Norway and around 15 in Svalbard. Data from in situ periglacial process monitoring, geodetic surveys and/or remote sensing of landform dynamics, and periglacial landform ages are also collected in the TSP project and may be included in the database.

Extensive datasets on ground temperature exist, mainly from southern Norway, from previous permafrost projects such as the PACE project and the Dovrefjell monitoring programme (Etzelmüller et al. submitted), and from several PhD theses.

NORPERM – Structure and Access

The structure of NORPERM is shown in Figure 2. NORPERM is structured with "permafrost location" at the first level, corresponding to the locations where measurements are clustered. Overview information on climate, large-scale geomorphology, geology, etc., and photos are included at this level. At the next level are boreholes, (with either continuous temperature logging or sporadic manual measurements),

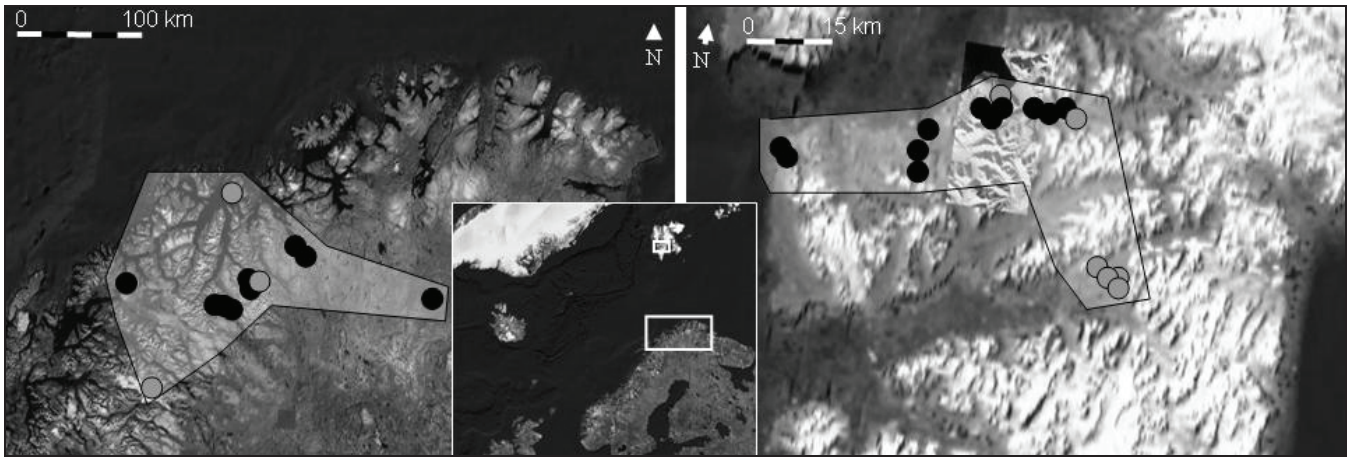

Figure 1. Left: the Norwegian part of the North Scandinavian Permafrost Observatory (69–70°N). Right: the Svalbard Nordenskioldsland Permafrost Observatory (78°N). Locations of TSP (black dots) and existing (grey dots) boreholes are shown. Based on Google Earth.

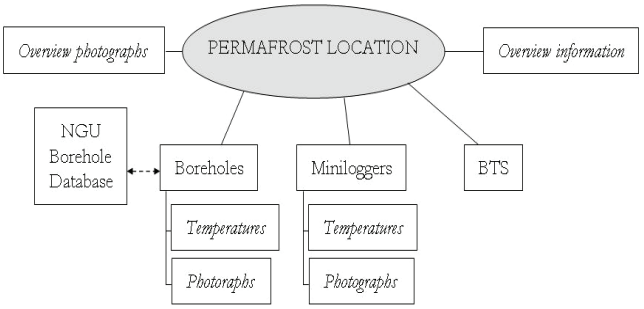

Figure 2. Overview of the structure of the NORPERM database.

shallow ground temperatures recorded with miniloggers, and BTS datasets. Photographs and summary graphics are included for each borehole and minilogger. The boreholes will also be registered in the national borehole database, which is under construction at NGU. Information and core samples from more than 6000 boreholes from mining exploration will be available through this service, and potential boreholes with negative ground temperatures will be included in NORPERM.

Relevant geographic, meteorological, geological, and geophysical data for the permafrost locations, existing at other institutions and available through Norway Digital (a national public cooperation of digital data between Norwegian national institutions), are linked to the NORPERM database. Metadata and data structure for boreholes follow the international standard format, and will be included in the International Global Terrestrial Network of Permafrost (GTN-P), which is the official international database for the international TSP IPY project. Data will be quality checked by TSP project scientists to ensure data quality.

NORPERM will be accessible through the websites of TSP NORWAY (www.tspnorway.com) and NGU (www.ngu.no). The dissemination of information is based on technologies for Internet distribution established through Norway Digital. Web map service (WMS) data will show the permafrost localities on both topographical and geological maps. Downloaded data will be available in standard formats as graphical plots, tables, pictures or "facts sheets."

Future Development

Current map visualization in NORPERM is in 2D. We aim at presenting NORPERM data in 3D in the near future, following guidelines given by a working group on visualization techniques at NGU. We also plan to present our results through Google Earth, as other types of IPY data are.

Three boreholes have been equipped with modem. Thus, real-time borehole temperature data will be available through our webpage (www.tspnorway.com).

References

Etzelmüller, B., Farbrot, H., Humlum, O., Christiansen, H.H., Juliussen, H., Isaksen, K., Schuler T., Ødegård, R. & Ridefelt, H. 2008. Mapping and modeling the distribution of permafrost in the Nordic countries. *Extended Abstracts of the Ninth International Conference on Permafrost, Fairbanks, Alaska, 29 June–3 July 2008*.

Potential Subsidence from Thawing of Near-Surface Ground Ice, Outer Mackenzie Delta Area, Northwest Territories, Canada

P.D. Morse
Department of Geography and Environmental Studies, Carleton University, Ottawa, ON, Canada
C.R. Burn
Department of Geography and Environmental Studies, Carleton University, Ottawa, ON, Canada
S.V. Kokelj
Water Resources Division, Indian and Northern Affairs Canada, Yellowknife, NT, Canada

Introduction

The outer Mackenzie Delta area (OMD), on the southeast coast of the Beaufort Sea, is within the continuous permafrost zone, and typically, permafrost occurs in unconsolidated sediments with greater than 20% visible ice content in the upper 15–20 m of the ground (Heginbottom et al. 1995). Kendall Island Bird Sanctuary (KIBS), OMD, protects 623 km^2 of wetland habitat important to migratory waterfowl and other birds, 60% of which is less than 1.5 m above mean sea level (Mackay 1963). Research on near-surface permafrost (NSP), defined here as the uppermost meter of permafrost, is necessary because of potential climate change impacts on ground conditions, specifically warming of permafrost (Smith et al. 2005) and sea level rise, which is currently 3.5 mm/a at Tuktoyaktuk (80 km east of KIBS) (Manson et al. 2005). Significant natural gas reserves have been identified beneath KIBS, and there are numerous other exploration leases in the region. Development of these resources would require construction of production platforms and distribution pipelines. Permafrost degradation in the OMD may lead to inundation and loss of both wildlife habitat and terrain for infrastructure construction.

The objective of this research is to estimate the potential subsidence from permafrost degradation at KIBS by (1) determining ground ice content of NSP in various surficial units; (2) determining the active layer thickness at each sample location; and (3) calculating the subsidence expected as the active layer thickens.

Surficial Units and Ground Ice

Ground ice contents were assessed in five surficial units within the two physiographic subdivisions at KIBS (Mackay 1963, Rampton 1988): (1) Tununuk Low Hills at the southwest, a rolling upland terrain usually less than 50 m above mean sea level, interspersed with broad, poorly drained depressions, covering approximately 30% of the area; and (2) Big Lake Delta Plain, a flat alluvial wetland, with numerous intersecting channels and lakes that may flood in spring or with storm surges. Tununuk Low Hills is a mosaic of thermokarst lake beds (TK), gravely sandy hills, ridges and terraces (G), ice-thrust hills and ridges (I), and till plains (TP). The physiography is due to Wisconsinan-advance glacial modification of permafrost in Pleistocene marine and fluvial deposits, post-glacial retreat with NSP aggradation, early Holocene thermokarst activity, and subsequent development of aggradational ice (Rampton 1987, 1988, Burn 1997). Big Lake Delta Plain, which consists of fine-grained river deposits (F), was exposed following the Wisconsinan glacial maximum through to the middle Holocene, and subsequently inundated by sea level rise or thermokarst lake development. It was then re-exposed between 0.5–1.5 ka ago due to fluvio-deltaic infilling and possible lake drainage (Rampton 1987, Taylor et al. 1996). Ground ice in F developed under saturated conditions with an aggrading surface from sediments deposited annually by spring flooding (Kokelj & Burn 2005).

Surficial Units and Ground Ice Sampling

The uppermost 1 m of permafrost was sampled at 72 sites in KIBS in 2006 and 2007. Cores were collected with a 5 cm diameter CRREL drill, and were sectioned into 10 cm intervals. Samples were collected along transects previously established within TK, G, I, TP, and F surficial units, and at a few other locations. Active layer thickness at each site was measured by probing the late-summer thaw depth (20–27 August 2007) (Mackay 1977).

Core sections were thawed, re-moulded, and allowed to settle. A saturated sediment layer with supernatant water on top was collected in a beaker, and excess-ice content was estimated with (Kokelj & Burn 2005, Eq. 1):

$$I_C = [(W_V*1.09)/(S_V+(W_V*1.09)]*100, \quad (1)$$

where I_C is the excess-ice content (%), W_V is the supernatant volume, and S_V is the saturated soil volume. The sample was then oven dried at 105°C to determine gravimetric moisture content (G_W).

Relation Between Surficial Units and Ground Ice

All surficial units had high ice content, with higher I_C in the upper 50 cm of permafrost (Table 1). Lowland NSP (F) was of higher ice content, 34%, than the uplands, on average 24%. In the uplands, the highest mean ice content in the uppermost 100 cm of permafrost was in TP, and the lowest was in G, but G also had the biggest range. In places, the ice content in organic-rich deposits at the base of hill slopes exceeded the hilltop ice content by an order of magnitude.

Table 1. Summary statistics for mean I_C (%) of the upper 50 and 100 cm of permafrost in surficial units of the OMD.

Surficial unit	Mean	Median	Min.	Max.	S.D.
F (n = 19)					
Upper 50 cm	36.6	36.8	20.0	53.5	9.7
Upper 100 cm	34.1	32.8	18.6	46.3	7.4
TK (n = 8)					
Upper 50 cm	26.0	23.3	16.6	38.2	8.0
Upper 100 cm	25.7	26.0	13.4	37.9	8.6
G (n = 16)					
Upper 50 cm	24.8	19.5	1.3	60.0	17.8
Upper 100 cm	20.2	19.2	0.8	39.5	12.3
I (n = 9)					
Upper 50 cm	23.2	24.1	7.8	36.3	8.9
Upper 100 cm	22.6	23.8	7.2	37.8	8.5
TP (n = 10)					
Upper 50 cm	32.7	34.1	20.9	47.6	8.4
Upper 100 cm	28.6	28.7	10.5	46.6	11.4

*n = number of cores used. Samples from hill slopes are not included.

Potential Near-Surface Permafrost Subsidence

Subsidence (*S*) due to a thermal disturbance was estimated for each surficial unit using mean upper 50 cm I_C (Table 1), and active layer thickness increases of 30% and 70%, respectively, after Mackay (1970, Fig. 3):

$$S = \{AL_1 /[(100 - I_C)/100]\} * \{I_C /100\}, \quad (2)$$

where AL_1 is the increase in active layer thickness (cm).

Predicted subsidence in the surficial units at KIBS (Table 2) is highest in F, yielding 26 cm of water with a 70% increase in active layer thickness. The greatest amount of subsidence in uplands occurs in TP, while subsidence in the remaining units is nearly uniform.

Subsidence is likely underestimated because I_C does not account for the 10% volume of air bubbles commonly found in larger ground ice bodies. Additional subsidence would likely occur from consolidation of thawed soil. In addition, the release of water would impact terrain stability in unconsolidated sediment, and thermal erosion would likely occur on slopes with modification of drainage patterns (Mackay 1970).

Conclusions

1. High ice content (>20% I_C) occurred in the uppermost 1 m of permafrost in all surficial units in KIBS, and ground ice content was highest in the uppermost 50 cm at the base of the active layer.

2. The highest ground ice content was in F, which accounts for nearly 60% of the habitat at KIBS.

3. An increase of 70% in active layer thickness F, which is typically less than 1.5 m above mean sea level, would decrease the elevation by 26 cm, and increase the chances of inundation during storm events.

Table 2. Thermokarst subsidence estimates based on mean active layer thickness (AL) and mean upper 50 cm I_C for surficial units of the OMD.

Surficial unit	Increase in thickness of active layer (cm)	Total depth of thaw (cm)	Subsidence (cm)
F (n = 19; AL = 64)			
30% increase	19	30	11
70% increase	45	71	26
TK (n = 8; AL = 35)			
30% increase	10	14	4
70% increase	24	33	9
G (n = 16; AL = 49)			
30% increase	15	20	5
70% increase	34	45	11
I (n = 9; AL = 48)			
30% increase	14	18	4
70% increase	34	44	10
TP (n = 10; AL = 47)			
30% increase	14	21	7
70% increase	33	49	16

*n = number of cores used. AL = mean active layer thickness (cm). Samples from hill slopes are not included.

References

Burn, C.R. 1997. Cryostratigraphy, palaeography, and climate change during the early Holocene warm interval, western Arctic coast, Canada. *Canadian Journal of Earth Sciences* 34: 912-925.

Heginbottom, J.A., Dubreuil, M.A. & Harker, P.A. 1995. Permafrost. In: *National Atlas of Canada,* 5th ed.

Kokelj, S.V. & Burn C.R. 2005. Near-surface ground ice in sediments of the Mackenzie Delta, Northwest Territories, Canada. *Permafrost and Periglacial Processes* 16: 291-303.

Mackay, J.R. 1963. *The Mackenzie Delta area, N.W.T., Canada.* Ottawa: Department of Mines and Technical Surveys, Geographical Branch Memoir 8, 202 pp.

Mackay, J.R. 1970. Disturbances to the tundra and forest tundra environment of the western Arctic. *Canadian Geotechnical Journal* 7: 420-432.

Manson, G.K., Solomon, S.M., Forbes, D.L., Atkinson, D.E., & Craymer, M. 2005. Spatial variability of factors influencing coastal change in the Western Canadian Arctic. *Geo-Marine Letters* 25: 138-145.

Rampton, V.N. 1987. Surficial Geology, Mackenzie Delta. Map 22. In: B.R. Pelletier (ed.), *Marine Science Atlas of the Beaufort Sea: Geology and Geophysics*. Ottawa: Geological Survey of Canada Miscellaneous Report 40.

Rampton, V.N. 1988. *Quaternary geology of the Tuktoyaktuk Coastlands, Northwest Territories*. Ottawa: Geological Survey of Canada Memoir 423, 98 pp.

Taylor, A.E., Dallimore, S.R. & Judge, A.S. 1996. Late Quaternary history of the Mackenzie–Beaufort region, Arctic Canada, from modelling of permafrost temperatures. 2. The Mackenzie Delta – Tuktoyaktuk Coastlands. *Canadian Journal of Earth Sciences* 33: 62-71.

Vegetation and Permafrost Long-Term Monitoring in the West Siberia Subarctic

N.G. Moskalenko, O.E. Ponomareva, G.V. Matyshak, P.T. Orehov
Earth Cryosphere Institute, Moscow, Russia
L.A, Kazantseva, E.V. Ustinova
Earth Cryosphere Institute, Tyumen, Russia

Long-term ecosystem monitoring in cold regions was carried out by few researchers (Timin et al. 1973, Bliss 1975, Bocher 1949, Broll et al. 2003, Burgess et al. 1999 and others). In this connection, results of long-term vegetation and permafrost monitoring since 1970 at the Nadym site in the West Siberia North can be of interest for researchers of Arctic and Subarctic regions.

The observation site is located 30 km south of the town of Nadym in the West Siberia northern taiga. This site is found on a flat boggy surface of the fluvial-lacustrine plain (third terrace) with altitude ranging from 25 to 30 m. The plain is composed of sandy deposits interbedded with clays, with an occasional covering of peat. Permafrost underlies the area sporadically. Patches of permafrost are closely associated with peatlands, tundras, mires, and frost mounds.

The annual geobotanical descriptions are carried out on fixed plots and transects in natural and disturbed conditions. Observations over vegetation dynamics were accompanied by soil descriptions, microclimatic observations, microrelief leveling, and measurements of permafrost temperature and seasonal thaw depths.

Flat peatland with a *Rubus chamaemorus-Ledum palustre-Sphagnum fuscum-Cladina stellaris* community is dominant on the fluvial-lacustrine plain (Fig. 1A). For this community, the complex horizontal structure caused by the presence of hummocks, interhummocks, pools, and in this connection, significant spatial variability of seasonal thaw depths (from 0.5 m in inter-hummocks up to 1 m and more in pools) is characteristic.

At the peatland in the first years after vegetation removal, cotton grass-cloudberry groupings formed over only 20% of the surface. Within 15 years on the disturbed peatland, continuous cloudberry-cotton grass-*Polytrichum-Sphagnum* cover had formed. This cover within 30 years, as a result of surface settlement, downturn of permafrost table up to 2–3 m, development of thermokarst, and bogging, was replaced by cotton grass-peat moss cover. The generated fragment of cotton grass-peat moss bog is present 35 years after disturbance (Fig. 1B)

The carried-out definitions of plant biomass have shown that, as compared with boggy communities in tundra communities, the biomass on the disturbed sites increased 2.5 times.

In this tundra, a *Ledum palustre-Betula nana*-lichen-*Polytrichum* plant community developed, replaced within 30 years after disturbance by a *Betula nana-Ledum palustre-Sphagnum*-lichen plant community, which developed here. On disturbed hummocky tundra, downturn of the permafrost table, rise in ground temperature, appearance of surface settlements, and formation in them of pools are observed; during the winter period, snow capacity has increased. It has been accompanied by a sharp increase in vegetation structure of *Betula nana* participation, having an average height of 1 m, and also *Polytrichum* mosses. The participation of these species has led to a substantial increase in plant biomass that was reflected in biodiversity, and abundance and biomass of small mammals in the disturbed tundra.

Evolution of soils on the disturbed flat peatland goes on in bog type, and bog oligotrophic soils are formed here. On the peatland, there are changes of hydrothermal regime and, as a consequence, changes of intensity and orientation of such major soil processes as respiration and transformation of organic material.

Background gas emission from the soil surface was measured. After that active layer left and measurements of gas emission from a permafrost surface directly after its opening and in 24 hours were carried out. On all investigated plots, sharp emission of the investigated gases (CO_2, CH_4), on some orders exceeding background emission, was observed (Table 1).

Measurements of ground temperatures in boreholes on the natural and disturbed peatland have shown (Fig. 1C) that distinctions in temperatures in natural and disturbed conditions have appreciably increased at a depth of 1 m (on 0.5°C). Temperature rise at a depth of 5 m was small, and at a depth of 10 m, it is not traced yet. Also we can see that the depth increase in ground temperature (on 0.8°C) for the period from 1972 to 2007, caused with rise in air temperature, is well defined. According to the Nadym weather station for 1970–2006, the trend in rise of air temperature has reached 0.04°C in a year.

The leveling of a peatland surface was carried out along a fixed transect once a year—at the end of August–the beginning of September—when seasonal thaw depth reaches maximum and surface position reflects the long-term process of frost heave. Marks of a surface were determined concerning a deep reference point.

It is established that the surface of flat peatland tested spasmodic rise in severe winters 1985, 1999, and for 32 years became 67 cm higher than in the beginning of observations. A feature of flat peatland frost heave is the rise of uniformity in the area. After 1999, the surface rise slowed down. The

Table 1. Gas emission (CH_4) from permafrost surface under disturbances (mg/m^2 per hour).

Landscape	Background	In 24 hours
Flat peatland	0.0624807	0.4265244
Palsa peatland	0.0003942	0.1820547

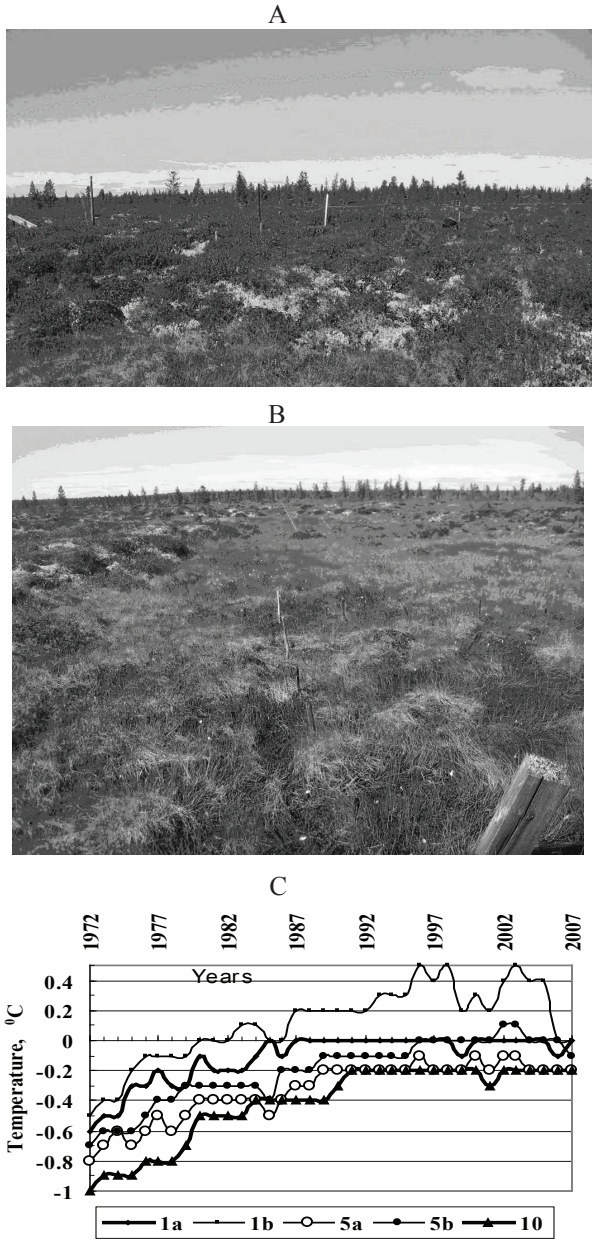

Figure 1. *Rubus chamaemorus-Ledum palustre-Sphagnum fuscum-Cladina stellaris* plant community on undisturbed peatland (A); *Eriophorum russeolum-Sphagnum Lindberg*ii plant community 33 years after removal of vegetation cover (B); and ground temperature (°C) in natural (a) and disturbed (b) conditions at the depths of 1, 5, and 10 m.

surface of flat peatland in recent years has become more stable (Fig. 2). These changes, as a whole, reflect a decrease in intensity of long-term frost heave, owing to climate warming and an increase of natural temperature background at human-induced impact.

Acknowledgments

This research was funded by the Polar Earth Science Program, Office of Polar Programs, National Science Foundation (ARC-0632400, ARC-0520578)

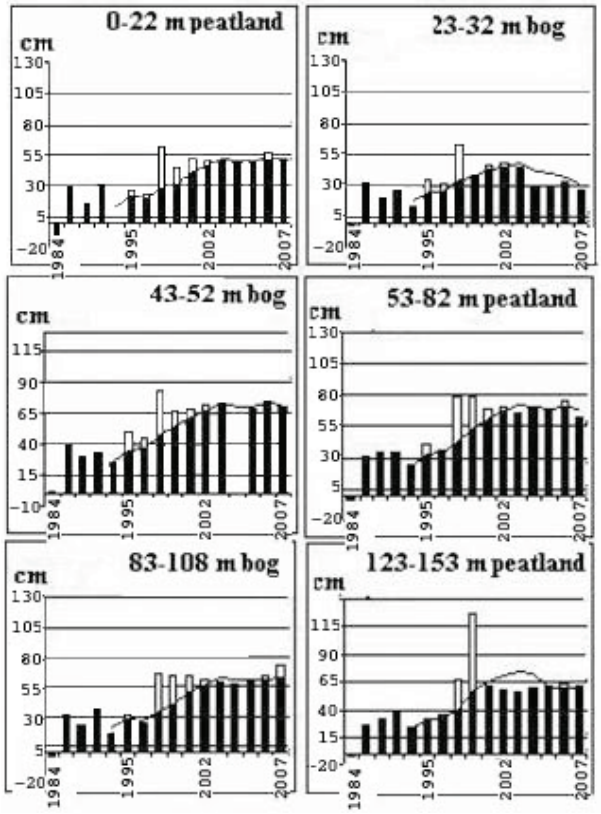

Figure 2. Diagram of changes of surface position along transect from its position in 1984 on data of repeated leveling and trend lines.

References

Bliss, L.C. 1975. Devon Island, Canada. *Ecolog. Bull*. 20: 17-60.

Bocher, T.W. 1949. Climate, soil and lakes in continental West Greenland in relation to plant life. *Medd. om Gronland* 147(2): 4.

Broll, G., Tarnocai, C. & Gould, J. 2003. Long-term high Arctic ecosystem monitoring in Quttnir paag National Park, Ellesmere Island, Canada. *Proceedings of the Eighth International Conference on Permafrost, Vol. 1, Zurich, Switzerland, 21–25 July 2003*: 85-94.

Burgess, M., Tarnocai, C., Nixon, N.M. et al. 1999. Active layer depth, and soil and ground temperature monitoring in permafrost areas of Canada. *Monitoring of Cryoshere.* Pushchino, 92-93.

Timin, M.E., Coller, B.D., Zich, J. & Walker, D.A. 1973. A computer simulation of the arctic tundra ecosystem near Borrow, Alaska. In: *U.S. Tundra Biome Rep. N 73-1*, San Diego State University: 1-82.

The Influence of Shrubs on Soil Temperatures in Alpine Tundra

Isla H. Myers-Smith
University of Alberta, Edmonton, Alberta, Canada
David S. Hik
University of Alberta, Edmonton, Alberta, Canada

Introduction

With a warming climate, northern ecosystems will face significant ecological changes such as permafrost thaw, increased forest fire frequency, and shifting ecosystem boundaries, including the spread of tall shrubs into tundra. In northern mountain ranges such as those in the southwestern Yukon, the shrub line will likely advance up mountain slopes with climate warming. In the last 50 years, rapid shrub expansion has been documented in arctic Alaska (Sturm et al. 2001a, Tape et al. 2006) and the Northern Yukon and NWT (Trevor Lantz, pers. com.) using repeat aerial photography. Paleoecological evidence suggests that tall shrubs last invaded tundra ecosystems in Alaska and northwestern Canada between 7,000 and 12,000 years ago, during the warm post-glacial period (Ritchie 1984). Growing season temperatures are again warming in Alaska and western Canada (Stafford et al. 2000), and concurrent with this trend, satellite imagery shows a greening of the Arctic (Stow et al. 2004). The correlation between warming and greening has been used to link climate change with shrub expansion (Sturm et al. 2001a); however, the exact mechanisms driving shrub increase are probably more complex. A combination of changes in nutrient mineralization, snow depth, microclimate, (Sturm et al. 2001b) disturbance (Trevor Lantz, pers. com.), and species interactions are most likely all contributing factors to shrub expansion patterns on the landscape

Influence of shrubs on soil temperatures

Increased shrubs in arctic and alpine tundra alter the partitioning of solar energy during the growing season, the distribution and physical characteristics of snow in the winter (Liston et al. 2002), and soil thermal dynamics year-round (Sturm et al. 2001b, Sturm et al. 2005a). In the winter, snow trapping by shrubs can insulate soils (by trapping heat) and has been proposed as a positive feedback mechanism promoting the expansion of shrubs in the Arctic (Sturm et al. 2001b, Sturm et al. 2005a). During spring, dark-colored shrubs that extend above the snow alter the albedo and accelerate local snowmelt (Sturm et al. 2005b, Pomeroy et al. 2006). In summer, shading by shrubs decreases soil temperatures under shrub canopies (Pomeroy et al. 2006). Though complex, the interactions between shrubs, snow, and soil warming may act as a positive feedback to shrub expansion (Fig. 4, Chapin et al. 2005). In addition, winter soil warming may enhance nutrient cycling and reduce soil carbon stores (Mack et al. 2004).

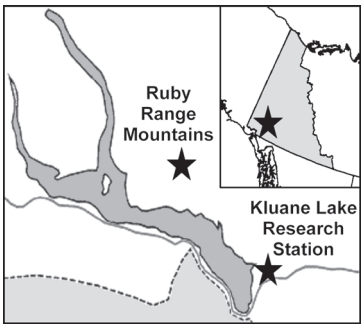

Figure 1. Map of the study region and the Ruby Range Mountain field site.

Study Site

The field site is located in the Ruby Range Mountains (61°20′N, 139°17′W, Fig. 1) adjacent to Kluane Lake. This area of the southwest Yukon is located at the convergence of the coastal and arctic air masses, and as a result, climate change could lead to increased variability in winter temperatures and precipitation. The study area varies in elevation, aspect, and proximity to glaciers, making it an ideal location to test a shrub expansion hypotheses.

Methods

To measure the influence of snow-capture by shrubs on soil warming, we manipulated willow (*Salix* spp.) cover to compare soil temperatures beneath plots with (a) intact shrubs, (b) shrubs removed, (c) artificial vegetation canopies, and (d) adjacent, shrub-free tundra. In September 2007, 6 artificial shrub and tundra plots were constructed by cutting down shrubs and affixing them to stakes in the soil in adjacent shrub-free tundra (Fig. 2).

The 6 manipulation plots and paired control monitoring plots are instrumented with snow stakes with iButton Thermochron temperature loggers (Dallas Semiconductor Corporation, Dallas, Texas, USA) at 2, 5, 25, 50, 100, and 150 cm along their length, and with Hobo micro station 12-bit temperature sensors (HOBO, Onset Computer Corp., Massachusetts, USA), installed at 2 and 5 cm below the soil surface. This experiment will test whether shrubs trap more snow than the adjacent tundra, whether this snow melts out earlier in the spring season, and how much the trapped snow insulates the soil.

Initial Results

Over the growing season of 2007, shrub plots were significantly cooler than tundra plots (for DOY 160 to 244, at 2 cm depth: 1.5°C cooler under shrubs, $F_{1,172} = 33.9$, $p < 0.001$, at 5 cm depth: 1.3°C cooler under shrubs, $F_{1,172} = 25.7$, $p < 0.001$, Fig. 3).

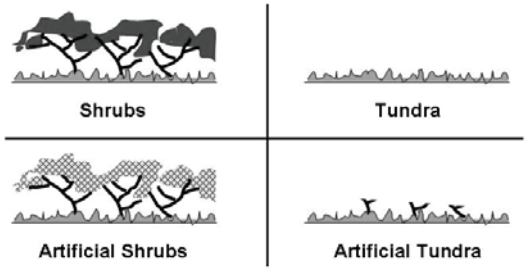

Figure 2. Manipulative experiment.

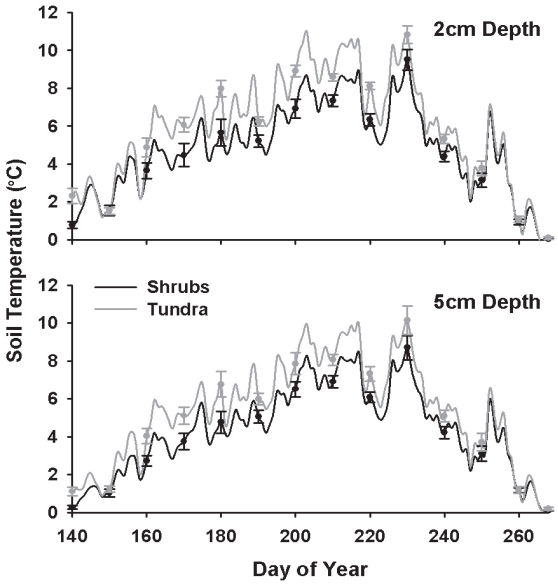

Figure 3. Mean daily soil temperatures (±SE) at 2 cm and 5 cm depth under shrub and tundra plots (n = 12).

Since the manipulation was conducted at the end of the 2007 field season, we were only able to collect one week of experimental data. During the last week of September, both the shrub and artificial shrub plots were cooler than the tundra and artificial tundra plots; however, these comparisons are not statistically significant. Data from the 2007–08 winter season will indicate whether shrub canopies trap more snow and if insulation results in soil warming.

Discussion

Increasing shrubs in arctic and alpine tundra will alter microclimates and soil thermal dynamics (Sturm et al. 2001b). Cooling of summer soil temperatures may reduce decomposition and resulting carbon loss. Warming of winter soils may, however, increase decomposition, accelerate nutrient cycling and promote the further expansion of shrubs (Sturm et al. 2001b, Sturm et al. 2005a). This study attempts to quantify the impact of shrubs on soil thermal dynamics. Shrubs cool soils during the growing season (Pomeroy et al. 2006 this study); however, the contribution of shrubs to winter soil thermal dynamics has been little explored in the literature. By manipulating shrub cover (removing above ground woody biomass and erecting artificial shrubs), the insulation provided by a shrub canopy and trapped snow can be isolated from the influence of understory vegetation and soils. If increasing shrubiness is resulting in warmer winter soils, this may lead to enhanced nutrient cycling and reduced soil carbon stores; however, the 2°C summer cooling may offset a winter warming response. By the summer of 2008, we will have collected data for a full winter season, and will be able to determine snow trapping and soil warming potential of willow shrubs in the alpine tundra of the Kluane Region.

Acknowledgments

We would like to thank Jodie Pongracz, Catherine Henry, Eric Vezeau, and Mark Wong for field assistance. Funding was provided by NSERC, NSTP, C/BAR, Yukon College NRI, the Alberta Ingenuity Fund, and ANIA's Grant-in-Aid Program.

References

Chapin, F.S. III, Sturm, M., Serreze, M.C. et al. 2005. Role of land-surface changes in Arctic summer warming. *Science* 310: 657-660.

Liston, G., McFadden, J.P., Sturm, M. & Pielke, R.A. 2002. Modelled changes in arctic tundra snow, energy and moisture fluxes due to increased shrubs. *Global Change Biology* 8: 17-32.

Mack, M.C., Schuur, E.A.G., Bret-Harte, M.S. et al. 2004. Ecosystem carbon storage in arctic tundra reduced by long-term nutrient fertilization. *Nature* 431: 440.

Pomeroy, J.W., Bewley, D., Essery, R. et al. 2006. Shrub tundra snowmelt. *Hydrological Processes* 20: 923-941.

Ritchie, J.C. 1984. Past and present vegetation of the far Northwest of Canada. University of Toronto Press: Toronto, Canada.

Stafford, J.M., Wendler, G. & Curtis, J. 2000. Temperature and precipitation of Alaska: 50 year trend analysis. *Theoretical and Applied Climatology* 67: 33-44.

Stow, D.A., Hope, A., McGuire, D. et al. 2004 Remote sensing of vegetation and land-cover change in Arctic Tundra Ecosystems. *Remote Sensing of Environment* 89: 281-308.

Sturm, M., Racine, C. & Tape K. 2001a. Increasing shrub abundance in the Arctic. *Nature* 411: 546-547.

Sturm, M., McFadden, J.P., Liston G.E. et al. 2001b. Snow-shrub interactions in Arctic tundra: A hypothesis with climatic implications. *Journal of Climatology* 14: 336-344.

Sturm, M., Schimel, J., Michaelson G. et al. 2005a. Winter biological processes could help convert arctic tundra to shrubland. *BioScience* 55: 17-26.

Sturm, M., Douglas, T. Racine, C. & Liston, G.E. 2005b. Changing snow and shrub conditions affect albedo with global implications. *Journal of Geophysical Research* 110: doi:10.1029/2005JG000013.

Tape, K., Sturm M. & Racine C. 2006. The evidence for shrub expansion in Northern Alaska and the Pan-Arctic. *Global Change Biology* 12: 686-702.

Estimation of the Extent of Near-Surface Permafrost in the Mackenzie Delta, Northwest Territories, Using Remote Sensing

T.-N. Nguyen, C.R. Burn, D.J. King
Department of Geography and Environmental Studies, Carleton University, Ottawa, ON, Canada
S.L. Smith
Geological Survey of Canada, Natural Resources Canada, Ottawa, ON, Canada

Introduction

Based on air temperature, permafrost should be continuous in the Mackenzie Delta (MD), northwest Canada (Henry & Smith 2001). However, the most recent Permafrost map of Canada, using sparse ground temperature data, classifies the MD as having discontinuous permafrost (Heginbottom et al. 1995). There has been little fieldwork investigating permafrost extent within the delta, yet, the determination of near-surface permafrost (NSP) extent, defined in this study as permafrost within 3 m from ground surface, is important for land-use planning, as terrain behaviour varies between frozen and unfrozen ground (Smith et al. 2001).

The objectives of this research were (1) to assess if the spatial distribution of near-shore vegetation associations can be used to predict NSP presence in the MD and, if so, (2) to apply remote sensing techniques to map these vegetation communities and estimate the proportion of ground underlain by NSP.

Vegetation and Permafrost in Mackenzie Delta

The MD stretches 200 km north–south and 60 km east–west (Mackay 1963). It is an alluvial landscape intersected by a network of channels and thousands of lakes, and is subjected to annual flooding. Spatial variation in channel shifting, flooding, and sedimentation is expressed by patterns of vegetation (Gill 1973).

Horsetail (*Equisetum* spp.) communities are the typical emergent plant associations, while Willow-horsetail (*Salix-Equisetum*) communities can be found with increasing distance from stream channels. Alders (*Alnus* spp.) are located at slightly higher elevations than the Willow-horsetail communities, since alder species are less tolerant of sedimentation. Spruce (*Picea glauca*) forests represent the climax community south of tree line. North of tree line, sedges (*Carex* spp.) and horsetails are common adjacent to channels, and Willow-horsetail and *Salix richardsonii* are widespread on more elevated sites (Pearce 1998).

In the MD, the thermal effect of water bodies and the shifting nature of channels affect the age, distribution, temperature, and thickness of permafrost (Smith 1975). On point bars, taliks have been recognized near channels by various authors (Gill 1973, Smith 1975). The presence of a talik, where winter freeze-back does not reach the top of permafrost, is due to the slow establishment of permafrost beneath newly exposed ground, and to deep snowdrifts blown off the channels and trapped in near-shore willow stands (Dyke 2000).

Vegetation and Permafrost Sampling

Field sites were selected so that several representative vegetation classes were present at each site. A line transect methodology was adopted for vegetation sampling and permafrost probing. A total of 52 transects were laid in summer 2006. The majority of transects were between 100 m and 200 m long depending on the width of the vegetation zones found at each site. Transects were established perpendicular to the shoreline and crossing the successional sequence of vegetation (Fig. 1). Vegetation was sampled using point and line-intercept methods and was identified at the genus level for shrubs and trees, and at the functional-type level for herbs. Plant presence and frequency were calculated to provide an indication of how dominant a plant type is in a community. The ground was probed using water-jet drilling to detect NSP in each vegetation association. Since the active layer thickness rarely exceeds 1.5 m in the MD, NSP was considered absent if unfrozen ground was recorded to 3 m depth (Kokelj & Burn 2005).

Relation Between Vegetation and Permafrost

There was a clear association between presence of permafrost in the upper 3 m and different vegetation communities. On point bars and alluvial islands, Horsetail

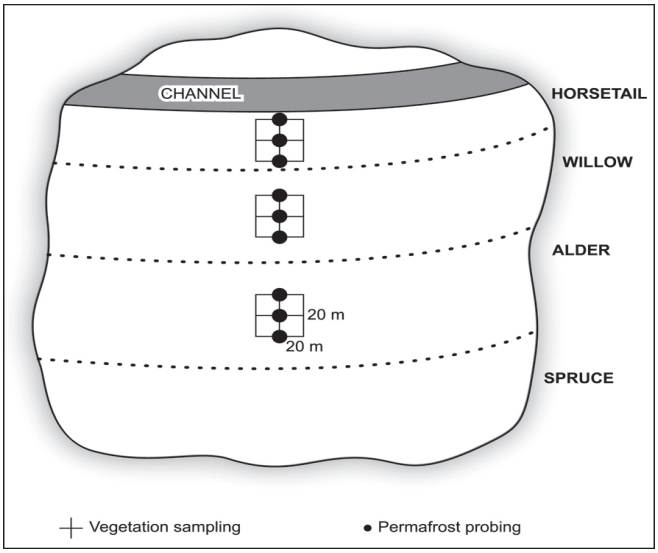

Figure 1. In each 20 m x 20 m plot, the water-jet drilled hole in the centre was complemented with two others. Each plot was assigned a single NSP presence or absence label based on the rule of majority. Spruce forests were not the focus of this research since the presence of permafrost is ubiquitous there with thin active layer thicknesses (Kokelj & Burn 2005).

Table 1. Relation between NSP and vegetation associations.

Vegetation association	Presence of NSP (% of plots)
Southern delta	
Horsetail (n=8)	0
Willow-horsetail (n=19)	0
Alder (n=25)	96
Central delta	
Horsetail (n=11)	9
Willow-horsetail (n=20)	10
Alder (n=26)	100
Northern delta	
Horsetail-sedge (n=18)	100
Willow-horsetail (n=12)	17
Salix richardsonii (n=15)	100

and Willow-horsetail communities were not associated with NSP. NSP was present beneath all other vegetation associations and in other land surface types (Table 1).

Image Data Analysis

Permafrost cannot be directly imaged by airborne or satellite-based sensors, but its presence may be inferred from surface characteristics, especially vegetation. In this study, SPOT-5 images of the MD, captured in July 2006 with a nominal ground pixel size of 10 m x 10 m, were classified for vegetation characteristics associated with NSP. Using relations of these characteristics with field survey data, the proportion of ground underlain by NSP was estimated.

In addition to spectral data produced directly by SPOT-5, data transformations such as vegetation indices, texture analysis and PCA were used to generate additional image information for classification. Training and testing data were chosen randomly among field sampled plots. Maximum Likelihood classifications were used to generate maps of vegetation associations with accuracies above 80%.

Estimation of Near-Surface Permafrost Extent

To estimate the extent of NSP in the MD, the land surface was categorized into three types: (1) Alluvial islands (AI), (2) Point bars (PB), and (3) all other types. PB occupied about 18% of the land surface and the extent of AI in the southern delta was calculated to be about 5%. The extent of NSP in the delta is:

$$\sum_{i=1}^{d}\left(\sum_{j=1}^{L}\left(\sum_{k=1}^{n} V_k * P_k\right)\right) \quad (1)$$

where d are the delta regions, L the land surface types, n the vegetation classes underlain by NSP, V the land fraction occupied by n, and P the land fraction occupied by L.

In the southern delta, 93% of the land surface was found to be underlain by NSP. Zones with presence of NSP represented 95% and 96% of the land surface in the central and northern delta, respectively.

Conclusions

1. On point bars and alluvial islands, Horsetail and Willow-horsetail communities were not associated with NSP. NSP was present beneath all other vegetation associations and in other land surface types.
2. Zones with presence of NSP represent 93%, 95%, and 96% of the land surface in the southern, central, and northern delta, respectively. This indicates that the MD is part of the continuous permafrost zone.
3. The technique developed in this study was useful in the mapping of NSP over large areas in a dynamic environment and could form the basis of a mapping tool that could be used to aid in land-use planning.

References

Dyke, L.D. 2000. Shoreline permafrost along the Mackenzie River. In: L.D. Dyke & G.R. Brooks (ed.), *The Physical Environment of the Mackenzie Valley, Northwest Territories: a Baseline for the Assessment of Environmental Change*. Ottawa: Geological Survey of Canada Bulletin 547: 143-151.

Gill, D. 1973. A spatial correlation between plant distribution and unfrozen ground within a region of discontinuous permafrost. *Proceedings of the Second International Conference on Permafrost, Yakutsk, U.S.S.R., July 13-28, 1973*: 105-113.

Heginbottom, J.A., Dubreuil, M-A. & Harker, P.A. 1995. *Permafrost. National Atlas of Canada,* 5th ed.

Henry, K. & Smith, M.W. 2001. A model-based map of ground temperatures for the permafrost regions of Canada. *Permafrost and Periglacial Processes* 12: 389-398.

Kokelj, S.V. & Burn, C.R. 2005. Near-surface ground ice in sediments of the Mackenzie Delta, Northwest Territories, Canada. *Permafrost and Periglacial Processes* 16: 291-303.

Mackay, J.R. 1963. *The Mackenzie Delta Area, N.W.T., Canada*. Department of Mines and Technical Surveys, Geographical Branch, Memoir 8.

Pearce, C.M. 1998. Vegetation patterns and environmental relationships in an Arctic riparian wetland. In: S.K. Majumdar, E.W. Miller & F.J. Brenner (eds.), *Ecology of Wetlands and Associated Systems*. Pennsylvania Academy of Science, 258-280.

Smith, M.W. 1975. Microclimatic influences on ground temperatures and permafrost distribution, Mackenzie Delta, Northwest Territories. *Canadian Journal of Earth Sciences* 12: 1421-1438.

Smith, S.L., Burgess, M.M. & Heginbottom, J.A. 2001. Permafrost in Canada, a challenge to northern development. In: G.R. Brooks (ed.), *A Synthesis of Geological Hazards in Canada.* Ottawa: Geological Survey of Canada Bulletin 548: 241-264.

Employing a Coupled Permafrost Water Balance Model to Study Possible Changes in Permafrost

D.J. Nicolsky
Geophysical Institute, University of Alaska Fairbanks PO Box 757320, Fairbanks, AK 99775, USA
V.E. Romanovsky
Geophysical Institute, University of Alaska Fairbanks PO Box 757320, Fairbanks, AK 99775, USA
M.A. Rawlins
Jet Propulsion Laboratory, California Institute of Technology, Pasadena, CA 91109, USA

Introduction

Thawing and freezing of arctic soils is affected by many factors, with air temperature, vegetation, snow accumulation, and soil moisture among the most significant. Here we describe the coupling of a Permafrost Model (Sazonova & Romanovsky 2003, Nicolsky et al. 2007) and the pan-Arctic Water Balance Model (PWBM, Rawlins et al. 2003), developed at the University of Alaska Fairbanks and the University of New Hampshire, respectively. Additionally, we present resultant simulated soil temperature and moisture dynamics, depth of seasonal freezing and thawing, river run-off, and water storage across the pan-Arctic. The coupled models simulate the snow/ground temperature with a 5-layer snow and 23-layer soil model. In the soil model, the layers thicken with depth and span a 60 m thick column. The PWBM has two soil storage zones: a root zone that gains water from infiltration and loses water via evapotranspiration and horizontal and vertical drainage, and a deep zone that gains water via root zone vertical drainage and loses water via horizontal drainage. Forcing data (i.e., air temperature, precipitation) are taken from ERA40 datasets and from several of the IPCC 4th Assessment model simulations of future arctic climate. We validate our model simulations by comparing soil moisture and thermal profiles with observational data collected within the pan-Arctic.

Coupling of Two Models

The coupling captures thresholds and non-linear feedback processes induced by changes in hydrology and subsurface temperature dynamics, and hence helps us to study the spatial and temporal variability of permafrost dynamics as well as potential future alterations to permafrost and the terrestrial arctic water cycle. Through explicit coupling of the Permafrost Model with the PWBM, we are able to simulate the temporal and spatial variability in soil water/ice content, active layer thickness, and associated large-scale hydrology that are driven by contemporary and future climate variability and change. Choosing appropriate climate forcings is clearly a significant challenge.

Acknowledgments

This research was funded by ARCSS Program and by the Polar Earth Science Program, Office of Polar Programs, National Science Foundation (OPP-0120736, ARC-0632400, ARC-0520578, ARC-0612533, IARC-NSF CA: Project 3.1 Permafrost Research), by NASA Water and Energy Cycle grant, and by the State of Alaska.

References

Nicolsky, D.J., Romanovsky, V.E., Alexeev, V.A. & Lawrence, D.M. 2007. Improved modeling of permafrost dynamics in a GCM land-surface scheme. *Geophysical Research Letters* 34: L08501.

Rawlins, M.A., Lammers, R.B., Frolking, S., Fekete, B.M. & Vo¨ro¨smarty, C.J. 2003. Simulating pan-Arctic runoff with a macro-scale terrestrial water balance model. *Hydrological Processes* 17: 2521-2539.

Sazonova, T.S. & Romanovsky, V.E. 2003. A Model for Regional-Scale Estimation of Temporal and Spatial Variability of the Active Layer Thickness and Mean Annual Ground Temperatures. *Permafrost and Periglacial Processes* 14(2): 125-139.

Influence of a Hydrothermal Soil Regime on the Radial Increment of Larch and Pine in Central Yakutia

Anatoly N. Nikolaev
Permafrost Institute, SB RAS, Yakutsk, Russia

Introduction

Central Yakutia (eastern Siberia, Russia) has a dominant growth of larches, for it is situated on the area of permafrost distribution. According to sustainable zoning of permafrost soils of Yakutia, the observed area refers to the Central Yakutia taiga-alas provinces of permafrost and pale soils (Elovskaya & Konorovskiy 1978). It has severe, long, and low-snow winters and hot, short, and droughty summers with significant insolation, low annual and winter temperatures, high seasonal and daily amplitudes, and small amount of deposits (Gavrilova 1973). Hydrothermal soil condition is one of the important factors influencing tree species growth. Long-term observation of the thermal soil regime in Central Yakutia has enabled the use of tree-ring chronology not only to reveal the relations between radial increment, atmospheric temperature, and precipitation, but also to analyze the influence of the hydrothermal soil regime on growth and development of larch (Nikolaev & Fyodorov 2004, Fyodorov et al. 2007).

Materials and Methods

Tree-ring chronology was examined at Spasskaya Pad and Tyungyulyu, 25 km northwest and 45 km northeast from Yakutsk accordingly, in Central Yakutia, the scientific stations of Institute of Biological Cryolitozone Problems of the SB RAS.

Due to the fact, that Spasskaya Pad site has areas of larch and pine forests nearby, it was possible to carry out the comparative analysis of the growth of these two species in conditions of permafrost. The forest areas are situated in the Lena and Amga interfluve, which has one of the most droughty climates in Central Yakutia. The width of year rings was measured with the LINTAB-III measuring instrument (Rinn 1996) in the laboratories of cryogenic landscapes of Melnikov Permafrost Institute SB RAS. Dendroclimatology standard research and the analysis technique were applied during dating and construction of tree-ring chronology (Vaganov et al. 1996, Shiyatov et al. 2000, Holmes 1983, 1998, Methods … 1990, Rinn 1996). As a result, we got 2 generalized tree-ring chronologies on the station Spasskaya Pad, one of which is for larch kayander (*Larix cajanderi Mayr.)* (SPPV) and the other for scotch pine *(Pinus sylvestris L.)* (SPP12), which have been constructed. Other tree-ring chronologies on larch have been made up at station Tyungyulyu (TYNG).

The comparative analysis of larch and pine growth depending on external conditions at Spasskaya Pad station was carried out. It is known that these two species are the basic forest-forming ones in Central Yakutia. Growth of trees is influenced not only by climatic factors such as atmospheric temperature and deposits, but also hydrothermal soils conditions. Larch prefers moderately fertile and moderately moistened loamy ground, and grows worse in dry and crude areas. In contrast to larch, pine grows on well aerated dry sandy and sabulous soils.

The soil temperature condition influence on radial trees increment at Spasskaya Pad was analyzed. Here data from Pokrovsk meteorological stations were used. This meteorological station has more homogeneous data in comparison with data of the Yakutsk meteorological station, which has some series disorder as a result of its relocation in 1930, 1952, and 1964 (USSR Climate Directory 1975) and soil condition changes since 1989 caused by an increase in subterranean water.

Results and Discussion

Correlation analysis of larches tree-ring chronology from Spasskaya Pad with soils temperature conditions at various depths shows that considerable correlation occurs during winter period. The higher the soil temperatures, the faster soils warm up, which promotes timely beginning of active tree growth in the vegetation beginning. Summer temperatures do not limit radial trees increment. During this period trees have enough amount of heat for favorable growth.

The similar analysis of pine radial increment has shown, that winter soil temperatures until the end of May have a positive relation to radial tree increments both at active layer table and zero annual amplitudes of active layer at 20 cm and 120 cm depth. A positive influence of temperature occurs in spring months in soil layers at 40–80 cm, which leads to early soil thawing and the beginning of pine growth processes. However, unlike larch, a significant negative influence of summer months' temperature on pine growth occurs at some depths. Probably this is due to a significant deficiency of soil water content in drier soils, where heats causes a drying up effect.

The correlation analysis of larch tree-ring chronology at Tyungyulyu with soil temperature conditions at different depths shows the presence of significant correlation; it is the same for Spasskaya Pad at winter period. It is also revealed, that the soil's summer temperature value has no significant influence on radial tree increments. In some cases, the soil high temperature means its negative relation with larch growth, which features for pine from Spasskaya Pad.

Correlation analysis of tree-ring chronology for larch with soil water content changes was carried out. Results show good correlation occurs during the whole vegetative period. However, it is necessary to note that the most significant ratios fall at the autumn period of the previous season. This

is due to the fact that larch in the beginning of the vegetative period uses the cumulative soil water reserve of the previous year. Thus water content of the soil's upper layers, that is, up to 50 cm, during its seasonal freezing shows significant correlation with the radial larch increment. Also soil water content of September and October at depths of 80–100 show good correlation with the annual increment It is possible to explain this by the fact that the larch root system basically uses water from the soil bottom lifts by the end of the vegetative period, since during summer, soil thawing passes gradually and is accompanied with dehydration of the soils upper horizons.

Conclusions

Thus, it is possible to approve that radial larch increment on permafrost soil is closely related to the active layer soil temperature and water content during the vegetative season. It is also significant that the application of dendroclimatological research technique helped to receive interesting results while studying the reaction of forest-forming species to climatic and soil conditions in the zone of permafrost distribution.

Acknowledgments

The research is executed with support of the grant of the Russian Federal Property Fund 06-05-96117 (r_vostok_a) and the integration project of SB RAS #71.

References

Elovskaya, L.G. & Konorovskiy, A.K. 1978. *Zoning and Melioration of Permafrost Soils in Yakutia.* Novosibirsk: Nauka, 175.

Fyodorov, P.P., Nikolaev, A.N. & Desyatkin, A.R. 2007. Revealing of hydrothermal soil regime influence on Larch radial increment in Central Yakutia. *Proceedings of Conference on New Dendroecological Technique*, *Irkutsk*.

Gavrilova, M.K. 1973. *Climate in Central Yakutia*. Yakutsk: Yakutsk Book Press, 120 pp.

Holmes, R.L. 1983. Computer-assisted quality control in tree-ring dating and measurement. *Tree-ring Bulletin*, 44: 69-75.

Holmes, R.L. 1998. *Dendrochronology Program Library-Users Manual-Laboratory of Tree-Ring Research*. Tucson, Arizona USA: University of Arizona, Updated September 1998 (the electronic version).

Methods of Dendrochronology. 1990. In: E. Cook et al. (eds.), *Application in Environmental Sciences.* Dordrecht: Kluwer Acad. Publ., 394 pp.

Murton, J.B. & French, H.M. 1994. Cryostructures in permafrost, Tuktoyaktuk coastlands, western Arctic Canada. *Canadian Journal of Earth Sciences* 31: 737-747.

Nikolaev, A.N. & Fyodorov, P.P. 2004. Influence of climatic factors and thermal permafrost soils regime of Central Yakutia on Larch and Pine radial increment (by the Example of Spasskaya Pad station). *Dendrology* 6: 1-11.

Rinn, F. 1996. *Referense Manual. Computer Program for Tree Ring Analysis and Presentation*. TSAP version 3.5. Heidelberg, Germany, 264 pp.

Shiyatov, S.G., Vaganov, E.A., Kirdyanov, A.V., Kruglov, V.B., Mazepa, V.S., Naurzbaev, M.M. & Khantemirov, R.M. 2000. *Dendrochronology Technique*. 1: Bases Dendrochronology Basic Foundation. Tee-ring Data Acquisition Tutorial and Methodological Manual. Krasnoyarsk: KrasGU Press, 80 pp.

Vaganov, E.A., Shiyatov, S.G. & Mazepa, V.S. 1996. *Dendroclimatological Research in the Ural-Siberian Subarctic Region*. Novosibirsk: Nauka, 246 pp.

Soil Temperature. 1975. In: USSR Climate Directory, 4th ed., Vol. 8. Yakutsk: Yakutsk Hydrometeorological Service Board Press, 570 pp.

The Effect of Soil Moisture and Ice Content on the Thermal Conductivity of Organic Soil Horizons Underlain By Discontinuous Permafrost

Jonathan A. O'Donnell
Department of Biology and Wildlife, University of Alaska Fairbanks
Vladimir E. Romanovsky
Geophysical Institute, University of Alaska Fairbanks
Jennifer W. Harden
United States Geological Survey, Menlo Park, CA
Kenji Yoshikawa
Water and Environmental Research Center, University of Alaska Fairbanks
A. David McGuire
Institute of Arctic Biology, University of Alaska Fairbanks

Introduction

Permafrost temperatures in Alaska have warmed in recent decades in response to changing climatic conditions at high latitudes (Lachenbruch & Marshall 1986, Osterkamp & Romanovsky 1999). In Interior Alaska, where forests are underlain by discontinuous permafrost, mean annual ground surface temperature (MAGST) often exceeds 0°C, yet permafrost can exist in a stable state (< 0°C) due to thermal offset (the difference between MAGST and mean annual permafrost surface temperature, or MAPST; Burn & Smith 1988). Thermal offset persists because the thermal conductivity of ice is greater than that of water, so soils conduct heat more effectively in winter than in summer.

Soil thermal models typically use a fixed thermal conductivity value for frozen and thawed soils. This bimodal approach, however, may be too simplistic to accurately predict soil temperatures and active layer depth (Overduin et al. 2006). Thermal conductivity of organic soil horizons varies considerably with moisture and ice content and is a critical control on active layer depth (Yoshikawa et al. 2003). Organic horizon type, which varies in bulk density, moisture field capacity, and extent of decomposition, may also influence thermal conductivity values. The primary objective of this study is to evaluate the effects of soil moisture and ice content on the thermal conductivity of three organic horizon types from black spruce forests of Interior Alaska.

Methods

We conducted a laboratory experiment to examine the effects of moisture and ice content on the thermal conductivity of organic soils collected from black spruce forests underlain by permafrost. Soil samples were collected from three moderately drained and three poorly drained black spruce forests in Interior Alaska. Organic soils were divided into three distinct horizons (live/dead moss, fibric, mesic/humic), that differ with respect to bulk density and extent of decomposition. Feather moss (*Hylocomium splendens and Pleurozium schreberi*) was the dominant moss species from the moderately drained stands, whereas *Sphagnum* spp. (most commonly *S. fuscum)* dominated forest floor cover in the poorly drained stands.

In the lab, all samples (n = 5 per site per horizon, total = 90 samples) were saturated and dried at air temperature, during which time we weighed each soil block and measured thermal conductivity using a KD2 Pro Thermal Properties Analyzer (Decagon Devices, Inc., Pullman, WA, USA) to generate a thermal conductivity—moisture content relationship for each sample from each horizon type. Measurements of thermal conductivity as a function of ice content are in progress. In 2005, we measured VWC in the field near Hess Creek, Alaska, using ECH2O probes (Decagon Devices, Inc., Pullman, WA) in replicate plots. Following field measurements, all probes and soil blocks were calibrated (O'Donnell et al. in review).

Results

Volumetric water content (VWC) of feather moss species, such as *Hylocomium splendens*, is generally around 10% (by volume) during summer months (Fig. 1). VWC of *Sphagnum* spp. is generally higher, ranging from 15–40% (by volume; Fig. 1).

We observed strong positive and linear correlations between thermal conductivity and organic VWC across all

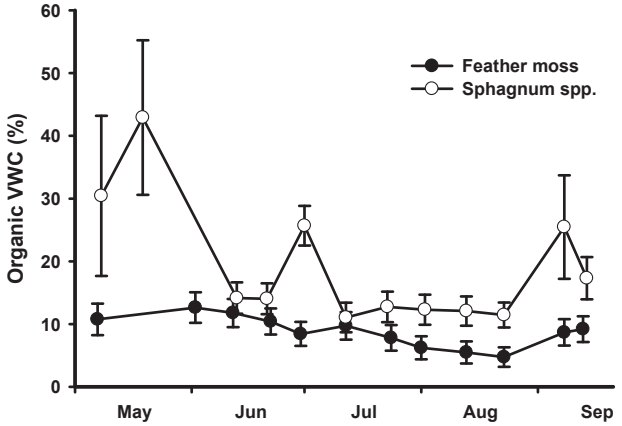

Figure 1. Seasonal variation in volumetric water content (VWC) of fibric organic matter near Hess Creek, Alaska (O'Donnell el al. in review).

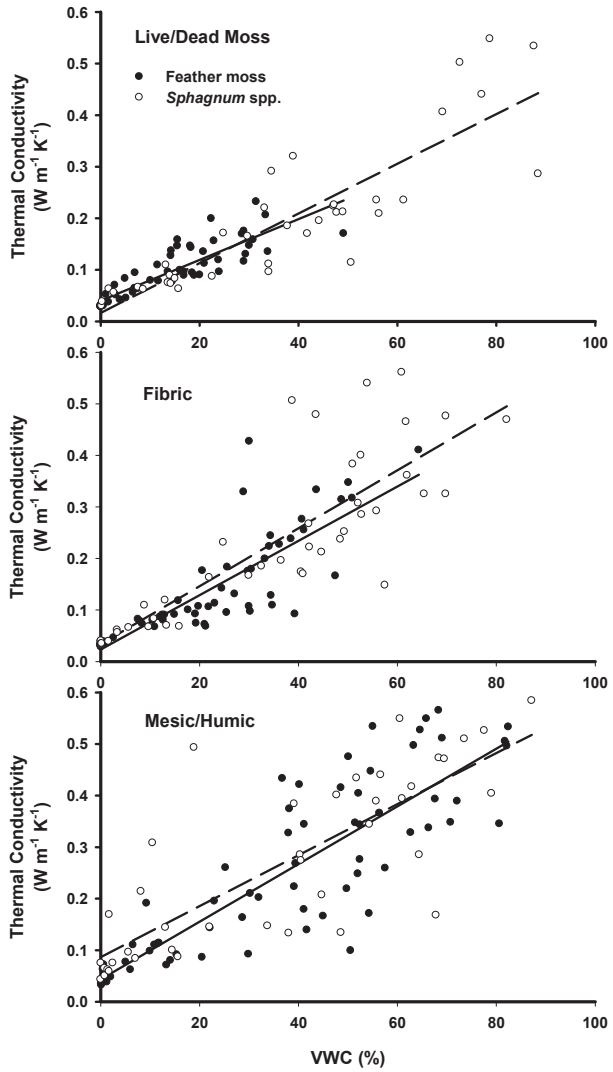

Figure 2. Linear regressions between thermal conductivity and volumetric water content in live/dead moss (top panel), fibric organic matter (middle panel), and mesic/humic organic matter (bottom panel). The regressions were fit separately for feather moss (solid line) and Sphagnum (dashed line).

organic horizons and moss types (range of R^2 values: 0.53–0.76; all P values < 0.0001). Increasing VWC of feather moss from 10 to 40% increased thermal conductivity nearly three-fold, whereas increasing VWC of Sphagnum from 10 to 60% increased thermal conductivity by five-fold (Fig. 2, top panel). We did not observe a very strong difference between feather moss- and *Sphagnum*-derived organic matter (fibric, mesic/humic). On average, increasing VWC of fibric horizons by 50% resulted in a four-fold increase in thermal conductivity (Fig. 2, middle panel). Similarly, increasing VWC of mesic/humic horizons by 70% resulted in a three-fold increase in thermal conductivity values (Fig. 2, bottom panel).

Discussion

Thermal conductivity of organic soil horizons in black spruce forests of Interior Alaska is positively correlated with moisture content. Thus, during the summer, variability in soil moisture content will greatly influence rates of heat transfer from surface to deep soil layers (Yoshikawa et al. 2003). During winter, heat fluxes through the active layer are primarily governed by ice content. However, unfrozen water can persist in deep peat and mineral soils during freeze-up and cooling of the active layer, modifying soil thermal properties and heat transfer (Romanovsky & Osterkamp 2000). Increased unfrozen water content during winter may reduce the thermal offset and increase the potential for permafrost thaw.

To evaluate the stability of permafrost in black spruce stands of Interior Alaska, we have developed a simple model to predict thermal offset (modified from Kudryavtsev 1981). This approach combines field measurements of soil moisture with laboratory measures of thermal conductivity and moisture, reported here. A comparative analysis of the observed thermal offset values with calculated values is currently in progress and will be discussed.

References

Burn, C.R., & Smith, C.A.S. 1988. Observations of the "thermal offset" in near-surface mean annual ground temperatures at several sites near Mayo, Yukon Territory, Canada. *Arctic* 41: 99-104.

Kudryavtsev, V.A. (ed.) 1981. *Permafrost*, short edition. MSU Press (in Russian).

Lachenbruch, A.H., & Marshall B.V. 1986. Changing climate: Geothermal evidence from permafrost in the Alaskan Arctic. *Science* 234: 689-696.

O'Donnell, J.A., Turetsky, M.R., Harden, J.W., Manies, K.L., Pruett, L.E., Shetler, G. & Neff, J.C. In review. Interactive effects of fire, soil climate and moss on CO2 fluxes in black spruce ecosystems of interior Alaska.

Osterkamp, T.E., & Romanovsky V.E. 1999. Evidence for warming and thawing of discontinuous permafrost in Alaska. *Permafrost and Periglacial Processes* 10: 17-37.

Overduin, P.P, Kane, D.L., & van Loon, W.K.P. 2006. Measuring thermal conductivity in freezing and thawing soil using the soil temperature response to heating. *Cold Regions Science and Technology* 45: 8-22.

Romanovsky, V.E. & Osterkamp, T.E. 2000. Effects of unfrozen water on heat and mass transport processes in the active layer and permafrost. *Permafrost and Periglacial Processes* 11: 219-239.

Yoshikawa, K., Bolton, W.R., Romanovsky, V.E., Fukuda, M. & Hinzman, L.D. 2003. Impacts of wildfire on the permafrost in the boreal forests of interior Alaska. *Journal of Geophysical Research* 108: (D1): 8148, doi:10.1029/2001JD000438.

.

Irreversible Damage? Human Activity, Cumulative Impacts, and Recovery Rates of the Antarctic Soil Environment

Tanya A. O'Neill
Department of Earth and Ocean Sciences, University of Waikato, Hamilton, New Zealand
Megan R. Balks
Department of Earth and Ocean Sciences, University of Waikato, Hamilton, New Zealand

Antarctic soils are vulnerable to disturbance because of their physical properties and extremely slow natural recovery rates due to the low temperatures and, in many regions, low levels of precipitation. As most human activities (tourism and national science programs) are concentrated in ice-free regions, the potential for human impacts on the soil landscape is great. Ice-free areas make up less than 0.4% of the total area of the continent, but are home to the majority of the historic huts, research stations, and biologically-rich sites, thereby attracting a short-sharp influx of tourists and science personnel each summer. Consequently, as continent-wide tourist numbers top 30,000 for the 2007/2008 summer season (www.iaato.org), concerns about cumulative effects, and the ability of the most frequented sites to recover after human disturbance, are also increasing.

Current information is insufficient to accurately predict how or to what extent the physical features at particular sites may be affected by repeat visits. This knowledge gap will impede our ability to effectively manage sites of value, and may consequently prove detrimental to the natural assets of the Antarctic ice-free regions.

This poster introduces a doctoral study that seeks to bridge the gap by quantifying the cumulative impacts of human activities on soils in the Ross Sea Region. Specific objectives are to (1) investigate the accuracy of EIAs (Environmental Impact Assessment) at predicting impacts of human activities on the Antarctic soil environment; (2) quantify the relationship between soil vulnerability (based on a soil vulnerability index), cumulative impact, and soil rates of recovery; and (3) elucidate a chronology of visible changes in the site "foot-print" at high human-impacted sites. Through this research we will establish baseline data relating to soil recovery rates in the Antarctic, an area of limited previous study. We will investigate sites where an EIA was conducted (such as the Greenpeace World Park base at Cape Evans, pipelines from McMurdo to Scott Base and beyond, and the proposed wind generation site on Crater Hill), and reassess the impacts on the soil environment following the completion of the activity to test the accuracy of EIA predictions. Such a detailed investigation into the effectiveness of the current EIA scheme with respect to *forecasted impacts* has not been conducted before. For our cumulative impact and recovery rate studies, we have deliberately chosen sites where the nature and timing of the disturbance have been well constrained, so recovery rates can be quantified (such as reassessing the K123 excavation pits and campsites in the Wright Valley, formed over three field seasons; and resurveying the 1992 Scott Base active-layer disturbance site of Campbell and others). In year three of this project, we will apply our Ross Sea Region methodologies to sites in the Antarctic Peninsula, where tourism and human disturbance is of an exponentially higher magnitude. Key heavily visited sites to investigate could include but not be limited to Barrientos Island (Aitcho Islands group), Hannah Point, Livingston Island, and Baily Head, Deception Island. Such comparisons could be used to model the likely impacts of the Ross Sea Region to increased tourist loading and associated pressures.

Our approach will begin to provide the basis for predicting how the Antarctic terrestrial environment will react to future human disturbance and climate change. It will assist environmental managers and Antarctic decision makers by allowing better predictive and managerial capability. There is the potential to document impacts of global warming on the terrestrial environment (soil and permafrost degradation), particularly in the warming Antarctic Peninsula. In the longer term there is the potential to produce a continent-wide map of ice-free regions using soil environment vulnerability classes based on cumulative effects and rates of recovery. This would involve the international coordination of resources to produce a GIS overlay of spatial information ranking soil vulnerability. Improved soil vulnerability data could be used by decision makers to identify or redefine Antarctic Specially Managed Areas (ASMA), Antarctic Specially Protected Areas (ASPA) (assist in developing or refining site specific guidelines), areas that are more resilient, could potentially have preference over others on the tourism itinerary, and identify others to focus future monitoring efforts. This information would be invaluable to the Committee for Environmental Protection (CEP) and aid in their Comprehensive Environmental Evaluation (CEE) assessment.

It is hoped that advancement of knowledge in the field of cumulative impacts will improve the highly criticized area of cumulative impact monitoring within the EIA system of the Madrid Protocol (1991). It is also hoped that this study will contribute to a more comprehensive tourism management system that will better incorporate tourism activities into the current EIA system. which coupled with an internationally standardized and quality EIA prior to an activity commencing, and coordinated environmental monitoring post-event, will ensure all possible environmental protection mechanisms are in place to preserve the integrity of the natural assets of the Antarctic ice-free regions.

The Role of Sea Ice in Coastal and Bottom Dynamics in the Baidaratskaya Bay

S.A. Ogorodov
Lomonosov Moscow State University, Faculty of Geography, Moscow, Russia

Sea ice, as a zonal factor associated with the high-latitude position of arctic seas, plays an important role in the evolution of their coastal zone. The ongoing development of oil and gas fields and the construction of relevant engineering facilities in the coastal and shelf areas (navigation channels, water scoop, terminals, drilling platforms, submarine pipelines) require new information on the effect of sea ice on the dynamics of coasts and sea floor. The effect of sea ice on coastal and bottom dynamics is one of the most important factors that determines the selection of a site for pipelines crossing from an offshore slope to land, method and a value of pipeline deepening. In Russia, special studies of sea ice impacts (first of all, the effect of ice gouging) were carried out in the areas of construction of submarine pipelines: the Baidaratskaya Bay of the Kara Sea (Fig. 1), the Pechora Sea, and the Sakhalin Island shelf.

The so-called "Nothern-Europe Gas Pipeline" must directly connect Russia and Germany through the bottom of the Baltic Sea to 2011. To provide gas for this pipeline, the project "Yamal-Europe" pipeline design, which lines would cross the Baidaratskaya Bay of Kara Sea, was renewed. Since 2005 and in connection with renewing of the project, investigations on coastal zone dynamics and sea ice effects was continued after a 10-year break.

Ice gouging is a destructive mechanical impact of ice onto the underlying surface. This impact onto the shore and bottom of the arctic seas is due to ice dynamics and mobility, hummocking, and formation of grounded hummocks, and it is controlled by hydrometeorological factors and coastal topography. In the Baidaratskaya Bay, the sea ice impact is observed in the coastal zone within the altitudes from first meters above the sea level down to 26 m depths.

Sea coasts are subjected to ice impact during the periods of both ice formation in autumn and fast-ice destruction and seas clearing of ice in spring. The relief of coasts composed of coarse debris material features a wide occurrence of ridges formed under the ice-push effect (Fig. 2). In autumn and in early winter, young sea ice (20–40 cm thick) can be pushed onto land during periods of surge. While moving, this solid ice cover cuts off beach sediments and forms ridges of unsorted material from it.

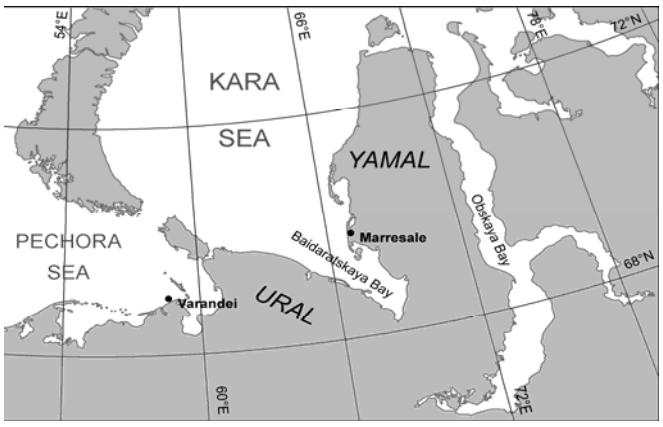

Figure 1. Location of research area

On maritime lowlands that can be flooded during high storm surges, sea ice can be brought inland as far as tens and even hundreds of meters, causing surface and building destruction.

The mechanical action of ice on the sea bottom lasts from the onset of ice formation until the sea is completely free of ice. After young ice freezes to the sea floor in the water edge zone, this new strip of ice serves as a protective buffer. The ridges of hummocks closest to the coast develop above submarine bars. Because of decreased sea depth over these bars, they become the centers of hummocking; hence, the number of hummock ridges commonly corresponds to the number of submarine bars. Due to the onshore pushing impact of sea ice, ice gouges in this zone are mostly oriented normally to the coastline (Fig. 3).

Further in the sea, the pattern of hummock ridges and barriers is irregular and controlled by hydrodynamic factors, particularly by the location of the fast ice edge during periods when storm wind is blowing. Storm winds destroy the fast ice edge and form a new ridge of hummocks or single-grounded hummocks. The ice gouges plowed in this case are either chaotic or parallel to the coastline. This is due to the prevailing along-shore drift of hummock formations. The fast ice edge (within Baidaratskaya Bay, at about 10–15

Figure 2. Ural Coast of Baidaratskaya Bay; ice-pushed ridge.

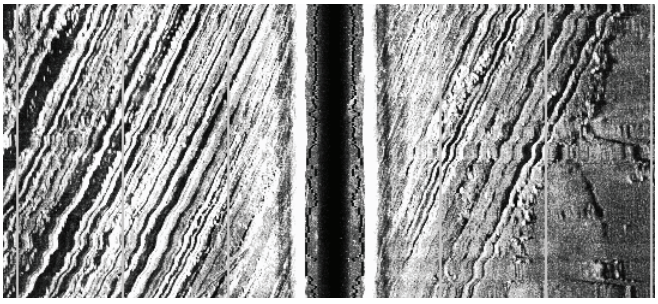

Figure 3. Sonar record at 12 m depth: Parallel and normally oriented to the shore ice gouges formed by multi-keels ice dam.

m depth) is the zone where ice impact on the sea floor is the strongest. Here, hummock ridges and barriers reaching the floor develop during the whole winter.

Within a beyond-fast-ice polynia up to 19–20 m depths sea ice influence on the bottom is also high, since hummocks frozen into the ice fields drift here during the winter as single large bergs which have high kinetic energy due to their mass. As a result, the largest ice gouges can reach 1.8 m deep, 10–40 m wide, and several km long (Fig. 4). They are oriented conformably with the direction of tidal currents—lengthwise the Baidaratskaya Bay.

The main method of indirect estimation of ice gouging intensity is the estimation of density and deepness (Fig. 5) of ice gouges. Meanwhile, the lifetime of such forms essentially can vary according to sea depth, types of sediment, and duration of the dynamically-active period; so the question about sea ice gouging intensity of the coasts and bottom is directly connected with the problem of safety of ice gouging forms.

Investigations on the Baidaratskaya Bay, Kara Sea, show that the frequency of occurrence and the density of ice-gouging forms is the largest at 17–19 m depth; but that does not mean that the intensity of ice gouging is lower in shallow depths with rarer occurrence and smaller depths of ice gouges.

The effect of coastal hummock ridges and barriers on beaches and in shallow areas (down to a depth of 7–10 m) can be traced only immediately after fast ice is destroyed. The life period of ice-gouged forms developed on sand beaches and shallow areas is very short—until the first summer storm. These forms, whose depth is mainly < 0.5 m here, commonly disappear with first strong waves in summer and autumn. Therefore, as a rule, the age of ice gouges in shallow areas does not exceed one year. Due to high hydrodynamic activity here, the gouges quickly smooth over, and the gouge density in shallow areas is lower than in the zone of the fast ice edge.

At depths of 14–16 m, the occurrence and density of gouges turn out to be lower than at higher depths, though ice gouging is the most intense (most of the mobile systems of hummocks and grounded hummocks are formed here). The above situation is due to more active hydrodynamics at smaller depths, where the effect of waves still manifests itself and the velocities of tidal currents are higher. Due to this, the gouges can exist over several years here (as distinct from their short existence in shallow areas), gradually smoothing over and vanishing. The lifetime of ice gouges is substantially determined by proportion between the freezing period and the dynamically-active period, and hence differs in diverse seas. For example, in the Pechora Sea, with a dynamically-active period two times longer in comparison with the Kara Sea, it is quite difficult to find ice gouges at the same depth. Another significant factor for the lifetime of a gouge is wave action. While comparing ice gouges at Baidaratskaya Bay at 12–14 m depth, the fewer number of gouges in the western part as compared with the eastern one is obvious. Indeed, the frequency of strong waves higher than 3 m, which can transfer sediments at stated depths, is a few times higher on the western coast as compared with the eastern one.

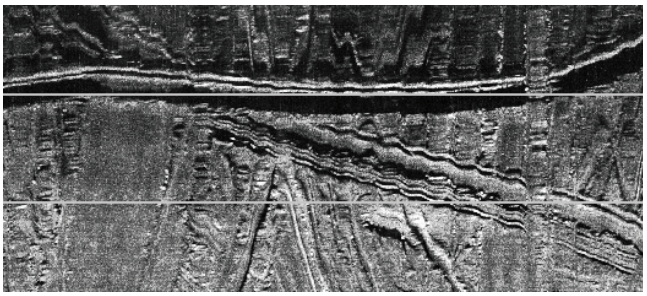

Figure 4. Sonar record, 19 m depth: Largest and deepest ice gouges.

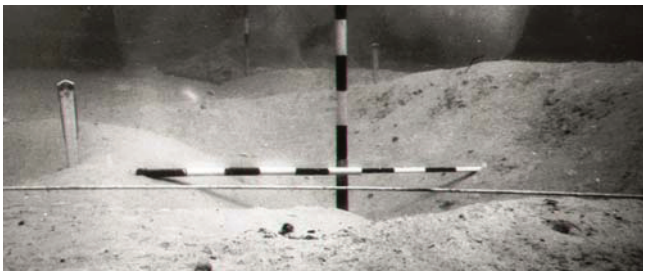

Figure 5. Winter underwater photo at a depth of 7 m: ice gouge deepness measurement. Stamukhi generated holes and gouges will become level by the first strong summer storm.

Deeper than 19 m, the ice gouges occur rather frequently. However, ice formations, particularly grounded hummocks, rarely occur at these depths. This situation is caused by low hydrodynamic activity and low sedimentation rates. Under such conditions, the gouges, especially large ones, can exist on the floor surface over decades. Thus, low intensity of ice gouging is compensated by a long life of gouge forms. This "accumulation" effect gives a wrong idea of high intensity ice gouging here.

The depth of ice-gouging forms depends not only on sea depth, ice thickness, and intensity of sheer stress, but also on composition and the state of bottom deposits. The safety of ice gouging forms probably depends also on plasticity, mobility, and granulometric composition of sediments. Attempts to find regularity between field data about occurrence and density of gouges on the one hand and the type of sediments on the other hand were not successful, except single examples of correspondence. Observations show that ice gouges, especially large ones, have considerable lengths, sometimes up to several kilometers; that is, hummocks can constantly gouge the bottom for a long time due to their large kinetic energy. Therefore hummocks can gouge bottom sections with rather different characteristics of the sediments.

Solifluction Phases During the Late Holocene in Sierra Nevada (Southern Spain)

Marc Oliva
Department for Physical and Regional Geography and Landscape Research Laboratory, University of Barcelona
Lothar Schulte
Department for Physical and Regional Geography and Landscape Research Laboratory, University of Barcelona

Introduction

Sierra Nevada, at latitude 37°N in southern Spain, is the highest massif in the Iberian Peninsula, reaching 3478 m a.s.l. at the Mulhacén peak and concentrates an important number of solifluction features. Dynamic control shows that nowadays most of these solifluction lobes are inactive and a few are weakly active.

The present climate conditions do not trigger intense solifluction processes, although sedimentological profiles of several lobes show enhanced solifluction activity during the last millennia. The alternation of edaphic layers and solifluction deposits implies different environmental conditions and reflects climate variations during the Late Holocene; colder and/or wetter periods promote solifluction, while warm periods induce soil formation.

Headwaters of Rio Seco and San Juan Valleys have a significant number of vegetated solifluction lobes. We have analysed the stratigraphy of many of them, and we provide the first chronology for solifluction activity during the Late Holocene in the southernmost last glaciated massif in Europe (Schulte et al. 2002).

Materials and Methods

Sedimentological and pedological studies according to the FAO system (2006) were carried out on more than 30 lobes placed between 2500–3000 m in these two valleys. A bulk sample of 0.5 kg was taken from each horizon or unit; laboratory analyses were done in the Institute of Geography of the University of Bern (Switzerland) on dry and sieved samples (< 2 mm).

For grain size measurements, organic matter was oxidized with 30% H_2O_2, and micro-aggregates were dispersed with Na_2CO_3. Silt (2–63 μm) and clay (<2 μm) fractions were determined with a Micromeritics SediGraph 5100 system, and sand fractions (63–2000 μm) were quantified by wet sieving. Organic carbon (OC) and the ratio C/N were measured with an Elemental Analyzer. The amorphous and crystalline pedogenic iron (Fe_o and Fe_d) were extracted according to Mehra & Jackson (1960). For AMS dating purposes, pollen grains from organic layers were concentrated and processed in the Angstrom Laboratory of Uppsala (Sweden).

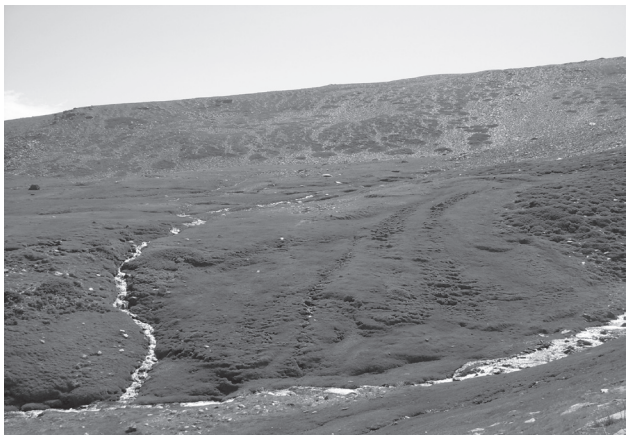

Figure 1. Solifluction lobes in San Juan valley.

Results

Solifluction phases are characterised by high percentage of gravels, a sandy loam fine fraction, and low OC contents (Fig. 2), while edaphic layers have a finer matrix with little amount of gravels, high OC contents (up to 30%) and increasing Fe_d values, depending on soil development intensity and weathering.

We present the lithostratigraphy of a solifluction lobe radiocarbon dated in San Juan Valley (Fig. 3), near late-lying snow patches with abundant supply of water. The bottom of the lobe corresponds to an organic layer that was buried by a solifluction deposit characterised by a high percentage of gravels and low OC contents, perhaps during the Neoglacial period. The warm climate conditions dominant during the Roman Warm Period and the Medieval Warm Period induce edaphic processes and peat formation (OC up to >25%) at this altitude. During the Little Ice Age, solifluction is reactivated with two pulses of significant percentage of gravels and decrease in OC values. In between these slope deposits, there is a thin organic layer, probably developed at the end of the 17th and beginning of the 18th centuries, a relatively

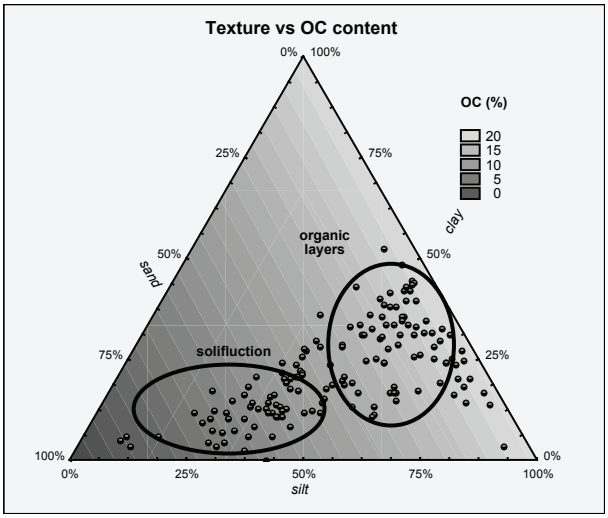

Figure 2. Comparison between texture and OC content in solifluction deposits and edaphic layers.

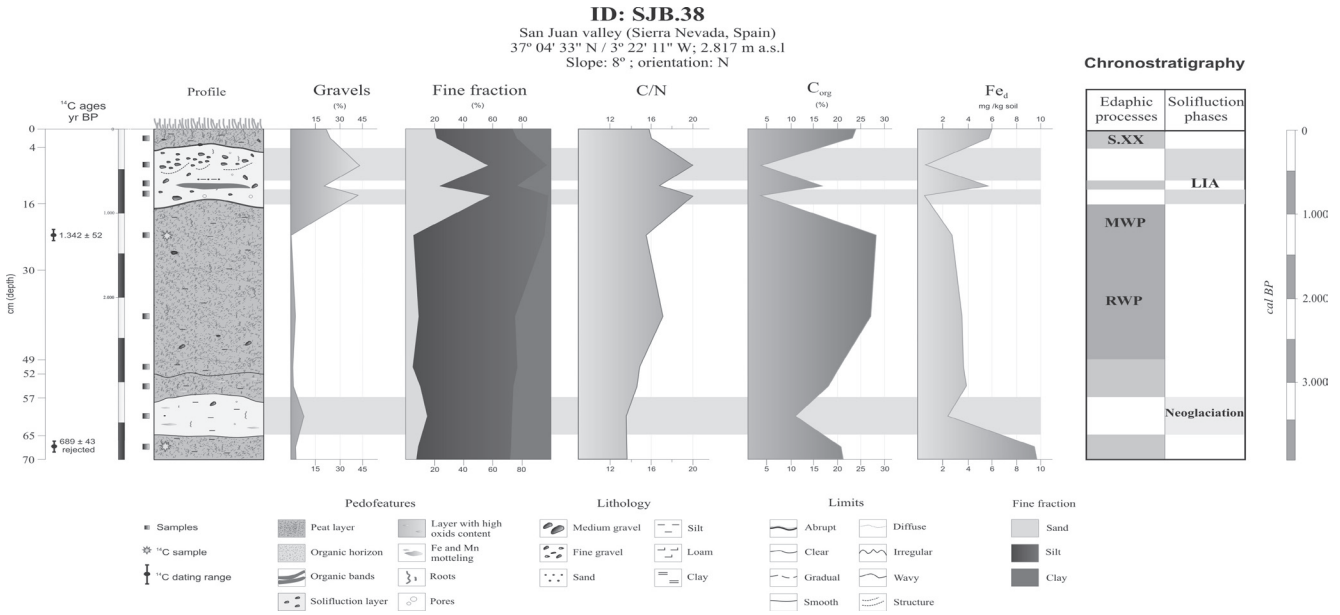

Figure 3. Lithostratigraphy of a solifluction lobe in San Juan Valley.

warm period in Andalusia (Rodrigo et al. 1999). The upper organic horizon of this vegetated lobe is the consequence of the increasing temperature trend of the 20th century.

Conclusions

Considering the chronostratigraphy of several lobes we can deduce different solifluction phases during the Late Holocene in Sierra Nevada: ?–3400, 3000–2700, 1400–1200, 650–300 and 250–100 cal. yr BP. Especially widespread are slope deposits corresponding to the two main pulses of the Little Ice Age (650–300 and 250–100 cal. yr BP) and the Neoglaciation (?–3400 and 3000–2700 cal. yr BP), mostly the two main Holocene solifluction phases in Sierra Nevada. On the other hand, intense soil development and peat formation was dominant during the Roman Warm Period (2700–1400 cal. yr BP) and the Medieval Warm Period (1200–650 cal. yr BP). These Late Holocene solifluction phases match with other mountain environments timing, such as in the Alps (Gamper 1983, Veit 1988), and correlates either with regional (Jalut et al. 2001) and global proxies (Stuiver & Braziunas 1993), suggesting the sensitivity of geomorphic processes in this high semiarid massif to Holocene climate variability.

Acknowledgments

This research was financially supported by the Spanish Ministry of Education, projects AP-2004-4548 and Fluvalps-3000 (CGL2006-01111).

References

FAO. 2006. *Guidelines for Soil Description*. UN, 133 pp.

Gamper, M.V. 1983. Controls and rates of movement of solifluction lobes in the eastern Swiss Alps. *Proceedings of the Fourth International Permafrost Conference. Fairbanks, Alaska, July 18–22, 1983:* 328-333.

Jalut, G., Esteban-Amat, A., Bonnet, L., Gauquelin, T. & Fontugne, M. 2000. Holocene climatic changes in the Western Mediterranean from South-East France to South-East Spain. *Palaeogeogr., Palaeoclimatol., Palaeoecol*. 160: 255-290.

Mehra, O. & Jackson, M. 1960. Iron oxide removal from soils and clays by dithionit-citrate systems buffered with sodium bicarbonate. *Clays and Clay Minerals* 7: 317-327.

Rodrigo, F.S., Esteban-Parra, M.J., Pozo-Vázquez, D. & Castro-Diaz, Y. 1999. A 500-year precipitation record in Southern Spain. *International Journal of. Climatology* 19: 1233-1253.

Schulte, L., Marcos Garcia-Blanco, J.de, Gómez Ortiz, A, Palacios Estrema, D., Tanarro Garcia, M., Fernández Fernández, A. & Ramos Sainz, M. 2002. Evolución Glaciar y periglaciar del Circo del Mulhacén (Sierra Nevada, Península Ibérica). *Publicaciones del Instituto Geológico y Minero de España*. Serie Geología 1: 491-499.

Stuiver, M. & Braziunas, T.F. 1993. Radiocarbon and 14C ages of marine samples to 10,000 B.C. *Radiocarbon* 35: 137-189.

Veit, H. 1988. Fluviale und solifluidale morphodynamik des spät- und postglazials in einem zentralalpinen flusseinzugsgebiet (Südliche Hohe Tauern, Osttirol). *Bayreuther Geowissenschaftliche Arbeiten* 13: 1-167.

Block Fields, Block Slopes, and Rock Glaciers: A Polygenetic Block Accumulation on the Schafstein (Rhoen Mountains, Germany)

Ch. Opp
Philipps-University Marburg, Germany

Introduction

Different forms of block accumulation are widespread in Central European Mid-Mountains. In most of the cases, they are described as block slopes (German: *Blockhalden*) and block fields (German: *Blockmeer*) and other German terms; in rare cases they are described as rock glaciers (Zurawek 2002).

The biggest known extension of block accumulation located in Germany is the basaltic hill of the Schafstein, in the central part of the Rhoen Mountains. This block accumulation was described in the 1960s by Mensching (1960), who called it *Blockmeer*, and in the 1990s by Halfmann (1991), who called it *Blockhalde*.

The first step of this study was to collect information from literature about the features of different forms of block accumulation (cf. Table 1).

Results

With the help of a self-developed mapping method, different features (cf. Table 1) of the Schafstein block accumulation were surveyed, for instance, block forms on the surface, weathering features, etc. The structure and the thickness of the block accumulation were measured with the help of refraction seismic techniques. For measuring air temperature below and between the blocks, dataloggers were used. Rock and soil samples were taken to determine the mineralogical composition with regard to weathering differences and transport mechanisms.

The small-scale survey of the block forms shows that the central part of the Schafstein block accumulation has edged blocks at the upper part and shaped blocks at the bottom of the block accumulation. A special feature at the bottom of the block accumulation is a characteristic wall and depression structure, with more than 30° inclination between the walls (cf. Fig. 1), caused by different tensions of different ice cement-saturated parts of the block accumulation. Refraction seismic measurements have proved that the central part of the block accumulation has a thickness of about 30 and 40 m. During summer time, when air temperature was about 30°C, we measured -1°C air temperature in between the block

Figure 1. Wall and depression structure in the central part of the block accumulation, the fossil rock glacier.

Table 1. Features of different forms of block accumulation (block field, block slope, and rock glacier), compiled after Däuble (2004, changed) from different literature sources.

Feature	Block field	Block slope	Rock glacier
General feature: accumulation of blocks with only a few or no amount of fine particles, with only rare or no vegetation cover			
Size	no details	some 10 m up to some 100 m long, >20 m broad	60...1500 m long, 60...3000 m broad
Thickness	no general details; mostly >1 m	no general details; some meters	10...100 m
Slope inclination	<20°	>20°	seldom more than 10°; border slopes 35°
Relief location	on plateaus and slopes; not necessarily closely connected to the source of blocks	below a bare rock	on slopes
Block size	no general details, different	at least head size, >2 m	mostly 0.6...1 m
Block form	edged or shaped	edged	no details
Block formation	in situ chemical and physical weathering with transport	in situ chemical and physical weathering with transport	physical weathering, primarily by frost
Block transport	solifluction, sliding	falling, sliding	cohesion transport of the ice cement
Surface structure	no details	no details	longitudinal and transverse bulges, depressions
Necessary climate	tropic or periglacial	periglacial, arid, semi-arid	periglacial

Figure 2. Rock glacier features on the bottom of the north and northwest slope of the Schafstein block accumulation.

accumulation (Opp 2005). Nearly all studied features prove that the central part of the Schafstein block accumulation represents a fossil rock glacier (cf. Fig. 2), while the western part represents a block field, and the eastern part is a block slope.

Acknowledgments

The author is especially grateful to Mrs. Däuble (Berlin) and Dr. M. Gude, who were included in the field research.

References

Däuble, F. 2004. Blockmeer–Blockgletscher–Blockhalde? *Ergebnisse neuer Untersuchungen am Schafstein/ Rhön*. Unpubl. FB Geographie, Marburg, 162 pp.

Halfmann, J. 1991. Die Struktur der Vegetation auf periglazialen Basalt-Block-Halden des hessischen Berglandes. *Dissertationes Botanicae* 168: 212 pp.

Mensching, H. 1960. Periglazial-Morphologie und qurtäre Entwicklungsgeschichte der Hohen Rhön und ihres östlichen Vorlandes. *Würzburger Geographische Arbeiten* 7: 39 pp.

Opp, Ch. 2005. Geographische Beiträge zur abiotischen Ausstattung des Biosphärenreservats Rhön. *Beiträge Region und Nachhaltigkeit* 2: 71-83.

Zurawek, R. 2002. Internal structure of a relict rock glacier, Sleza Massif, Southwest Poland. *Permafrost & Periglacial Processes* 13: 29-42.

Occurrence of Permafrost and Ground Frost Phenomena in Mongolia

Ch. Opp
Philipps-University Marburg, Germany

Introduction

Because of the climatic peculiarities and of the extreme continental location, the formation of permafrost and ground frost phenomena in Mongolia are widespread (Opp & Barsch 1993). Most of them belong to different forms of discontinuous and periodic permafrost. Types of ground frost occur in dependence from the zonal climatic, soil, and vegetation conditions. Zones of ground frost are distinguishable by their location above the sea level, by their area, by their spatial share, by their distribution within the zone, and by the thickness of the permafrost (cf. Table 1).

On the basis of observations, measurements, and interpretations during five field trips between 1989 (Barsch et al. 1993) and 1998 (Opp 1998, 2005), selected results are imparted.

Results

Seasonal average periods of freezing of discontinuous permafrost were established between October and May. The corresponding periods of thawing were established from late April until late September (cf. Fig. 1). The processes and periods of freezing and thawing can differ in dependence from the site conditions. Such examples were proved in dependence from the exposition (northern and southern slopes), or in river valleys (cf. Fig. 2) Characteristic differences of temperatures and pH values between the top and the bottom position of thufurs (earth hummocks) were analysed.

The degradation of many thufur fields in Mongolia is caused by climate (warmer winters) and land use changes (higher share of grazing animals) during the last decade.

Thermokarst bank erosion is caused by deep thawing during the summertime and lateral erosion by river water. The erosion rate of bank caving processes is much higher at the natural levee side in southern exposition than at other river bank positions. Within the river valley of the Orkhon River, south of the city of Darkhan, a maximum value of 1.5 m per year of backward erosion of the river bank, caused by permafrost degradation, were measured (Opp 1998, 2006). This "fluvio-cryo-thermo-erosion" of the river banks is a characteristic phenomenon of many rivers in northern Mongolia.

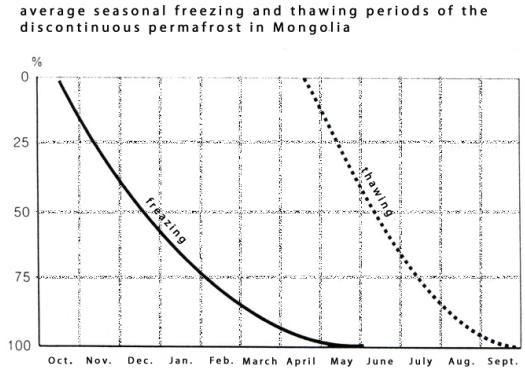

Figure 1. Average seasonal freezing and thawing periods of discontinuous permafrost within the Orchon catchment (northern Mongolia).

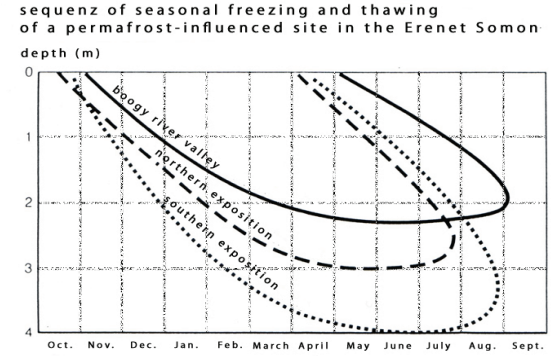

Figure 2. Sequence of seasonal freezing and thawing of a permafrost-influenced site near Erdenet (northern Mongolia).

Table 1. Selected features of the belts of frozen ground in Mongolia (Source: National Atlas of Mongolia, Ulan Bator, 1990).

belts of frozen ground	altitude a.s.l	area		portion within the permafrost area	dominant maximum thickness of permafrost		temperature in 20 m depth
			portion within the country		in valleys	on slopes and on watersheds	
	(m)	(km²)	(%)	(%)	(m)	(m)	(°C)
discontinuous permafrost	1200–2800	175,280	11.2	40–80	20–500 (bis 1000)		-5 bis +1
discontinuous permafrost	700–2600	350,560	22.4	1–40	5–50 (bis 100)	5-20	-5 bis +5
sporadic permafrost	600–1900	460,110	29.4	<1	5–10	-	-5 bis +5
seasonal ground freezing	600–1800	579,050	37	-	-	-	+3 bis +10

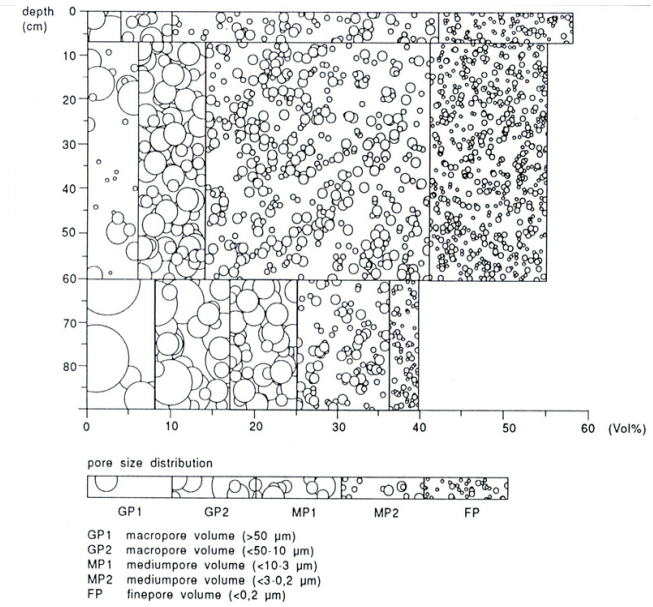

Figure 3. Pore size distribution of a Gelic Fluvisol (Turbel) within the Orkhon floodplain (northern Mongolia).

A warmer climate and an intensive use of pastures of the river valleys are the main reasons for permafrost and ground frost degradation in Mongolia. Effects on soils were proved with the help of cylinders measuring specific soil-physic parameters (pore volume, pore-size distribution, soil density, saturated vertical water conductivity) which, for example, allow statements about natural and man-made soil degradation and ground frost degradation processes. Though the pore volume in the upper soils of these sites is on average bigger than 50%, it is striking that their macro pore volume content is very small. The percentage of quickly-draining coarse pores is zero (cf. Fig. 3).

One reason for this seems to lie in the permafrost of the subsoil. The permafrost table during the summer measurement was at a depth of 90 cm.

Systems of polygonal ice wedges were observed on wet meadows near the river. A different distribution of the soil moisture of the ice wedges—wetter margin of the polygon, drier core of the polygon—was established by the different colouring of the grass. Besides that, ice wedge gaps of a width of 10 up to 40 cm are typical for a soil surface which was deformed by ice push and shrinking. The biggest ice wedge gaps (depth and width) were found in direct proximity of the Orkhon River.

Acknowledgments

The author is especially grateful to Prof. Dr. Barsch (Potsdam), Dr. Böttcher (Magdeburg), Dr. Tulgaa (Ulan Bator) and Mr. Enktuvshin (Ulan Bator), who were included in the field research.

References

Barsch, H., Opp, Ch. & Steinhardt, U. 1993. Geoökologische Probleme in der Waldsteppe der nördlichen Mongolei. *Potsdamer Geographische Forschungen* 3: 1-89.

Opp, Ch. & Barsch, H. 1993. Geomorphological processes in the Mountain Forest Steppe of Northern Mongolia. *Z. Geomorph. N.F., Suppl.-Bd*. 92: 145-157.

Opp, Ch. 1998. Bodenökologische Aspekte dauerfrostbeeinflusster Standorte in der Mongolei. *Mitteilungen Deutsche Bodenkundliche Gesellschaft* 88: 121-124.

Opp, Ch. 2005. Natürliche und nutzungsbedingte Land- und Bodendegradationsprozesse, untersucht am unteren Orchon (Nord-Mongolei). *Erforschung Biologischer Ressourcen der Mongolei* 9: 475-494.

Opp, Ch. 2006. Natural and land use caused land and soil degradation processes, a case study from the lower Orkhon region (northern Mongolia). *Proceedings of the Conference "Soil as a connecting link – function of natural and anthropogenic ecosystems in transition." Irkutsk September 4–7, 2006*: 480.

Reaction of Northern Taiga Ecosystems on Human-Induced Degradation of Permafrost in West Siberia

P.T. Orekhov
Earth Cryosphere Institute, Moscow, Russia, 744001

The development of the oil and gas industry has a considerable effect on permafrost ecosystems. Major and highly dynamic human-induced changes of the Western Siberia ecosystems have been caused due to the establishment and maintenance of the transport infrastructure of the oil and gas industrial system. Even a single facility, such as a main gas pipeline due to its length, is likely to have a drastic effect on ecosystems of different natural environment zones. The study of human impact on permafrost ecosystems appears to be especially urgent, taking into consideration an indirect effect of the disturbed vegetation, soil, and micro-topography on permafrost conditions.

This investigation has been conducted within the area of the Nadymsky Station of the SB RAS (Siberian Branch, Russian Academy of Science) Earth Cryosphere Institute, located in the northern taiga subzone of Western Siberia. The site occupies the area of sporadically distributed permafrost, and it is characterized by varied permafrost conditions. The permafrost patches are found in peat bogs, hilly lands, and frost heave areas. Mean annual temperatures of rocks vary within a range of +1.0 to -2.0°C.

Tundra ecosystems are widespread in peat bogs of the northern taiga. Perennially frozen grounds under the tundra ecosystems are referred to as the continuous permafrost zone. The temperature of perennially frozen ground varies from -0.5 to 1°C. A thickness of a seasonally thawed layer is within the range of 0.8 to 1.2 m in peat and mineral frost heave mounds and 0.5 to 0.7 m in peat mounds.

Associations of tundra plants such as grass, dwarf shrubs, moss, and lichen make up the specific vegetation cover of peat bogs. Dominant plants among those are *Ledum palustre, Vaccinium vitis-idaea, Rubus chamaemorus, Carex globularis, Cladina stellaris, C. rangiferina, Sphagnum fuscum,* and *Polytrichum commune* (Moskalenko 1999). In the almost complete ground cover of the undisturbed tundra ecosystems, lichens appear to be prevailing, that is, *Cladina stellaris and C. Rangiferina.* Apart from those, *Cetraria islandica* is commonly found among the ground cover plants together with *C. cucullata* and peat mosses. Foliage cover of the ground vegetation makes up 70%. The prevalent dwarf shrubs are presented by *Ledum palustre, Betula nana, and Vaccinium vitis-idaea.* Commonly found are *Vaccinium uliginosum*, *Carex globularis*, and *Rubus chamaemorus.* Foliage cover of the grass-and-dwarf shrub layer is 40–45%. The frost peat mounds vegetation cover is comprised of *Polytrichum strictum, Cladonia coccifera,* and *Cladina stellaris; Rubus chamaemorus* is abundant in the grass-and-dwarf shrub layer. In the natural tundra ecosystems, a total abundance of small mammal populations on average makes up 16.9 ± 1.1 species/10 pitfall trapnights. Biomass of small mammals is 259.4 ± 25.6 g/10 pitfall trapnights (Fig. 1).

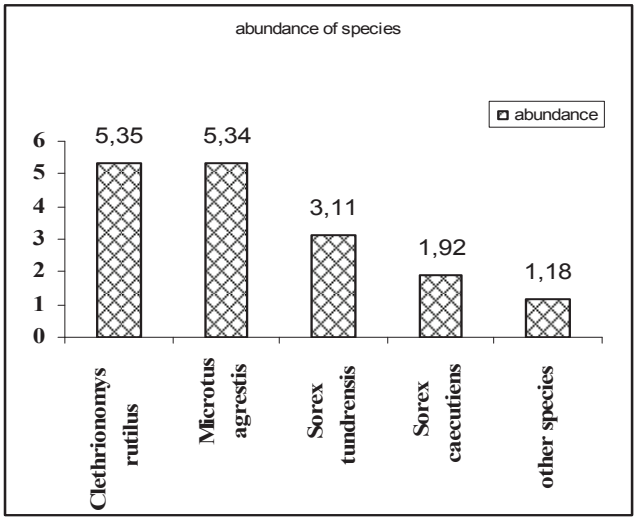

Figure 1. Abundance of small mammal species in the natural tundra ecosystems.

In 1971 in this area, the route was cleaned up to lay the gas pipeline Nadym-Punga. As the route was cleaned up, the vegetation cover was removed, the micro-topography was disturbed, and the upper peaty layer was withdrawn. The pipeline was laid in-ground with the earth fill made later. The pipeline laying lead to disturbance of the tundra ecosystems that resulted in an increase of water due to deteriorated drainage conditions, an increased number and enlarged area of hollows, bog formation, thermokarst activation, and finally, in peat surface subsidence with the top layer of the permafrost ground being dipped down to 6 m and, in areas with a thinner permafrost layer, being completely degraded.

Secondary ecosystems formed by 32 years after the occurrence of the primary disturbance. Ground cover of the secondary ecosystems has mosses prevailing, that is, *Polytrichum commune* and *Cladina stellaris. C. rangiferina* is not commonly found. Foliage cover makes up about 75%. Apart from those, species found in the ground cover are *Cetraria islandica* and *C. cucullata*. Among dwarf shrubs covering 40–45% of the ground surface*, Betula nana, Vaccinium uliginosum*, and *Empetrum nigrum* are growing abundantly. Species commonly found include *Calamagrostis Langsdorfii, Carex canescens, C. Globularis, Eriophorum russeolum, and E. vaginatum*. It should be noted that there are species which started growing abundantly along the pipeline, particularly, *Betula tortuosa* (height 5–7 m), *Salix viminalis* (height 3–5 m), and *Alnus* fruticosa, and these are species not specific for the tundra ecosystems (Sorokina 2003). Temperatures of top soil layers in September go up to 9.1°C.

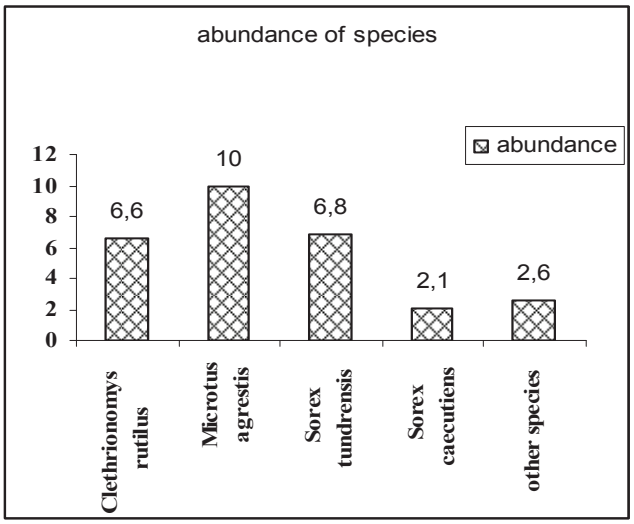

Figure 2. Abundance of small mammal species in the secondary ecosystems.

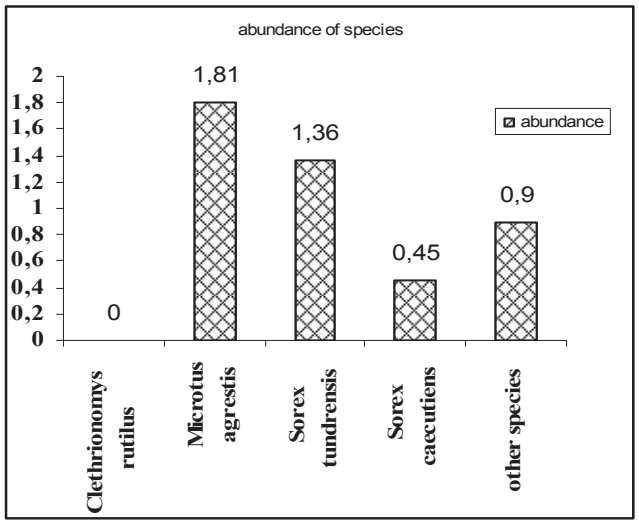

Figure 3. Abundance of small mammal species in the areas disturbed for the second time.

The comparative analysis applied to a community of small mammals has shown that the secondary ecosystems have significant growth of the species richness index that increased by 23.6% and the Shannon's diversity index that increased by 8.5%. A total abundance of small mammal populations on average makes up 28.1 ± 1.3 specisis/10 pitfall trapnights (Fig. 2). Biomass of small mammals is 522.2 ± 62.7 g/10 pitfall trapnights. A change has been observed in the dominance structure of small mammal communities (*Anthropogenic Changes* 2006). These changes in the population of small mammals of the secondary ecosystems compared to the natural ecosystems are associated with a great diversity of habitat conditions formed under the action of human-induced factors, particularly change in the hydrothermic condition of soils and formation of phytocenoses, having a greater variety of species.

In 2004 the gas pipeline was modified with the pipe replaced, which caused once again a disturbance of the secondary ecosystems. In 2005 the areas disturbed for the second time were partly flooded, followed by a formation of small, elongated lakelets up to 1.3 m deep, in which single species of *Utricularia sp.* were found. After the water level subsided as a result of the embankment being washed out in the third year after the secondary disturbance, sparse sedge-and-sphagnum groups were observed to form including single species of *Rubus chamaemorus*. A temperature of the soil top layer varies +4.5°C to +5.6°C. After the secondary disturbance occurred, the total abundance of small mammal species became 4.5 ± 0.9/10 pitfall trapnights. Biomass of small mammals is 60.9 ± 6.3 g/10 pitfall trapnights (Fig. 3).

With construction of pipelines, human-induced transformation of landscapes leads to change in ecosystem components such as vegetation, soil, topography, and rock top layers. This results in a change of snow cover dynamics, hydrological condition, and heat exchange in the bottom atmospheric layer. This in turn leads to impoundment, to change in thickness of seasonally frozen and seasonally thawed layers, to strengthening or weakening of a number of human-induced processes, and to reduced permafrost top layers, and in rare cases, to their degradation. Finally, there will be secondary ecosystems formed that differ considerably from the original ecosystems by multiple parameters.

Acknowledgments

I thank Elena A. Slagoda, Dmitry S. Drozdov, and Nataliya G. Moskalenko from the Earth Cryosphere Institute for logistic support. This research was funded by the grant of the Tyumen governor and the NASA Yamal LCLUC Project.

References

Moskalenko, N.G. (ed.) 2006. *Anthropogenic Changes of Ecosystems in West Siberian Gas Province*. Moscow: Earth Cryosphere Institute, 358 pp.

Moskalenko, N.G. 1999. *Anthropogenic Vegetation Dynamics in the Permafrost Plains of Russia*. Novosibirsk: Nauka, 280 pp.

Sorokina, N.V. 2003. *Anthropogenic Changes of West Siberia Northern Taiga Ecosystems*. Tyumen: Avtoreferat of candidate dissertation, 24 pp.